Mechanical Engineering Department G.I. Fekete
Ph. D. Thesis

Self-Preserving, Two-Dimensional Jets in Streaming Flow

A self-preserving, two-dimensional jet in streaming flow with pressure gradient and with the fluid in the jet the same as that of the surrounding flow, has been investigated experimentally. The fluid was air moving at effectively incompressible speeds.

Two-dimensionality was established and assessed as excellent, self-preserving conditions were obtained not only for the mean flow parameters, but for the components of the stress tensor as well, and reliable error limits were placed on all measured quantities.

Results are presented which show the non-dimensional velocity distribution, the rate of jet spread, the rate of velocity decay and the components of the stress tensor for six cases of jet excess to free stream velocity ratios. Several theories for jet growth and the value of the shear stress parameter are compared with the experimental results. Newman's theory is favoured since it is based on three fundamental equations, two momentum and one energy, with experimental input required only from a single flow whereas Vogel's theory is based only on two momentum equations with experimental input required from two measured flows (still air jet and small deficit wake).

SELF-PRESERVING, TWO-DIMENSIONAL JETS IN STREAMING FLOW

Self-Preserving Two-Dimensional Jets in Streaming Flow

by

G.I. Fekete

A thesis submitted to the Faculty of Graduate Studies and Research in partial fulfilment of the requirements for the degree of Doctor of Philosophy

Department of Mechanical Engineering
McGill University
Montreal, P.Q.

July, 1970

SUMMARY

A self-preserving, two-dimensional jet in streaming flow with pressure gradient and with the fluid in the jet the same as that of the surrounding flow, has been investigated experimentally. The fluid was air moving at effectively incompressible speeds.

Two-dimensionality was established and assessed as excellent, self-preserving conditions were obtained not only for the mean flow parameters, but for the components of the stress tensor as well, and reliable error limits were placed on all measured quantities; appropriate results to this effect are presented.

Results are presented which show the non-dimensional velocity distribution, the rate of jet spread, the rate of velocity decay and the components of the stress tensor for six cases of jet excess to free stream velocity ratios. Several theories for jet growth and the value of the shear stress parameter are compared with the experimental results. The latter fall between the Vogel and the Newman-Prandtl theories. Between these two no decision could be made due to lack of precise information on the jet in still air, from which experimental data is required in these theories. Newman's theory is favoured since it is based on three fundamental equations, two momentum and one energy, with experimental input required only

from a single flow whereas Vogel's theory is based only on two momentum equations with experimental input required from two measured flows.

Results of some intermittency measurements at the edge of the turbulent shear flow are also presented, but the limits of their accuracy are considered to be inadequate. Consequently, although the results are compared with two theories, no firm decision concerning the accuracy of either can be reached.

ACKNOWLEDGEMENTS

The author is indebted to Dr. B.G. Newman for his guidance and advice throughout the course of this work.

The help of Mr. A.A. Gustavsen in modifying the wind tunnel, his assistance with the construction of the working section, and the advice and help of Mr. O. Muehling with the construction of the slot lips are very much appreciated.

Mr. W.M. Vogel deserves special mention; his expertise with electronic instrumentation made it possible to complete the experimental programme on time. He also supplied information on the finer points of computer programming and a few of his sub-routines were used as parts of some of the computer programmes used in carrying out the calculations.

Discussions with Messrs. D. Guitton, R.P. Patel and W.M. Vogel concerning turbulent flows and flow measurements proved fruitful.

Thanks are due to Mrs. T. Miller for the typing of the manuscript and to Miss D. McKeown for her help with the illustrations.

The work was supported by the Defence Research Board of Canada under D.R.B. Grant Number 9551-12.

TABLE OF CONTENTS

NOTATION

A	Lateral rate of strain
B	Longitudinal rate of strain
b	Slot width
C_1	Constant in Equation (16)
C_2	Constant in Equation (16)
C_3	Constant in Equation (20)
C_4	Constant in Equation (19)
C_5	Constant in Equation (21)
C_6	Constant in Equation (22)
dL_o/dx	Rate of jet growth
E	$\frac{L_o}{U_o}\frac{\partial U_o}{\partial x} = E$
F	$\partial L_o/\partial x = F$
f	Function of η in Equation (1.a)
G	Excess to free stream velocity ratio U_o/U_1
g	Function of η in Equations (1.b, c, d)
H	$\overline{(q_o^2)}^{1/2}/U_o$
H_S^2	Suffix S = jet in still air
k	ln 2
k_1	Constant in Equations (11) and (15)
k_2	Constant in Equations (11) and (15)
L	Average dissipation length scale of large eddies in turbulent motion
L_o	Length scale of mean motion
l	Scale of largest eddies
ln	logarithm
m	Exponent of x giving the variation of u_1 in downstream direction to achieve self-preserving flow

q^2	$u^2 + v^2 + w^2$ twice kinetic energy of turbulence per unit mass
q_o^2	Twice kinetic energy of turbulence at y = 0
R_T	Eddy viscosity Reynolds number
T	Period of time
T_m	Arithmetic mean absolute temperature
T_a	Ambient absolute temperature
T_w	Absolute temperature of hot wire
U	Mean velocity in direction x
U_o	Velocity scale of mean motion
U_1	Free stream velocity
u_1	Fluctuating velocity about the mean in direction x
u	Velocity scale of large eddies in turbulent motion
$\sqrt{\overline{u^2}}/U$	Free stream turbulence
V	Mean velocity in direction y
v	Fluctuating velocity about the mean in direction y
W	Mean velocity in direction z
w	Fluctuating velocity about the mean in direction z
XTE	Measured from tunnel exit plane
x	Coordinate direction
Y	Average position of bounding surface separating rotational turbulent fluid from irrotational free stream fluid
y	Position from the axis of symmetry and coordinate direction
z	Coordinate direction

Greek notation

α, β	Constants used by Vogel - see Equations (10) and (12)
γ	Intermittency factor
ΔT_a	Small change of ambient air temperature

δ	Small change of velocity or space coordinate
ν	Kinematic viscosity of fluid
ν_T	Eddy viscosity due to total turbulent motion
ν_{TM}	Mean eddy viscosity due to "rest" of turbulent motion
ρ	Density of fluid
σ	Standard deviation of boundary between rotational and irrotational fluid from mean position or deviation of position of superlayer or Standard deviation of measurement
τ	$-\rho\ \overline{uv}$ Reynolds shear stress

Computer notation equivalents

$\sqrt{\overline{u^2}}/U_o$	RMSU/U.	Longitudinal turbulent intensity (non-dimensional)
$\sqrt{\overline{v^2}}/U_o$	RMSV/U.	Cross-stream turbulent intensity (non-dimensional)
$\sqrt{\overline{w^2}}/U_o$	RMSW/U.	Lateral turbulent intensity (non-dimensional)
$\overline{q^2}/U_o^2$	Q^2/U_o^2	Twice kinetic energy of turbulence (non-dimensional)
$\overline{uw}/U_o^2$	UW/U_o^2	Non-dimensional shear stress
$\overline{uv}/U_o^2$	UV/U_o^2	Non-dimensional shear stress
y/L_o	Y/LO	Non-dimensional cross-stream coordinate
$\overline{uv}$	MUV	Shear stress calculated from momentum equations
U_o^2	SUO	Scaling velocity squared

1. INTRODUCTION

When boundary-layer control problems are considered the flow in the vicinity of slotted flaps, blown flaps or jet flaps frequently involves either a quasi-two-dimensional jet or wake in a pressure gradient, or a wall jet in a pressure gradient the outer part of which is very similar to half a free jet.

Considerable theoretical and experimental work has been carried out in studying two-dimensional wall jets, free jets in still air, uniform streaming flow, and pressure gradients, and jets in uniform streaming flow, but only theoretical attention has been paid to the case of self-preserving two-dimensional jets and wakes in pressure gradients.

The conditions for the existence of this class of flows were set out by Townsend (1956), Patel and Newman (1961), and Newman (1967), and their theories based on integral methods were developed by Gartshore (1965), Vogel (1969), Newman (1968) and Gartshore and Newman (1969). Unfortunately, no experimental data is available to verify these theories. The only relevant experiments were carried out by Gartshore (1967), but even the two wakes he investigated were only approximately self-preserving. Since in the analysis of self-preserving flows fewer assumptions have to be made than in the analysis of related non-self-preserving flows, the former are of fundamental importance to provide insight for the more complicated flow cases.

Hence it is considered very important that the reliability of the available theories be verified experimentally. To this end the basic objective of this work has been to obtain reliable experimental data, in particular for two-dimensional, self-preserving jets in pressure gradients.

Before a detailed objective for the work can be set out the flow, the flow parameters and the axis system are shown in Fig. 1, and Townsend's (1956) criteria for self-preservation are given:

$$U = U_1 + U_o f(\eta) \tag{1a}$$

$$\overline{u^2} = U_o^2 g_{11}(\eta) \tag{1b}$$

$$\overline{v^2} = U_o^2 g_{22}(\eta) \tag{1c}$$

$$\overline{uv} = U_o^2 g_{12}(\eta) \tag{1d}$$

where $\eta = y/L_o$ and functions f and g are functions of η only.

Newman (1967) showed that, if U_1 the free stream velocity, is not equal to zero, self-preservation is possible only if:

$$\frac{U_o}{U_1} = \text{constant} = G \tag{2a}$$

$$U_1 \propto x^m \tag{2b}$$

$$\text{where } m = -\frac{\sqrt{2+G}}{3\sqrt{2+2G}} \tag{2c}$$

$$\frac{L_o}{x} = \text{constant} \qquad (2d)$$

It can be seen that the flow has to advance into an adverse pressure gradient so that the free stream velocity decreases in accordance with Equation 2.b.

A more detailed objective for the work can then be set out as follows: to establish a two-dimensional flow; to adjust the pressure gradient to obtain a self-preserving flow judged by mean-flow parameters; to prove that self-preservation as set out by Townsend's criteria does in fact exist for the stress tensor; to carry out a number of experiments that will permit the assessment of the accuracy of the measurements; to measure the rate of growth of the jet and the stress tensor for a range of excess jet velocity to free stream velocity ratios; to review the existing theories, and to discuss them and the assumptions on which they are based in the light of the experimental results.

2. EXPERIMENTAL ARRANGEMENT

The general layout of the apparatus is shown in Fig. 2 and Fig. 3.a. It is based on the McGill 17" x 30" Blower Wind Tunnel, Wygnanski and Gartshore (1963). Recent modifications to the tunnel include the addition of filters* to the air intake to reduce dust accummulation on hot wires; openings and doors cut in the side walls of the contraction section to permit mounting of a jet box, and the addition of a 5 HP variable speed D.C. motor drive to reduce tunnel turbulence at low tunnel air speed. This latter modification was completed only towards the end of the experimental programme. At high air speeds a constant rpm 25 HP A.C. motor drives the fan and tunnel speed is controlled by the fan's variable inlet vanes. When these are used to reduce the tunnel speed to below about 50 ft. per second the turbulence increases to about 0.8% and at very low tunnel speeds the turbulence intensity rises to about 1.5%, Patel (1970).

The jet box is supplied with air by a centrifugal compressor which is preceded by an air filter and is followed by a bleed valve for speed control then a water cooled heat exchanger to cool the jet air to tunnel temperature, and by two throttling valves in the hoses which duct the air to the ends of the jet box.

---

* American Air-Filter, Series 2000 DRI-Pak bag type filter units with fibreglass pre-filters.

The most important component of the apparatus is the jet box the suitable construction of which governs the two-dimensionality of the jet. The outside of the jet box was made as uniform as possible in cross section along the length of the box and putting the box into the contraction section of the tunnel as shown in Fig. 8 was expected to give rise to a well behaved two-dimensional flow in the free stream. Jet box construction details are shown in Fig. 4, and Fig. 5 shows photographs of the jet box with the top cover plate removed. Air is supplied to the jet box at its two ends, the air streams entering the opposite ends of a $1\frac{3}{4}$" high by 4" wide channel, the front of which consists of a two-dimensional orifice plate. This is followed by a deep cell honeycomb, a small settling chamber, and the slot plates. If the gap between the slot plates is uniform and the pressure upstream and along the gap is uniform one expects a two-dimensional jet to issue from the slot. The orifice plate opening was calculated, first assuming that the pressure is constant in the settling chamber and then using continuity and Bernoulli's equations. This simple first order analysis holds only if the flow makes a sharp 90° turn in the orifice plate. This requirement was effectively met by adding the aforementioned deep cell honeycomb immediately downstream of the orifice plate. Previous experience, Fekete (1963), with two-dimensional jets suggested that lack of two-dimensionality is caused mainly by:

a) the slot lip radius not being uniform along the slot causing varying degrees of initial jet

spread due to 'Coanda' effect - it is desirable to have a uniform zero radius, that is a perfectly sharp edge,

b) the surfaces that lead to the slot lip not being uniform and not being flat when they are expected to be, resulting in cross flows, and

c) the non-uniformity of the slot gap width.

To eliminate difficulties arising from the above causes, the slot was made about nine inches long in the flow direction so that, having approximately quarter inch gap width, one could expect the two-dimensional channel flow to be fully developed at least as far as the mean flow parameters were concerned, see Patel (1968). The plates were stress relieved, ground, stress relieved and ground again until they were flat within $\pm$ .002 in. over their surfaces; a rather long process. The flatness of the plates was checked on a surface plate and their parallelity by rubbing the plates together using a dye. The lip edges were honed square with a hand stone. To have the least possible variation in gap width along the 30 inch length of the slot the downstream portions of the slot are not supported at the plate ends, the two plates being spaced by two by three inch shims between tabs at their upstream ends. In addition to the clamping screws jack screws were inserted into the tabs so that deflection of the plates when under pressure could be counteracted by tightening the jack screws. The plate edges at the entry were also kept sharp, for

simplicity of construction and to give uniform entry into the channel.

Before the jet box was finally assembled it was clamped and the slot width and flow two-dimensionality were checked. After appropriate jack screw adjustments the nominal slot width was 0.240 inches and the deviation from this dimension along the slot length with and without flow is shown in Fig. 6. Fig. 6 also shows the same information obtained after the jet box's final assembly in place in the tunnel. These measurements were made with a dial indicator device. It can be seen that the maximum variation of slot gap width over its length was .004 in. without flow and .002 in. - that is less than one percent - when flow took place. Fig. 7 shows total pressure profiles in the slot exit plane at various positions along the length of the slot for the clamped slot box. It can be seen that the two-dimensionality was exceedingly good, within about 1% in total pressure. Two-dimensionality of the jet in streaming flow will be discussed in Section 4.

Flanges on the jet box fit into the cut-outs in the tunnel sides and the box can be mounted into or removed from the tunnel quite readily. Small screw jacks embedded in the flanges permit the adjustment and alignment of the jet box in the wind tunnel. Jet box reference pressure can be measured at two static pressure taps one at each end of the box settling chamber.

The tunnel working section (see Fig. 8) which consists of two sides, 'end plates' for the flow, top and bottom adjustable

louvres and a perforated plate at its downstream end is supported on an angle iron frame and is bolted to the tunnel exit plane. The whole section is mounted on castors so that it can be simply moved and it is provided with four elevating screws for levelling and alignment. The effective end plates for the flow consist mainly of six large 'plexiglas' windows, three of which are removable giving generous access to the working section.

The traversing gear (see Fig. 9) is based on a lead screw having twenty threads per inch. The lead screw carries a slider along an aluminum channel which is placed vertically into the working section of the tunnel. The bearing blocks at the ends of the channel, in addition to supporting the lead screw, fit into channels embedded in the top and bottom louvres so that the traversing gear can be slid manually from one side of the working section to the other. This provides movement in the z coordinate direction. A synchro receiver is mounted on one end of the lead screw which projects through a slot above the top louvres. The synchro transmitter, driven by a small D.C. motor, is coupled directly to a mechanical counter a unit change in the last digit of which corresponds to 0.01 in. of vertical travel of the traversing gear. This arrangement permits the adjustment of the traversing gear in the y direction within an accuracy of $\pm$ .005" and allows flow traverses to be made at a satisfactory speed. Probes are supported at the end of a long boom made of thin wall steel tubing, the probe lead wires being carried back through the tube. The boom is clamped

to the traversing gear slider in such a manner that it can be moved along its axis manually a total distance of 20 inches giving motion in the x direction. Furthermore, the boom support is such that the boom axis can be tilted in two mutually perpendicular planes so that slanting wires can be aligned with the mean flow direction.

The instrumentation used is shown diagrammatically in Fig. 10, it is also shown with the general layout of the apparatus in Fig. 3.b. Flow quantities were measured by a Disa constant temperature hot wire anemometer. The signal was linearized and the rms values of the turbulence quantities were obtained by means of a Hewlett Packard or a Disa RMS meter. Time averaging of the signals was done by using a voltage-to-frequency converter in conjunction with a digital counter to which a printer was coupled to reduce fatigue and to minimize the occurrence of errors during long experimental runs. The hot wires used were mainly standard or modified Disa miniature probes although a few measurements were made with the new gold-plated, wide-spaced, prong Disa probes when they became available. Details of the probes will be discussed more extensively in Section 3.

Jet box reference pressures were measured by a vertical water-filled manometer; the wind tunnel and the working section reference pressures were checked by inclined alcohol-filled 'Lambrecht' manometers while tunnel and room temperatures were observed on conventional thermometers.

3. EXPERIMENTAL PROCEDURE

The general pattern of experimentation and the use of equipment and instruments were governed by the fact that the wind tunnel was used by two experimenters alternatively for approximately six to eight week periods. This meant that the working section and the jet box had to be installed and later removed, this being done three times during the course of the present experiments. Furthermore, while either of the two experimenters using the wind tunnel worked during the day a third experimenter worked at night using the jet box air supply and some or all of the instrumentation in conjunction with a different apparatus. This meant that the working section and jet box were aligned three different times, perhaps more than usual care was taken to check out and calibrate the instruments, and the instrument gain varied at times from test to test. In addition anemometers and linearizers failed and were replaced by new instruments, and although of lesser importance the data acquisition section of the instrumentation was replaced due to the fact that initially borrowed instruments were used. This was very tedious at the time, but it guaranteed that the experiments were not carried out using the same experimental set-up and the same instrumentation through all the tests. Consequently, if the measurements were repeatable and/or consistent under these circumstances one would gain some confidence concerning their accuracy in addition to their repeatability.

In order to ascertain that the flow is self-preserving not only as assessed by the mean flow components, but also by the terms of the stress tensor (Equation 1) a test was run in which all the flow parameters were measured at several streamwise stations.

There was also a conscious effort made to assess the measurement accuracy. To this end the above-mentioned test for which standard Disa wires were used was repeated using hot wires of a different material the flow being effectively the same for both cases. The standard Disa wires N-21, S-8, 0.0002 in. dia. platinum plated tungsten having an aspect ratio of 225 are shown in Fig. 11a and were operated at an overheat ratio of 1.8 resulting in the wire to air temperature difference, $T_w - T_a$, being equal to 200°C. The wires for the comparison check N-3, S-3, 0.0004 in. dia. made of platinum -20% iridium, having an aspect ratio of 110 are shown in Fig. 11b, and were operated at an overheat ratio of 1.45 which gave rise to $T_w - T_a$ being 556°C. It can be seen that the transducer operating parameters were very different for the two runs, there being a slight difference in the slanted wires' geometry as well, as can be seen in Fig. 11, hence one would expect that the experimental results obtained with them on effectively identical flows would give a fair measure of the accuracy or rather the expected inaccuracy of the measurements. Details of these experimental runs will be discussed after other factors have been assessed.

It was expected that movement of the flexible hoses supplying air to the jet box would alter somewhat the two-dimensionality of the jet. Tests showed that this was so, but the effect was not substantial. Nevertheless, 18 in. long wooden cradles were clamped to the jet box ends and these cradles supported the hoses firmly in the same position during all of the tests.

The air supply to the two ends of the jet box was then regulated using the two throttling valves in the supply hoses until the maximum total pressures in the jet at the slot exit were equal at a position of nine inches on either side of the centre line.

The following procedure was followed to set up the self-preserving flow. First the jet was set to maximum velocity then the tunnel speed was adjusted so that the excess to free stream velocity ratio, G, was about one half, the louvres on the top and bottom of the working section having been pre-set in an arbitrary fashion to give an adverse pressure gradient. The maximum jet velocity and the free stream velocity were then measured at several streamwise stations using total and static probes. After the louvre spacing was re-set a few times by trial and error the excess to free stream velocity ratio, G, was almost constant. It was noted with interest that the down-stream variation of G was affected more by the width of the gap, about $1\frac{1}{2}$ in. left between the tunnel exit and the first louvre, the following three slots of order $\frac{1}{2}$ in. width, and

also the gap between the last louvre and the perforated plate at the end of the working section, than by the spacing between the louvres, order of $\frac{1}{8}$ in., in the portion of the working section where the measurements were taken. Following this, hot wire traverses were made at various downstream stations and it was found that Townsend's criterion, Equation 1.a, and Newman's criterion, Equation 2.a, for self-preservation were satisfied. Two dimensionality was then checked by the use of hot wires and a great number of exploratory measurements were made so that detailed experimental procedure could be established for the actual test runs.

A test was run to find the length of time required for signal averaging to obtain an acceptable degree of accuracy. Table I shows the results of these tests and it can be seen that if we consider a 95% confidence limit an averaging time of ten seconds results in the mean velocity being within $\pm \frac{1}{4}\%$ of its 'real' value. On the other hand the corresponding figure for $\sqrt{u'^2}$ is only $\pm$ 1.5%, and even if the averaging time is increased to fifty seconds the result obtained can be expected to be only within $\pm \frac{3}{4}\%$ of its 'real' value.

The preliminary tests showed also that it required nearly one hour to take one normal wire profile: mean and rms voltages using ten second averaging time intervals. Furthermore, it was noted that in each profile the mean velocity measured at the same point at the beginning and at the end of the traverse differed usually by between $\frac{1}{2}$ to 1 percent.

When several profiles were taken the first one was repeated at the end of the run. Interestingly enough, provided test conditions were maintained as constant as possible, the change in velocity at the reference point from the start of the run to its end was again of the order of one percent. The possible reasons for this will be discussed later, for the moment it is important only that one has had to contend with a drift of the order of one per cent in mean velocity at the best of times. The longer a particular run, the greater is the probability that the test conditions will not remain constant. In the light of these conflicting requirements a reasonable and practical choice had to be made for the length of time over which time averaging of individual measurements was to be carried out. A time interval of ten seconds was chosen. This made it possible in some cases to take all measurements for a particular flow case during one uninterrupted run. The interval was also sufficient to result in mean velocities of satisfactory accuracy, and although the accuracy of the individual turbulence signals was less than desired it was hoped that more than one profile per run would be taken in the self-preserving region of the flow, giving sufficient data which could then be averaged resulting in satisfactory accuracy.

It was also important to establish the effect of ambient temperature change on the hot wire output signal since Collis' (1957) law applies to wires of infinite aspect ratio and it is known from experience that wires having an aspect ratio of an

order of 200 do not behave according to it, hence error estimates derived from Collis' relation would have been unreliable. The tests carried out were not sufficiently extensive (ΔT_a of 8°F for example) to be definitive but were sufficient to show that the percentage error in the linearized mean voltage was of the order of 0.2% for a one degree Fahrenheit change of the ambient temperature when the overheat ratio was kept constant, and it was of the order of 1% per °F when the wire operating resistance was kept constant for the standard platinum plated tungsten wires. (For the platinum iridium wires where the difference between the wire operating and ambient temperature is almost three times as large as for the standard wires the error is negligible for a few degrees change in ambient temperature.) This suggests that it is advantageous to carry out the measurements by keeping the overheat ratio constant and then even if the ambient temperature changes by a few degrees during the course of an experimental run the error in mean velocity will still be within one percent. On the other hand measurement of the cold resistance, effectively ambient temperature, before each measurement would be very time consuming and impractical. It was done only at the beginning and at the end of a traverse; this means that for a particular traverse the wire operating resistance was kept constant. It is required then that the jet and free stream temperatures should not differ by more than about $\frac{1}{4}$°F if one wishes to obtain reasonable accuracy. Furthermore, the ambient temperature needs to be maintained within one degree while a specific traverse is being measured if one wishes the

mean velocity measurement to be accurate within one percent.

The sensitivity of the measurements to changes in ambient temperature would explain then the previously mentioned half to one percent drift in the reference velocity from the beginning to the end of measurement of a profile and also of a complete run, keeping in mind that the overheat ratio was kept constant and the cold resistance was measured at the start and at the end of each profile. In fact the records show that the cold resistance did often vary sufficiently to give a half percent error. In later measurements the results were rejected when the difference in wire cold resistance between start and end of any profile indicated an ambient temperature change larger than one half degree F. The results were also rejected when the mean voltage varied by more than one percent. To maintain the ambient temperature within one degree F in a laboratory in which other people were active presented the greatest single experimental difficulty, but the requirement was met for the runs for which data are presented.

The foregoing indicated the possible errors in mean voltage hence mean velocity due to ambient temperature changes. The effect of ambient temperature change on the slope of the wire calibration curve was also established by the tests, showing again that the error was considerably less when the overheat ratio was maintained constant than when the wire operating temperature was constant. (See Table II.)

Having information concerning the scatter of data which depends on the length of signal time averaging and the effect of ambient temperature changes on the output signal, it was possible to carry out an error analysis for all the quantities which were to be measured, to give an indication of the order of magnitude of the errors one might expect. The analysis was based on ten second averaging time with 2σ confidence limit, assuming that the data for the longitudinal turbulence was representative for all turbulence components; and on operation with a particular constant overheat ratio during wire calibration and the overall test run, which means in effect that during the measurement of any one profile the wire resistance was constant, and for this condition a probable ambient temperature variation of plus or minus $\frac{1}{2}°F$ was considered. An allowance of temperature difference of $2\frac{1}{2}°F$ was also made between calibrating and flow air temperatures. The results are shown in Table III. It can be seen that one of the most important parameters, the non-dimensional shear stress parameter, could be expected to be within an accuracy of plus or minus seven percent. This order of accuracy is satisfactory for this measurement provided it can actually be achieved experimentally.

It needs to be mentioned that no cross wires were used during this work, Jerome et al. (1969), only normal and single slanted ones, and that the preliminary measurements indicated that the turbulence intensities could be expected to be less than 15%, - this was confirmed during all the test runs - hence

there was at least no need to worry about high intensity turbulence corrections, see Guitton (1968). Further output signals were not smoothed, all data points were calculated using the actual output signal values for any one point. There is only one test run which is an exception to this, and the reason for data smoothing and its effect on the results will be discussed in Section 4. Champagne's (1965) longitudinal cooling corrections were applied to all slanted wire results.

One may mention also some of the difficulties encountered which gave rise to rejection of data for individual profiles or for complete runs, such as bursting of air supply hoses, failure of a hot wire or passage of a cold front in the middle of a run the latter completely upsetting test conditions, but one failure is particularly noteworthy because it took some time to find its cause. It was found during one run that the wire cold resistance changed arbitrarily over a narrow range although there was no measurable change in the test conditions. At first the anemometer control unit then the hot wire to probe support connection was suspected to cause the trouble. After these were disproven it was found that most wires of the probe cable strand were broken at their joint with the 'BMC' connector, changing the wire resistance with slight movement of the connector. Since this connector was located within and supported by the probe support boom it was a most unexpected failure and difficult to trace. It is suspected, however, that the wires

were nearly broken during previous experiments or accidental mishandling and the vibration of the support boom, although slight, was sufficient to sever those wires or additional wires in the strand to cause failure.

It was also found during the preliminary measurements that hot wire calibration in the calibrating drum was not convenient although it could be done satisfactorily. It was difficult and time-consuming to obtain and maintain appropriate calibrating air temperature, to align slanting wires with the flow and, since the calibrating drum was supplied with air from the jet box compressor, after calibration was completed and air supply reconnected to the jet box one had to wait about one hour until the tunnel came up to working temperature before measurements could be made. This was extremely time-consuming and the wires were calibrated for most runs in the free stream of the wind tunnel, except for the self-preservation and accuracy assessment runs for which the above lengthy procedure had to be followed for the following reason. Although it was possible to adjust both the jet box and tunnel wind speeds the adjustment was very coarse and since the jet box, tunnel and working section reference pressures fluctuated considerably it was not possible to reproduce the same flow conditions once the tunnel or jet-box flow-controls were changed. But in order to calibrate wires in the wind tunnel the tunnel speed had to be changed. So for the self-preservation and accuracy assessment runs and also for preliminary measurements the tunnel controls were not touched once the particular flow was set up, only the

drive motors were started or stopped and the calibration was carried out in the drum, controlling the calibrating air speed by moving a sluice valve near the drum.

The particular procedure used for the accuracy assessment runs can then be summarized. A particular self-preserving flow having been set up previously it was assumed that it could be reproduced since neither tunnel nor jet box speed settings had been changed. Using a normal wire the flow centre line was found at a particular downstream station. The slanted wire to be used was positioned at the flow centre line and it was aligned with the mean flow direction. Adjustments were made until mean voltage output was within about $\frac{1}{3}$ per cent when the wire was rotated over 360° several times in 90° increments. Hot wire instrumentation was checked out, zeros, set points, gain, etc., adjusted and normal wire N-3 was calibrated in the drum. Tunnel and jet were started, windows were opened appropriately - room was used as constant temperature plenum chamber - until constant room and flow temperatures were achieved. At the same time the flow was traversed with the hot wire and its cold resistance, i.e. flow temperature, was measured in the jet and the free stream, the heat exchanger water supply being altered until no difference could be detected between jet and free stream temperature. The first measurement was made at the centre line, the flow was then traversed from bottom to top, and the last measurement was made at the centre line again. Both the mean and the rms voltages were recorded

the averaging time for both signals being ten seconds. Wire cold resistance was measured before the first and last centre line reading. This procedure was repeated for subsequent profiles at other streamwise locations, always maintaining the same hot wire overheat ratio and making adjustments to the window openings as the need arose to maintain room temperature variation within one degree F. Finally the first profile was repeated. After this the wire was calibrated again. On another day slanted wire (S-3) profiles were taken at the same downstream positions. The procedure was essentially the same as for the normal wire measurements except that four traverses were made at each streamwise station the wires being rotated 90° between traverses, and mean voltage readings were taken only at the centre line reference positions, at other points in the flow only rms values being recorded.

Readings were taken at two downstream stations XTE = 51.8 and 59.8 for the evaluation of intermittency, the turbulence signal being differentiated, amplified and recorded on light sensitive paper using a galvanometer with a frequency response of up to 3000 cps at a paper speed of 12 inches per second. The length of the recordings per point was about six seconds.

The same procedure was repeated later using hot wires N-21 and S-8 except that no intermittency readings were taken. This was the more significant run since standard Disa wires were used, and the results of this run were to be used to see if the flow was self-preserving in its turbulence as well as

mean properties.

It appears clear from the foregoing that the runs designed for the assessment of self-preservation and of measurement inaccuracy, although eminently suitable to check self-preservation, were likely to accentuate the inaccuracy, and that it was possible to devise procedures to obtain improved results when no comparison of results obtained using different wires was required for a particular flow case. The changes in procedure adopted to this end follow. Both normal and slanted wires were calibrated in the wind tunnel in the free stream of the flow at the start of a run by appropriately adjusting the tunnel speed. The excess velocity to free stream ratio was then set followed by normal wire traverses at several stations, slanted wire traverses at one, the furthest downstream station, and the recording for ten seconds per wire position on magnetic tape of the differentiated turbulence signal for the later evaluation of intermittency - all taken during one uninterrupted run. Some of the runs were unfortunately interrupted by some calamity, which usually involved a sudden temperature change, resulting in fewer measured profiles for some runs than intended, and no intermittency recordings. These latter experiments were carried out during the summer, third apparatus setup, when the room temperature could not be as readily moderated as during the winter time.

The evaluation of the intermittency records was done by looking at the charts and making a judgement as to which

portions represent rotational, which represent irrotational flow and obtaining by scaling the proportion of turbulent to total interval, the intermittency γ. No electronic circuitry was constructed based on the conclusions of Gartshore (1965).

In the two cases where direct recording on light sensitive paper was made 12 inches of record represented one second recording time. When the signal was recorded on magnetic tape the recording was done at a rate of 60 inches of tape per second and the play-back at 1.5 inches per second. A Sanborn recorder was used to produce a permanent record which could then be evaluated by several people without the danger of the record fading away. This recorder was operated at a paper speed of 20 mm. per second giving an approximate chart length of 16 inches per each second of original signal. A paper speed of 100 mm. per second was also tried, but this did not improve resolution or readability over the record obtained at 20 mm. per second, consequently the latter was used for all the records taken. In addition the signal was processed through a band width filter having a low cut-off at 2000 cps. and a high cut-off at 5000 cps. in order to eliminate high frequency noise and low frequency fluctuations which made the record difficult to read. This is certainly a somewhat arbitrary procedure but it was used only after considerable experimentation of changing the band width and observing the readability of the records obtained. The argument is that since evaluation of the record is a matter of judgement and a difficult one at that, one wants to make a record which is as little ambiguous as possible; and

as long as the conditions under which the record was made are clearly stated the merit of the method can be judged. Furthermore, the original signal is preserved on the tape and can be processed again in any desired manner. This method involves also the reasonable fundamental assumption that if turbulence exists at any one time it will have components which lie between 2000 and 5000 cycles per second.

Gartshore (1965) states that the individual intermittency values are unlikely to be within $\pm 2\frac{1}{2}\%$ of their real value. During the present work the effect of sample length on an individual intermittency value was assessed and it was found that γ varied by about $\pm 5\%$ as additional chart increments were evaluated when the total sample length was ten seconds. This value was reached in an asymptotic manner the corresponding error at 5 second total sample length being $\pm 8\%$. It should be noted that this error includes some effect of judgement as to what is laminar or turbulent on the chart, although a particular individual is likely to be reasonably consistent in this respect. This suggests that no appreciable gain in accuracy can be expected with this method if sample lengths are increased to over ten seconds.

4. EXPERIMENTAL RESULTS

4.1 Two-dimensionality

The two-dimensionality check of the jet total pressure Fig. 7 has already been mentioned in Section 2. The two-dimensionality of the whole flow is shown in Figs. 12, 13 and 14 over eighteen inches of the central span of the working section at a downstream position where final measurements were later made for the first, second and third tunnel set-ups respectively. It can be seen that the flow is two-dimensional, the mean velocities being within $\pm$ 1%. Perhaps a better measure of the existence of two-dimensionality is shown when the measured shear stress compares favourably with the shear stress calculated using the integrated momentum equations, with the spread of the jet and the excess to free stream velocity ratio as experimental inputs. This is a very stringent criterion for the evaluation of two-dimensionality because the existence of even a limited degree of three-dimensionality in a flow will cause momentum imbalance and noticeable disagreement between the calculated and measured shear stress values. Guitton (1970) in fact shows that for a small flow divergence of the order of 2°, the discrepancy between the calculated and the measured shear stress may be of the order of 20%. It can be seen from Figs. 15.8 to 22.8 that there is remarkably good agreement between the calculated and the measured shear stress distributions up to a value of $y/L_o \doteqdot 1.2$ for all flow cases which were investigated, indicating excellent two-dimensionality.

At values larger than $y/L_o \doteq 1.2$ the flow is intermittent, that is, the flow is not turbulent all the time, hence the measured values of $\overline{vu}/U_o^2$ are smaller than those calculated from the equations which assume that the flow is at all times fully turbulent throughout.

4.2 Self-Preservation

The results for the test run, Ref. No. 279-297, G = 0.59, designed to test self-preservation are shown in Figs. 15. Measurements of mean quantities and the longitudinal component of turbulence were carried out at nine streamwise stations and for the rest of the turbulence quantities at five stations, all quantities having been measured at the furthest downstream station twice, at the beginning and at the end of the run. Fig. 15.a shows the excess to free stream velocity ratio to be constant the experimental scatter being within $\pm 1\frac{1}{2}\%$ of the mean value. Fig. 15.b shows the rate of the spread of the jet to be constant and Fig. 15.c shows that the maximum, free stream, and excess jet velocities decay as predicted by Equation 2.b. It can be seen that Newman's criteria for self-preservation, Equations 2, are met satisfactorily the experimental scatter being small. The non-dimensional excess velocity profiles are given in Fig. 15.1 and their independence of the downstream coordinate is even better than one would normally expect. The experimental points fit the usual exponential function rather well over most parts of the flow. Fig. 15.2 gives $\sqrt{u^2}/U$ as a function of the non-dimensional cross stream coordinate η,

$\sqrt{u^2}/U_o$ is shown in Fig. 15.3, $\sqrt{v^2}/U_o$ in Fig. 15.4, $\sqrt{w^2}/U_o$ in Fig. 15.5, $\overline{q^2}/U_o^2$ in Fig. 15.6, $\overline{uw}/U_o^2$ in Fig. 15.7, and $\overline{uv}/U_o^2$ in Fig. 15.8. Careful examination of the results shows that if one excludes some of the upstream stations, i.e. XTE < 42.8, not only is the scatter of the data within the error estimates given in Table III, but most of the data points lie within the bounds defined by the measurements taken at XTE = 51.8 at the beginning and at the end of the test run. This leads one to conclude that self-preservation does in fact exist in the turbulence components of the flow as well as in its mean components.

4.3 Expected Accuracy of Measurements

As was mentioned in Section 3 two test runs were carried out using transducers of very different operating characteristics for the two runs, the flow being nominally the same in both cases. In the light of the results of the self-preservation tests only results that are far downstream are presented, XTE > 45.8 in., for the two test runs Ref. 279-297 and 193-207, for comparison in Figs. 16. Table IV shows the experimental error obtained from the combined flow plots compared to the results of the error analysis. The experimental errors compare favourably with those of the error analysis, in fact they are almost identical except for the quantity $\sqrt{u^2}/U$ where one expects an error of $\pm$ 1.5% and experiences $\pm$ 4.5% experimentally. This is a large discrepancy and it is disturbing at first sight, in particular since this is one measurement where calibration and temperature errors cancel out almost entirely, the rms and mean

signals having been taken one after the other without moving the probe. Two reasons suggest themselves for the discrepancy. First the frequency response of the two wires is not the same, that of the platinum - 20% iridium wire being lower than that of the standard platinum plated tungsten wires. The effect of this, however, would be felt at the highest frequencies, typically larger than order of 10 Kh, and it is known from spectral measurements that at those high frequencies there is only a very small contribution to the turbulence intensities. One is led to consider the second reason for the discrepancy, that the two flows although expected to be identical are in fact not. Immediate evidence for this assumption is supplied in Fig. 16.2 which shows the plot of $\sqrt{u^2}/U$ versus η. One can see that one of the flows is not entirely symmetrical although the discrepancy is slight. Also, if one remembers that the two flows were considered identical mainly due to the fact that all tunnel and jet box controls were untouched while the measurements were carried out over a period of several days, one would be surprised if the two flows were truly identical. This could suggest that these tests are of little value, but on the contrary the whole point of carrying out the tests in this manner was to simulate or rather obtain and evaluate the effect on measurement accuracy of all the possible factors which may still be present when one believes that all reasonable precautions have been taken to get reliable measurements. As a consequence one can be very confident that the measurements presented have an accuracy falling within the limits shown in

Table IV. It may be a matter of opinion whether these limits are sufficiently tight, but the author feels that, when there is evidence, as was shown, that these limits are not estimates, but values based on analysis and experiment, they are very satisfactory.

4.4 Results for Various Excess to Free Stream Velocity Ratios

In the following tests all measurements for a particular U_o/U_1 = G ratio were taken during one uninterrupted run the wires having been calibrated in the wind tunnel.

Figs. 17 show the results for G = 0.265, Figs. 18 for G = 0.44, Figs. 19 for G = 0.68, Figs. 20 for G = 0.74, Figs. 21 for G = 0.79, and Figs. 22 for G = 0.95.

Points of interest are that the measured shear stresses agree well with those calculated from the momentum equations, that the data in Figs. 21 are presented both as calculated from individual (standard procedure) and also from smoothed voltages, that the data presented in Figs. 19 and Figs. 20 were obtained by using the new wide prong Disa wires, and that the run for which results are shown in Figs. 20 was carried out by using the new D.C. motor wind tunnel drive to obtain low free stream turbulence.

It can be seen from Figs. 21 that, as expected, voltage smoothing reduces the scatter and this can be significant in particular for the shear stress data especially in the region

of $\eta = 1$ which is usually the region of greatest interest. This indicates that one should smooth the voltages before they are processed further to obtain improved results, but except for this example for which the smoothed voltage plots are given in Figs. 21.9 to 21.14, this was avoided on purpose in this paper to eliminate factors of judgement which would then necessarily influence the final results. The basic data and the calculated results are available in numerical form and could be requested by those interested in processing them in any manner. Figs. 23 show examples of the numerical information. The basic hot wire and voltage information is given in Fig. 23.a*, dimensional calculated results without longitudinal cooling in Fig. 23.b, and non-dimensional results including the effects of longitudinal cooling in Fig. 23.c.

The use of the DC tunnel drive was disappointing in that the free stream turbulence $\sqrt{u^2}/U$, was not reduced remaining about 0.8% as was the case for all the other runs. The reason for this is most likely that the free stream part of the flow is not very extensive. This latter fact is responsible also for limiting the excess to free stream velocity ratio G to a maximum value of one. That the upper value of G obtainable would be limited was expected even before the experimentation

---

* Scale factor other than zero means that the given voltage value has to be divided by $\sqrt{10}$. The standard Disa platinum plated tungsten wire is designated by '1' under the heading of wire material, while the platinum -20% iridium wire is designated by the number '2'.

was started because of the 17 in. height of the tunnel working section. However, limiting the G values within a certain range is not as great a disadvantage as it may seem because the greatest variation between theoretically predicted shear stress and growth values occurs approximately in the G range to which the present experiments were restricted, namely $0 < G < 1$. And, although it would be desirable to have results for a greater range of G values, one of the fundamental purposes of the investigation, i.e. to show which of the many available theories is most likely to be correct, can be satisfied within the possible range of excess to free stream velocity ratios.

Figs. 19 and Figs. 20 which show the results obtained using the wide pronged Disa wires cannot give an indication of any shift in trend of the results as compared to those measured by standard Disa wires. In order to see if there is an effect due to these probes results are plotted for all of the test runs as follows. The values for the rate of jet growth dL_o/dx are plotted against G in Fig. 24 together with several curves of theoretical predictions. Theories will be discussed in Section 5, for the moment it is significant only that the experimental points follow a theoretical trend, the small deviations from a smooth line representing an experimental scatter rather than any pronounced effect which could be attributed to the different transducers. Similarly the experimental values of the non-dimensional shear stress at $\eta = 1$ are plotted in Fig. 25. Although the scatter appears to be large it is

still within the expected $\pm$ 7% limit of the mean value and certainly does not show any dependence on the transducer material or configuration.

This is a fair enough conclusion, but if we wish to use the experimental data to check the accuracy of the theoretical predictions we must select the data points which are likely to be the more accurate ones. Then the two runs designed to assess inaccuracy should perhaps be rejected for this purpose because ironically, although they give a good measure of measurement inaccuracy, by their very nature they are likely to be less accurate than the latter, main tests in each of which all measurements were carried out during an uninterrupted run. One can possibly expect then, an accuracy for the non-dimensional shear stress to be within $\pm$ 5%. This course of action is suggested when one examines Fig. 25.

One interesting feature of these flows was that within the limited range of excess to free stream velocity ratios investigated there was no need to re-adjust the louvre settings for the flows to remain self-preserving. It was mentioned previously that when the first self-preserving flow was set up with $G \doteq \frac{1}{2}$, the variation of G with x appeared to be influenced more by the large upstream gap than by the detailed setting of the louvres in the section where measurements were finally made. Now it may be just fortuitous that due to the fact that the G range was small, the working section along

which measurements were made was relatively short, 20 in. max., and the manner in which the flow rates varied resulted in appropriate streamwise pressure gradients of sufficient accuracy that all flows measured were self-preserving. On the other hand, one may see at least as a partial reason for this state of affairs a tendency of the flow to self-preservation once the initial adverse pressure gradient starts the flow in a certain direction. The pressure gradient that follows is not very different from that which it should theoretically be in order to keep the flow self-preserving. Newman and Gartshore (1969) have shown that wakes and jets that are nearly self-preserving tend to revert to a self-preserving condition. The present observations lend support to their contention.

4.5 Intermittency

Intermittency results are plotted in Fig. 26 for the flow case with G = .95. It should be noted that the same recordings for this case were evaluated independently by three different people. It can be seen that when least square fit probability integral curves are fitted to the three sets of results one obtains a large variation, of the order of $\pm$ 10%, in the value of σ/L_o. When one looks at the graph one may think, especially in the light of the comments made in Section 3 concerning the accuracy of each individual point, that one sees only an experimental scatter. However, the evaluation

by the three individuals also results in a variation of Y/L_o due to which some of the scatter is hidden in Fig. 26. If we consider that one is not even certain to what degree the charts, from which these differing results were obtained, represent the intermittency one is bound to question whether measuring intermittency using present techniques is a worthwhile proposition. The outlook becomes more optimistic, however, when data presented in Figs. 27 and 28 for G = .74 and .79 respectively are examined where the evaluation of the individual points was done in a random manner by the same three people. The σ/L_o values for the flows appear more consistent. Fig. 29 shows the intermittency results for G = .57, which are the ones obtained by the author from recordings made directly on light sensitive paper (the results of Figs. 26, 27 and 28 having been from processed signals and charts as described in Section 3). Two streamwise stations in the same flow are evaluated to see if σ/L_o is independent of x, remembering that Townsend (1956) found a substantial variation in the case of his small deficit wake with increasing downstream distance. In the present case σ/L_o = .305 at XTE = 51.8 and it has a value of .315 at XTE = 59.8 which in the context of the accuracy of evaluation can be considered a constant σ/L_o = .31. It is perhaps worth noting that during the preliminary measurements a value of σ/L_o = 0.33 was obtained for effectively the same flow, but using a different recorder which was operated at a paper speed of 24 inches per second. When one looks at Fig. 32 where all the σ/L_o values are plotted against G one

sees reasonable consistency in the results and considering all the factors one may put a probable accuracy limit of $\pm$ 10% for the σ/L_o results.

5. REVIEW OF THEORIES AND COMPARISON WITH EXPERIMENTAL RESULTS

5.1 General

From a theoretical standpoint two avenues of attack have been taken to obtain solutions not only for the two-dimensional turbulent jets considered here, but also for the related flows such as wakes, wall jets, etc. Of the two, the field methods, i.e. the use of digital computers to solve the differential equations by using finite difference techniques after an appropriate grid system has been chosen (Spalding and Patankar, 1967), appear to offer great promise for the future. Unfortunately, substantial empirical information is needed initially, and so far the methods are not readily usable. Furthermore, since the field methods involve to a very large extent computer methodology, they are outside the scope of this investigation. Hence no solution of the present problem will be attempted using these methods, the task being left to those whose main interest lies in that field. It is hoped, however, that the data obtained during the present experiments will be useful in perfecting such methods.

The second approach is based on an integral concept; that is, the parameters which govern the flow, the rate of growth and the shear stress parameter are established by considering the overall flow and integrating the boundary-layer form of the equations of motion across the particular flow. Since the number of equations is insufficient to solve the problem, additional

equations can be obtained by carrying out the integration between various limits and by using empirical or semi-empirical auxiliary equations. The methods in this category differ from each other mainly in their choice of the limits of integration and of the auxiliary equations, and the inclusion or exclusion of the energy equation in the primary equations. Of particular interest are the work of Gartshore* (1965), Vogel (1968), (1969), and Newman (1968) and the relevant ideas of Townsend (1956, 1966, 1969).

Fundamental to all three investigations is the use of the boundary-layer form of the momentum equation as the basic equation. For a turbulent flow and with the assumption that the streamwise change of the difference of normal stresses $\frac{\partial}{\partial x}(\overline{u^2} - \overline{v^2})$ is negligible compared to the other terms, this equation reduces to

$$U \frac{\partial U}{\partial x} + V \frac{\partial U}{\partial y} + \frac{\partial(\overline{uv})}{dy} = U_1 \frac{dU_1}{dx} \qquad (3)$$

the mean continuity equation is used

$$\frac{\partial U}{\partial x} + \frac{\partial V}{\partial y} = 0 \qquad (4)$$

---

* Bradbury (1965) presented independently an approach which is essentially similar to Gartshore's. Since both are based on Townsend's hypotheses the method should strictly be called the Gartshore-Bradbury formulation of Townsend's hypothesis. For simplicity, however, it will be identified in this paper with Gartshore.

also the mean velocity profile which is found to be valid experimentally as

$$U = U_1 + U_o \, e^{-k\eta^2} \qquad (5)$$

where $k = \ln 2$ and $\eta = y/L_o$ if one considers the notation as defined in Fig. 1. It is interesting to note that Equation (5) also holds very closely for non-self-preserving flows and even for the outer regions of wall-jets provided η is defined appropriately, (Forstall and Shapiro (1950), Bradshaw and Gee (1960), Patel and Newman (1961)).

It is not the intention here to go into the details of the work of the quoted investigators, but to summarize the methods they used and in particular to list the assumptions they made and the means whereby the validity of the assumptions may be checked. It will then be possible to discuss the merits of the assumptions and the various methods in the light of the present experiments.

It should be noted that in general when wakes and jets are studied the purpose is to predict the development of the mean flow parameters.

5.2 Gartshore

Gartshore (1965) followed Squire and Trouncer (1944) in integrating the momentum equation, Equation (3), twice: first

between the limits of $y = 0$ and $y = \infty$ and then between the limits of $y = 0$ and $y = L_o$ to obtain additional information. He then proceeded to find the shear stress which has now to be known as $y = L_o$, by showing that the shear stress could be related to the scale of the largest eddies, ℓ, in the flow, by considering Townsend's (1956) large eddy equilibrium hypothesis which postulated that the large eddies gain energy from the mean motion at the same rate as they are losing energy to the remaining turbulent motion throughout a significant part of their lives. Thus

$$\frac{\nu_{TM}}{U_o L_o} \propto -\left(\frac{\ell}{L_o}\right)^2 \qquad (6)$$

The scale of the largest eddies, (ℓ), was predicted by considering the effect of the mean rates of strain $\partial U/\partial y = A$ and $\partial U/\partial x = B$ on the vorticity of a large eddy. The instantaneous vorticity equations were simplified by considering Grant's (1958) conclusion that simple large eddies as postulated by Gartshore can exist only if they do not possess v-component of velocity. Further the diffusion terms were neglected and solutions were obtained for the average vorticity over a period of time T for two flows, one having both lateral and longitudinal mean rates of strain (A and B) and the other with longitudinal rate of strain (B) only. It was also assumed that both of the above flows started with the same circulation thus the average eddy size was defined. Following Townsend's

(1956) suggestion, the life time of the eddy was made inversely proportional to the lateral rate of strain

$$T \propto \frac{1}{|A|} \tag{7}$$

Then noting that ν_{TM} the mean eddy viscosity due to the "rest" of the turbulent motion is proportional to ν_T, the eddy viscosity due to total turbulent motion, since a universal eddy structure was assumed, and absorbing the various constants of proportionality into the new ones

$$\left.\frac{\nu_T}{U_o L_o}\right|_{A+B} = \left.\frac{\nu_T}{U_o L_o}\right|_{A \text{ only}} \frac{\sinh \beta \frac{B}{|A|}}{\beta \frac{B}{|A|}} \tag{8}$$

or a more convenient effectively equivalent linear expression

$$\frac{R_{T_o}}{R_T} = 1 - \beta \frac{B}{|A|} \quad \text{where } R_{T_o} = \frac{1}{\alpha} \tag{9}$$

Newman (1967) obtained the same results by considering the turbulent vorticity equation, his approach being more general than that of Gartshore.

Gartshore calculated the two experimental constants by considering the small deficit wake to obtain α, and the jet in still air which has a finite value of B/A to get β. Thus three coupled differential equations were obtained which Gartshore solved numerically. To obtain a solution the initial

values of all variables must be known for each particular flow.

With one notable exception, the majority of the assumptions made cannot be directly tested and Gartshore had to rely on an agreement between theory and experiment to assess the validity of the assumptions. The large eddy equilibrium hypothesis is the exception, the validity of which can be directly tested experimentally. This is based on the additional assumption that the standard deviation, σ, of the boundary between the rotational and irrotational fluid from its mean position is proportional to the scale of the large eddies present in the flow. Then from Equation (6) $\frac{U_o L_o}{\nu_T}$ plotted versus $(\frac{L_o}{\sigma})^2$ should give a straight line. Gartshore (1966) showed that when $\frac{U_o L_o}{\nu_T}$ is calculated for five flows at $y = L_o$, the ordinate of principal interest, a straight line is obtained within an acceptable scatter of the experimental points.

5.3 Vogel

Vogel (1968) followed Gartshore and invoked Equations (2) and (5) to show that a closed form solution is possible and for self-preserving flows he obtained the growth parameter

$$\frac{dL_o}{dx} = \frac{2k\left|G\right|(3\sqrt{2} + G)\,\alpha}{\left[2k\,(.405G^2 + 1.494G + 1.414) + \alpha\beta\left|(4k-1)G^2 + (6k\sqrt{2} - 2 - \sqrt{2})G - 2\sqrt{2}\right|\right]} \qquad (10)$$

as a function only of the excess to free stream velocity ratio

G. The mean rate of strain ratio becomes

$$\left.\frac{B}{A}\right|_{y=L_o} = \frac{\frac{dL_o}{dx}\left|(4k-1)G^2 + (6k\sqrt{2} - 2 - \sqrt{2})G - 2\sqrt{2}\right|}{2k\left|G\right|(3\sqrt{2} + 2G)} \qquad (11)$$

and the shear stress parameter is from Equation (9)

$$\left.\frac{\overline{uv}}{U_o^2}\right|_{y=L_o} = \alpha\left(1 - \beta\frac{B}{A}\right) \qquad (12)$$

the constants $\alpha = .0533$ and $\beta = 9.1$ were established in Gartshore's manner using the small deficit wake in zero pressure gradient and the jet in still air. The above equations will be identified as the Gartshore-Vogel equations on the plots. Furthermore, Vogel showed that if, instead of Equation (9), the correct single-term, even-order expansion of the hyperbolic function is used, namely

$$\frac{R_{T_o}}{R_T} = 1 - \beta\left(\frac{B}{A}\right)^2 \qquad (13)$$

the results are not substantially changed. The calculated results do show, however, a peculiar behaviour. In particular, those for axisymmetric jets, for which Vogel also found the appropriate expressions, predict a maximum rate of growth for values of $\frac{U_o}{U_1}$ around 5 instead of ∞ as would be expected; a most unlikely behaviour. Vogel examined the manner in which the rates of strain behave and found that if B is calculated in the cartesian coordinate system as shown in Fig. 1, B becomes

zero for the two-dimensional case when G = .746. Then B/A is not even approximately constant and this contradicts the original postulate on which the derivation of Equation (9) or (13) is based; that an eddy travels in a mean flow which has constant homogeneous rates of strain. Of course, the rates of strain in jets and wakes are not homogeneous, but Vogel argued that the most reasonable approach is to evaluate the longitudinal rate of strain in a direction along which the strain ratio remains constant for self-preserving flows, namely along a line of constant y/L_o. Starting from the definition of the velocity component in the x-direction he found the velocity components in the now appropriate cylindrical polar coordinates, then assuming that dL_o/dx is small (the normal boundary layer approximation) so that $G/(dL_o/dx)$ is large for the regions of interest he obtained

$$\left|\frac{B}{A}\right| = \frac{-\frac{dL_o}{dx}\, m}{kG} \left[1 + \frac{G}{2}\right] \qquad (14)$$

Using Equation (9), the two constants are calculated again using the small deficit wake in zero pressure gradient and the jet in still air obtaining $\alpha = .0533$ and $\beta = 16.2$. The growth parameter becomes

$$\frac{dL_o}{dx} = \frac{2k\,|G|\,(3\sqrt{2} + 2G)\,\alpha}{2k\,(.405G^2 + 1.494G + 1.414) + \alpha\beta\left[G^2 + (2+\sqrt{2})G + 2\sqrt{2}\right]} \qquad (15)$$

and the shear stress parameter is obtained explicitly as a function of G by the use of Equations (2), (15) and (14) with either Equation (9) or (13). Vogel found the behaviour of the calculated growth parameter more reasonable for jets, but for large deficit wakes seeing the rapid rise of the growth parameter he naturally questioned the validity of the small growth parameter approximation he made and even the validity of the boundary layer approximation. The sole experimental values available being those of Gartshore's (1967) near self-preserving wakes, and in their region of G there is practically no difference between any of the theories, Vogel looked to future experimental data on self-preserving jets and self-preserving large deficit wakes for verification of his work.

It should be noted that he obtained almost identical results when he used either the linear Equation (9) or the quadratic approximation Equation (13) for the growth parameter.

5.4 Newman

Newman (1968), in addition to integrating the momentum equation twice between the same limits as Gartshore and Vogel, integrated the sum of the mean and the turbulence energy equations from $y = 0$ to $y = \infty$ and thus obtained three fundamental equations. The dissipation integral terms $\int_0^\infty \epsilon dy$ is expressed as $(\overline{q_o^2})^{3/2} \frac{Y}{L}$ on dimensional grounds where $q_o^2 = \overline{u^2} + \overline{v^2} + \overline{w^2}$ at $y = 0$, Y is the average position of the bounding surface which separates the rotational turbulent fluid from the

irrotational free stream fluid and L is the average dissipation length scale of the turbulent motion. He then first invoked Townsend's (1966) assumption that the turbulence is geometrically similar to find the expression for the shear stress, namely

$$\frac{\overline{uv}\Big|_{y=L_o}}{\overline{q_o^2}} = \text{constant} = C_1 \qquad (16)$$

As a consequence of the same assumption $\frac{L_o}{L}$ is also constant, say = C_2. The three basic equations for the half-momentum, full momentum, and the full mean and turbulence energy equation become respectively

$$F\left(\frac{.309}{G} + .275\right) + E\left(\frac{1.927}{G} + .955\right) = -C_1 H^2 \qquad (17)$$

$$F\left(\frac{1}{G} + .707\right) + E\left(\frac{3}{G} + 1.414\right) = 0 \qquad (18)$$

$$(F + 3E)\left[\frac{1.063}{G^2} + \frac{1.128}{G} + .307 + \left(\frac{.85}{G} + .508\right) H^2\right]$$

$$+ C_4 C_2 H^3 = 0 \qquad (19)$$

where $F = \frac{dL_o}{dx}$, $E = \frac{L_o}{U_o}\frac{dU_o}{dx}$, $H = \left(\frac{\overline{q_o^2}}{U_o^2}\right)^{1/2}$, $C_4 = \frac{Y}{L_o}$.

Or as an alternative Newman turned to Prandtl's expression

$$\tau \propto \rho L(\overline{q^2})^{1/2}\frac{\partial U}{\partial y}$$

to express the shearing stress. Then the shear stress parameter becomes

$$\left.\frac{\overline{uv}}{U_o^2}\right|_{y=L_o} = C_3 \frac{L}{L_o} \left(\frac{\overline{q_o^2}}{U_o^2}\right)^{1/2} \qquad (20)$$

and the first equation in the above set of three equations is modified to

$$F\left(\frac{.309}{G} + .275\right) + E\left(\frac{1.927}{G} + .955\right) = \frac{C_3}{C_2} H \qquad (17a)$$

It is then assumed that C_1, C_2, C_3 and C_4 are universal constants for all self-preserving flows, that a reasonable value or range of values can be taken from existing experimental data for C_1, C_4 and H and that a reliable value for F is available from the jet in still surroundings then C_2 and C_3 can be evaluated from the equations. With all the constants so established the problem is solved. It should be noted that it is possible to obtain all the empirical information required from a single flow, the jet in still air. Newman used values of Townsend's (1956) small deficit wake, Gartshore's (1967) nearly self-preserving wakes, Bradbury's (1965) and Heskestad's (1965) jets with little or no surrounding flow to obtain a range of plausible values for C_1 and calculated the growth and shear stress parameters for a range of G from Equations (17) to (19) for two values of C_1, $\frac{1}{3}$ and $\frac{1}{6}$, to cover the range of uncertainty.

Newman took Bradbury's jet value for C_4 and used for H_s^2 a range of .10 to .16 (guided by Bradbury's and Heskestad's measurements) to calculate the growth and shear stress parameters from Equations (17.a) to (19). He found that the results were only slightly affected by the variation of H_s^2.

Newman calculated also the variation of σ/L_o with G based on Townsend's prediction that the standard deviation σ of the bounding surface of the rotational flow regime from its mean position Y is proportional to L/H^3. Hence

$$\frac{\sigma}{L_o} = \frac{C_5}{C_2} H^{-3} \qquad (21)$$

and C_5 is established from measured intermittency values for a jet in still air.

5.5 Summary

Gartshore and Vogel used the "double integral method" with the shear stress parameter expressed as a function of the lateral and longitudinal rates of strain to obtain the rate of growth and the shear stress parameter as a function of the excess to free stream velocity ratio for jets and wakes. Several assumptions were required of which only Townsend's large eddy hypothesis could be verified directly, after an additional assumption was made. The effects of all assumptions were amalgamated into the constants of Equation (9), hence agreement or disagreement between final prediction and experiment could unfortunately not shed much light on the validity

of individual assumptions.

Vogel's work was more advanced than Gartshore's because he obtained a closed form solution for the shear stress and growth parameters and also used a more realistic coordinate system to evaluate the rate of strain ratio than Gartshore.

In order to evaluate the constants which are required to predict all self-preserving flows experimental data is required from two flows which have extreme values of excess to free stream velocity ratios.

Newman added an integral energy equation to the two integral momentum equations to predict the same parameters as Gartshore and Vogel. As a consequence more assumptions are made to evaluate all the terms of the equations, but most of the assumptions result in universal constants some of which can be directly verified by experiment, and although the validity of the whole can again be checked only by the final results, having three fundamental equations instead of two gives a more secure basis for the analysis. Furthermore, it is possible now to obtain all the required constants from experimental values of only a single flow, the jet in still air.

The constants used by Gartshore, Vogel and Newman are summarized in Table V.

5.6 Comparison with Experiment

Examination of Figs. 24 and 25, which present the calculated

values for the growth and shear stress parameters respectively with the values of the present and Gartshore's (1967) experiments, shows that as expected by Vogel Gartshore's theory gives unrealistic results, that Newman's theory using Townsend's assumption for the shearing stress is also unsatisfactory and that the results of the present experiment do lie between the predictions of Vogel's and Newman's theories, the latter using the Prandtl assumption for the shearing stress. Hence the latter two theories merit a closer examination together with considerations concerning the accuracy of the measurements.

It was shown in Section 4 that the accuracy of the measured shear stress parameter is expected to be within $\pm$ 5% and when the growth parameter was calculated from the experimental data its accuracy was found to be, within two σ limits, of the order of $\pm$ 5% . The experimental values are therefore re-plotted in Figs. 30 and 31 for the growth and shear stress parameters respectively showing the limits of the uncertainty of the measurements. It seems natural then to question the accuracy of the experimental constants which were used to calculate the theoretical curves of Vogel and Newman, and rather than plot a single curve for each, calculate the limits of their range and plot them accordingly.

Since the values for the shear stress parameters for the small deficit wake and the jet in still air and the value for B/A for the jet in still air used by Vogel could possibly be in error by $\pm$ 5% it is appropriate to re-calculate Vogel's theo-

retical curves using α = .056 and .051 and β = 17.3 and 15.1.

Newman already showed that a large variation of H_s^2 (.10 to .16) has little effect on the calculated results and since Bradbury (1965), Heskestad (1965) and Patel (1970) find values for H_s^2 as .13, .149, .122 respectively it is reasonable to use values of H_s^2 = .12 and .14 in the calculations. Patel finds that for a jet in still air C_4 = 1.68, Bradbury's jet value is 1.7 hence Newman's choice of C_4 = 1.7 seems appropriate; nonetheless values of 1.6 and 1.8 will be tried to see if the results are sensitive to this parameter. In reference (Newman, 1967) the available results for the growth parameter for a jet in still air have been tabulated. By neglecting some unlikely values on the basis of the conditions under which the tests were carried out Newman found an average value for $\frac{dL_o}{dx}$ of .104 with $\pm$2% variation. In the light of the measurements of Reichardt (1951), Heskestad (1965), Gartshore (1965) and Smith (1970) and of the present experiments only two percent variation appears to be somewhat optimistic. Optimistic or not the purpose at present is to find probable bounds for the values and to this end a maximum value of .108 and a minimum value of .100 will be used as experimental inputs for the calculations.

The bands of growth and shear stress parameter values calculated in this way are also plotted in Figs. 30 and 31. It can be seen that for jets having an excess to free stream velocity ratio G in excess of 2 the two bands overlap considerably. When G is less than two the two bands diverge

slightly for jets and considerably for wakes. The experimental results for the growth parameter, see Fig. 30, span principally the Newman bounds, but intrude also into the lower part of the Vogel bounds. The results for the shear stress parameter, see Fig. 31, lie more in the Vogel bounds, and furthermore, if one considers the Gartshore wake results, although not agreeing with either Vogel's or Newman's theories, favour the trend of Vogel's theory. However, before one comes to any conclusion it has to be kept in mind that Gartshore's wakes were only approximately self-preserving; they were only 140 diameters downstream of the wake producing body hence the eddy structure and the shear stress were not fully independent of the large eddies produced by the wake body (Townsend, 1956), and that due to the approximations made by Vogel that $\frac{dL_o}{dx}$ is small and $G/(dL_o/dx)$ is large his theory is somewhat tenuous at least in the wake region.

The values for σ/L_o with a probable uncertainty of $\pm$ 10% are plotted in Fig. 32 together with the values calculated from Equation (21), σ/L_o = .38 and .42 having been used to calculate C_5 for a jet in still air. It can be seen that although Townsend's small deficit wake measurements appear to be predicted by this theory neither Gartshore's nor the present measurements support it. Alternatively σ/L_o may be calculated using the original argument of Townsend, Gartshore and Newman concerning the balance of energy for the large eddies of the motion, an argument of which Townsend (1969) himself was later highly critical. According to this theory

$$\left(\frac{\sigma}{L_o}\right)^2 \underset{U}{\propto} \frac{(-\overline{uv})}{\frac{\partial U}{\partial y}} \frac{1}{U_o L_o}$$

Hence $$\left(\frac{\sigma}{L_o}\right)^2 \underset{U}{\propto} \frac{\overline{uv}}{U_o^2} = \frac{C_3}{C_2} H$$

therefore predicting that σ/L_o is approximately constant.

Then $$\frac{\sigma}{L_o} = \left(C_6 \frac{C_3}{C_2} H\right)^{1/2} \qquad (22)$$

and the constants are evaluated as in the case of Equation (21). The results calculated from Equation(22) are also plotted in Fig. 32. It can be seen that there is fair agreement now between theory and experiment. This somewhat surprisingly reinforces the usefulness of Townsend's large eddy energy equilibrium hypothesis. The next step is then to see how the present data fit with Gartshore's check of this hypothesis. To this end Gartshore's (1966) Figure 3 is reproduced in Fig. 33 and the results of the present experiments are added together with a value that Patel (1970) obtained recently for a jet in still air. Despite the possibility that the $(L_o/\sigma)^2$ values may be in error by as much as 20% Gartshore's proof of the validity of Townsend's large eddy equilibrium hypothesis is not convincing although the apparent linear trend predicted by Gartshore is discernible.

5.7 Discussion

The apparent inaccuracy of the intermittency measurements is unfortunate because it leaves the question of the validity of the Townsendian large eddy hypothesis in suspense. The measurements show that the hypothesis may hold, but they certainly do not supply definite proof that it does (see Fig. 33).

When the predicted variation of σ/L_o versus G (Fig. 32) is examined the theory based on the large eddy hypothesis does appear to give reasonable agreement with measurements, but since this is effectively only a different plot as compared to Fig. 33 with σ/L_o not squared, one can only conclude that if the proof of the large eddy hypothesis as stipulated by Gartshore (Fig. 33) is suspect so is the prediction of σ/L_o in Fig. 32.

The outcome of all this is that although one is uncertain the validity of the large eddy equilibrium hypothesis can not be rejected, and secondly if one wishes to pursue this subject any further a considerably simplified, more accurate and reliable method has to be found for the evaluation of intermittency. The only hopefully useful result of the intermittency measurements is that in spite of all the other difficulties the mean position of the superlayer y/L_o has been established within a band of $\pm$ 8% in value and the mean value itself is not likely to be in great error.

Turning to the reliable results, the variation of the growth parameter and the shear stress parameter with G (Figs. 30, 31), one is again uncertain whether theories based on the Newman-Prandtlian assumptions are likely to be more valid. There is fortunately recourse to checks of some of the universal constants used in the Newman formulation and of H^2, the variation of which with G can also be calculated. The universal constant C_4 obtained from the intermittency measurements (and this is the reasonably useful information obtained from these measurements) is shown in Table VI which also shows the ratios of C_3/C_2, neither of which alone can be obtained directly from the measurements; but their ratio is readily obtainable. It can be seen that well within the accuracy of the measurements these can be considered constants. Examination of Fig. 34 which shows the predicted and experimental values of H^2 versus G also lends support to the Newman-Prandtl theory. The only difficulty is that neither the theoretical growth nor the shear stress parameters agrees with the experimental results within the accuracy limits. (Figs. 30, 31.)

When one examines the experimental inputs, namely the growth parameter, H^2 and y/L_o for a jet in still air, that are required to predict the flows and the effect of their variation on the theoretical predictions, one finds as Newman did that a large variation in H_s^2 causes little change in the predicted values. Furthermore, calculations have shown that variations in Y/L_o for a jet in still air result in effectively no change in the predicted values of the growth and shear stress para-

meters. Hence the sole experimental input value which significantly affects the above parameters is dL_o/dx for a jet in still air. Newman's value of .104 for this has already been questioned in Section 5.6 and limits of .100 and .108 have been adopted for it in the subsequent calculations.

Now it is not the author's intention here to match his experimental results with any theory, but it is clear from Figs. 30 and 31 that this can be done provided an appropriate value for dL_o/dx for a jet in still air is chosen. However, to do this would be an entirely unsatisfactory approach. Instead one must ask what is a jet in still air? Newman in effect appears to give vent to his dissatisfaction with what he calls a jet in still air by labelling it 'jet in virtually still surroundings'. This does not appear to be satisfactory, however; one either has a jet in still air or one has a jet in uncontrolled slowly moving surroundings with consequent different growth rates. It is postulated here that a two-dimensional jet in still air issues from a slot in a wall, the streamlines being similar to those shown on page 609 of Schlichting (1960), and reproduced in Fig. 35.a. In Fig. 35.b approximate streamlines are shown for a jet in virtually still surroundings; it is clear that the two are quite different. One may also consult some experimental results. In addition to Reichardt's (1951) value for $dL_o/dx = .115$ quoted by Newman (1967) one finds that Heskestad (1965) obtained .112, Gartshore (1967) .115, and Smith (1970) found recently a value of .113. In all of the above cases measurements were carried out to a

non-dimensional downstream distance of x/b from 100 to 240 and except for Gartshore's measurements there was a vertical wall from which the jet issued.

One could clearly re-evaluate the growth rates of a jet in still air based on the above data, but due to the importance of this matter no such step will be taken. Neither is it feasible to make some quick measurements to decide the issue; it is necessary to approach this problem with a systematic full scale investigation of the jet in still air.

It would also be of great value to obtain information concerning the degree to which the growth and the shear stress parameters are affected by the level of the free-stream turbulence. It was assumed in this work that the levels of free stream turbulence encountered did not have a noticeable effect on the above parameters. However, if this assumption should be incorrect an additional complication would be introduced even if reliable experimental parameters were to be established for the jet in still air.

Further, to gain full confidence in the value of the theories, extensive measurements will have to be made of self-preserving wakes with a G of the order of -.5 to -.75.

From a pragmatic point of view, for the moment, either the Vogel polar theory based on Townsend's large eddy equilibrium hypothesis or the Newman-Prandtl theory will give reasonable results.

From a theoretical point of view the Newman theory is superior, being based on three fundamental equations and requiring experimental input from only one measured flow, the jet in still air. One can compare this to Vogel's theory based on two momentum equations and the somewhat tenuous large eddy equilibrium hypothesis requiring in addition two flows from which experimental information needs to be fed into the theory.

It may also be noted that, somewhat contradicting the statement made in the introduction, owing to the complexities of turbulent flows and the uncertainties involved, integral methods for solving turbulent flow problems are likely to be extremely valuable for a long time to come due to their satisfactory performance and relative simplicity.

6. CONCLUSIONS

Experimental apparatus was designed and constructed which permitted the setting up of self-preserving, two-dimensional jets in streaming flow with excess to free stream velocity ratios between zero and one. The working fluid was air, and all the flows were effectively incompressible. Extensive measurements were made of mean flow parameters, the stress tensor and intermittency. Two-dimensionality was found to be excellent, self-preserving conditions were obtained and reliable error limits were placed on all measured quantities. This is the first time that such measurements have been made.

Comparison with various proposed theories resulted in rejecting all except two. Between these two no decision could be made due to lack of reliable information on the jet in still air from which experimental information is required in the theories. Nevertheless, sufficiently accurate information is available to satisfy the immediate needs of the researcher.

Uncertainties in intermittency measurements suggest that a study be undertaken to evolve a simple and reliable method for measuring intermittency.

Uncertainties concerning the jet in still air make it imperative that a careful, thorough experimental study be undertaken to obtain reliable results for this most important fundamental flow.

REFERENCES

Bradbury, L.J.S. (1965) — The Structure of a Self-Preserving Turbulent Plane Jet. J. Fluid Mech. 23 (1) pp. 31-64

Bradshaw, P. and Gee, M.T. (1960) — Turbulent Wall Jets with and without an External Stream. ARC, R and M, No. 3252

Champagne, F.H. (1965) — Turbulence Measurements with Inclined Hot Wires. Boeing Scientific Researh Laboratorie: Document D1-82-0491

Collis, D.C. and Williams, M.J. (1957) — Two-Dimensional Forced Convection from Cylinders at Low Reynolds Numbers. Australian - Aero. Res. Labs., Rep. A-105

Fekete, G.I. (1963) — Coanda Flow of a Two-Dimensional Wall Jet on the Outside of a Circular Cylinder. McGill University, Mech. Eng. Dept. Report 63-11

Forstall, N. and Shapiro, A.H. (1950) — Momentum and Mass Transfer in Co-axial Gas Jets. J. App. Mech. 17, pp. 389-408

Gartshore, I.S. (1965) — The Streamwise Development of Two-Dimensional Wall Jets and Other Two-Dimensional Turbulent Shear Flows. McGill University, Dept. of Mech. Eng., Ph.D. Thesis

Gartshore, I.S. (1966) — An Experimental Examination of the Large-Eddy Equilibrium Hypothesis. J.F.M., 24, (1), pp. 89-98

Gartshore, I.S. (1967) — Two-Dimensional Turbulent Wakes. J.F.M., 30, pp. 547-560

Gartshore, I.S. and Newman, B.G. (1969) — The Turbulent Wall Jet in an Arbitrary Pressure Gradient. Aero. Quarterly, Vol. 20, pp. 25

Grant, H.L. (1958) — The Large Eddies of Turbulent Motion. J.F.M., 4 (2)

Guitton, D. (1968) — Correction of Hot Wire Data for High Intensity Turbulence, Longitudinal Cooling and Probe Interference. McGill University, Dept. Mech. Eng. Report 68-6

Guitton, D. and Patel, R.P. (1969)
An Experimental Study of the Thermo-wake Interference Between Closely Spaced Wires of a X-Type Hot Wire Probe
McGill University, Dept. Mech. Eng. Report 69-7

Heskestad, G. (1965)
Hot Wire Measurements in a Plane Turbulent Jet
Trans. ASME, (Series E, J. Appl. Mech., 32), 87, pp. 721-734

Jerome, F.E., Guitton, D. and Patel, R.P. (1969)
Experimental Study of the Thermal Wake Interference between Closely Spaced Wires of a X-type Hot Wire Probe
(To be published in Aero. Quarterly)

Newman, B.G. (1967)
Turbulent Jets and Wakes in a Pressure Gradient
Proc. GM Conference on Fluid Mechanics of Internal Flow, Elsevier Publishing Co., Amsterdam

Newman, B.G. (1968)
The Growth of Self-Preserving Turbulent Jets and Wakes
McGill University, Dept. of Mech. Eng. Report 68-10

Patel, R.P. and Newman, B.G. (1961)
Self-Preserving, Two-dimensional Turbulent Jets and Wall Jets in a Moving Stream
McGill University, Dept. of Mech. Eng. Report Ae.5

Patel, R.P. (1968)
Reynolds Stresses in Fully Developed Turbulent Flow down a Circular Pipe
McGill University, Dept. of Mech. Eng. Report 68-7

Patel, R.P. (1970)
Results to be presented in Ph.D. dissertation

Reichardt, H. (1951)
Gesetzmassigkeiten der Freien Turbulenz
VDI-Forshungsheft 414

Schlichting, H. (1960)
Boundary Layer Theory
McGraw-Hill Book Company Inc.

Smith, P. Arnot (1970)
Results to be presented in Master of Engineering dissertation.
Department of Mechanical Engineering, McGill University.

Spalding, D.B. and Patankar, S.V. (1967)
Heat and Mass Transfer in Boundary Layers
Morgan-Grampian, London.

Squire, H.B. and Trouncer, J. (1944)
Round Jets in a General Stream
ARC, R and M, No. 1974

Townsend, A.A. (1956)
The Structure of Turbulent Shear Flow
Cambridge University Press

Townsend, A.A. (1966)
The Mechanism of Entrainment in Free Turbulent Flows
J.F.M., 26, (4), pp. 689-715

Townsend, A.A. (1969)
Entrainment and the Structure of Turbulent Flow
Boeing Scientific Research Labs. Symposium on Turbulence, June 1969

Vogel, W.M. (1969)
An Analytic Solution for Flow Development of Symmetric Self-Preserving Jets and Wakes, Using an Integral Method
CASI Trans., Vol. 2, No. 2, pp. 105-10

Wygnanski, I. and Gartshore, I.S. (1963)
General Description and Calibration of the McGill 17 in. x 30 in. Blower Cascade Wind Tunnel
McGill University, Dept. of Mech. Eng. TN 63-7

TABLE I

INTEGRATION TIME REQUIREMENTS

XTE = 51.8 in $y \approx L_o$ Wire N-1 G = 0.57

	Integration Time, Seconds	Confidence Limit		
		68% σ	95% 2σ	99.7% 3σ
		$\epsilon \pm$ %	$\epsilon \pm$ %	$\epsilon \pm$ %
Mean Velocity	1	0.64	1.3	2.0
	5	0.22	0.44	0.7
	10	0.12	0.25	0.4
$\sqrt{\overline{u^2}}$	1	2.6	5.2	8.0
	5	1.0	2.0	3.0
	10	0.75	1.5	2.3
	50	0.34	0.7	1.0

TABLE II

EFFECT OF AMBIENT TEMPERATURE CHANGE ON HOT WIRE OUTPUT

	$\frac{\Delta E_L}{E_L}$	$\frac{\Delta(dE_L/dU)}{(dE_L/dU)}$
Wire overheat ratio, $\frac{R}{R_a}$ = CONST	0.002 ΔTa	0.001 ΔTa
Wire Temperature R = CONST	0.01 ΔTa	0.005 ΔTa

TABLE III

RESULTS OF ERROR ANALYSIS

Quantity	Error Analysis	Experiment Ref. No. 279-297
$\frac{\sqrt{\overline{u^2}}}{U}$	$\epsilon = \pm 1.5\%$	$\epsilon = \pm 1.5\%$
$\frac{\sqrt{\overline{u^2}}}{U_o}$	$\epsilon = \pm 2.5\%$	$\epsilon = \pm 2\%$
$\frac{\sqrt{\overline{v^2}}}{U_o}$, $\frac{\sqrt{\overline{w^2}}}{U_o}$	$\epsilon = \pm 6\%$	$\epsilon = \pm 6\%$
$\frac{\overline{uv}}{U_o^2}$, $\frac{\overline{uw}}{U_o^2}$	$\epsilon = \pm 7\%$	$\epsilon = \pm 6\%$

TABLE IV

RESULTS OF ERROR ANALYSIS

Quantity	Error Analysis	Experiment Ref. Nos. 279-297 and 193-207 combined
$\frac{\sqrt{\overline{u^2}}}{U}$	$\epsilon = \pm$ 1.5%	$\epsilon = \pm$ 4.5%
$\frac{\sqrt{\overline{u^2}}}{U_o}$	$\epsilon = \pm$ 2.5%	$\epsilon = \pm$ 2%
$\frac{\sqrt{\overline{v^2}}}{U_o}$, $\frac{\sqrt{\overline{w^2}}}{U_o}$	$\epsilon = \pm$ 6%	$\epsilon = \pm$ 6%
$\frac{\overline{uv}}{U_o^2}$, $\frac{\overline{uw}}{U_o^2}$	$\epsilon = \pm$ 7%	$\epsilon = \pm$ 6%

TABLE V

SUMMARY OF CONSTANTS USED BY GARTSHORE, VOGEL AND NEWMAN

	Gartshore	Vogel	Newman
α	0.083	0.0533	-
β	10.15	16.2	-
c_1	-	-	$\frac{1}{3}$ and $\frac{1}{6}$
c_4	-	-	1.7
H_S^2	-	-	.10 and .16
F_S	-	-	0.104

TABLE VI

TABULATED UNIVERSAL CONSTANTS

	G	$C_4 = Y/L_o$	C_3/C_2
Present Experiments	.265	—	.065
	.44	—	.064
	.68	—	.064
	.59	—	.060
	.57	1.84 XTE 51.8	—
		1.84 XTE 59.8	—
	.74	1.74	.064
	.79	1.62	.063
	.95	1.73 S.U. 1.70 M.O. 1.63 D.N.	.064
Bradbury's Jet	Not Constant	1.7	—
Patel	∞	1.68	—

FLOW, FLOW PARAMETERS AND AXIS SYSTEM

Fig. 1.

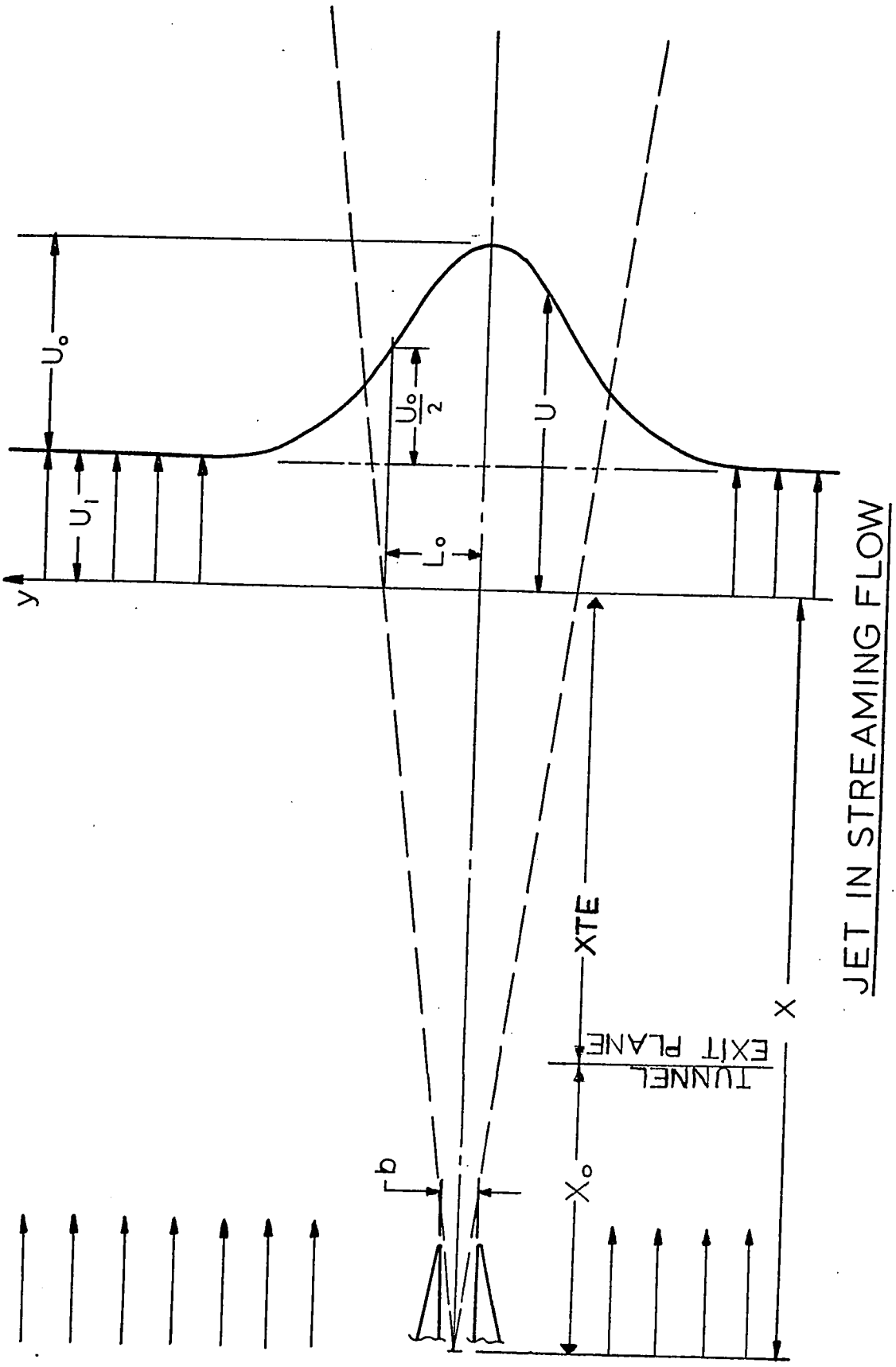

FLOW, FLOW PARAMETERS AND AXIS SYSTEM

Fig. 1.

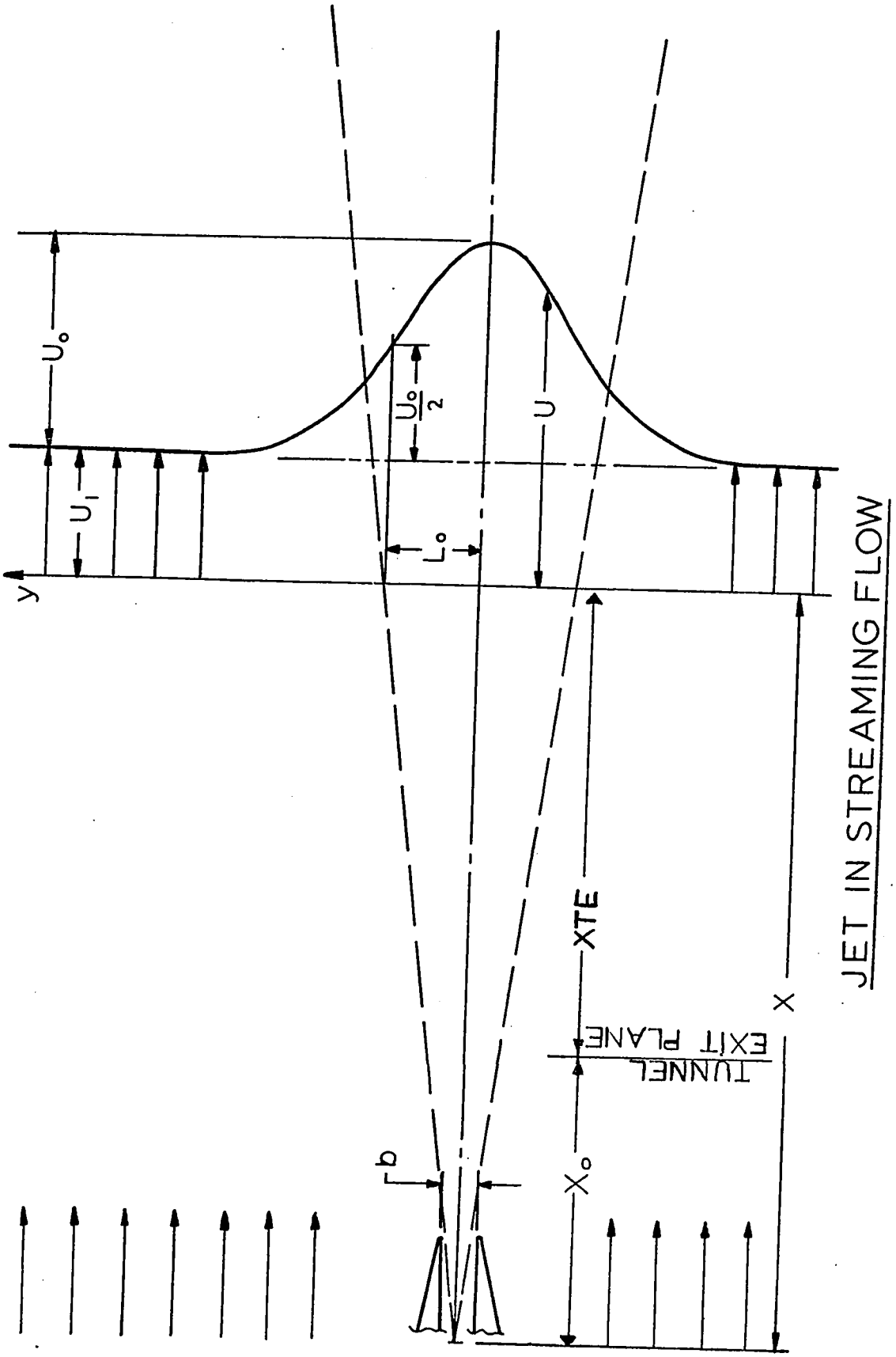

Fig. 3.a Photograph of the general apparatus layout

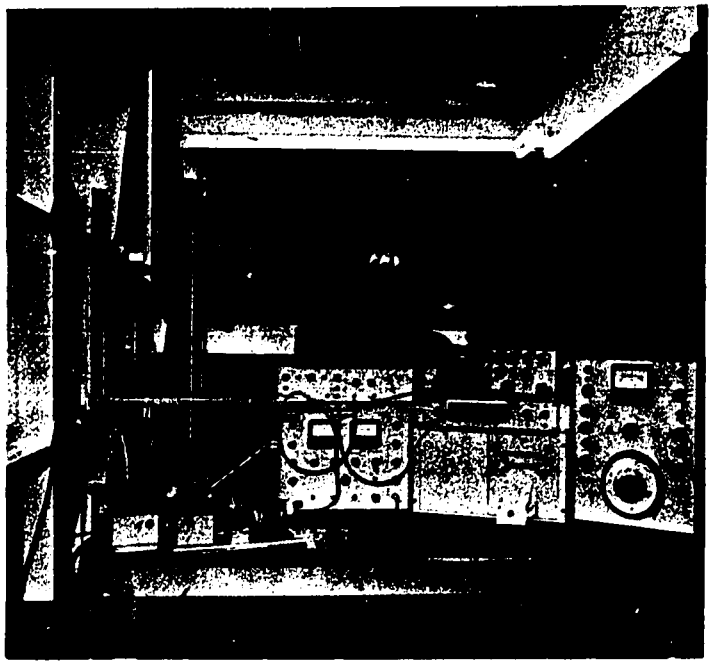

Fig. 3.b Photograph of instrument layout

Fig. 3.a Photograph of the general apparatus layout

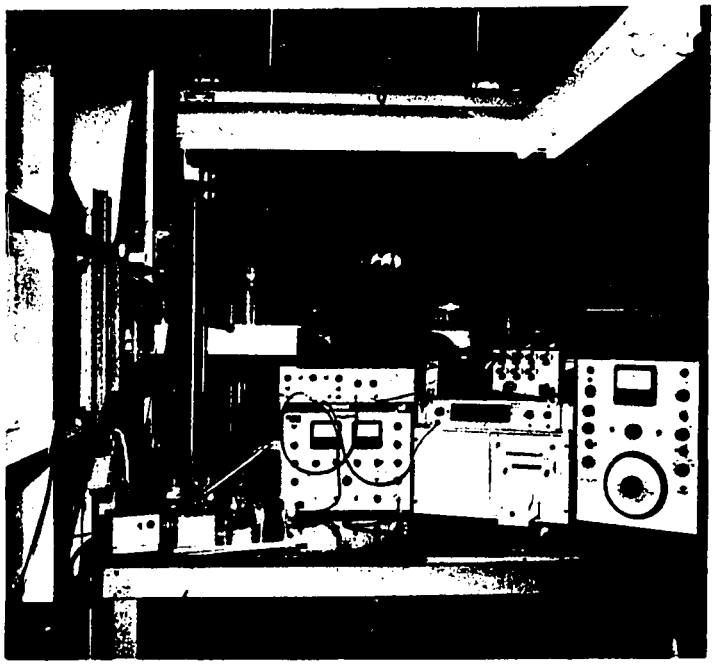

Fig. 3.b Photograph of instrument layout

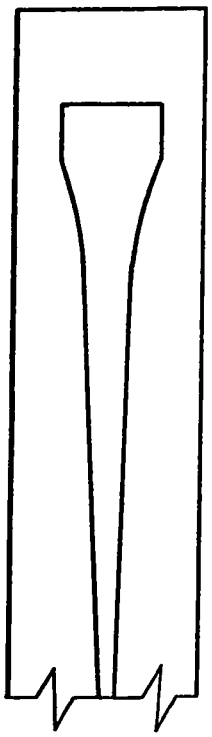

ORIFICE PLATE

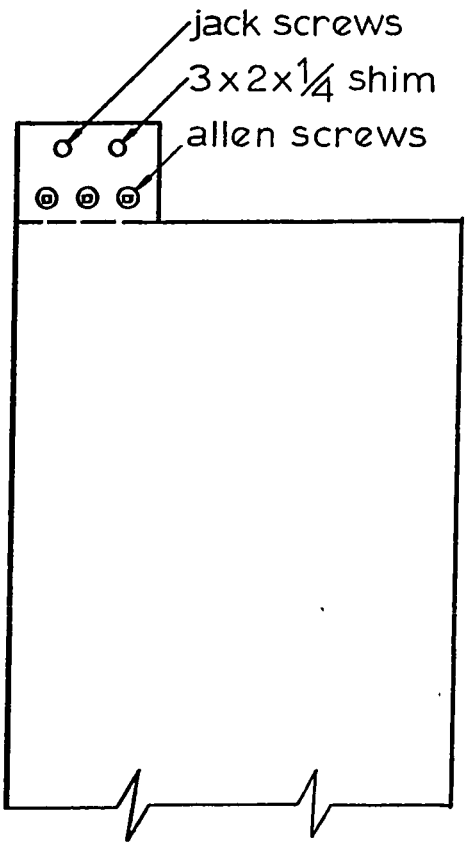

SPACING OF SLOT PLATES

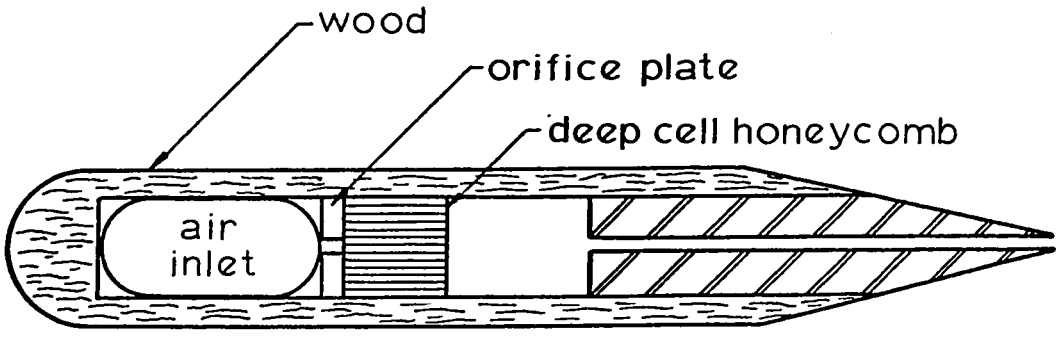

JET BOX

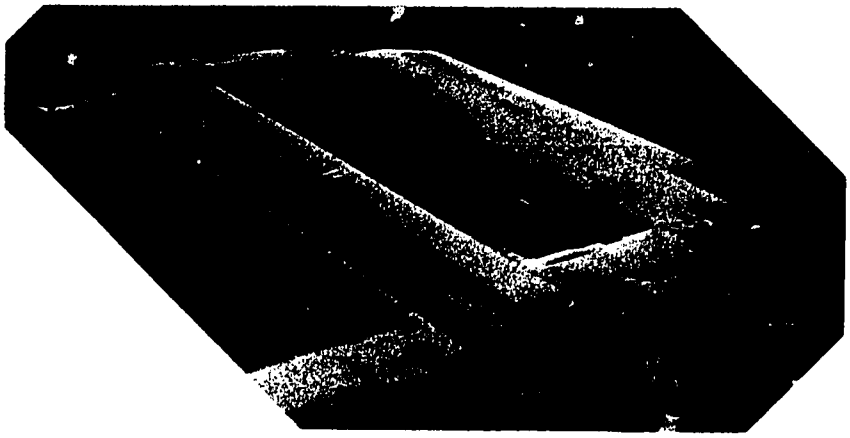

Fig. 5 (a). Photograph of jet box with top cover plate removed.

Fig. 5 (b). Photograph of jet box with top cover plate removed.

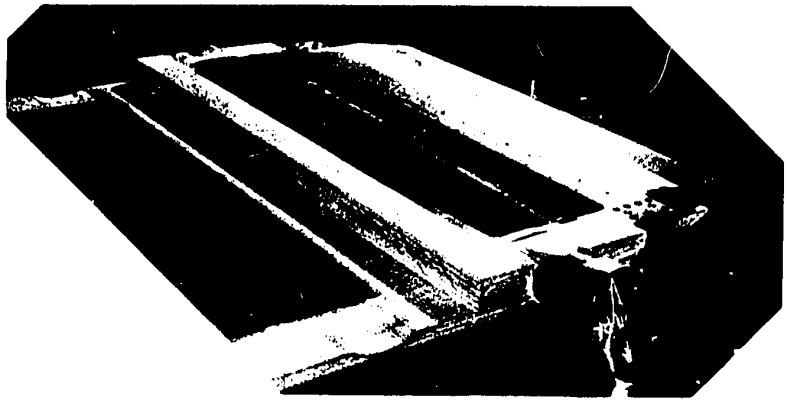

Fig. 5 (a). Photograph of jet box with top cover plate removed.

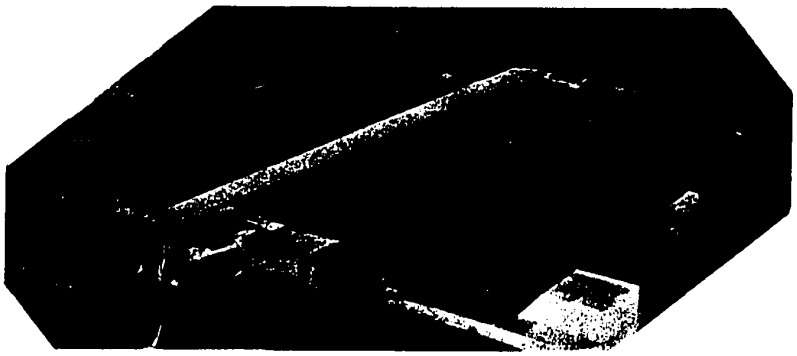

Fig. 5 (b). Photograph of jet box with top cover plate removed.

Fig. 6

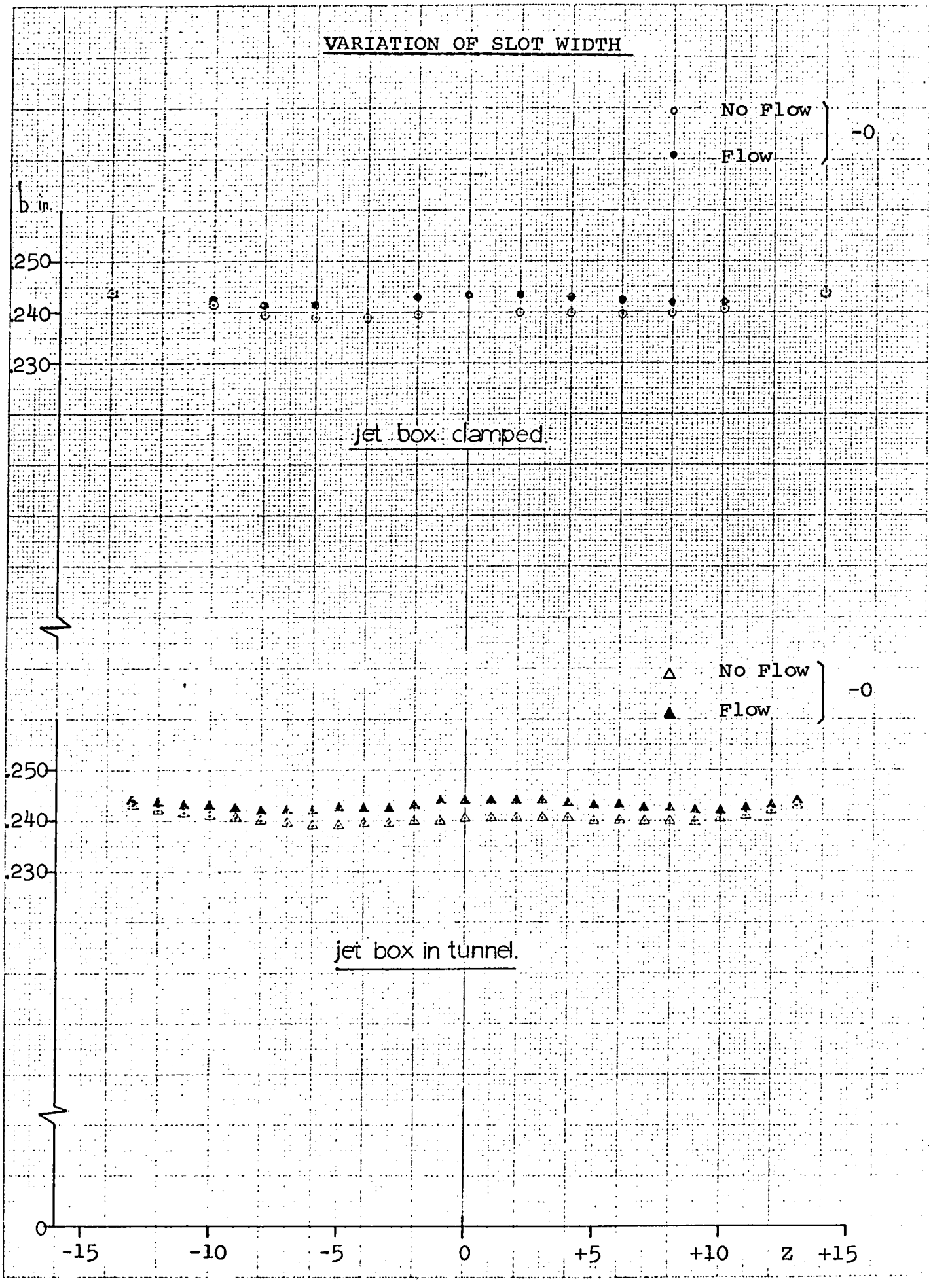
VARIATION OF SLOT WIDTH
No Flow
Flow
-0
b in.
.250
.240
.230
jet box clamped.
No Flow
Flow
-0
.250
.240
.230
jet box in tunnel.
0
-15
-10
-5
0
+5
+10
z
+15

Fig. 7.

TOTAL PRESSURE PROFILES IN SLOT EXIT PLANE

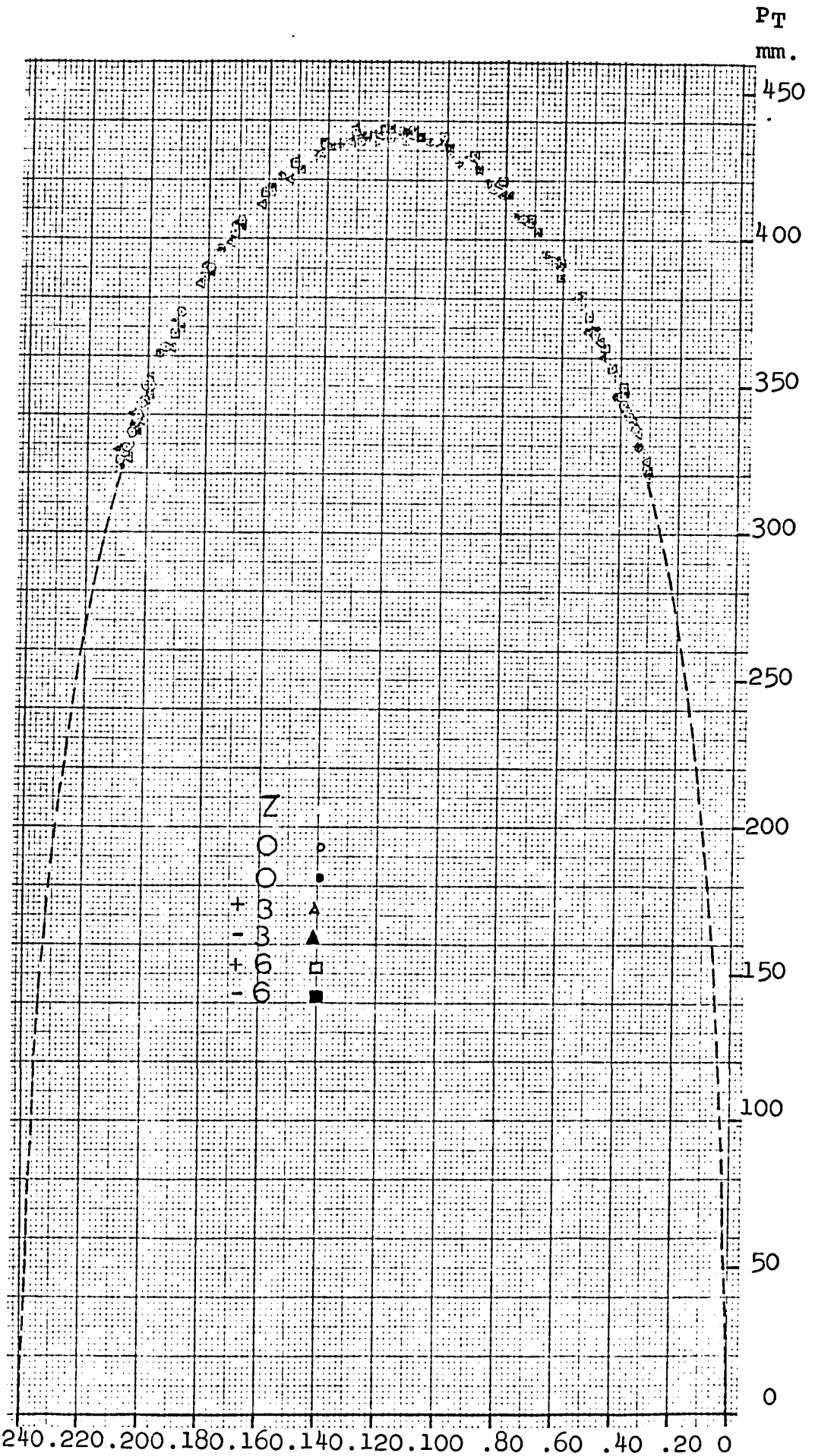

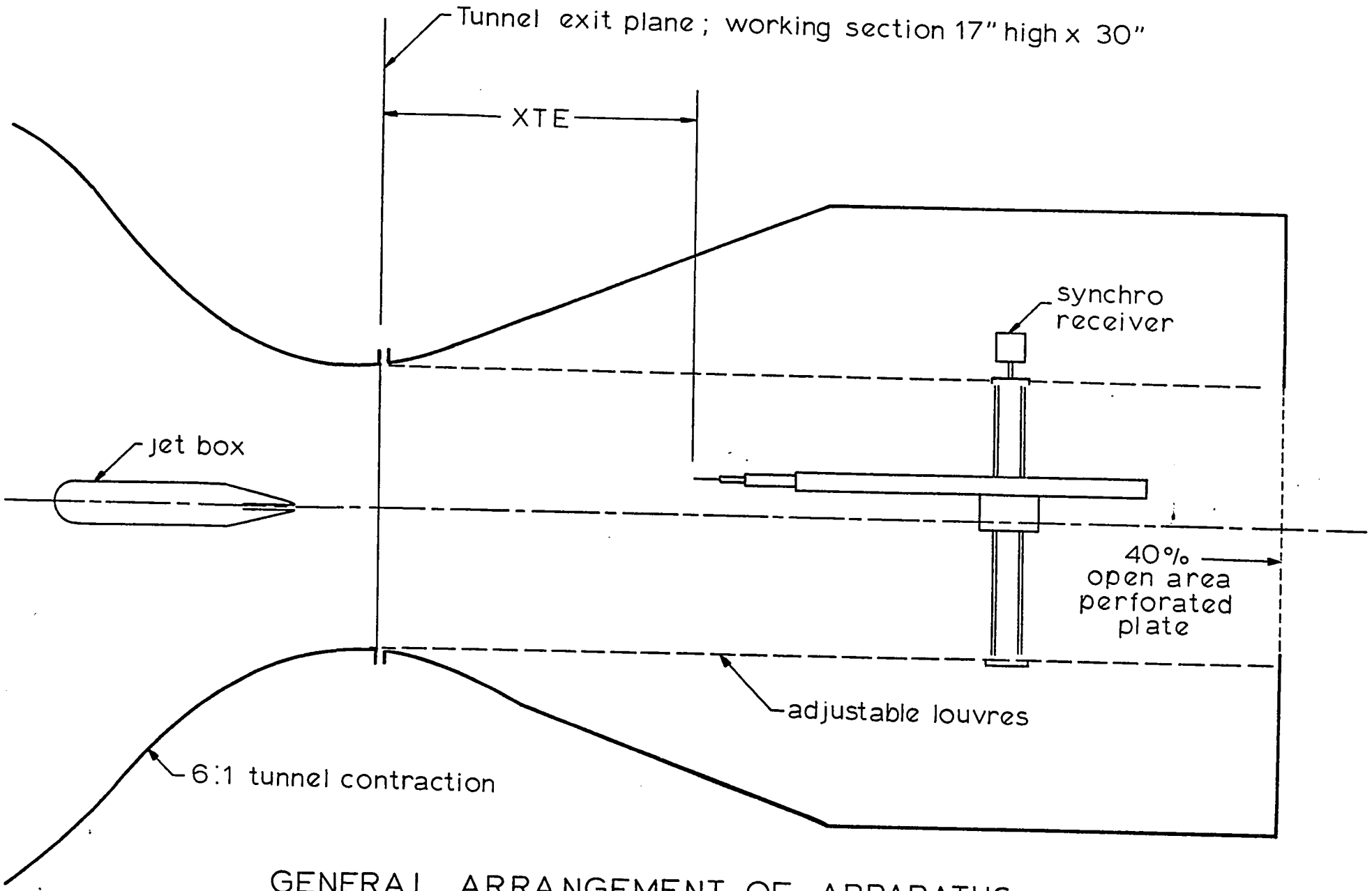

GENERAL ARRANGEMENT OF APPARATUS
Sketch of Working Section

Fig. 8.

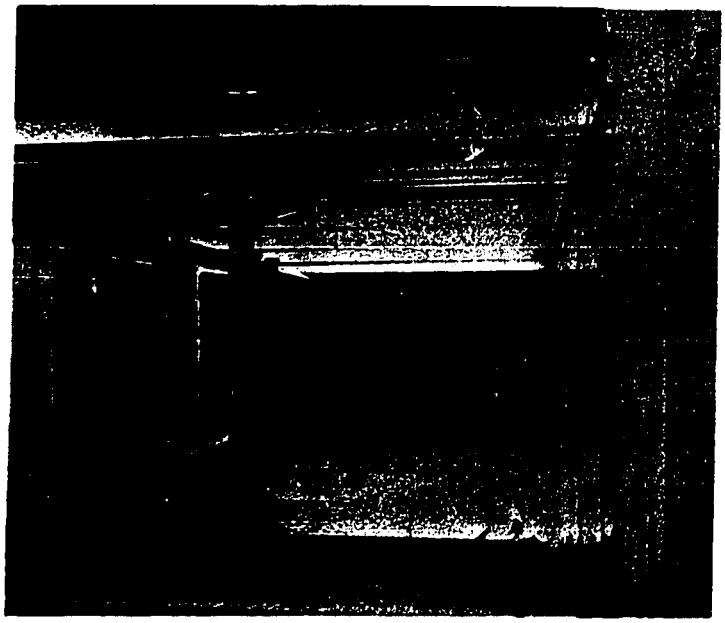

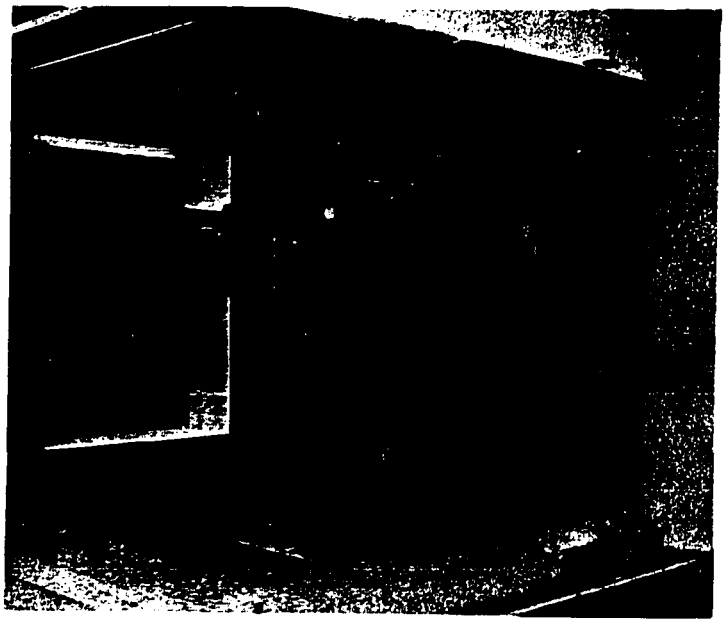

Fig. 9 **Photographs of traversing gear**

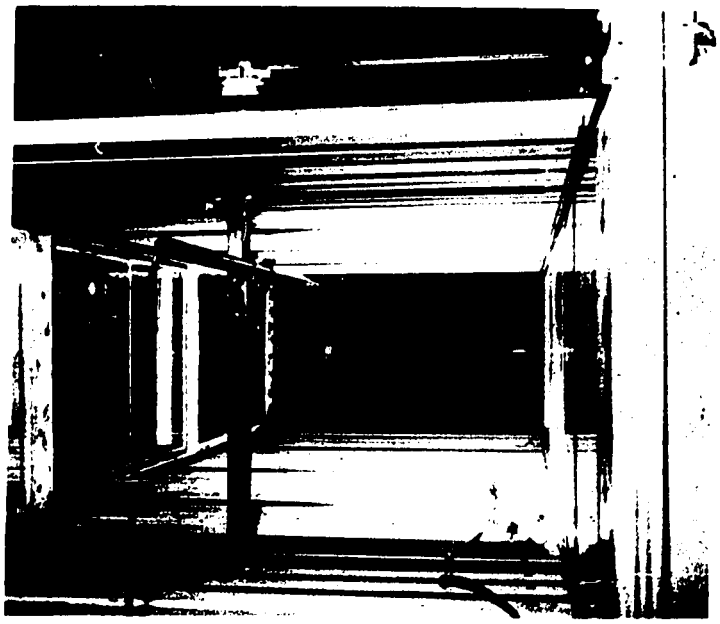

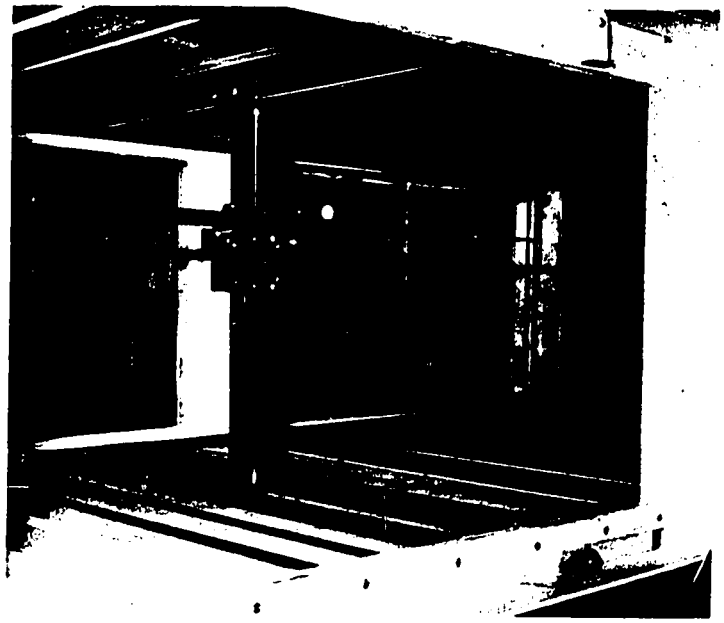

Fig. 9 Photographs of traversing gear

INSTRUMENTATION

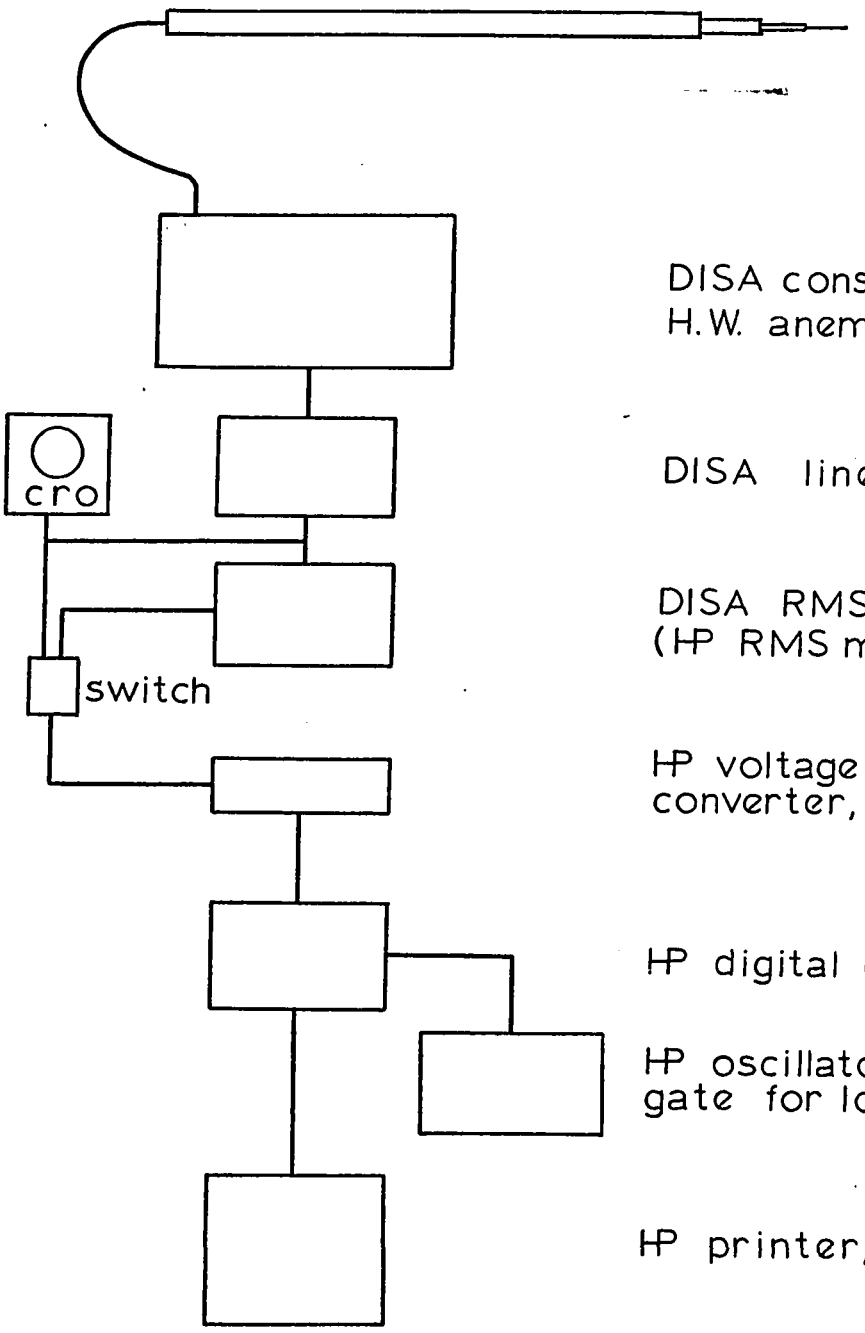

Synchro drive with counter for probe positioning in Y direction

Manometer	Jet box reference pressure
Manometer	Wind tunnel reference pressure
Manometer	Working section velocity pressure
Thermometer	Working section temperature
Thermometer	Room temperature
Barometer	Atmospheric pressure

SKETCHES OF HOT WIRES

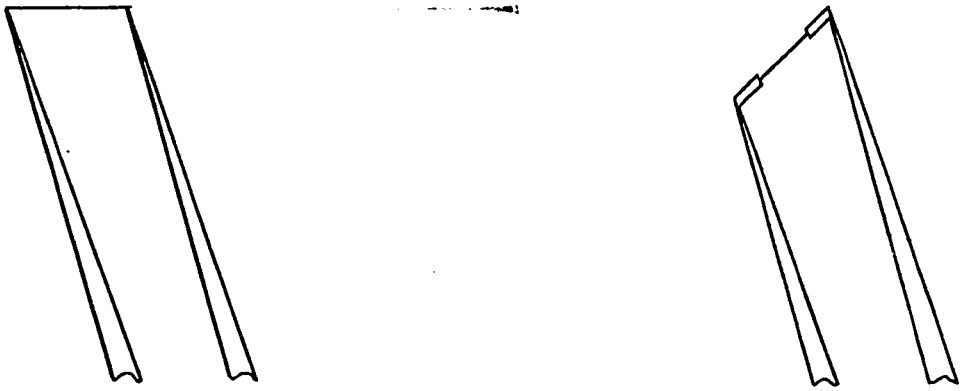

N-21 S-8

Fig. 11 (a). The .0002 dia. platinum plated tungsten wires

N-3 S-3

Fig. 11 (b). The .0004 dia. platinum-20% iridium wires.

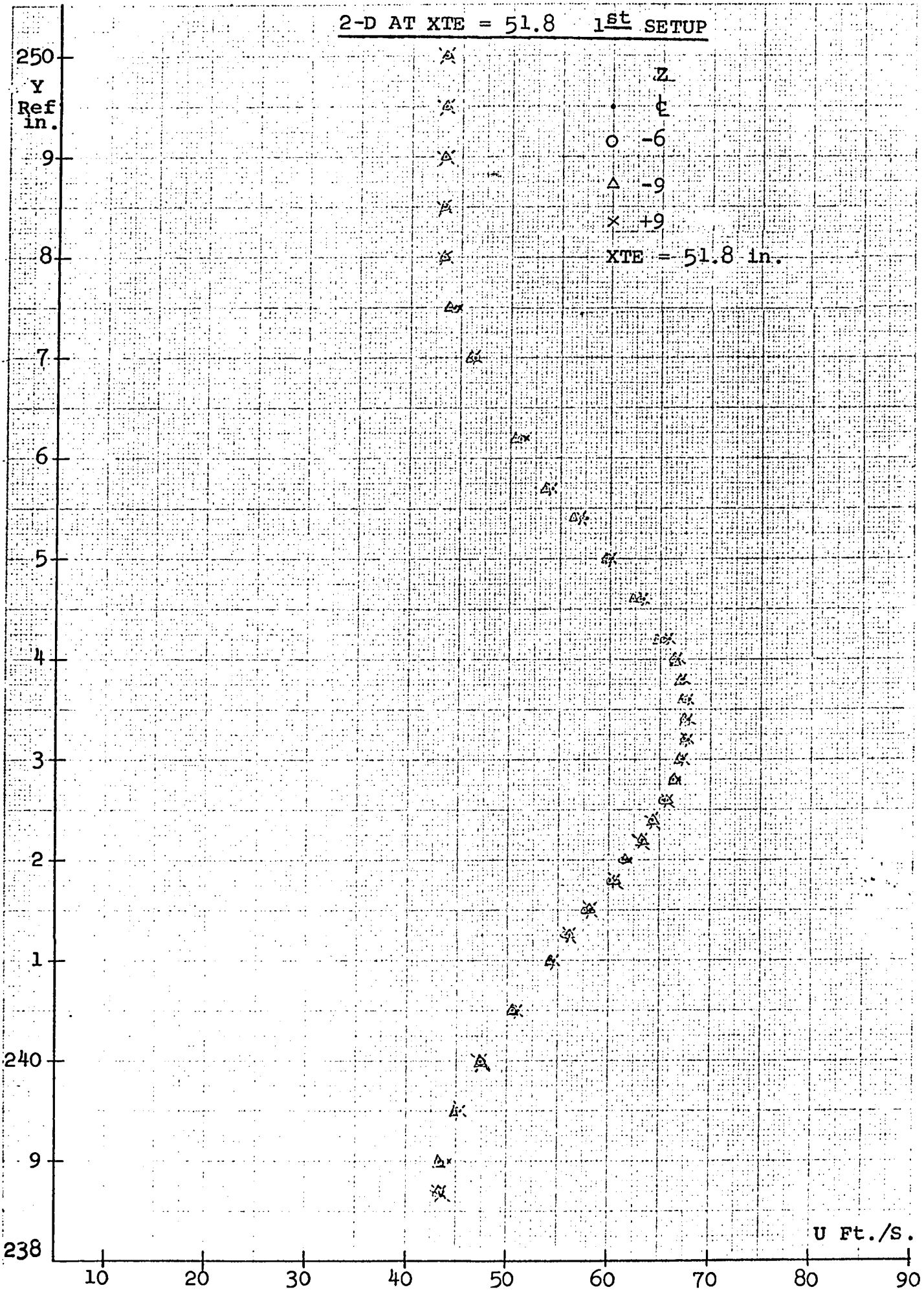
2-D AT XTE = 51.8 1st SETUP
Z
℄
o -6
△ -9
× +9
XTE = 51.8 in.
250
Y Ref in.
9
8
7
6
5
4
3
2
1
240
9
238
U Ft./S.
10
20
30
40
50
60
70
80
90

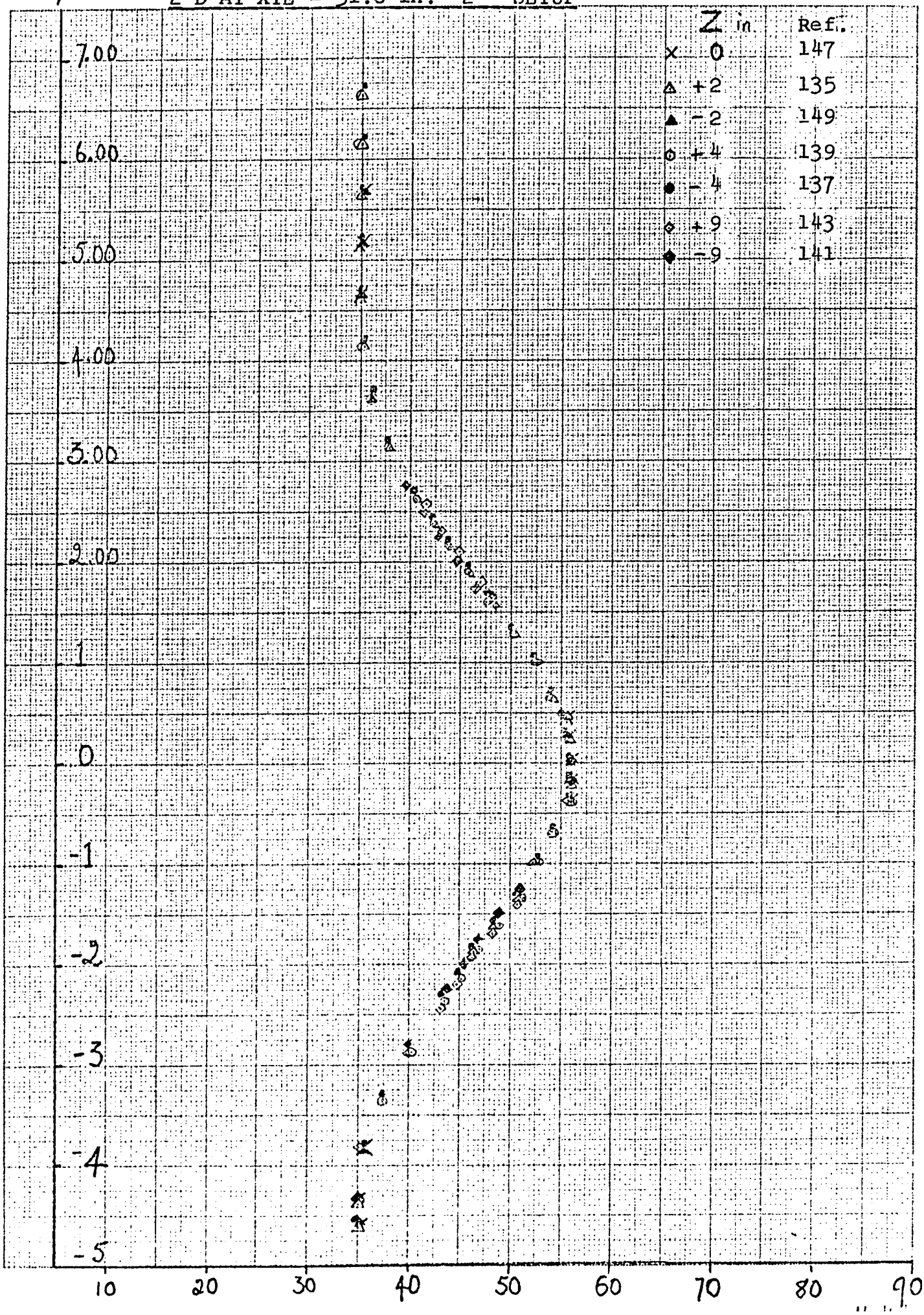
2-D AT XTE = 51.8 in. 2nd SETUP
y
Z in.
Ref.
× 0 147
△ +2 135
▲ −2 149
○ +4 139
● −4 137
◇ +9 143
◆ −9 141
7.00
6.00
5.00
4.00
3.00
2.00
1
0
-1
-2
-3
-4
-5
10
20
30
40
50
60
70
80
90

Fig. 14

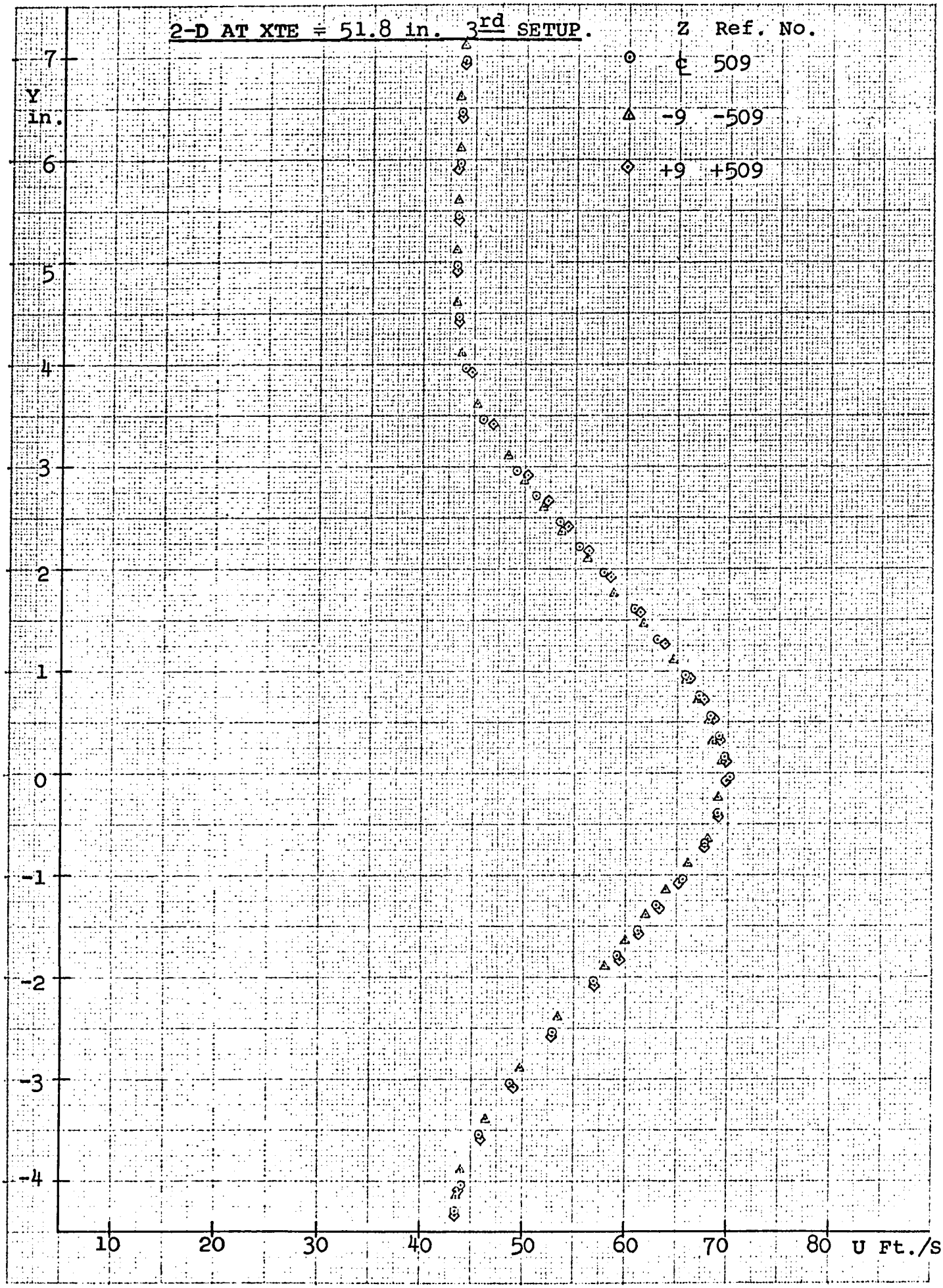
2-D AT XTE = 51.8 in. 3rd SETUP.
Z Ref. No.
℄ 509
-9 -509
+9 +509
Y in.
7
6
5
4
3
2
1
0
-1
-2
-3
-4
10
20
30
40
50
60
70
80
U Ft./S

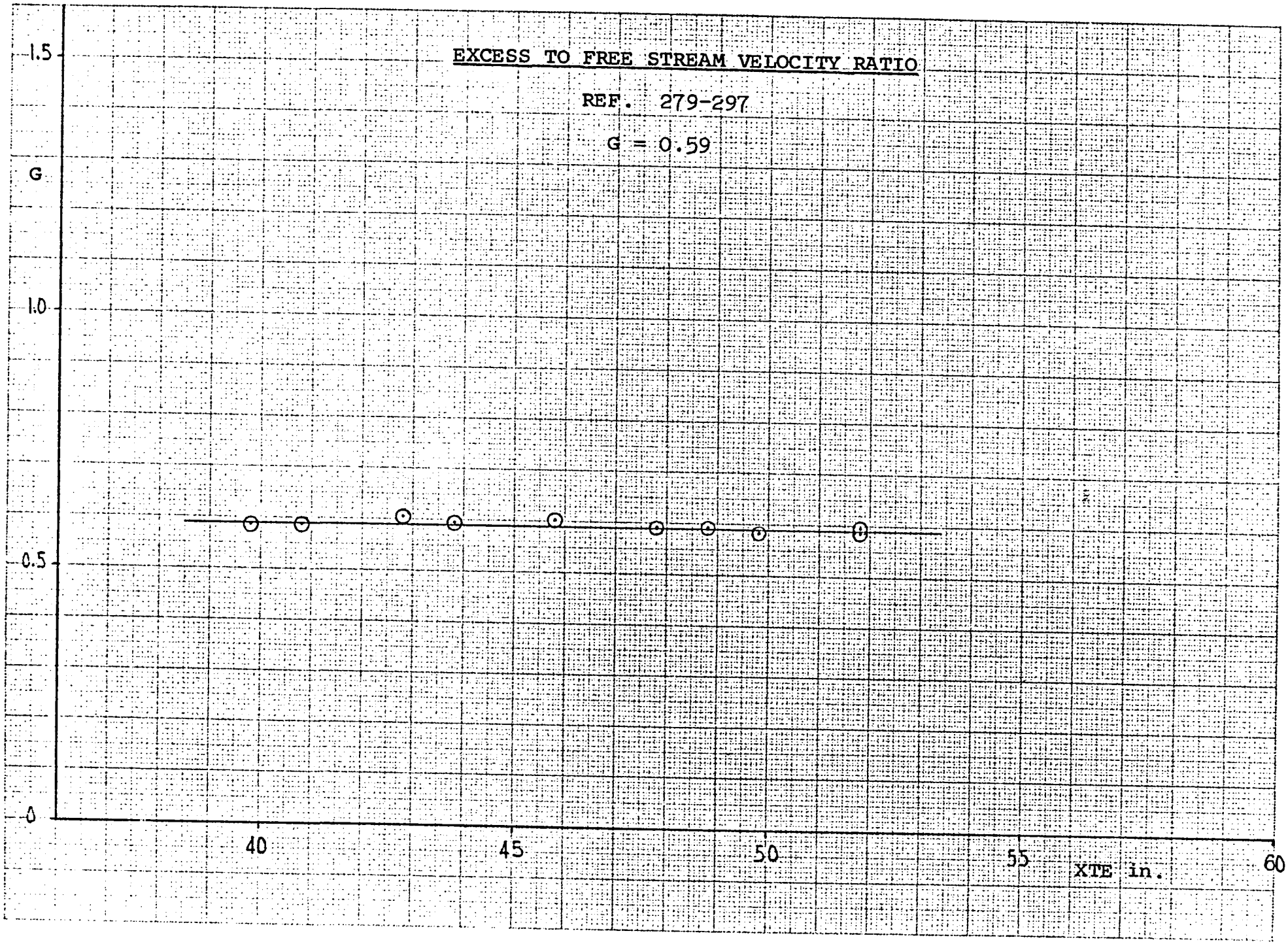
EXCESS TO FREE STREAM VELOCITY RATIO
REF. 279-297
G = 0.59
G
1.5
1.0
0.5
0
40
45
50
55
60
XTE in.

Fig. 15.a

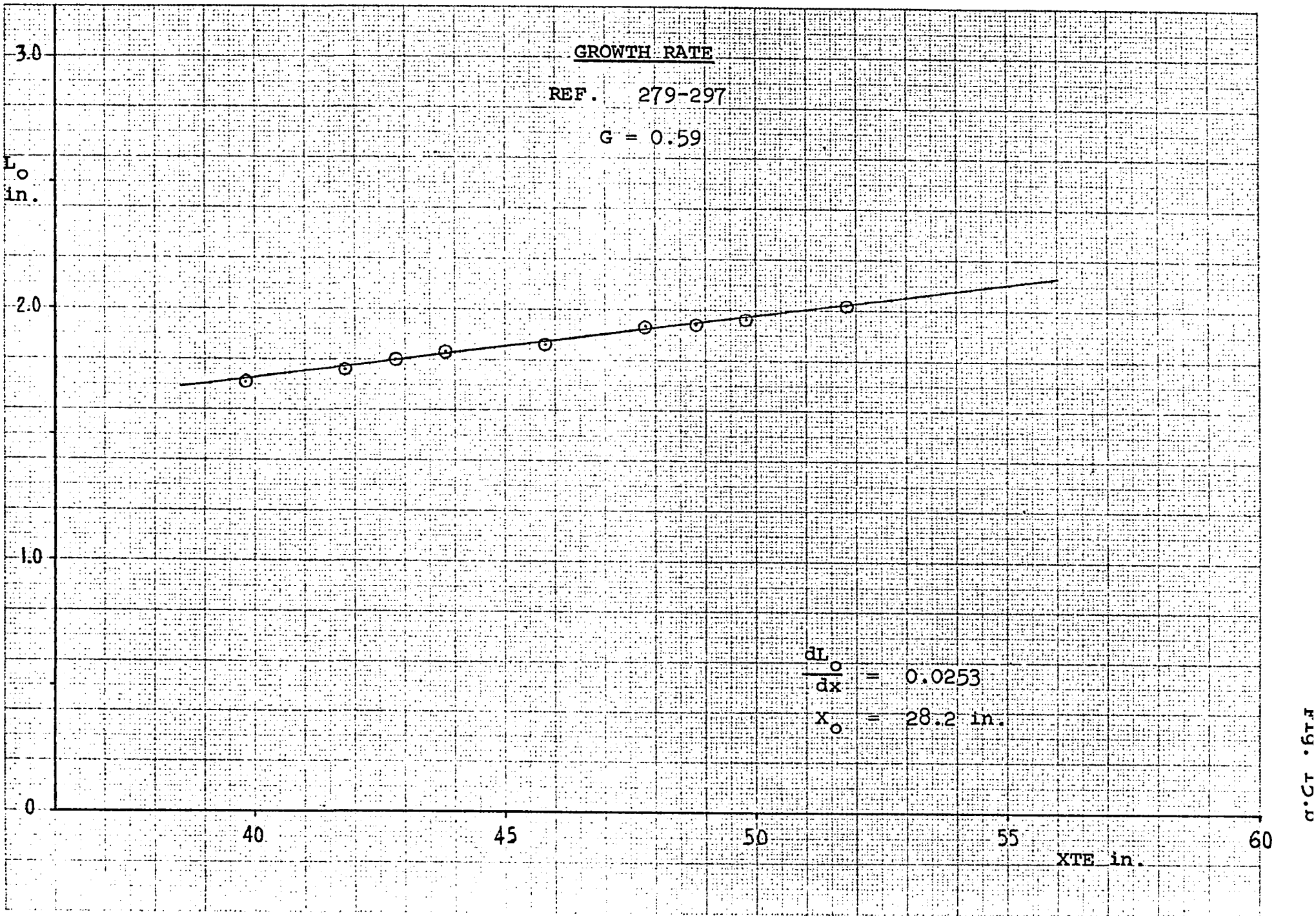
GROWTH RATE
REF. 279-297
G = 0.59
L_o in.
3.0
2.0
1.0
0
40
45
50
55
60
XTE in.
$\frac{dL_o}{dx}$ = 0.0253
x_o = 28.2 in.

Fig. 45

VELOCITY DECAY

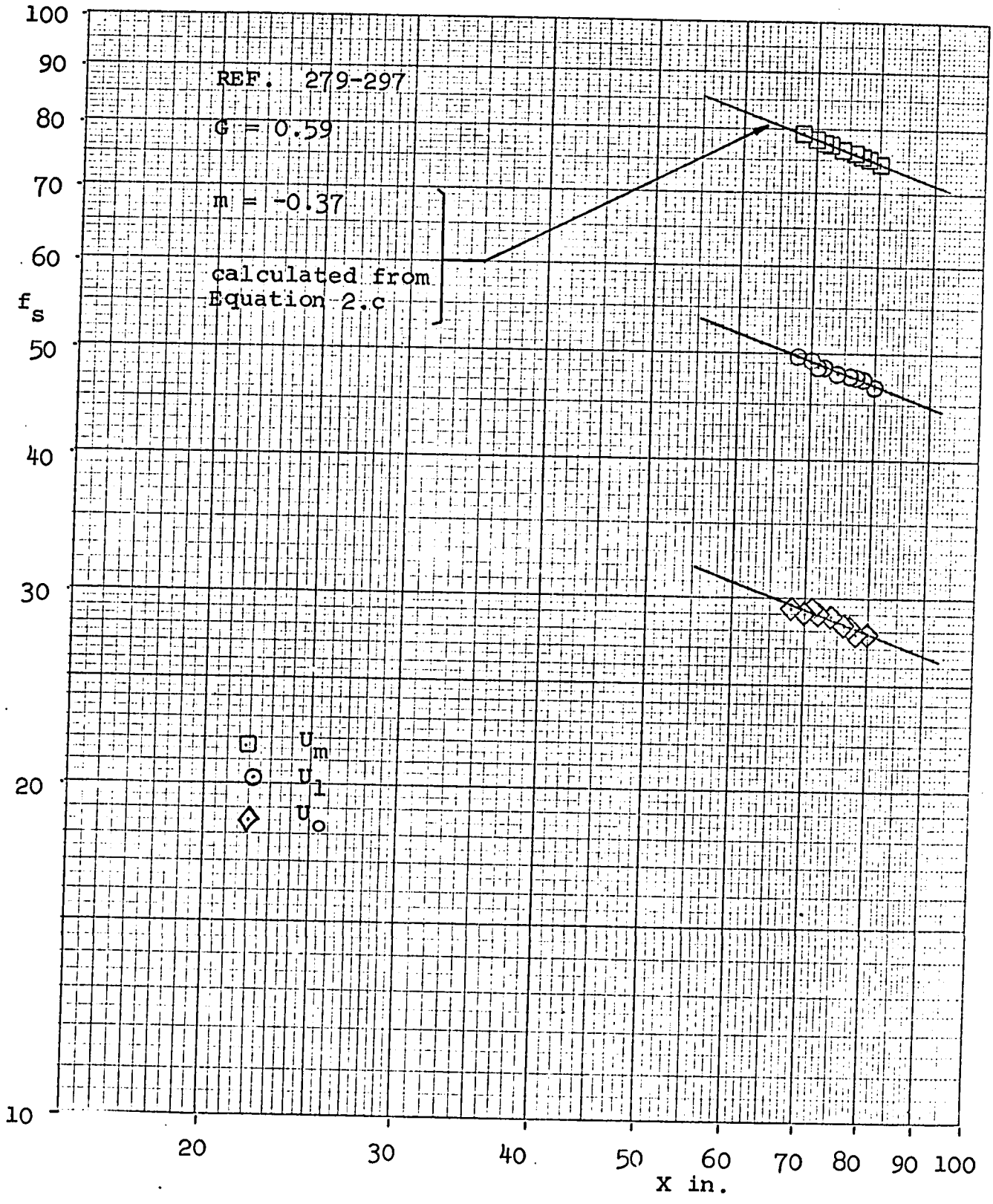

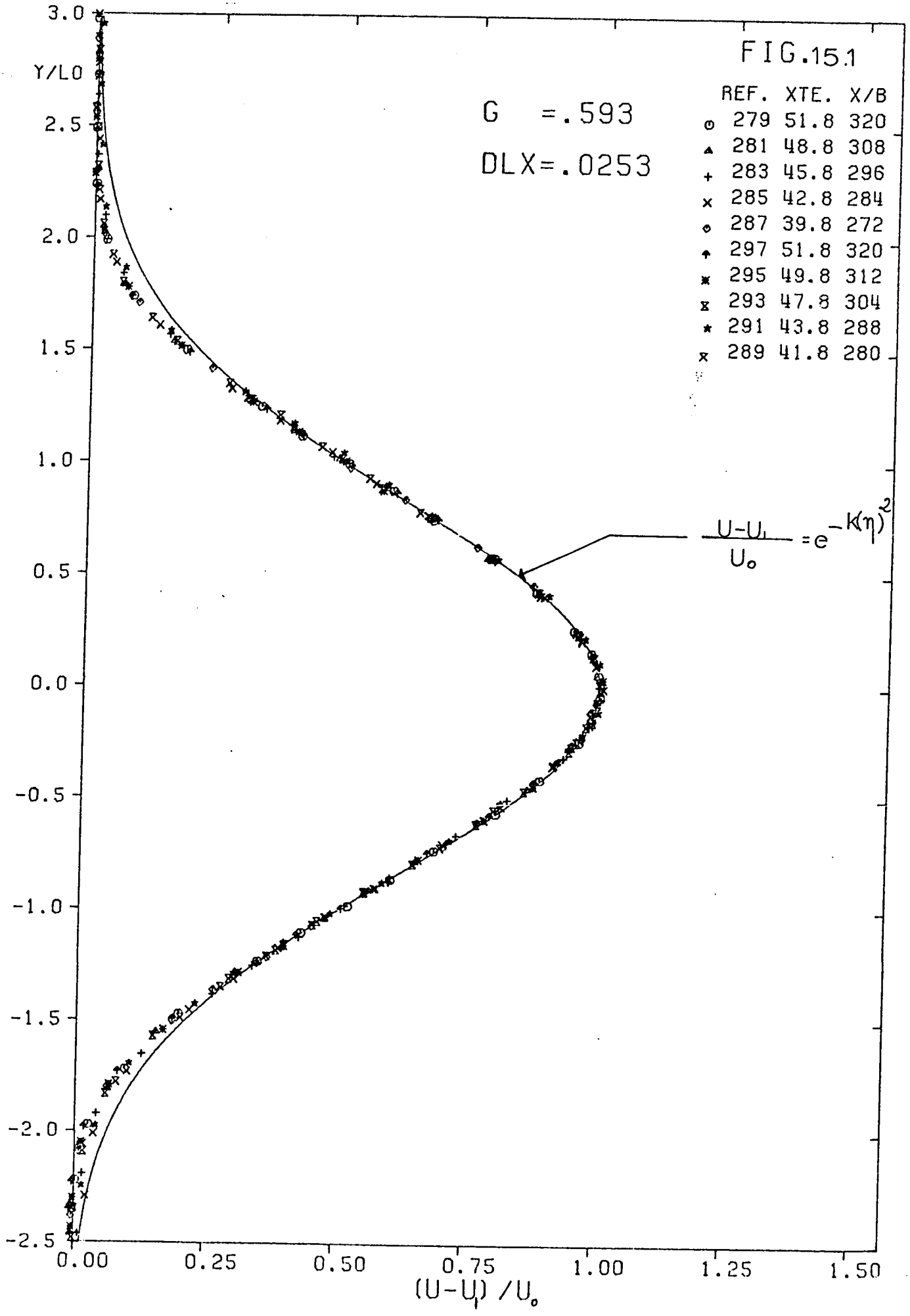
FIG.15.1
G =.593
DLX=.0253
REF. XTE. X/B
279 51.8 320
281 48.8 308
283 45.8 296
285 42.8 284
287 39.8 272
297 51.8 320
295 49.8 312
293 47.8 304
291 43.8 288
289 41.8 280
$\frac{U-U_1}{U_o} = e^{-K(\eta)^2}$
Y/LO
3.0
2.5
2.0
1.5
1.0
0.5
0.0
-0.5
-1.0
-1.5
-2.0
-2.5
0.00
0.25
0.50
0.75
1.00
1.25
1.50
$(U-U_1)/U_o$

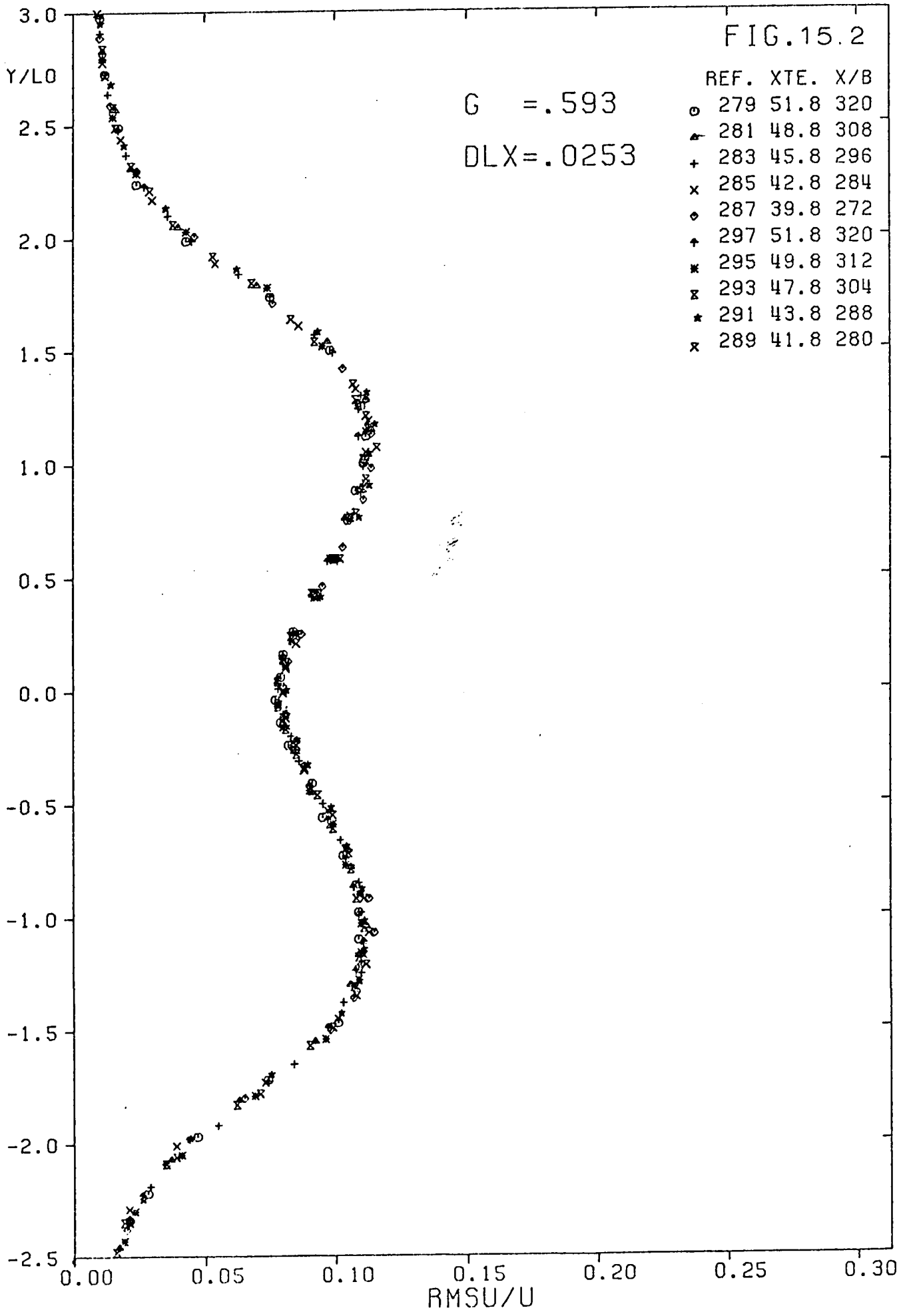
FIG.15.2
G =.593
DLX=.0253
REF. XTE. X/B
279 51.8 320
281 48.8 308
283 45.8 296
285 42.8 284
287 39.8 272
297 51.8 320
295 49.8 312
293 47.8 304
291 43.8 288
289 41.8 280
Y/LO
3.0
2.5
2.0
1.5
1.0
0.5
0.0
-0.5
-1.0
-1.5
-2.0
-2.5
0.00
0.05
0.10
0.15
0.20
0.25
0.30
RMSU/U

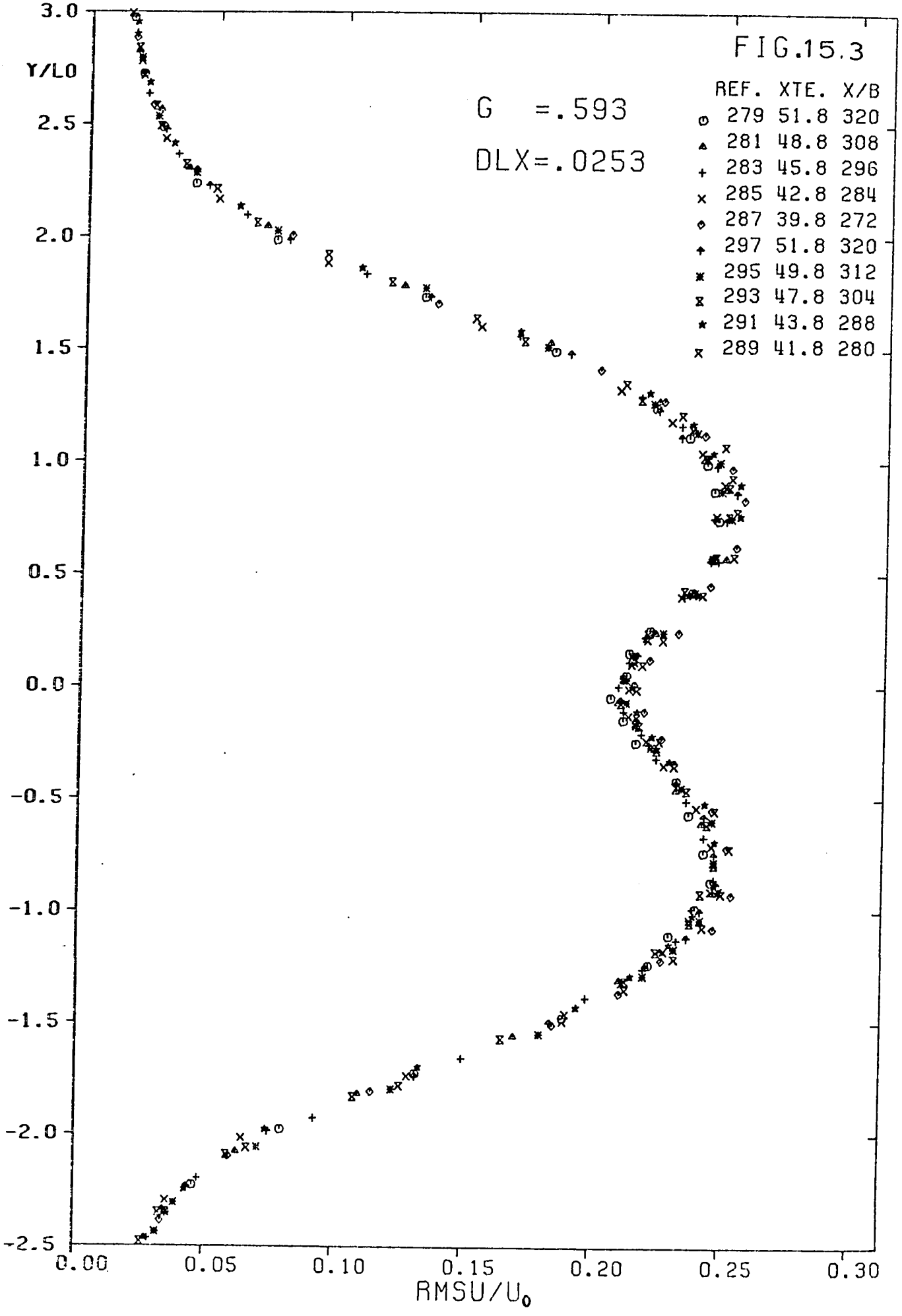
FIG.15.3
G =.593
DLX=.0253
REF. XTE. X/B
279 51.8 320
281 48.8 308
283 45.8 296
285 42.8 284
287 39.8 272
297 51.8 320
295 49.8 312
293 47.8 304
291 43.8 288
289 41.8 280
Y/L0
3.0
2.5
2.0
1.5
1.0
0.5
0.0
-0.5
-1.0
-1.5
-2.0
-2.5
0.00
0.05
0.10
0.15
0.20
0.25
0.30
RMSU/U0

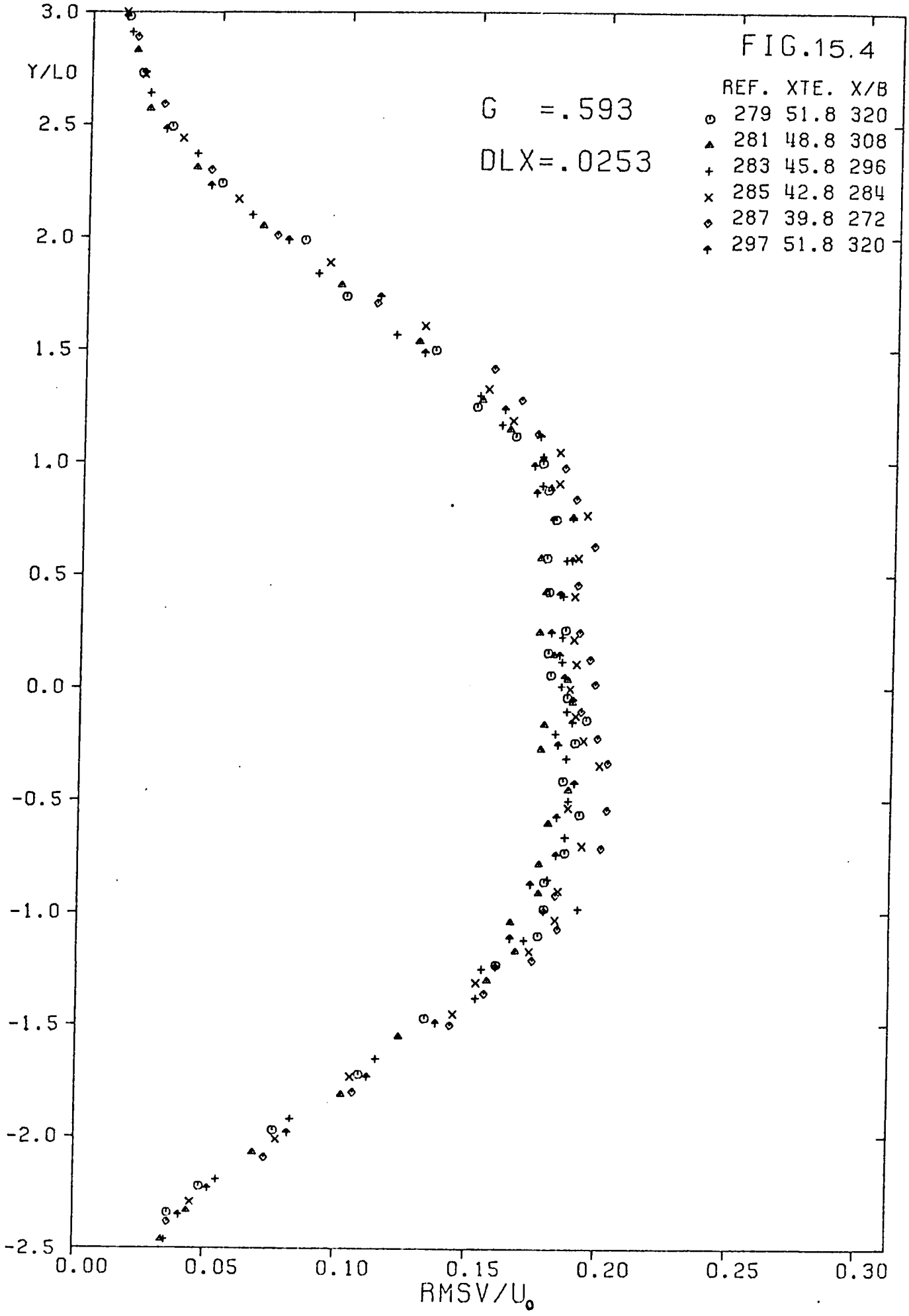
FIG.15.4
G =.593
DLX=.0253
REF. XTE. X/B
279 51.8 320
281 48.8 308
283 45.8 296
285 42.8 284
287 39.8 272
297 51.8 320
Y/LO
3.0
2.5
2.0
1.5
1.0
0.5
0.0
-0.5
-1.0
-1.5
-2.0
-2.5
0.00
0.05
0.10
0.15
0.20
0.25
0.30
RMSV/U0

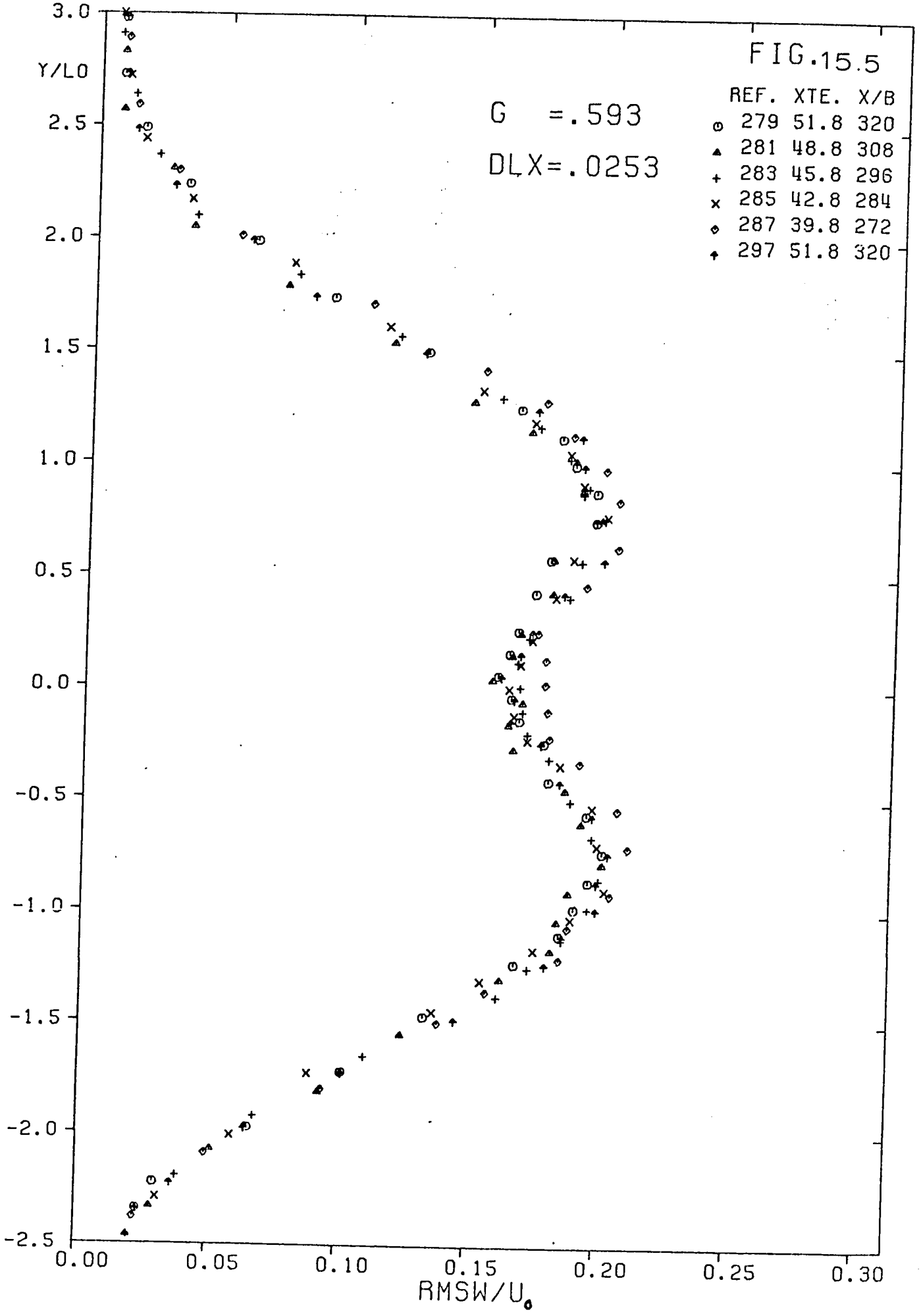
FIG.15.5
G =.593
DLX=.0253
REF. XTE. X/B
279 51.8 320
281 48.8 308
283 45.8 296
285 42.8 284
287 39.8 272
297 51.8 320
Y/LO
3.0
2.5
2.0
1.5
1.0
0.5
0.0
-0.5
-1.0
-1.5
-2.0
-2.5
0.00
0.05
0.10
0.15
0.20
0.25
0.30
RMSW/U∞

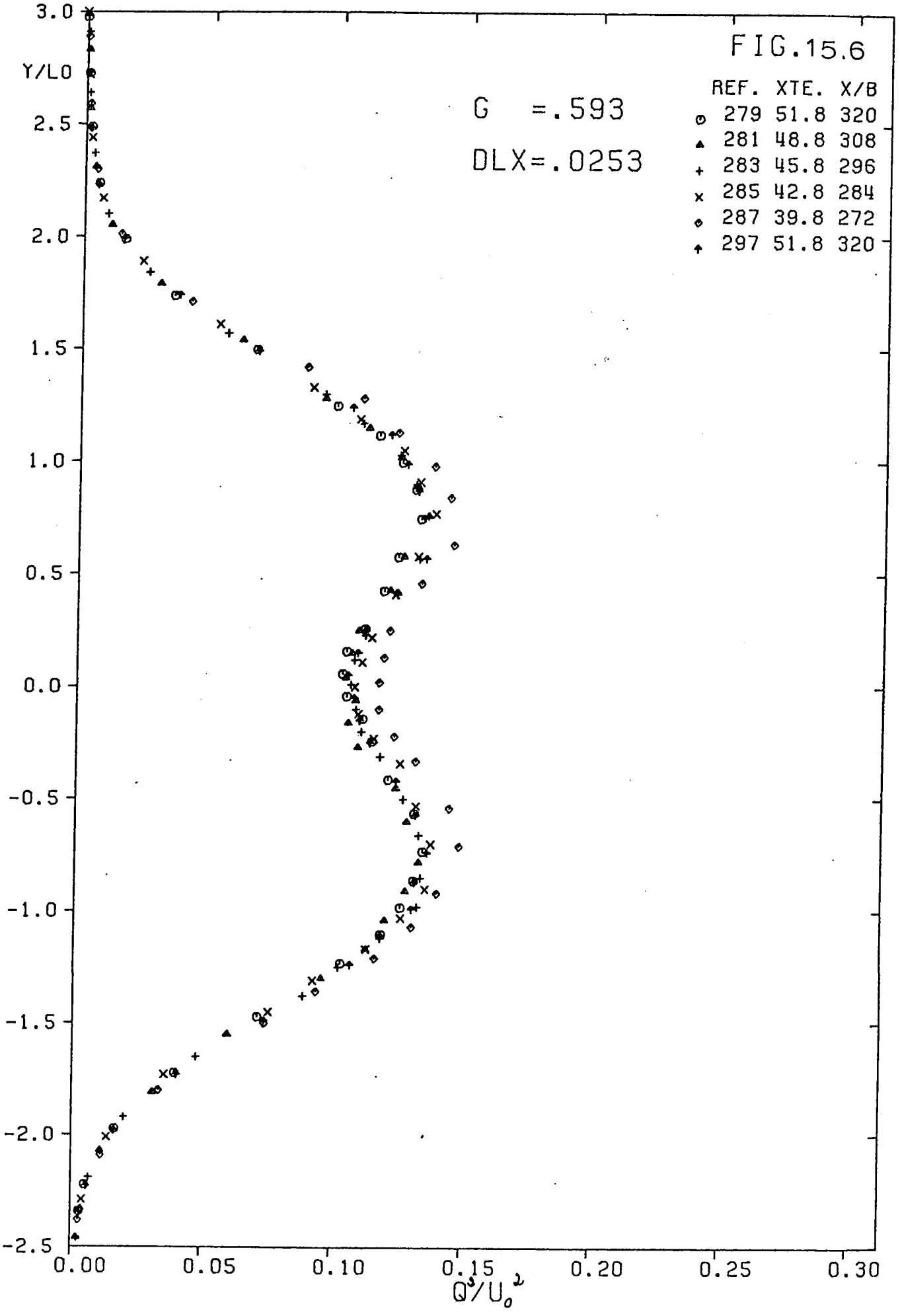
FIG.15.6
G =.593
DLX=.0253
REF. XTE. X/B
279 51.8 320
281 48.8 308
283 45.8 296
285 42.8 284
287 39.8 272
297 51.8 320
Y/LO
3.0
2.5
2.0
1.5
1.0
0.5
0.0
-0.5
-1.0
-1.5
-2.0
-2.5
0.00
0.05
0.10
0.15
0.20
0.25
0.30
Q^2/U_o^2

FIG.15.7

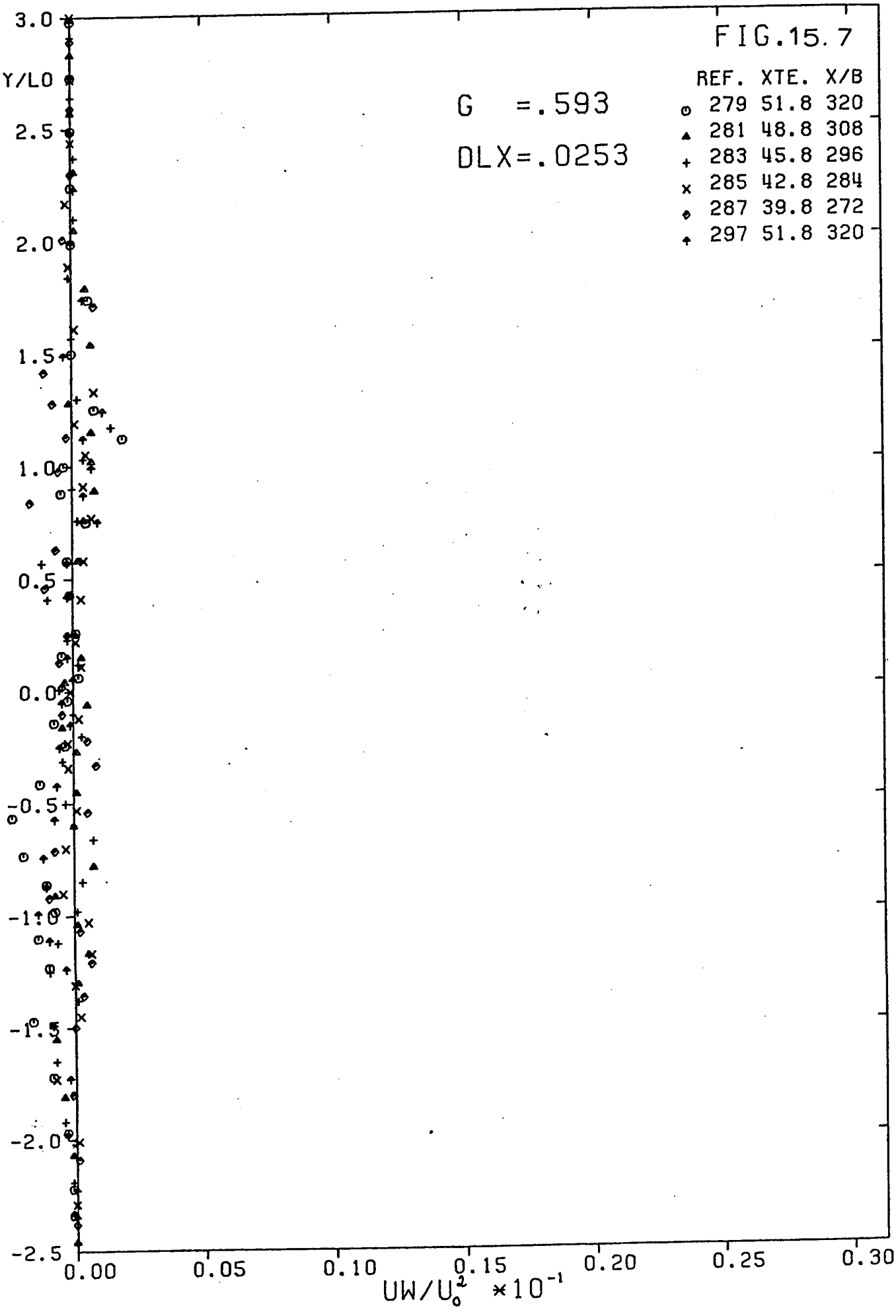
G =.593
DLX=.0253
REF. XTE. X/B
279 51.8 320
281 48.8 308
283 45.8 296
285 42.8 284
287 39.8 272
297 51.8 320
Y/LO
3.0
2.5
2.0
1.5
1.0
0.5
0.0
-0.5
-1.0
-1.5
-2.0
-2.5
0.00
0.05
0.10
0.15
0.20
0.25
0.30
UW/U$_o^2$ *10^{-1}

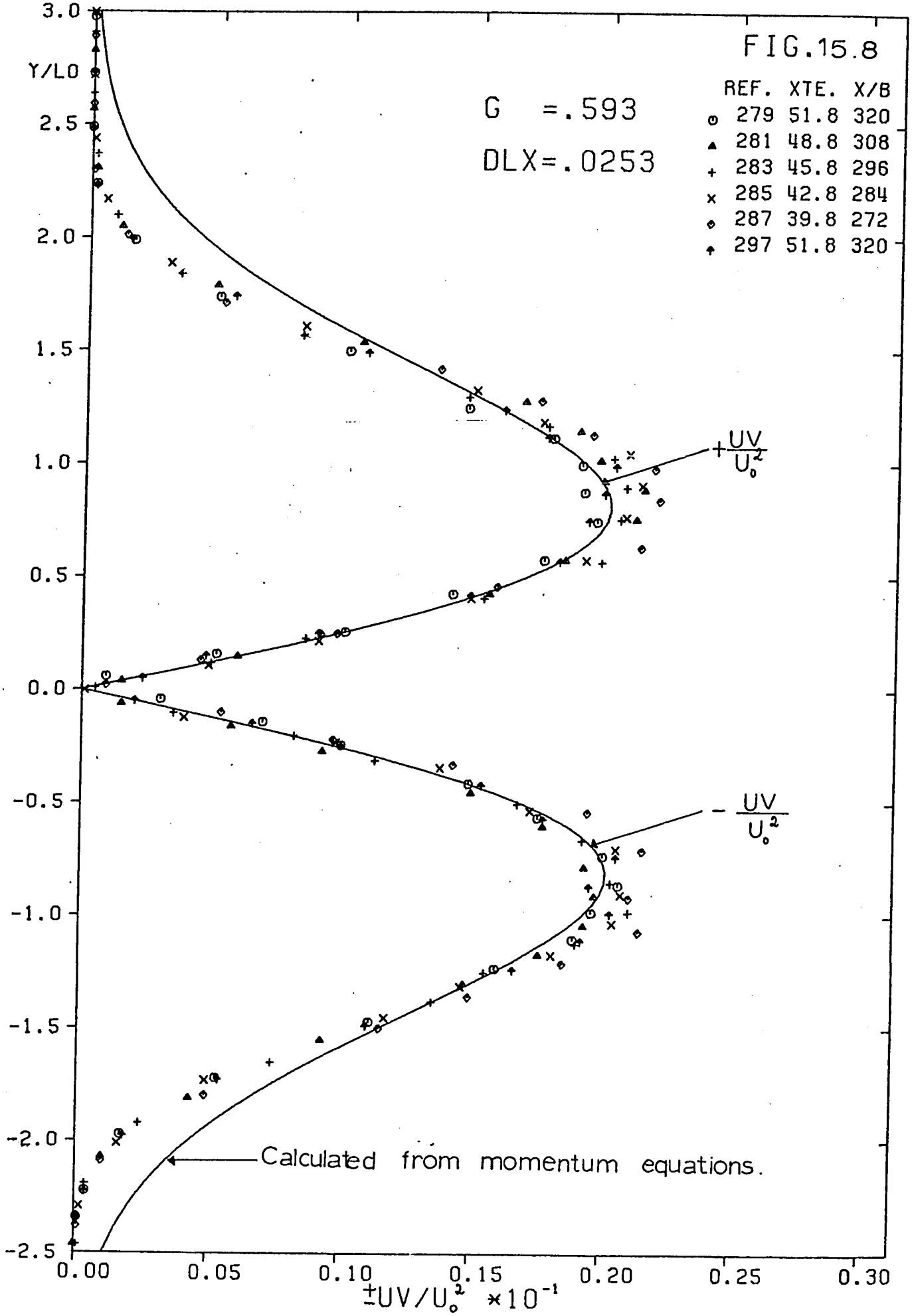
FIG.15.8
G =.593
DLX=.0253
REF. XTE. X/B
279 51.8 320
281 48.8 308
283 45.8 296
285 42.8 284
287 39.8 272
297 51.8 320
Y/LO
3.0
2.5
2.0
1.5
1.0
0.5
0.0
-0.5
-1.0
-1.5
-2.0
-2.5
+UV/U₀²
-UV/U₀²
Calculated from momentum equations.
0.00
0.05
0.10
0.15
0.20
0.25
0.30
±UV/U₀² ×10⁻¹

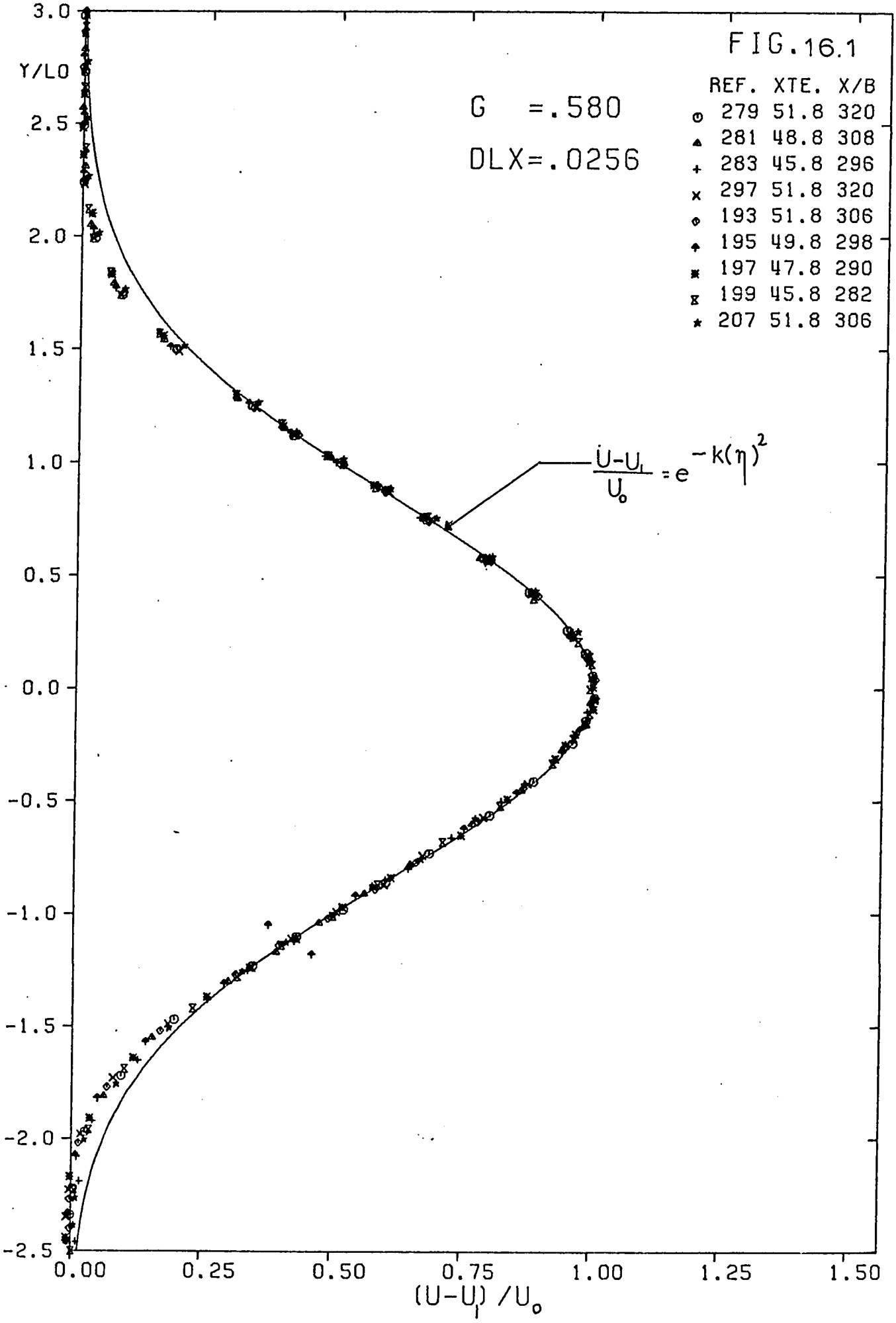
FIG. 16.1
G = .580
DLX = .0256
REF. XTE. X/B
279 51.8 320
281 48.8 308
283 45.8 296
297 51.8 320
193 51.8 306
195 49.8 298
197 47.8 290
199 45.8 282
207 51.8 306
$\frac{U-U_1}{U_0} = e^{-k(\eta)^2}$
Y/LO
3.0
2.5
2.0
1.5
1.0
0.5
0.0
-0.5
-1.0
-1.5
-2.0
-2.5
0.00
0.25
0.50
0.75
1.00
1.25
1.50
$(U-U_1)/U_0$

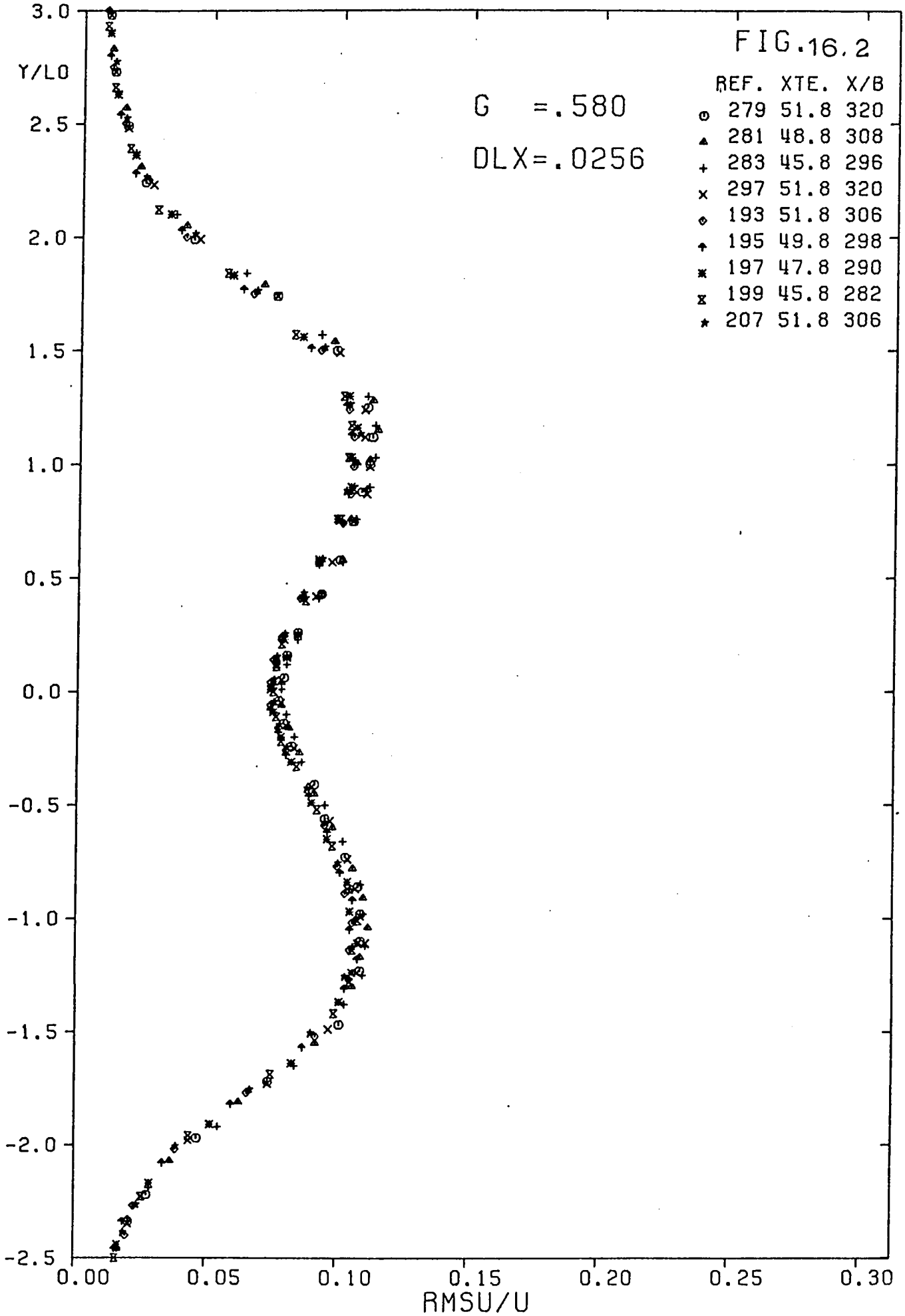
FIG.16.2
G =.580
DLX=.0256
REF. XTE. X/B
279 51.8 320
281 48.8 308
283 45.8 296
297 51.8 320
193 51.8 306
195 49.8 298
197 47.8 290
199 45.8 282
207 51.8 306
Y/LO
3.0
2.5
2.0
1.5
1.0
0.5
0.0
-0.5
-1.0
-1.5
-2.0
-2.5
0.00
0.05
0.10
0.15
0.20
0.25
0.30
RMSU/U

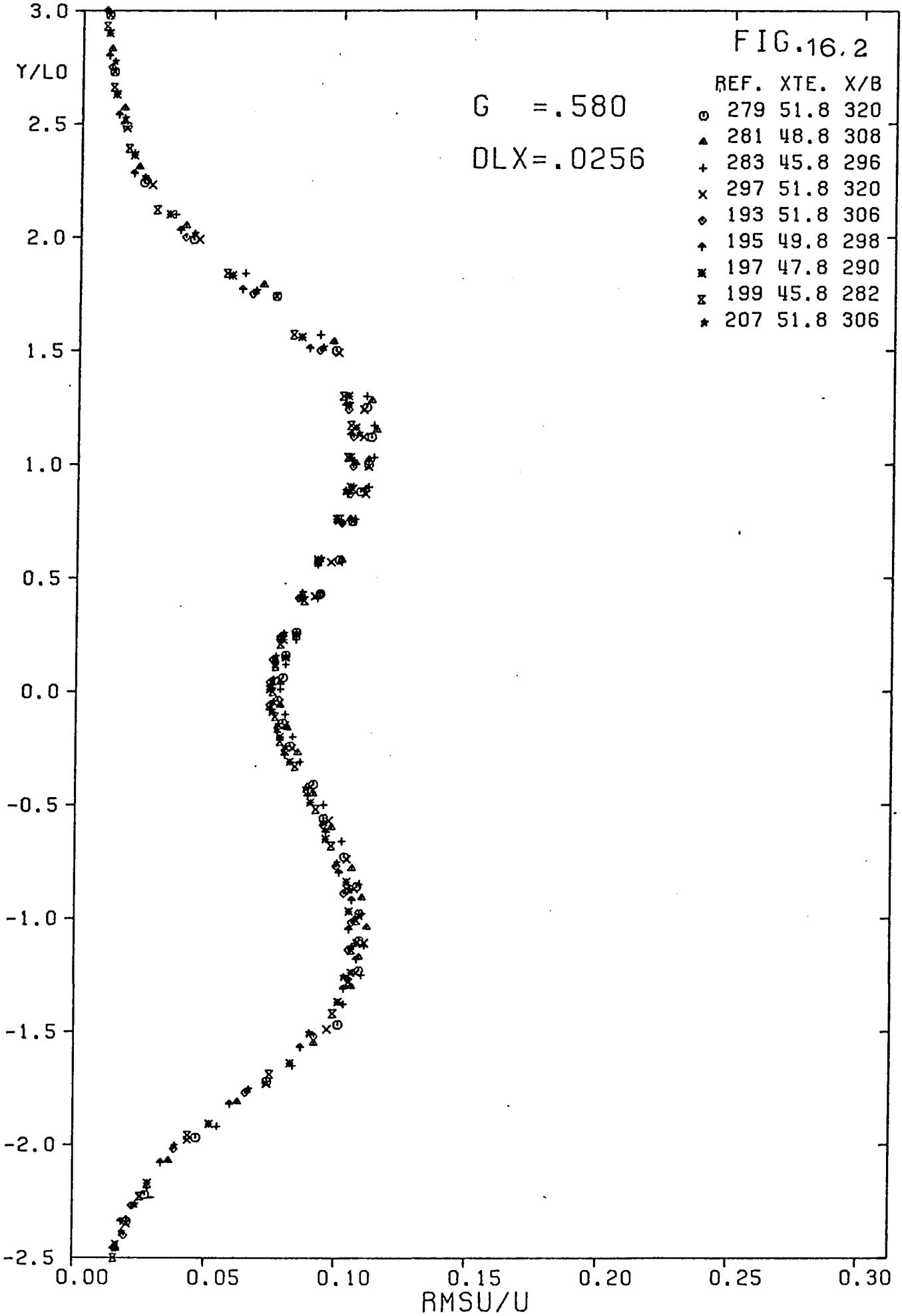
FIG.16.2
G =.580
DLX=.0256
REF. XTE. X/B
279 51.8 320
281 48.8 308
283 45.8 296
297 51.8 320
193 51.8 306
195 49.8 298
197 47.8 290
199 45.8 282
207 51.8 306
Y/LO
3.0
2.5
2.0
1.5
1.0
0.5
0.0
-0.5
-1.0
-1.5
-2.0
-2.5
0.00
0.05
0.10
0.15
0.20
0.25
0.30
RMSU/U

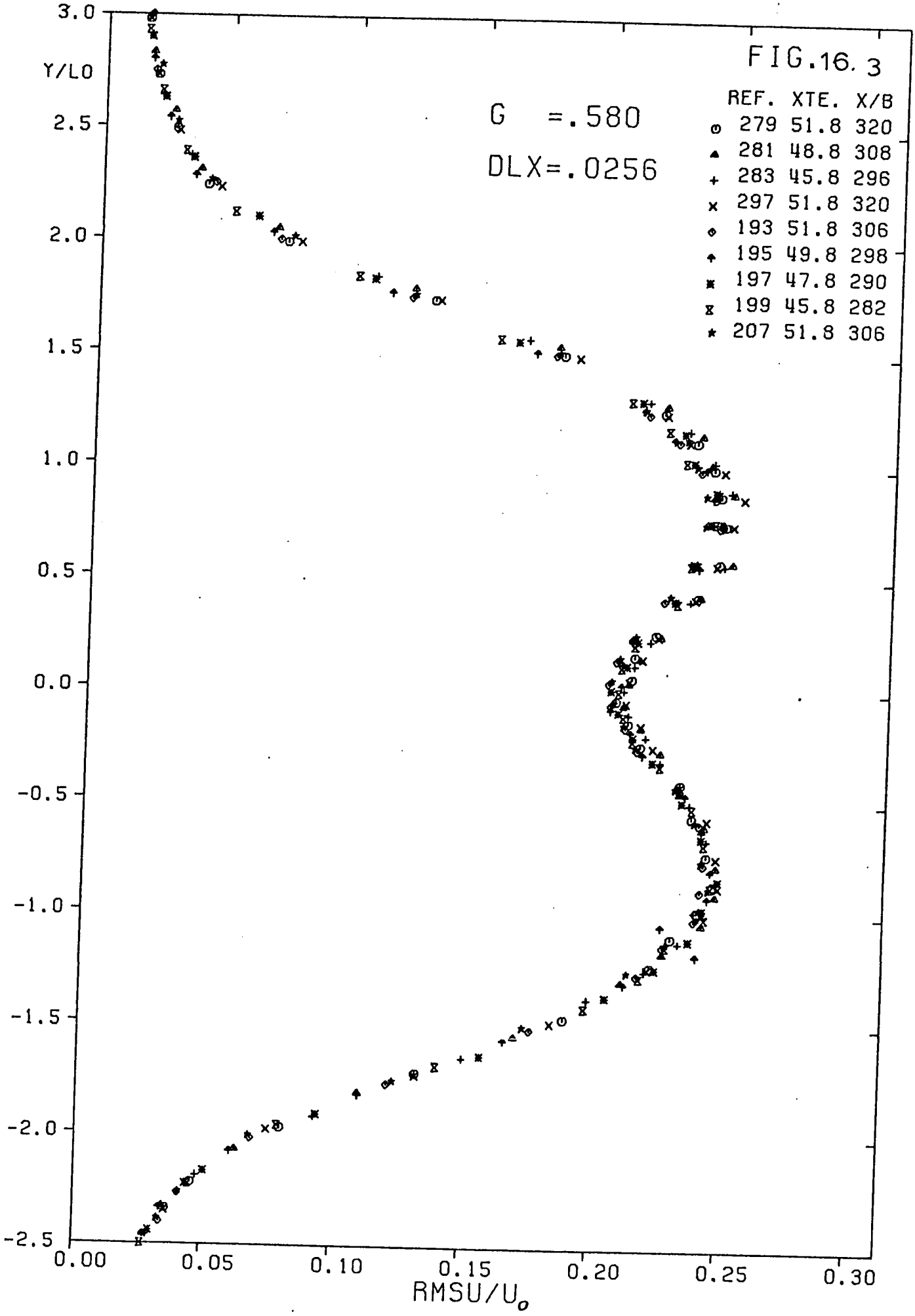
FIG.16.3
G =.580
DLX=.0256
REF. XTE. X/B
279 51.8 320
281 48.8 308
283 45.8 296
297 51.8 320
193 51.8 306
195 49.8 298
197 47.8 290
199 45.8 282
207 51.8 306
Y/LO
3.0
2.5
2.0
1.5
1.0
0.5
0.0
-0.5
-1.0
-1.5
-2.0
-2.5
0.00
0.05
0.10
0.15
0.20
0.25
0.30
RMSU/U$_o$

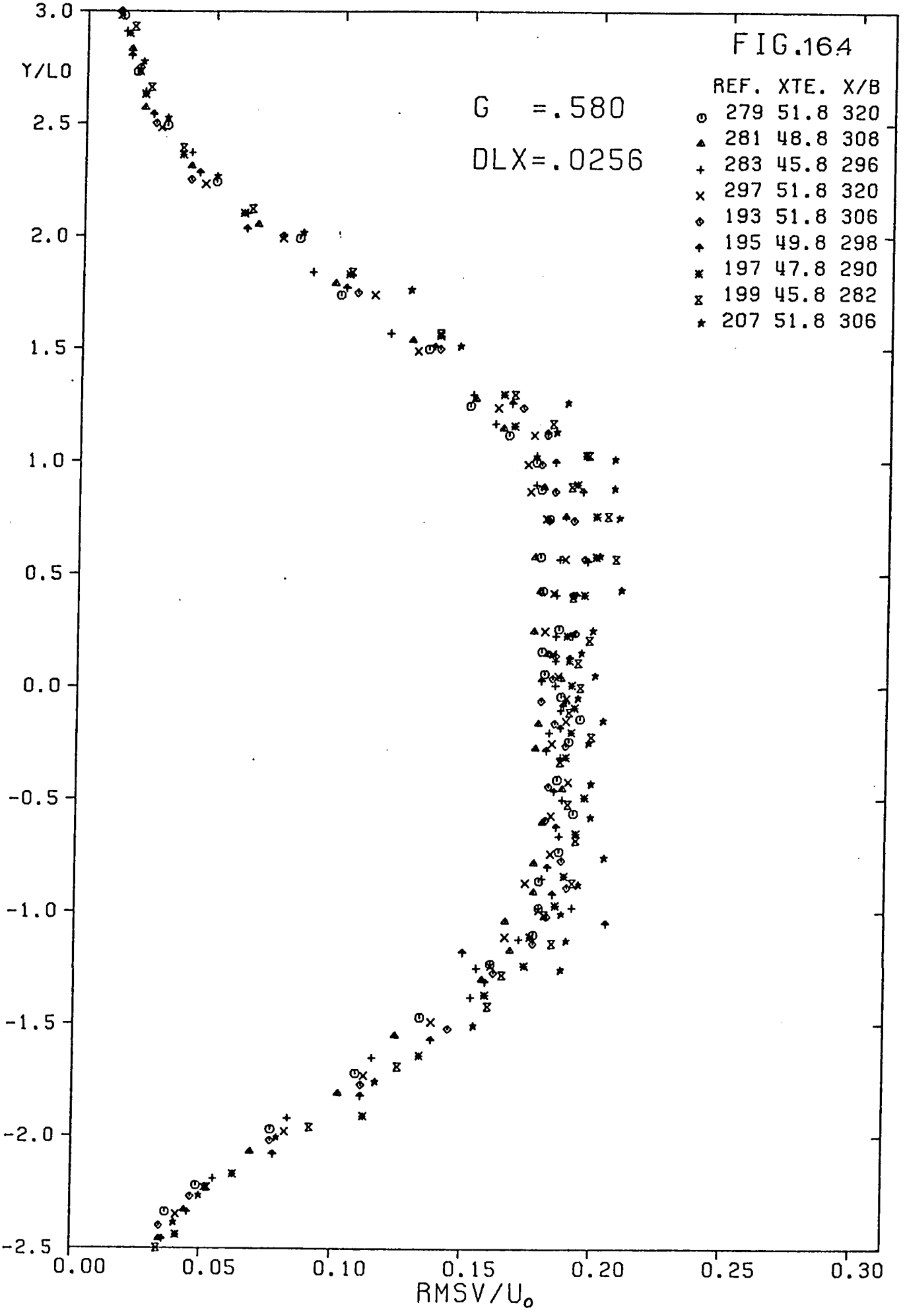
FIG.164
G =.580
DLX=.0256
REF. XTE. X/B
279 51.8 320
281 48.8 308
283 45.8 296
297 51.8 320
193 51.8 306
195 49.8 298
197 47.8 290
199 45.8 282
207 51.8 306
Y/LO
3.0
2.5
2.0
1.5
1.0
0.5
0.0
-0.5
-1.0
-1.5
-2.0
-2.5
0.00
0.05
0.10
0.15
0.20
0.25
0.30
RMSV/U$_o$

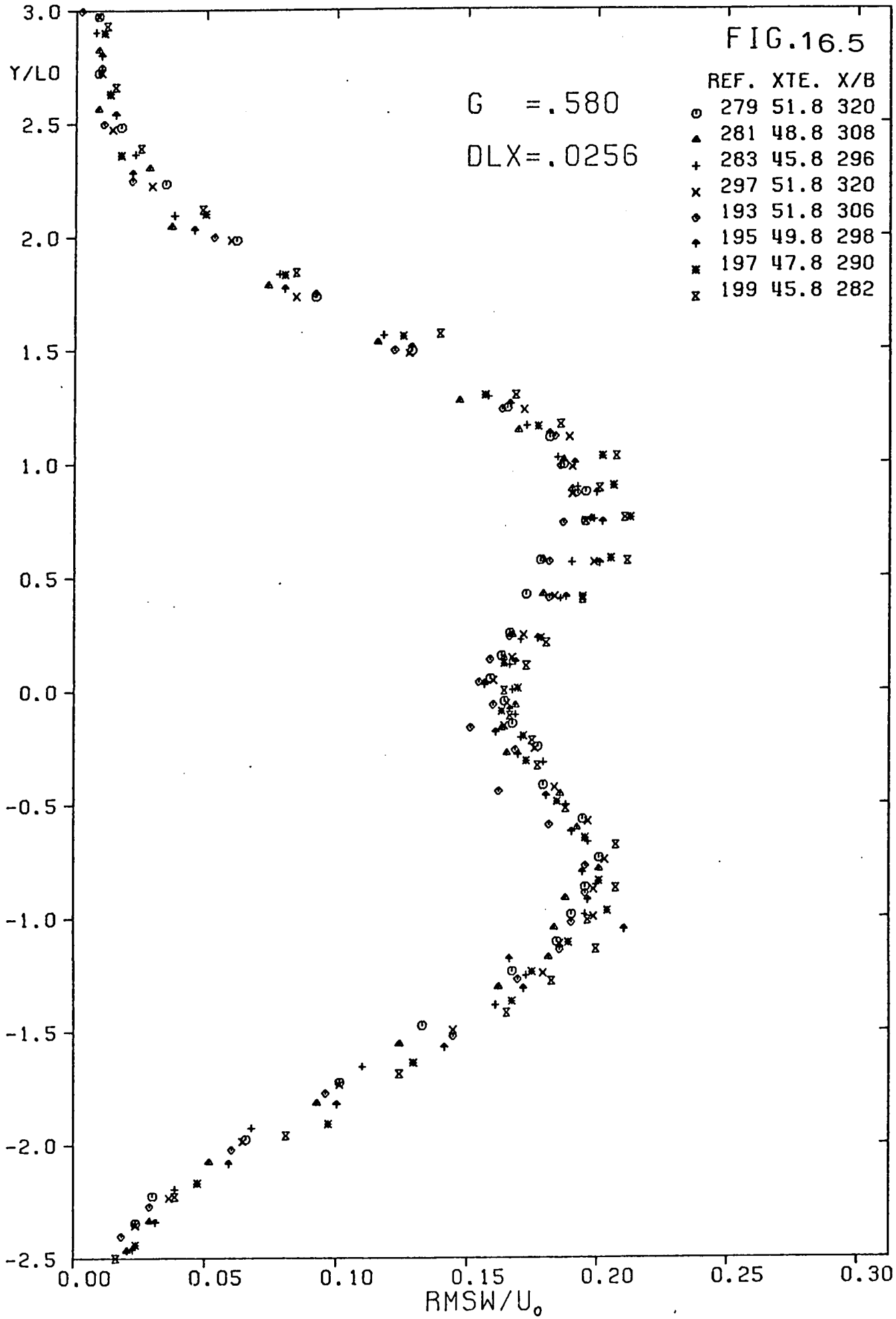
FIG.16.5
G =.580
DLX=.0256
REF. XTE. X/B
279 51.8 320
281 48.8 308
283 45.8 296
297 51.8 320
193 51.8 306
195 49.8 298
197 47.8 290
199 45.8 282
Y/LO
3.0
2.5
2.0
1.5
1.0
0.5
0.0
-0.5
-1.0
-1.5
-2.0
-2.5
0.00
0.05
0.10
0.15
0.20
0.25
0.30
RMSW/U0

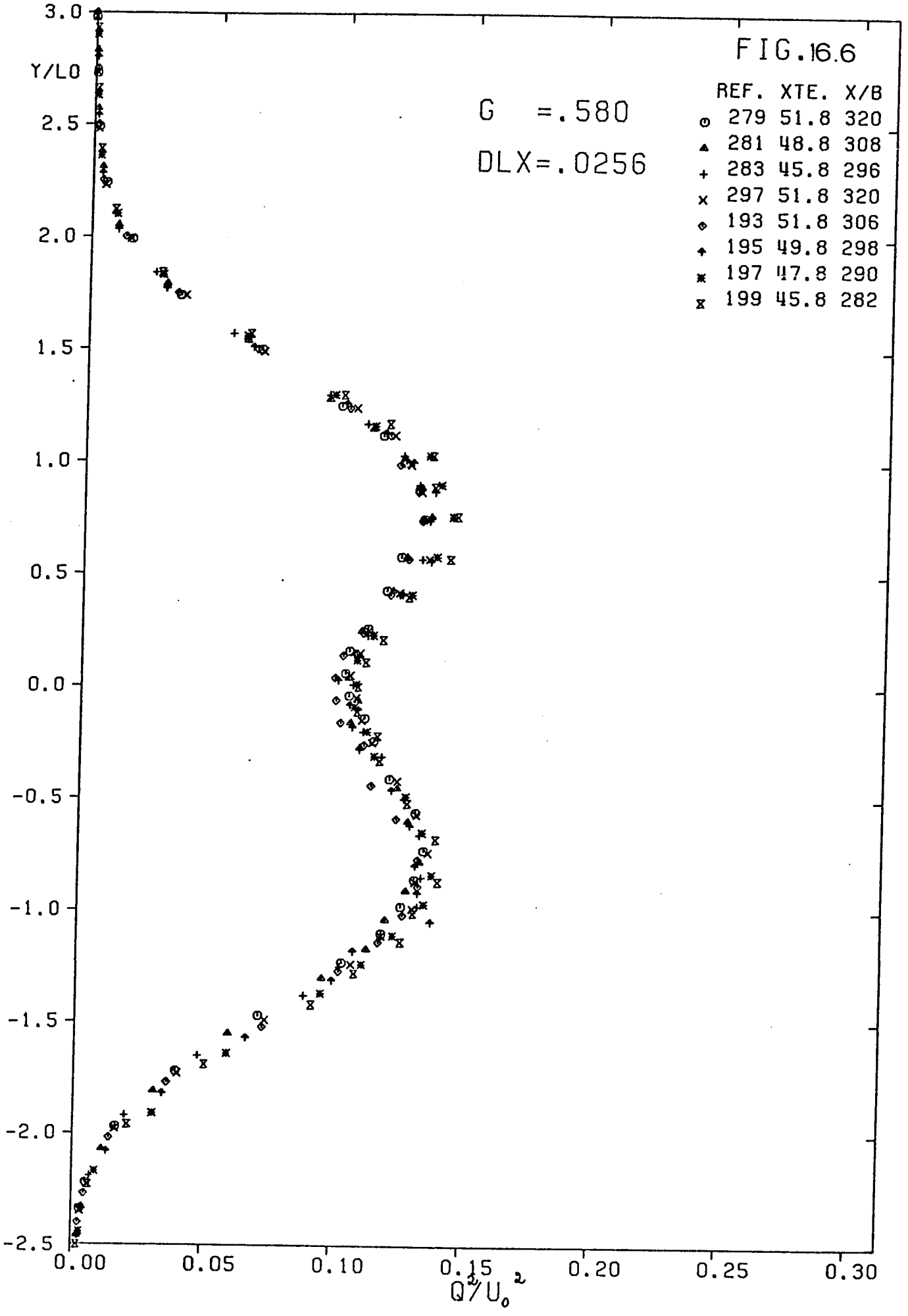
FIG.16.6
G =.580
DLX=.0256
REF. XTE. X/B
279 51.8 320
281 48.8 308
283 45.8 296
297 51.8 320
193 51.8 306
195 49.8 298
197 47.8 290
199 45.8 282
Y/LO
3.0
2.5
2.0
1.5
1.0
0.5
0.0
-0.5
-1.0
-1.5
-2.0
-2.5
0.00
0.05
0.10
0.15
0.20
0.25
0.30
Q²/U₀²

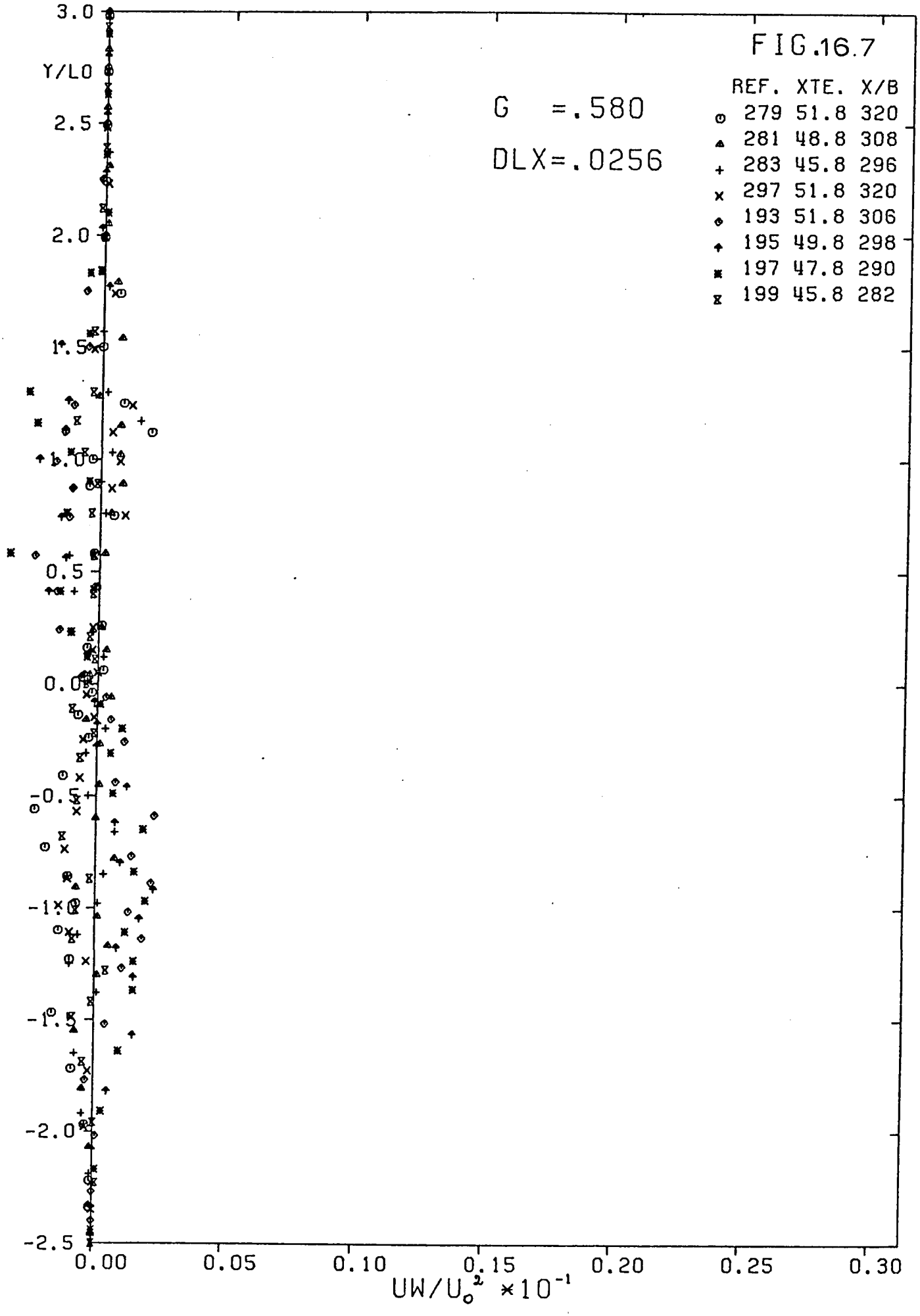
FIG.16.7
G =.580
DLX=.0256
REF. XTE. X/B
279 51.8 320
281 48.8 308
283 45.8 296
297 51.8 320
193 51.8 306
195 49.8 298
197 47.8 290
199 45.8 282
Y/LO
3.0
2.5
2.0
1.5
1.0
0.5
0.0
-0.5
-1.0
-1.5
-2.0
-2.5
0.00
0.05
0.10
0.15
0.20
0.25
0.30
UW/U$_o^2$ ×10^{-1}

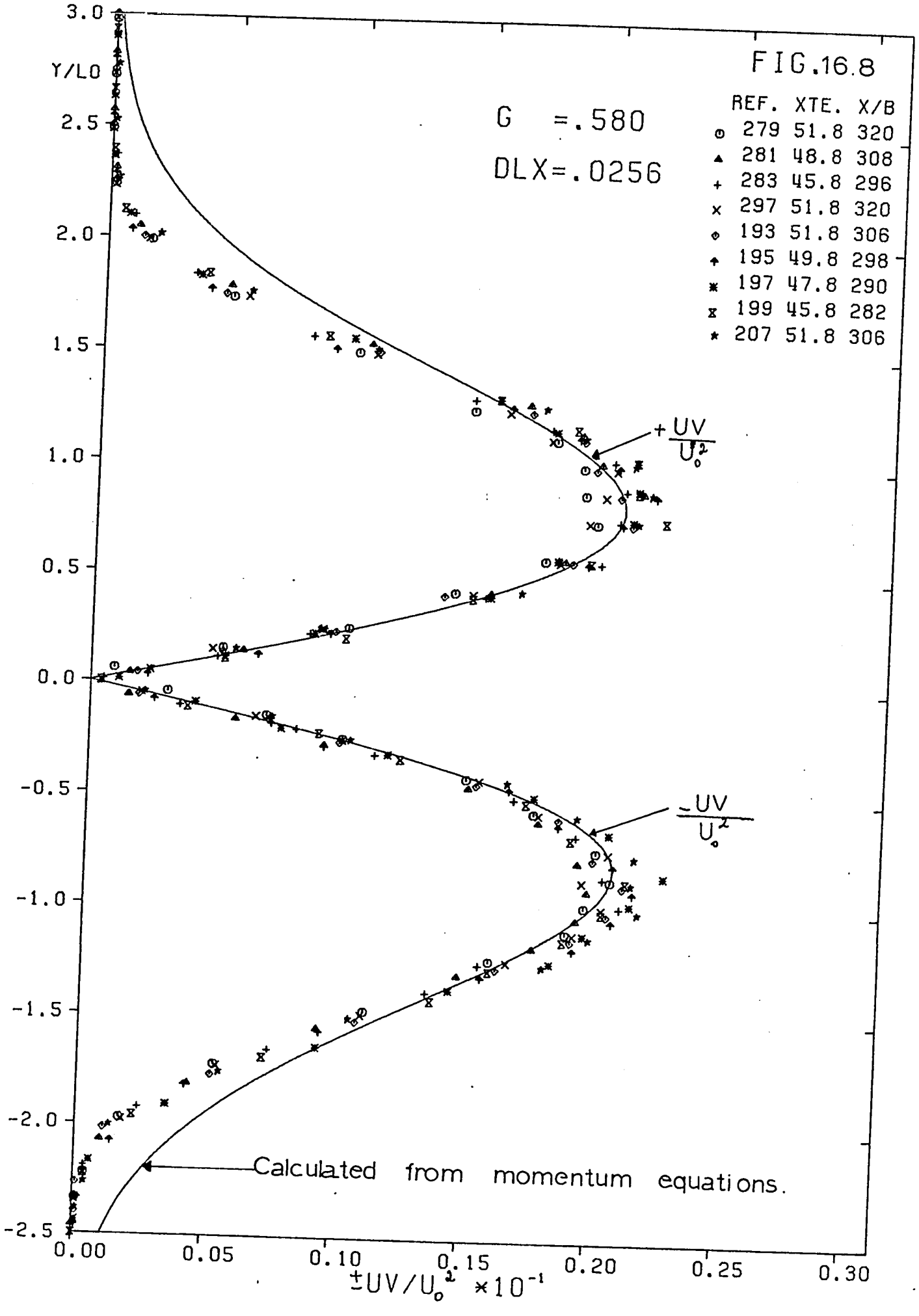
FIG.16.8
G =.580
DLX=.0256
REF. XTE. X/B
279 51.8 320
281 48.8 308
283 45.8 296
297 51.8 320
193 51.8 306
195 49.8 298
197 47.8 290
199 45.8 282
207 51.8 306
+UV/U₀²
-UV/U₀²
Calculated from momentum equations.
Y/LO
±UV/U₀² ×10⁻¹
3.0
2.5
2.0
1.5
1.0
0.5
0.0
-0.5
-1.0
-1.5
-2.0
-2.5
0.00
0.05
0.10
0.15
0.20
0.25
0.30

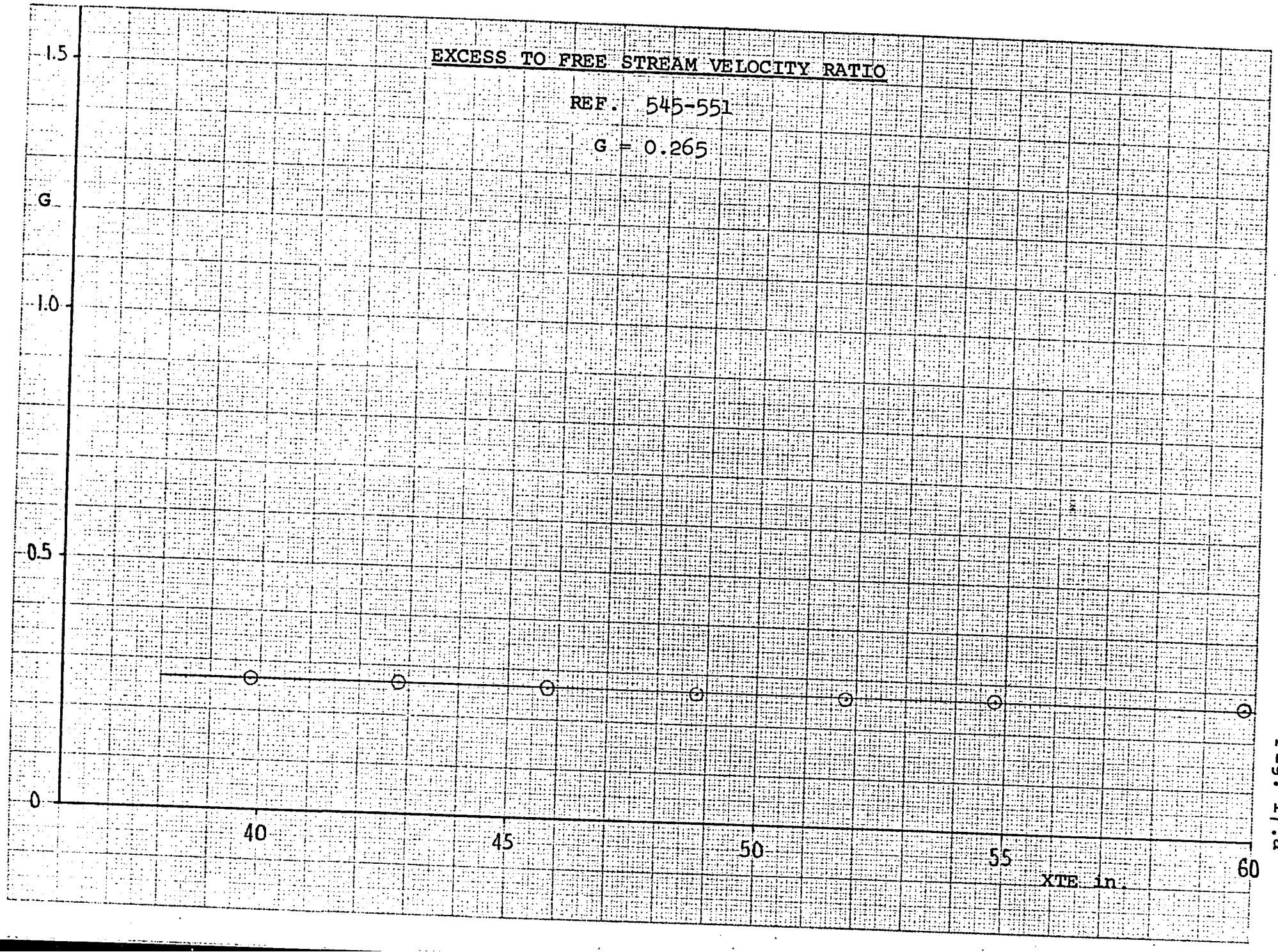
EXCESS TO FREE STREAM VELOCITY RATIO
REF. 545-551
G = 0.265
G
1.5
1.0
0.5
0
40
45
50
55
60
XTE in.

Fig. 17.a

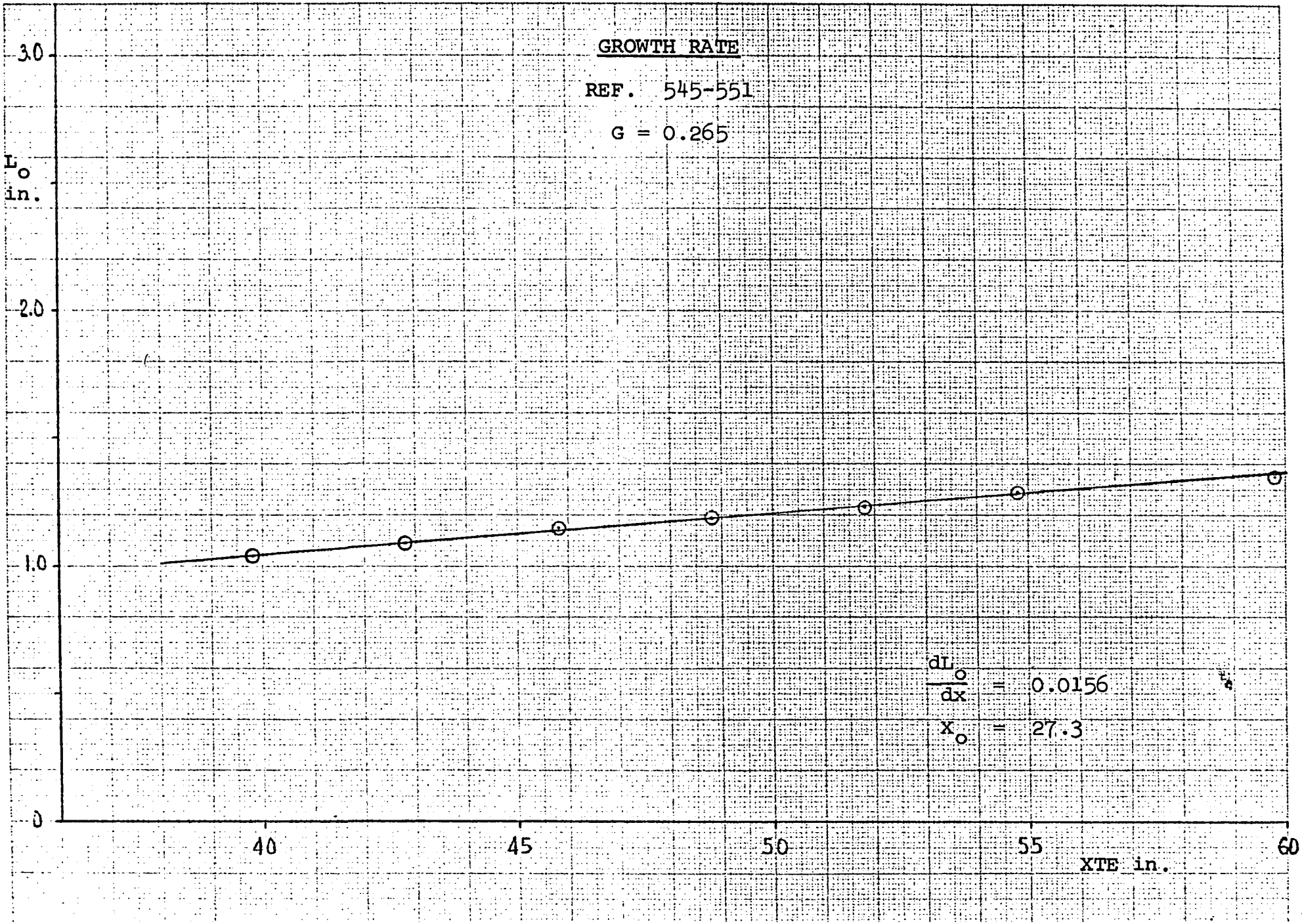
GROWTH RATE
REF. 545-551
G = 0.265
L_o in.
3.0
2.0
1.0
0
40
45
50
55
60
XTE in.
$\frac{dL_o}{dx}$ = 0.0156
x_o = 27.3

Fig. 17.a

VELOCITY DECAY

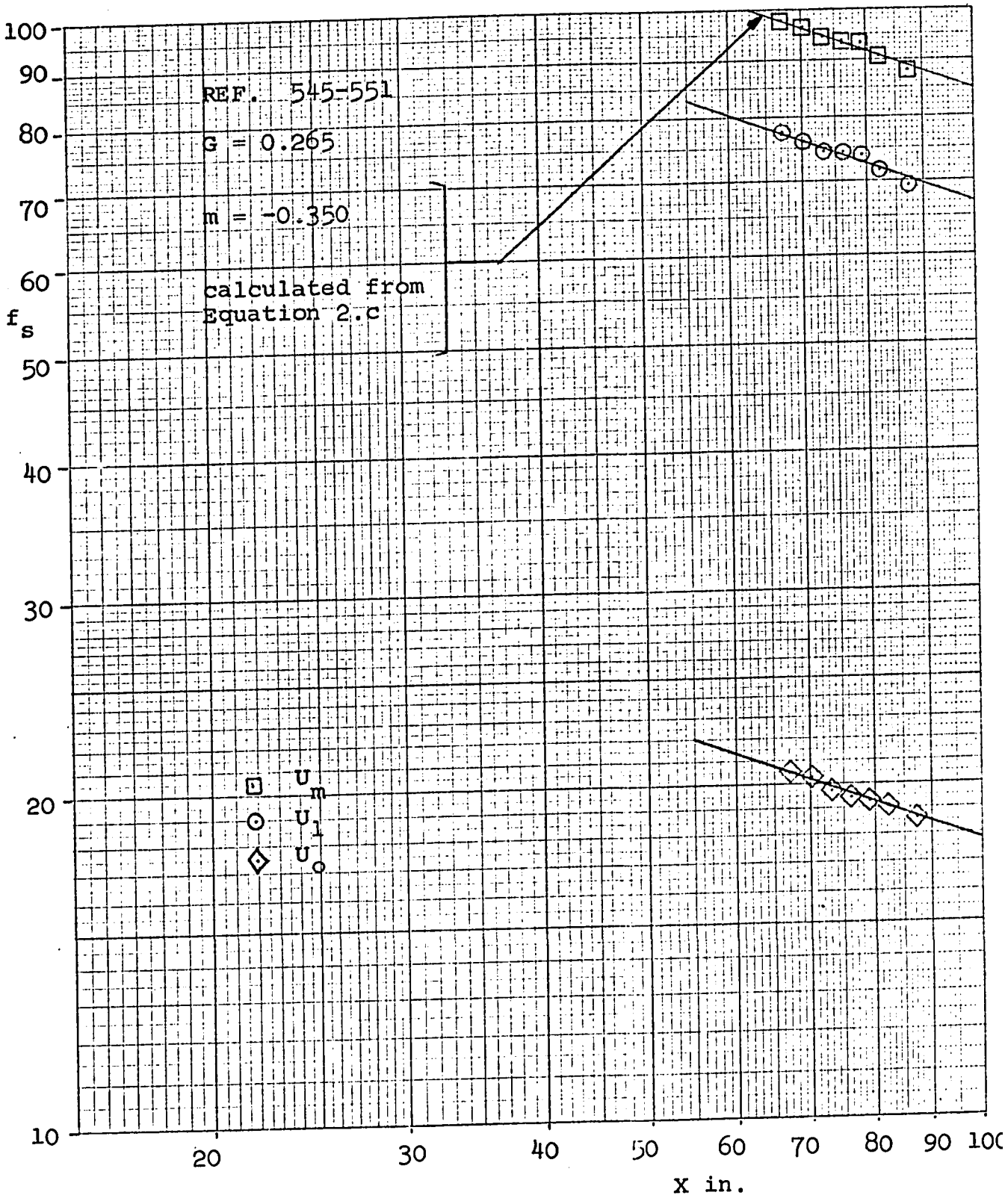

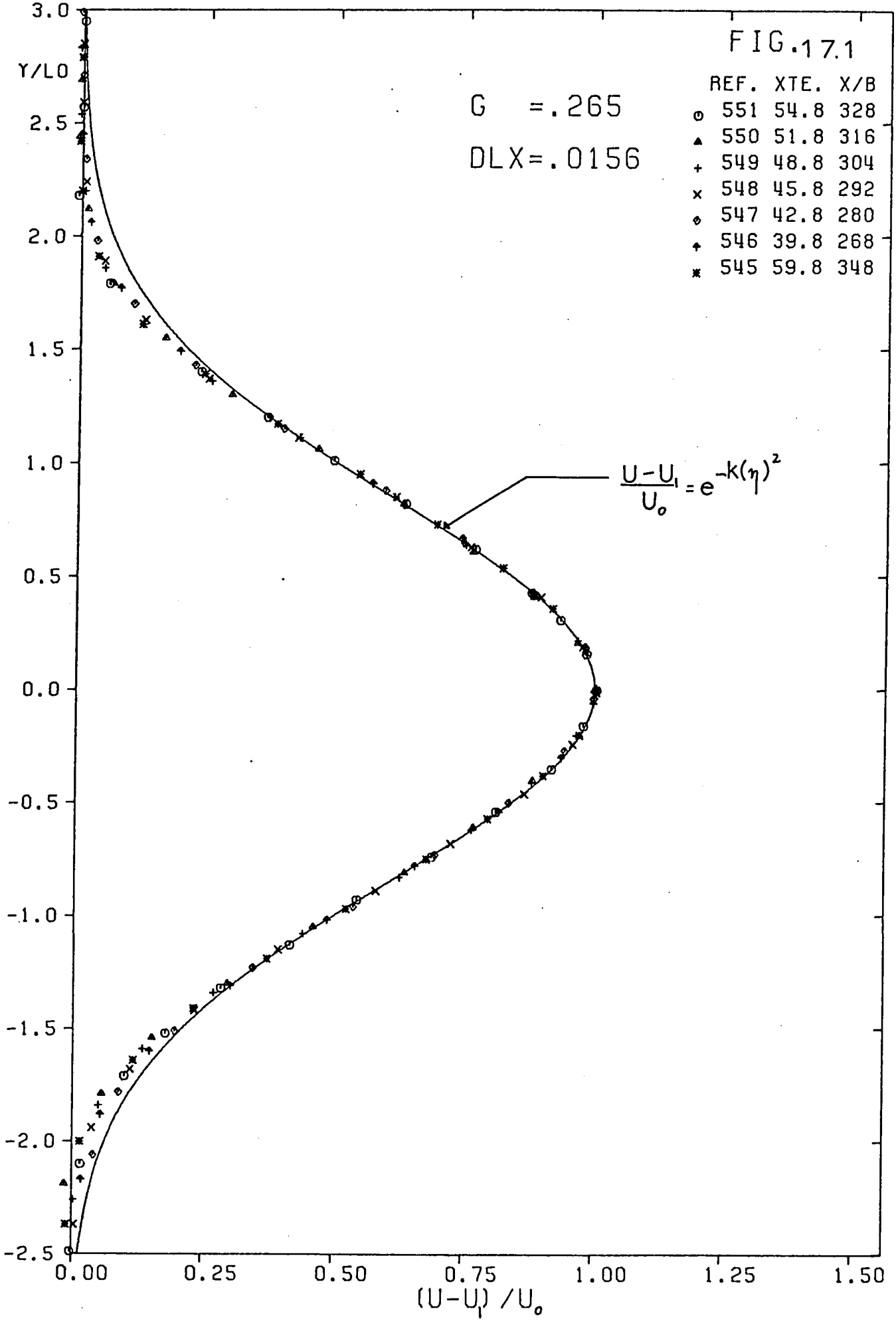
FIG.17.1
G =.265
DLX=.0156
REF. XTE. X/B
551 54.8 328
550 51.8 316
549 48.8 304
548 45.8 292
547 42.8 280
546 39.8 268
545 59.8 348
$\frac{U-U_1}{U_o} = e^{-k(\eta)^2}$
Y/LO
3.0
2.5
2.0
1.5
1.0
0.5
0.0
-0.5
-1.0
-1.5
-2.0
-2.5
0.00
0.25
0.50
0.75
1.00
1.25
1.50
$(U-U_1)/U_o$

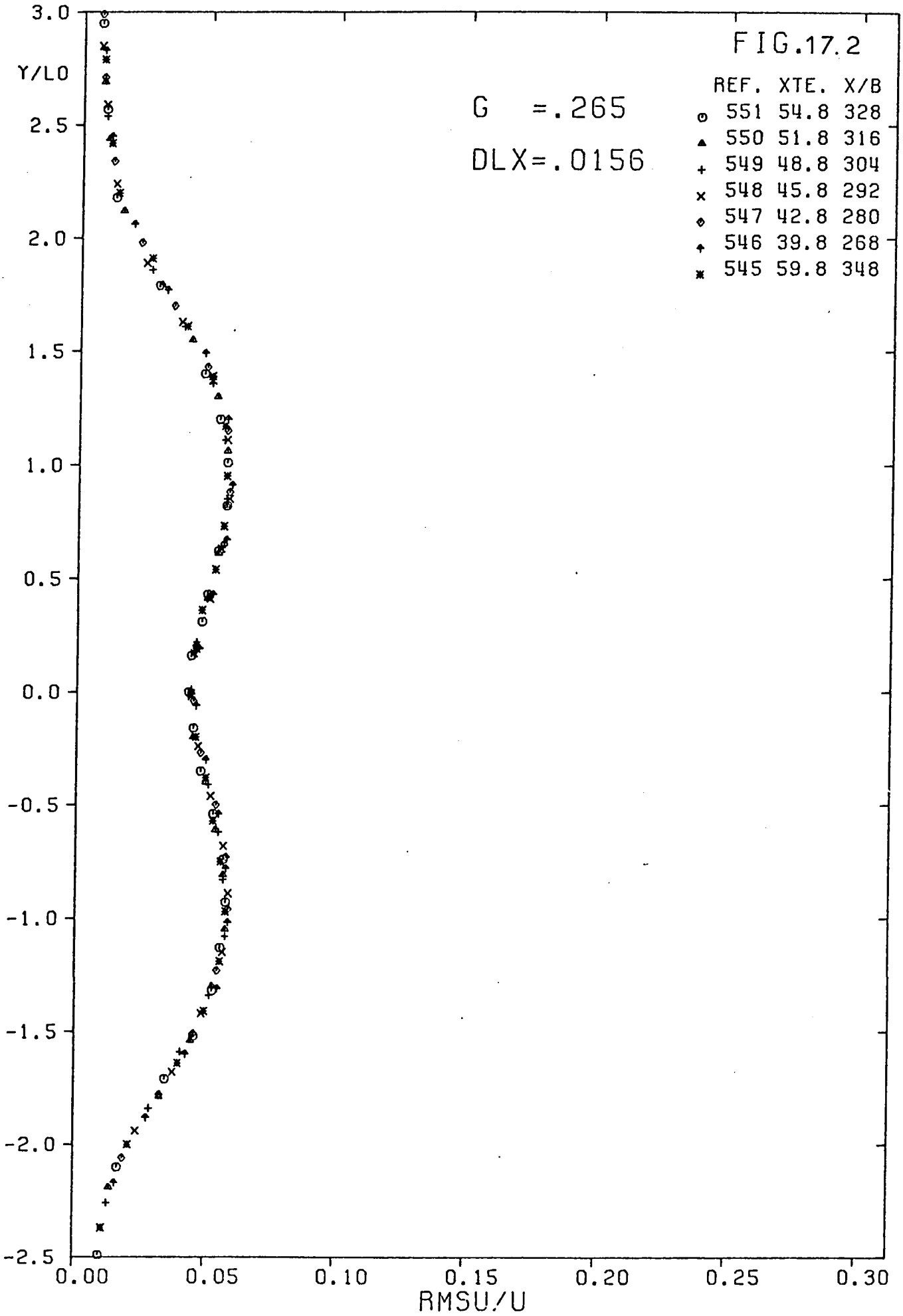
FIG.17.2
G =.265
DLX=.0156
REF. XTE. X/B
551 54.8 328
550 51.8 316
549 48.8 304
548 45.8 292
547 42.8 280
546 39.8 268
545 59.8 348
Y/LO
3.0
2.5
2.0
1.5
1.0
0.5
0.0
-0.5
-1.0
-1.5
-2.0
-2.5
0.00
0.05
0.10
0.15
0.20
0.25
0.30
RMSU/U

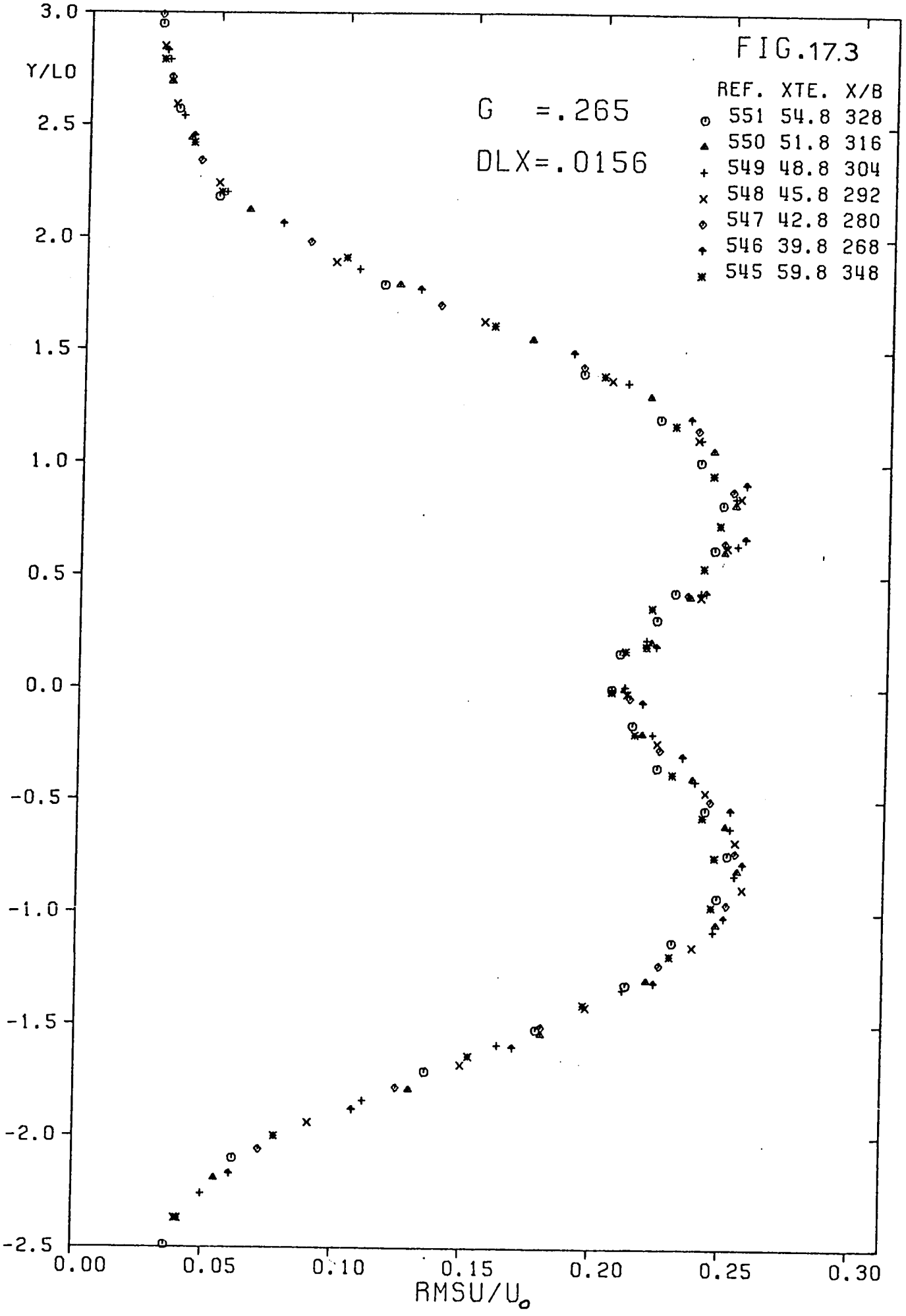
FIG.17.3
G =.265
DLX=.0156
REF. XTE. X/B
551 54.8 328
550 51.8 316
549 48.8 304
548 45.8 292
547 42.8 280
546 39.8 268
545 59.8 348
Y/LO
3.0
2.5
2.0
1.5
1.0
0.5
0.0
-0.5
-1.0
-1.5
-2.0
-2.5
0.00
0.05
0.10
0.15
0.20
0.25
0.30
RMSU/U$_o$

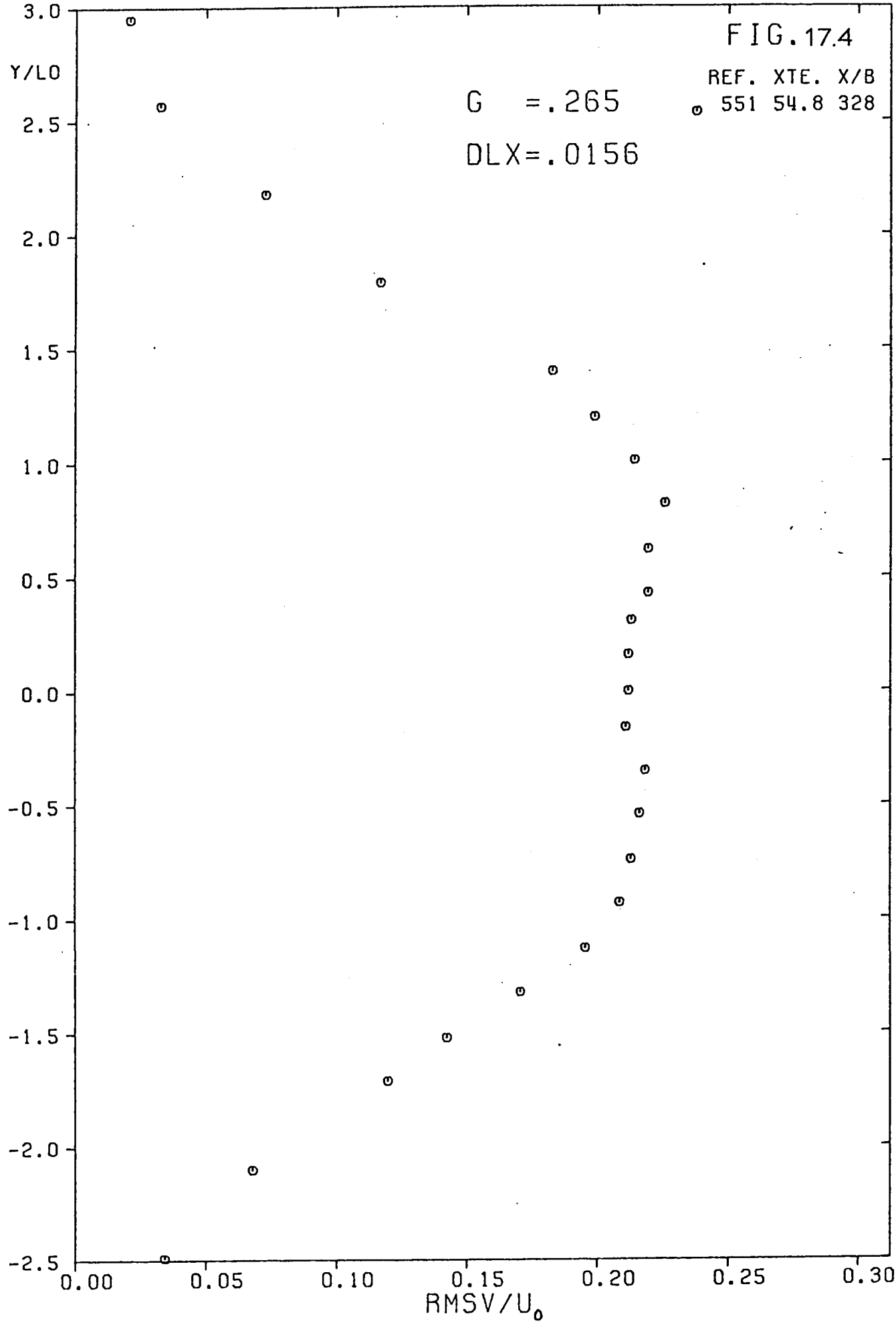
FIG. 17.4
REF. XTE. X/B
551 54.8 328
G =.265
DLX=.0156
Y/LO
3.0
2.5
2.0
1.5
1.0
0.5
0.0
-0.5
-1.0
-1.5
-2.0
-2.5
0.00
0.05
0.10
0.15
0.20
0.25
0.30
RMSV/U0

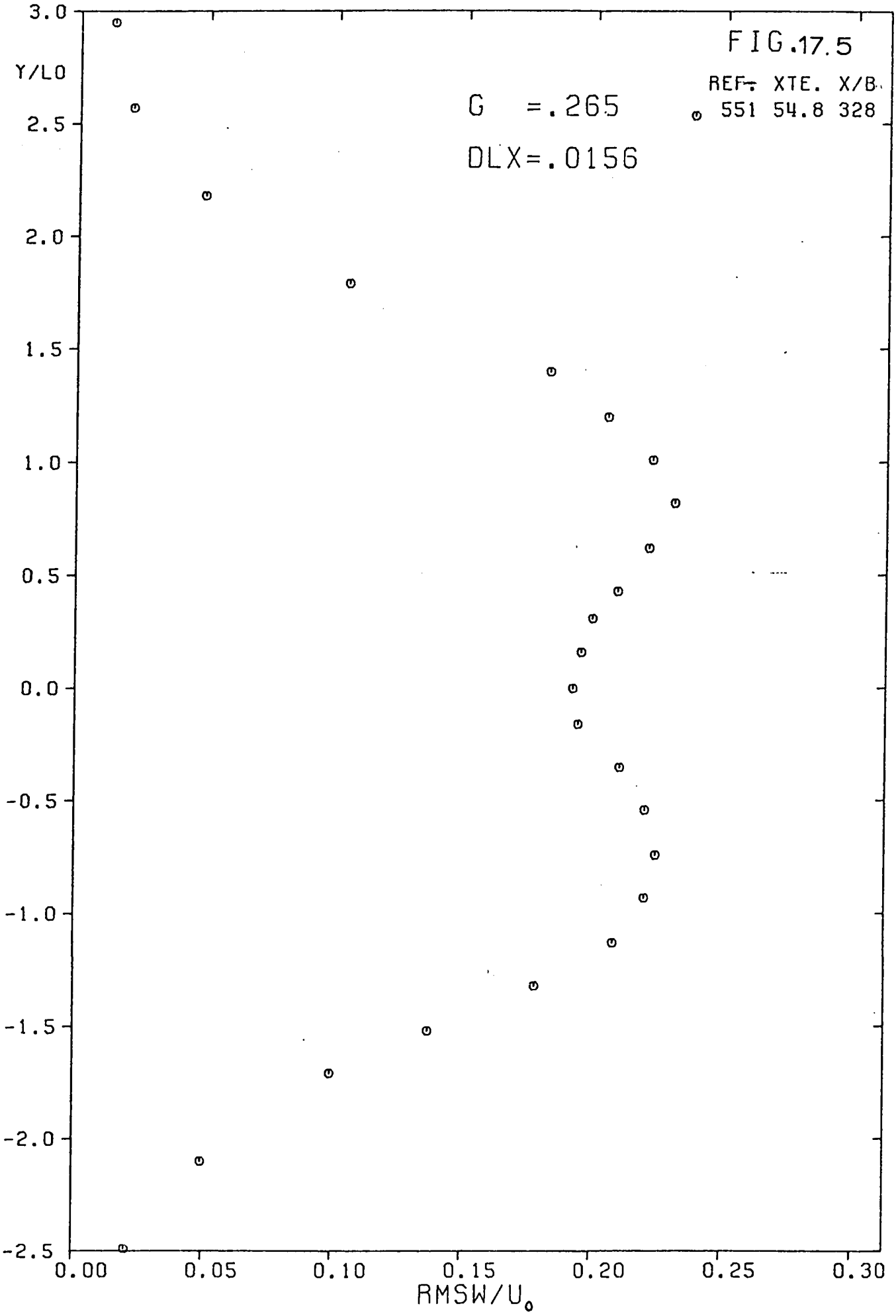
FIG.17.5
REF: XTE. X/B
551 54.8 328
G =.265
DLX=.0156
Y/LO
3.0
2.5
2.0
1.5
1.0
0.5
0.0
-0.5
-1.0
-1.5
-2.0
-2.5
0.00
0.05
0.10
0.15
0.20
0.25
0.30
RMSW/U0

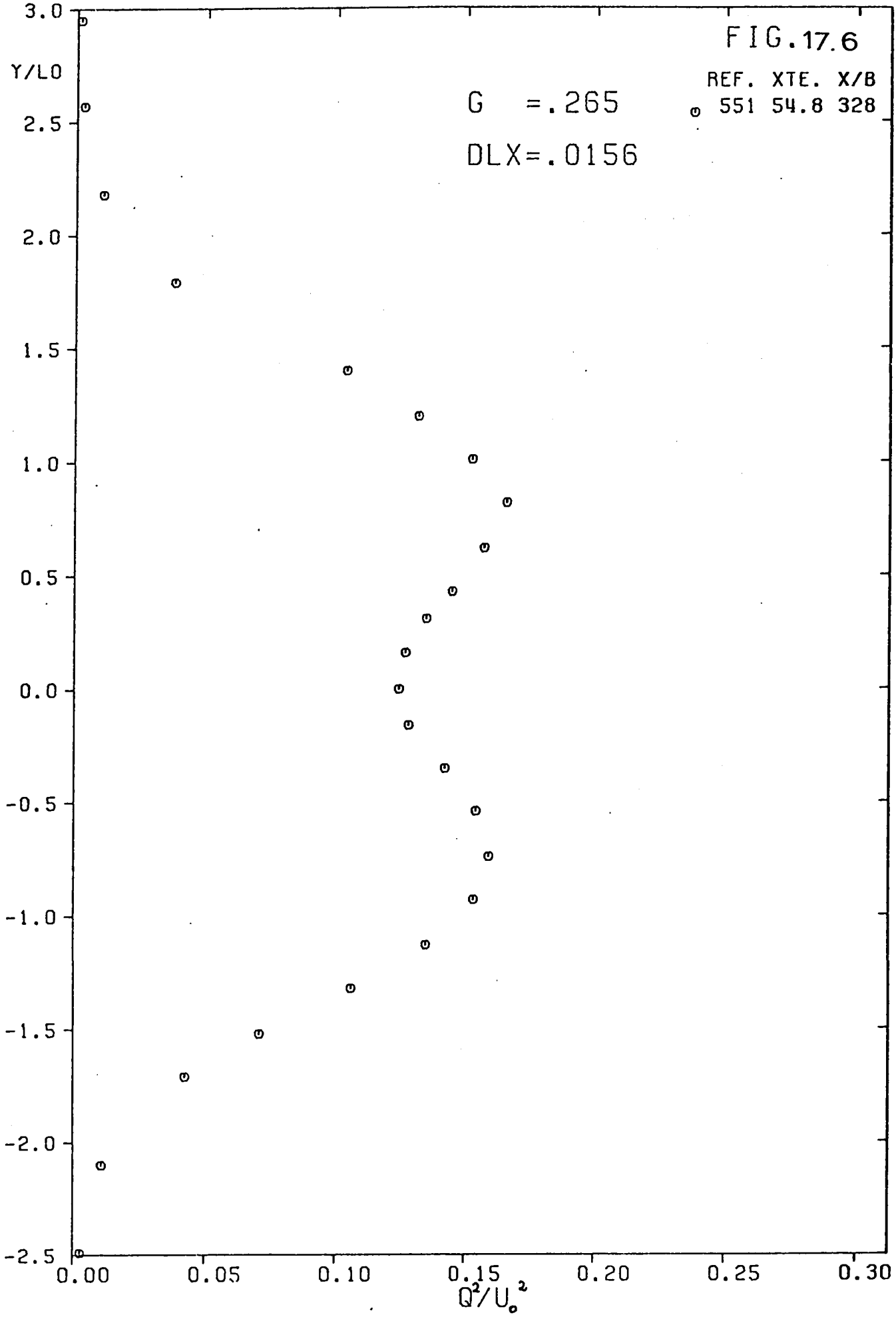
FIG.17.6
REF. XTE. X/B
551 54.8 328
G =.265
DLX=.0156
Y/LO
3.0
2.5
2.0
1.5
1.0
0.5
0.0
-0.5
-1.0
-1.5
-2.0
-2.5
0.00
0.05
0.10
0.15
0.20
0.25
0.30
Q^2/U_o^2

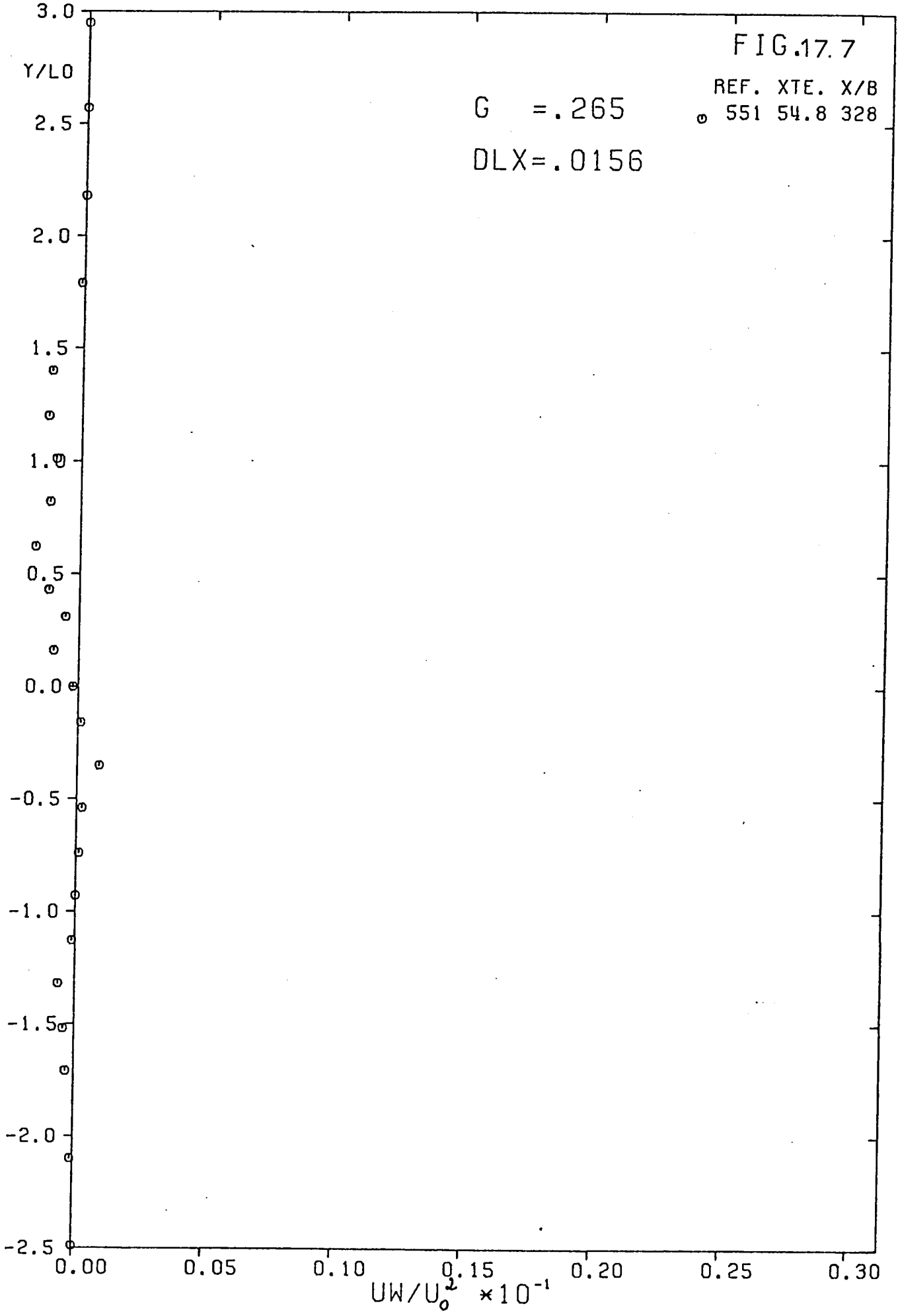
FIG.17.7
REF. XTE. X/B
551 54.8 328
G =.265
DLX=.0156
Y/LO
3.0
2.5
2.0
1.5
1.0
0.5
0.0
-0.5
-1.0
-1.5
-2.0
-2.5
0.00
0.05
0.10
0.15
0.20
0.25
0.30
UW/U$_o^2$ *10^{-1}

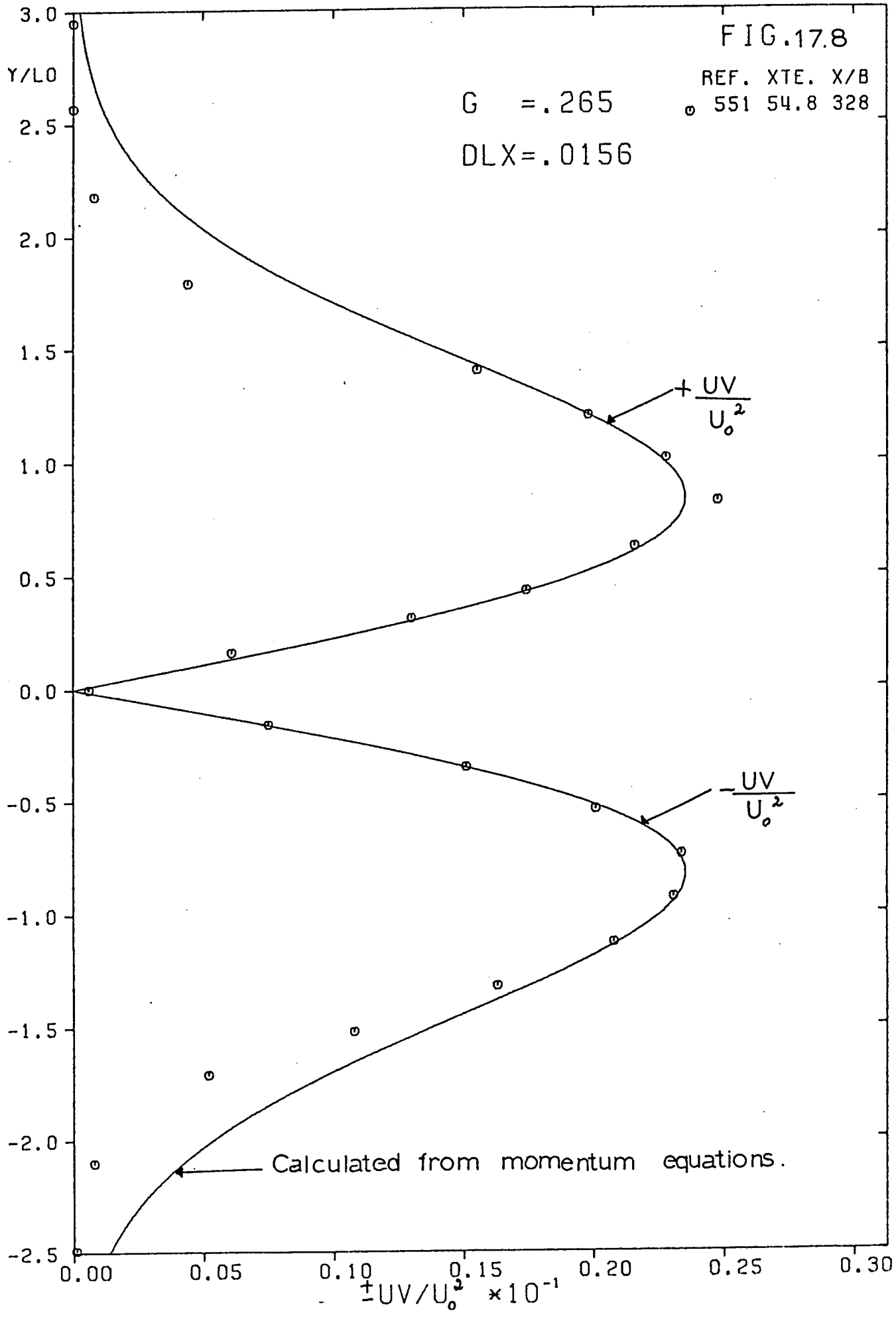
FIG.17.8
REF. XTE. X/B
551 54.8 328
G =.265
DLX=.0156
Y/LO
3.0
2.5
2.0
1.5
1.0
0.5
0.0
-0.5
-1.0
-1.5
-2.0
-2.5
+ UV/U₀²
- UV/U₀²
Calculated from momentum equations.
0.00
0.05
0.10
0.15
0.20
0.25
0.30
±UV/U₀² ×10⁻¹

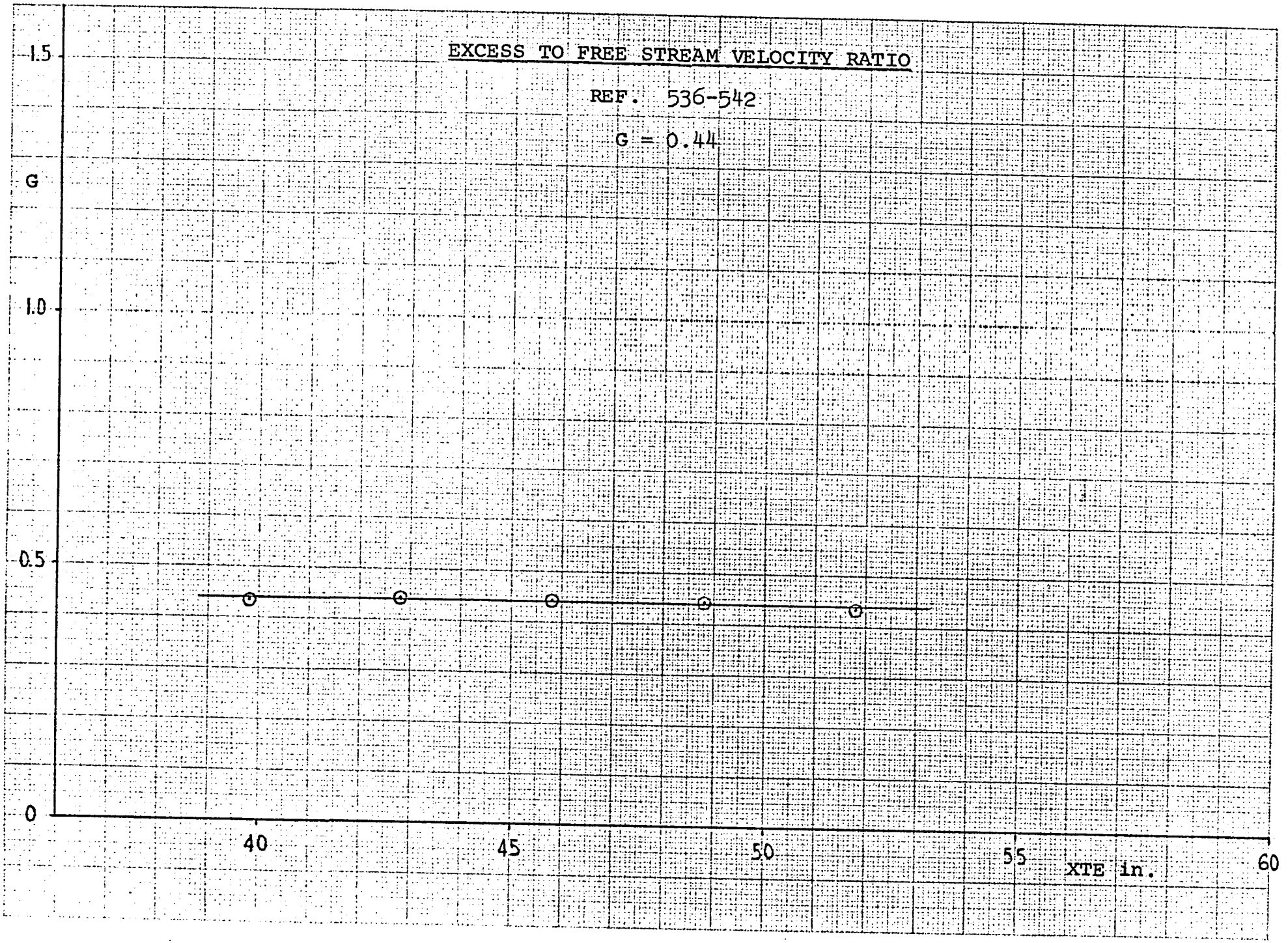
EXCESS TO FREE STREAM VELOCITY RATIO
REF. 536-542
G = 0.44
G
1.5
1.0
0.5
0
40
45
50
55
60
XTE in.

Fig. 18.a

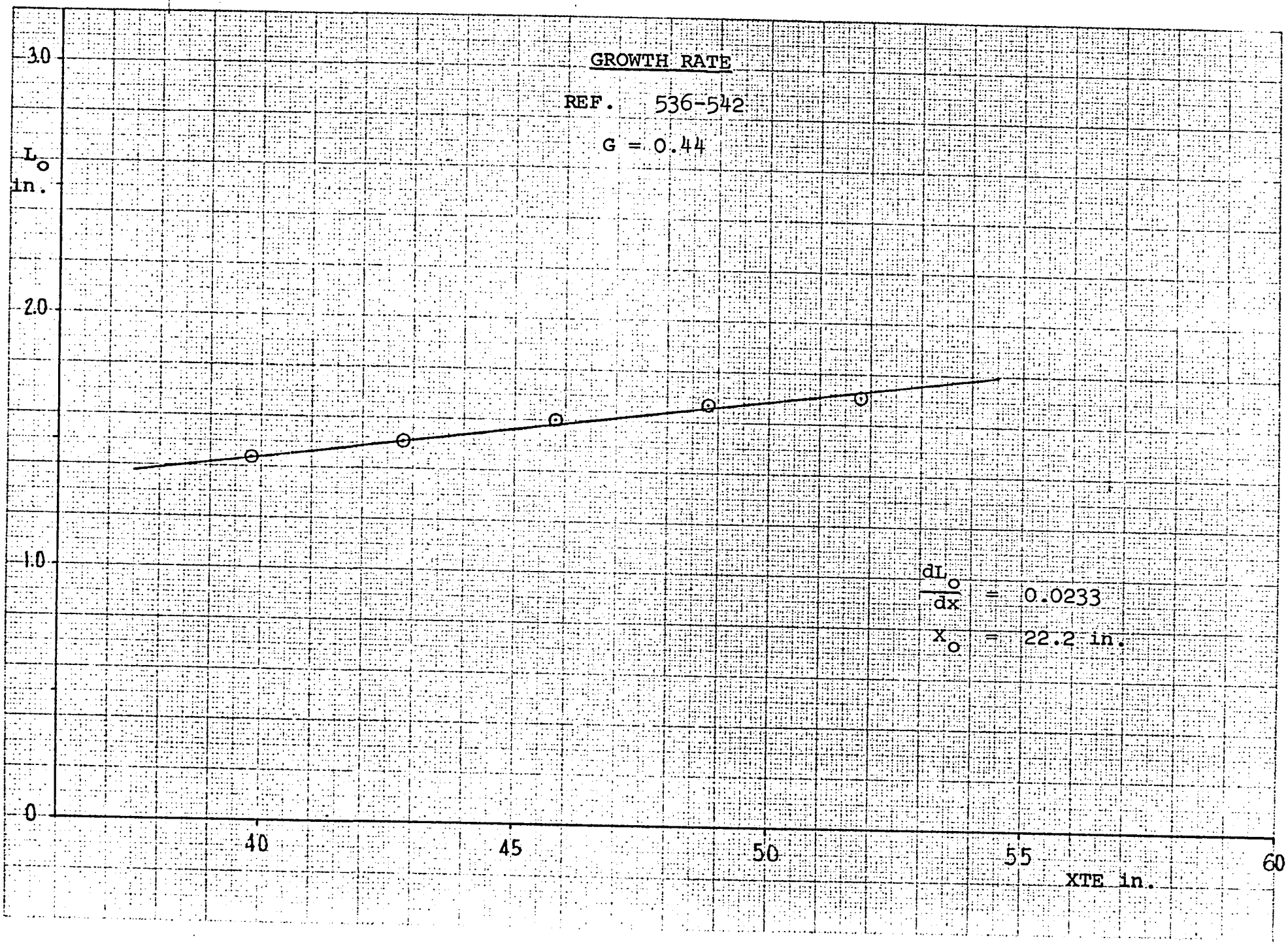
GROWTH RATE
REF. 536-542
G = 0.44
L_o in.
3.0
2.0
1.0
0
40
45
50
55
60
XTE in.
$\frac{dL_o}{dx}$ = 0.0233
x_o = 22.2 in.

Fig. 18.b

VELOCITY DECAY

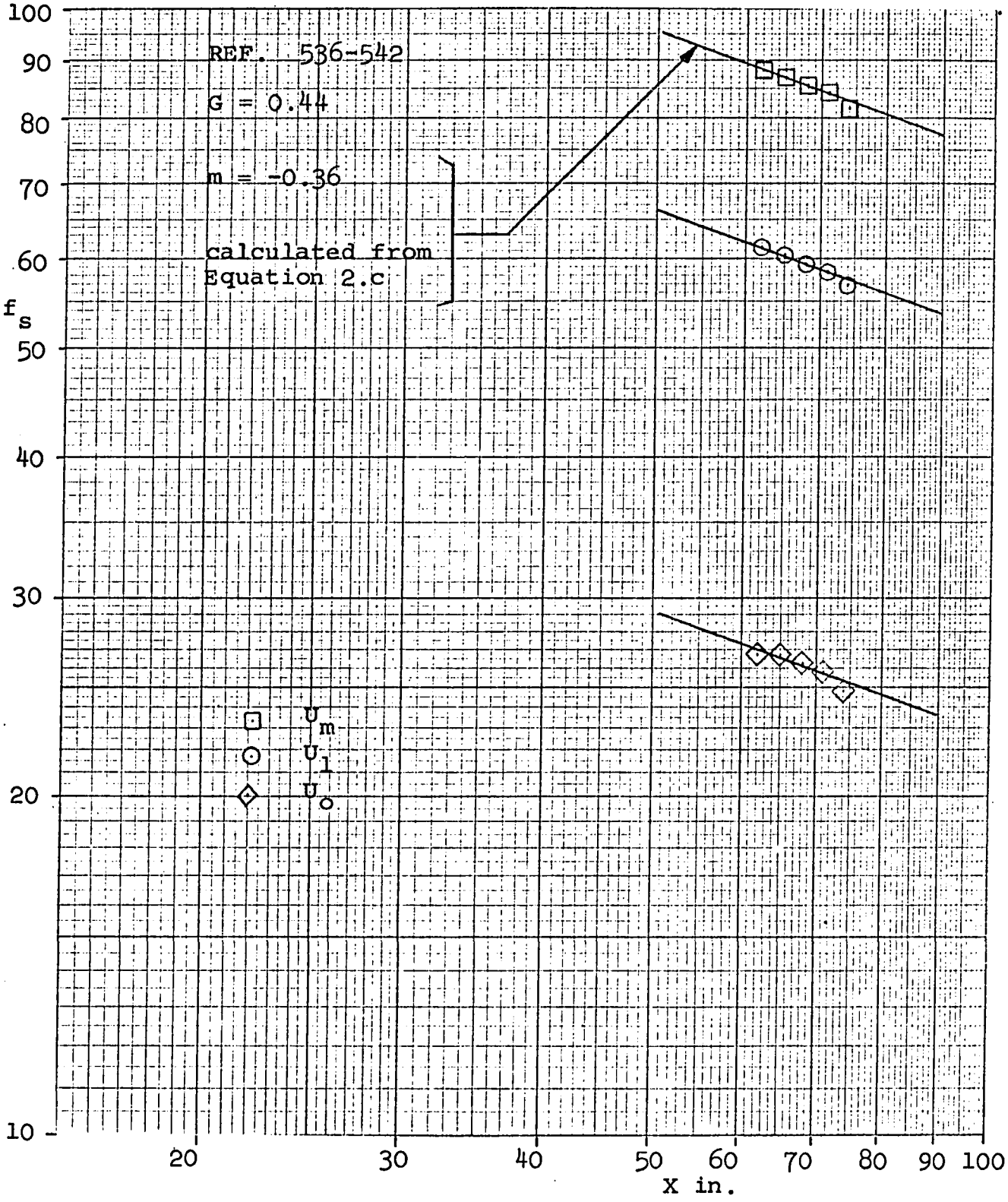

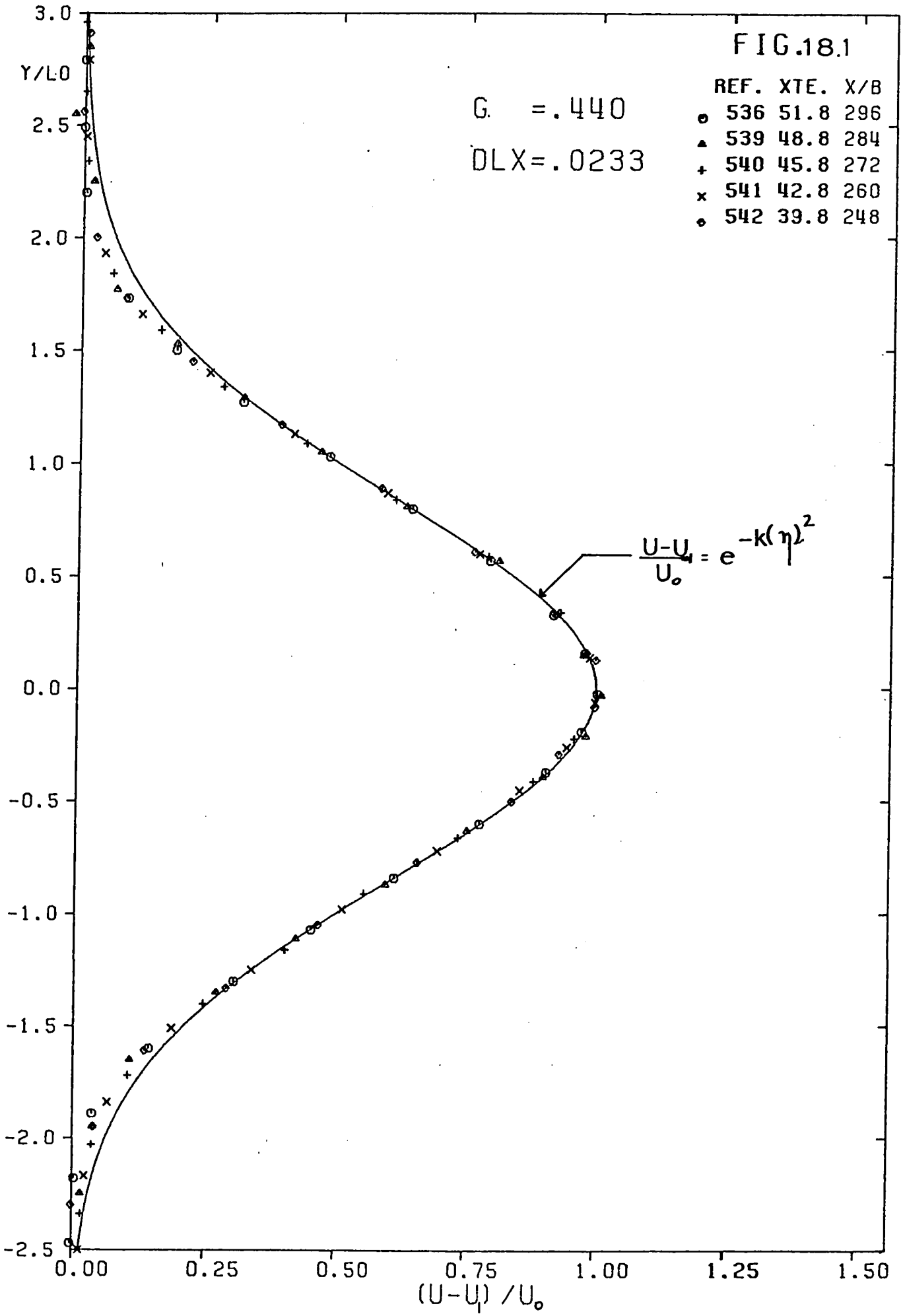
FIG.18.1
G. =.440
DLX=.0233
REF. XTE. X/B
536 51.8 296
539 48.8 284
540 45.8 272
541 42.8 260
542 39.8 248
$\frac{U-U_1}{U_o} = e^{-k(\eta)^2}$
Y/LO
3.0
2.5
2.0
1.5
1.0
0.5
0.0
-0.5
-1.0
-1.5
-2.0
-2.5
0.00
0.25
0.50
0.75
1.00
1.25
1.50
$(U-U_1)/U_o$

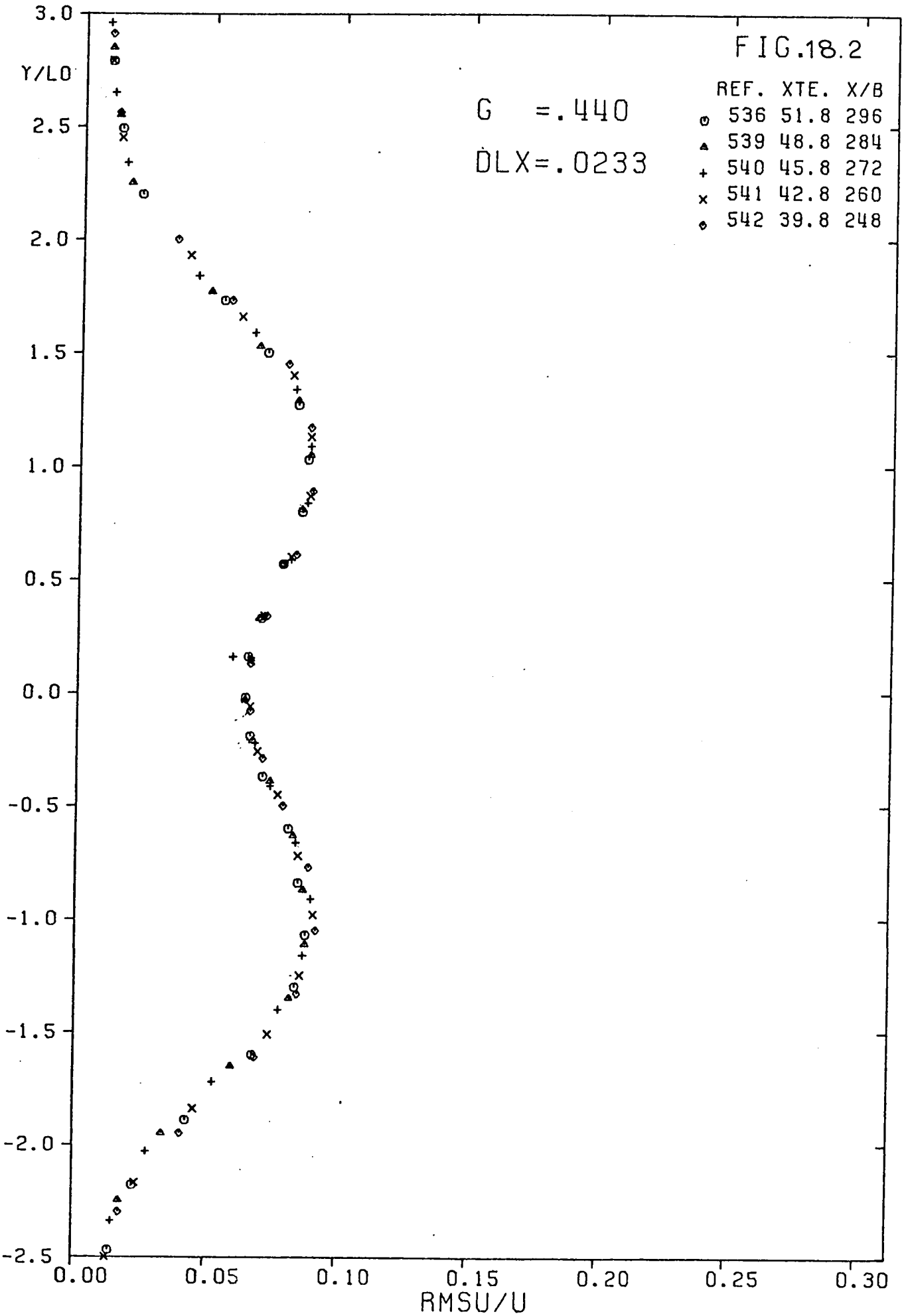
FIG.18.2
G =.440
DLX=.0233
REF. XTE. X/B
536 51.8 296
539 48.8 284
540 45.8 272
541 42.8 260
542 39.8 248
Y/LO
3.0
2.5
2.0
1.5
1.0
0.5
0.0
-0.5
-1.0
-1.5
-2.0
-2.5
0.00
0.05
0.10
0.15
0.20
0.25
0.30
RMSU/U

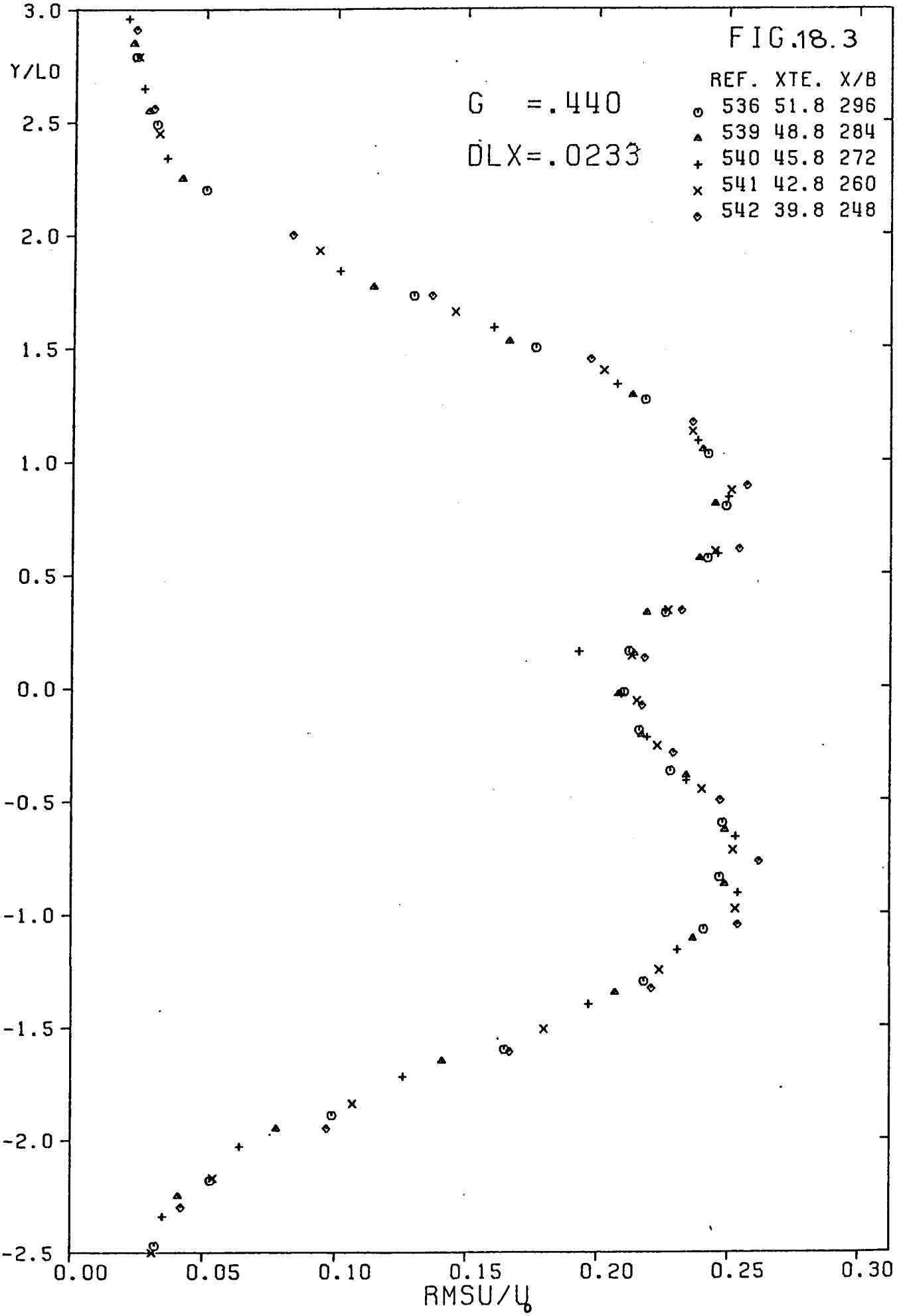
FIG.18.3
G =.440
DLX=.0233
REF. XTE. X/B
536 51.8 296
539 48.8 284
540 45.8 272
541 42.8 260
542 39.8 248
Y/LO
RMSU/U0
3.0
2.5
2.0
1.5
1.0
0.5
0.0
-0.5
-1.0
-1.5
-2.0
-2.5
0.00
0.05
0.10
0.15
0.20
0.25
0.30

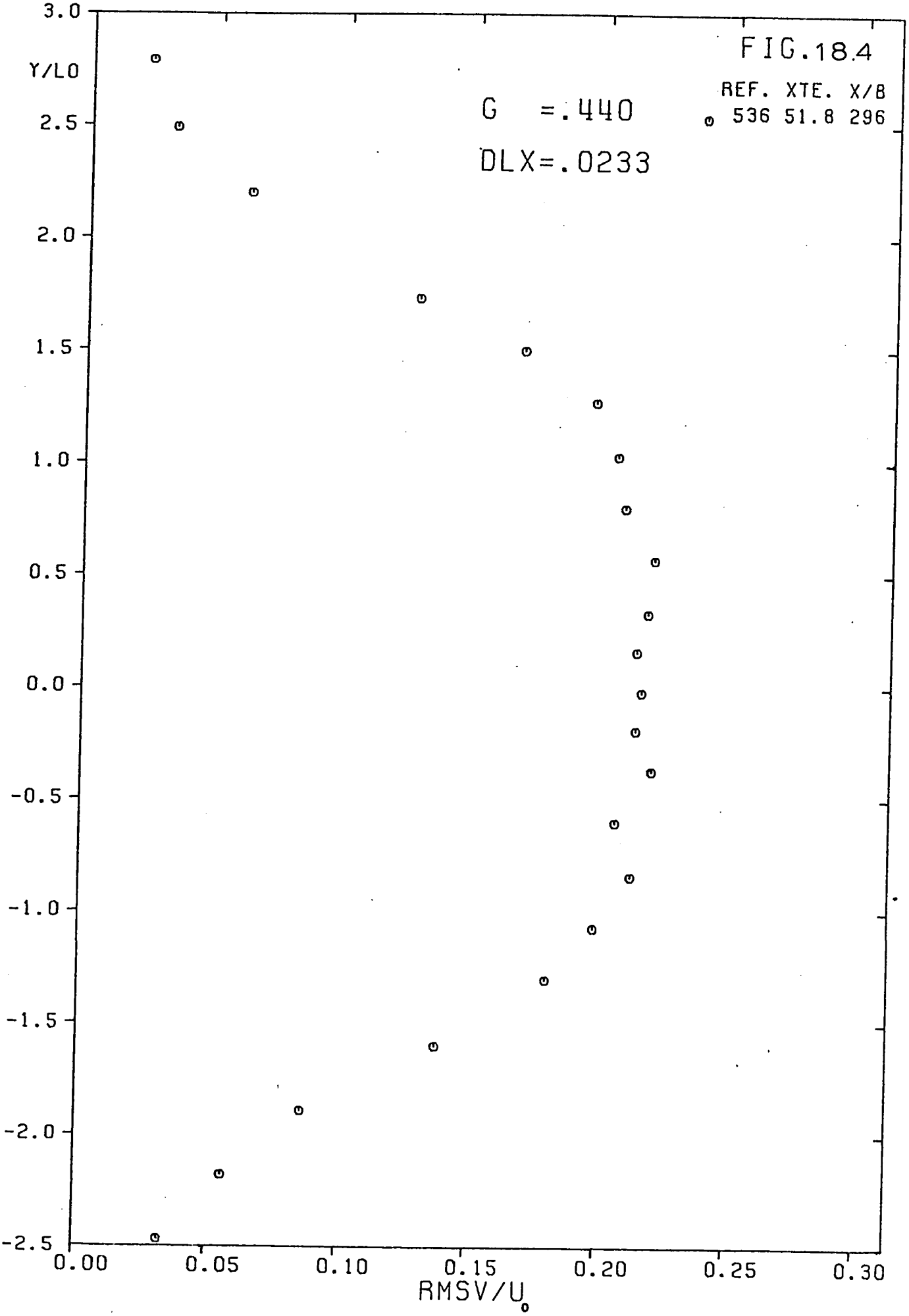
FIG.18.4
REF. XTE. X/B
536 51.8 296
G =.440
DLX=.0233
Y/LO
3.0
2.5
2.0
1.5
1.0
0.5
0.0
-0.5
-1.0
-1.5
-2.0
-2.5
0.00
0.05
0.10
0.15
0.20
0.25
0.30
RMSV/U0

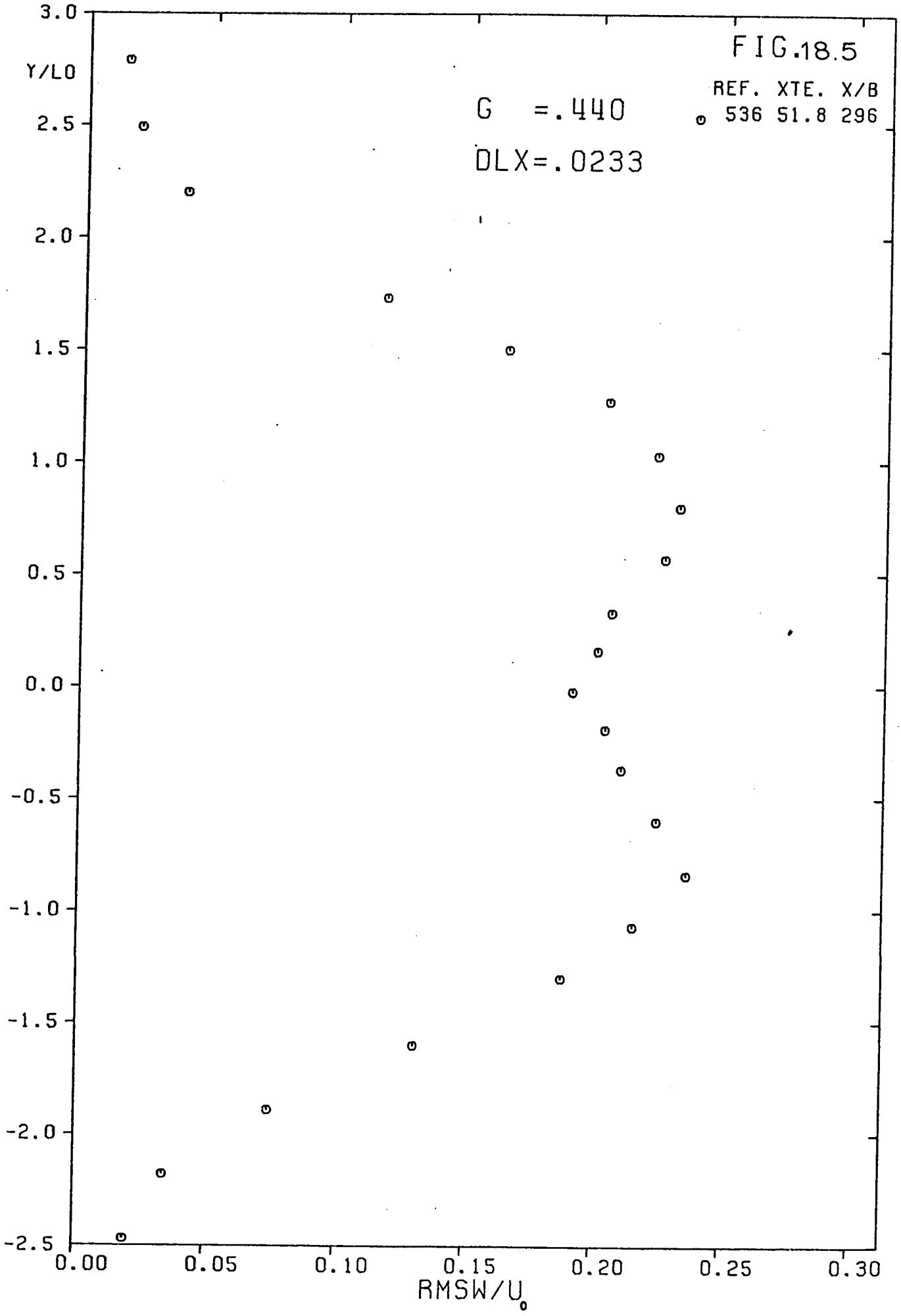
FIG.18.5
REF. XTE. X/B
536 51.8 296
G =.440
DLX=.0233
Y/LO
3.0
2.5
2.0
1.5
1.0
0.5
0.0
-0.5
-1.0
-1.5
-2.0
-2.5
0.00
0.05
0.10
0.15
0.20
0.25
0.30
RMSW/U0

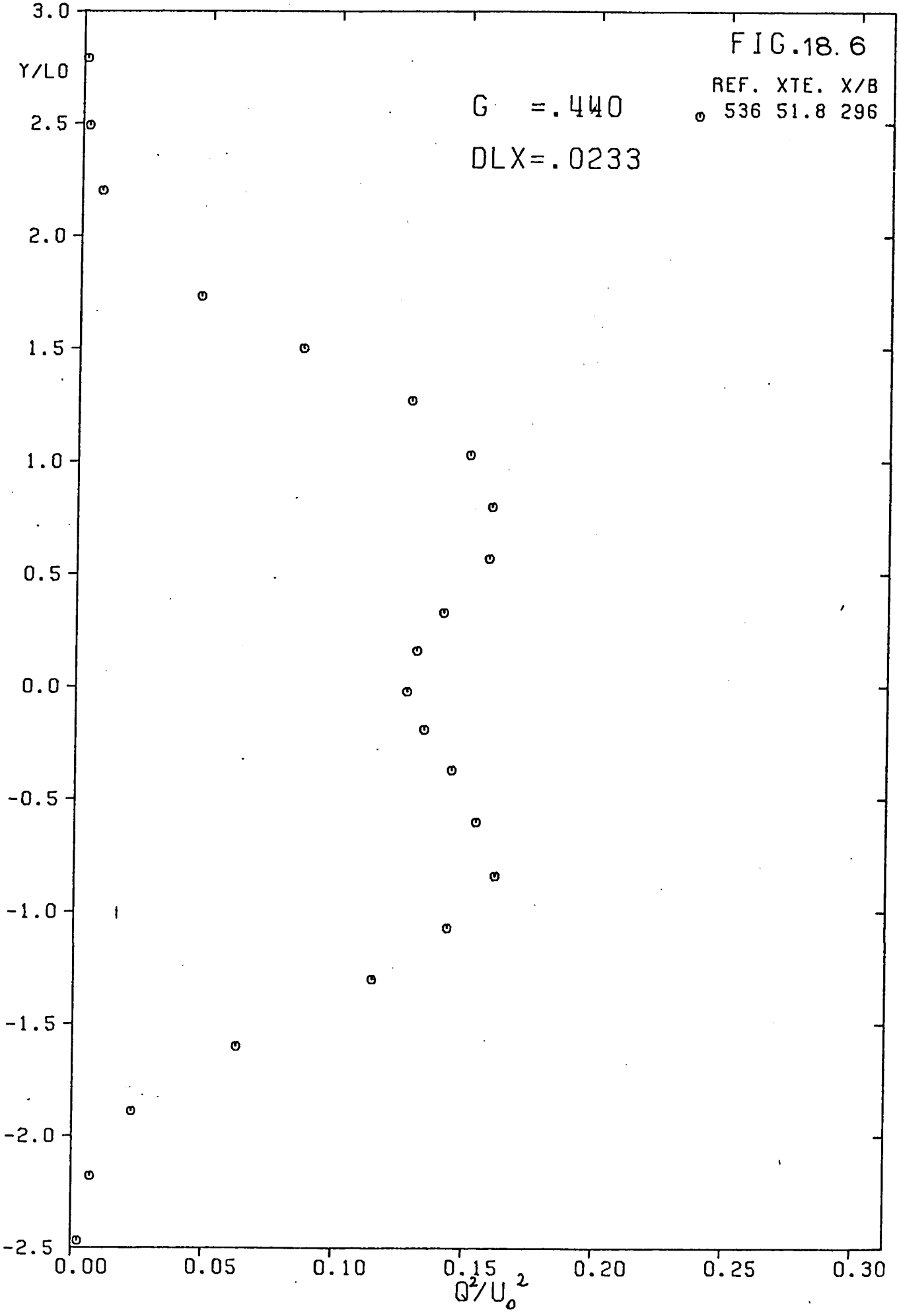
FIG.18.6
REF. XTE. X/B
536 51.8 296
G =.440
DLX=.0233
Y/LO
3.0
2.5
2.0
1.5
1.0
0.5
0.0
-0.5
-1.0
-1.5
-2.0
-2.5
0.00
0.05
0.10
0.15
0.20
0.25
0.30
Q^2/U_o^2

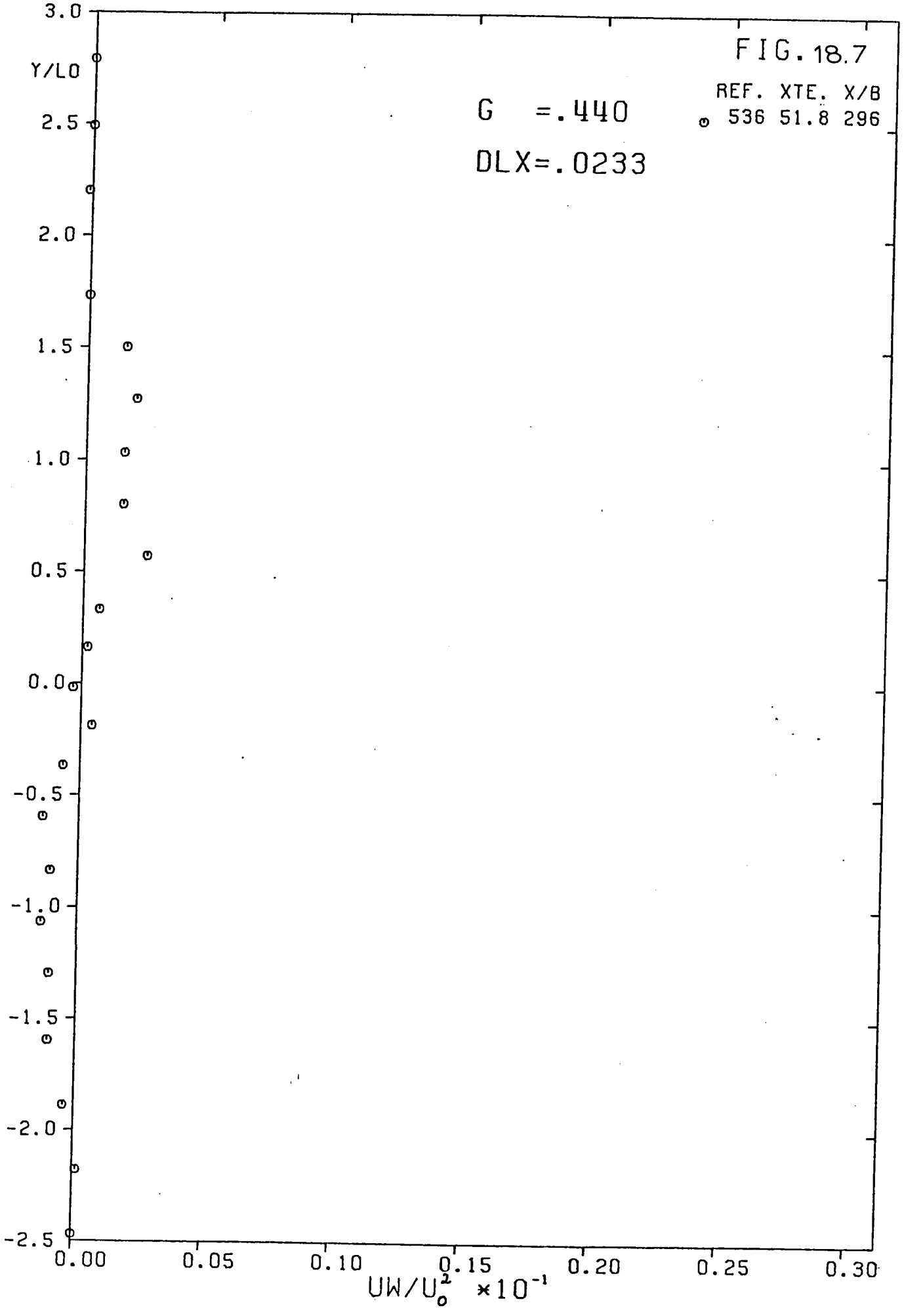
FIG. 18.7
REF. XTE. X/B
536 51.8 296
G =.440
DLX=.0233
Y/LO
3.0
2.5
2.0
1.5
1.0
0.5
0.0
-0.5
-1.0
-1.5
-2.0
-2.5
0.00
0.05
0.10
0.15
0.20
0.25
0.30
UW/U$_o^2$ *10^{-1}

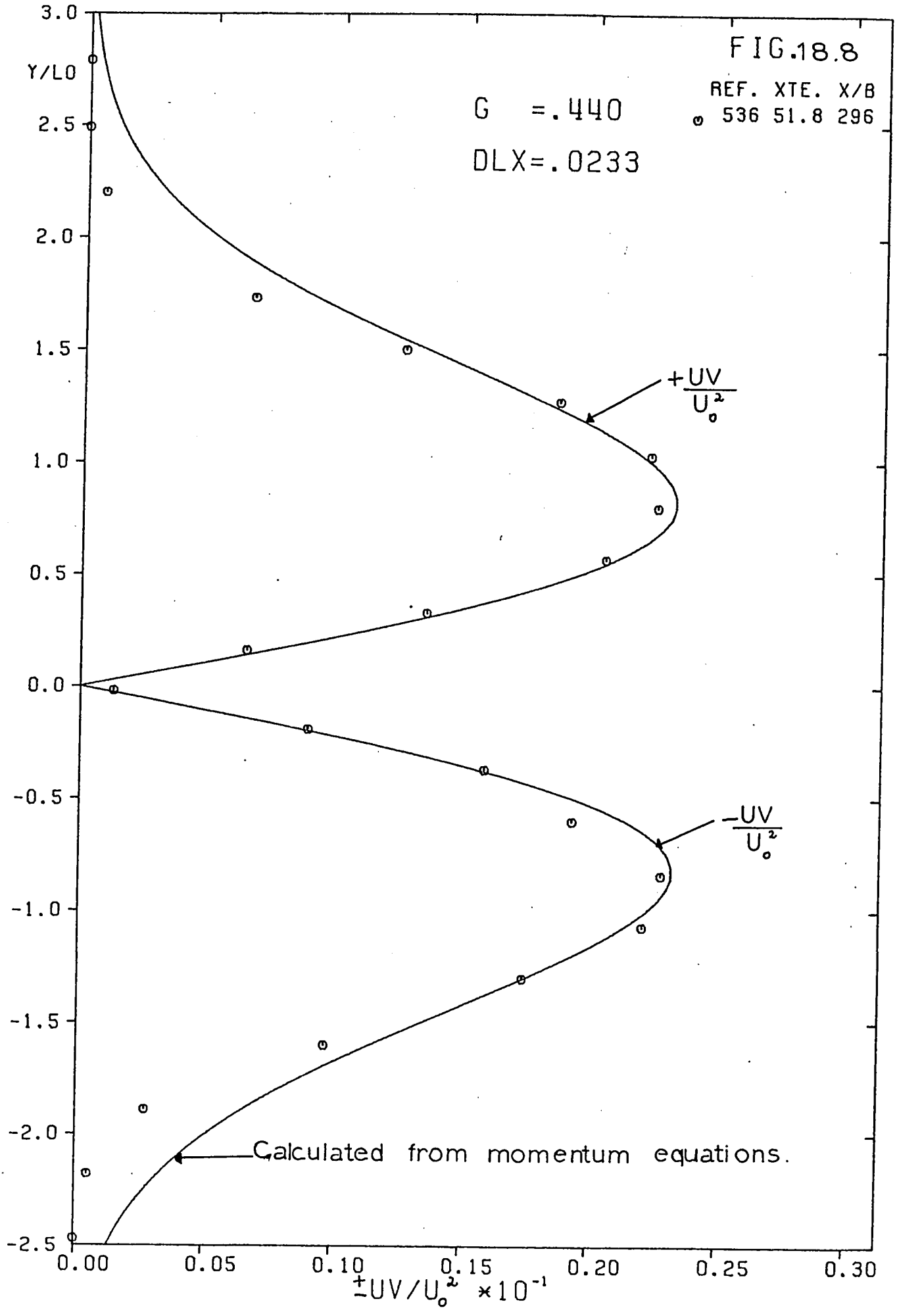
FIG.18.8
REF. XTE. X/B
536 51.8 296
G =.440
DLX=.0233
Y/LO
3.0
2.5
2.0
1.5
1.0
0.5
0.0
-0.5
-1.0
-1.5
-2.0
-2.5
+UV/U₀²
-UV/U₀²
Calculated from momentum equations.
0.00
0.05
0.10
0.15
0.20
0.25
0.30
±UV/U₀² ×10⁻¹

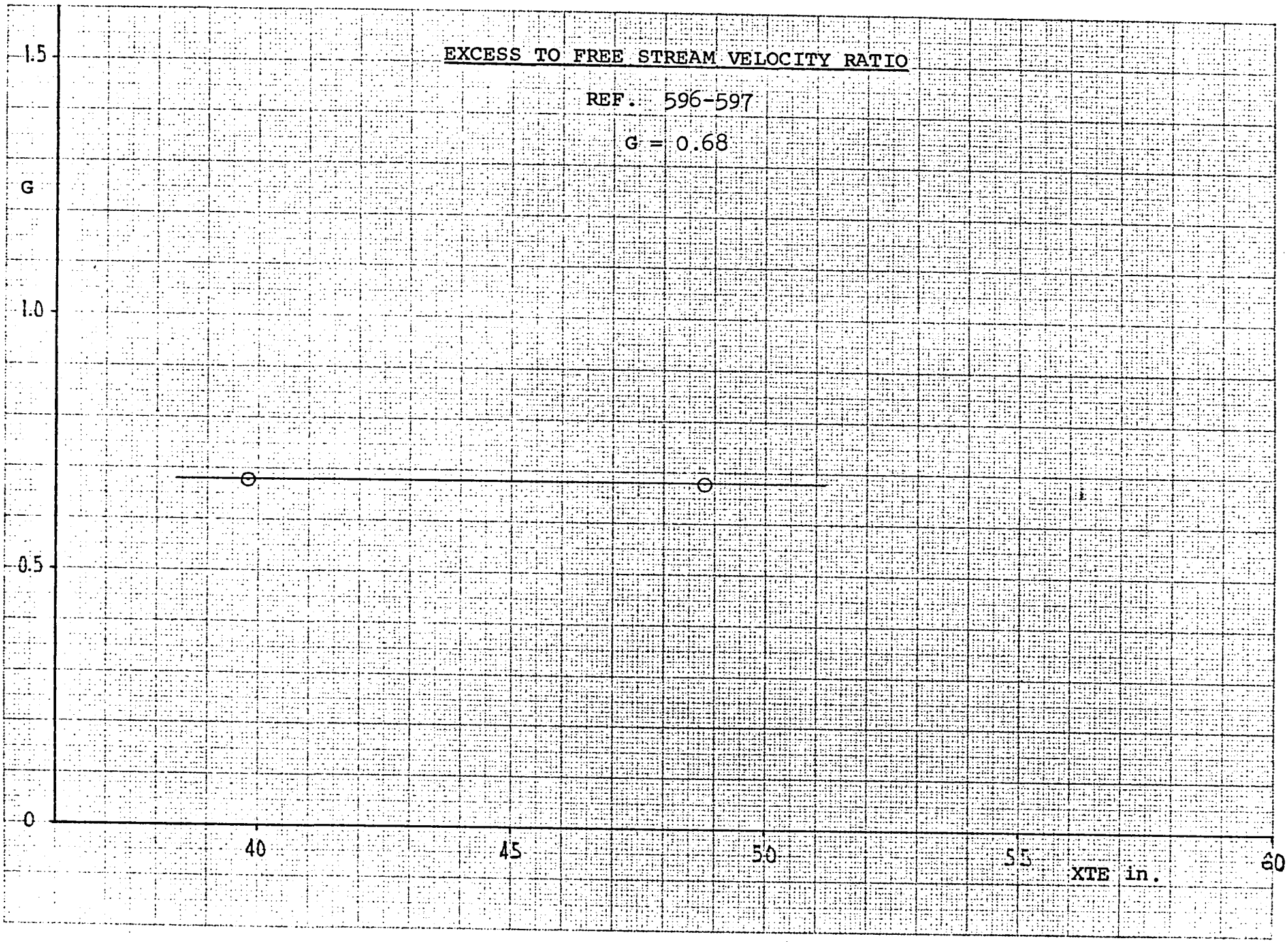
EXCESS TO FREE STREAM VELOCITY RATIO
REF. 596-597
G = 0.68
G
1.5
1.0
0.5
0
40
45
50
55
60
XTE in.

Fig. 19.a

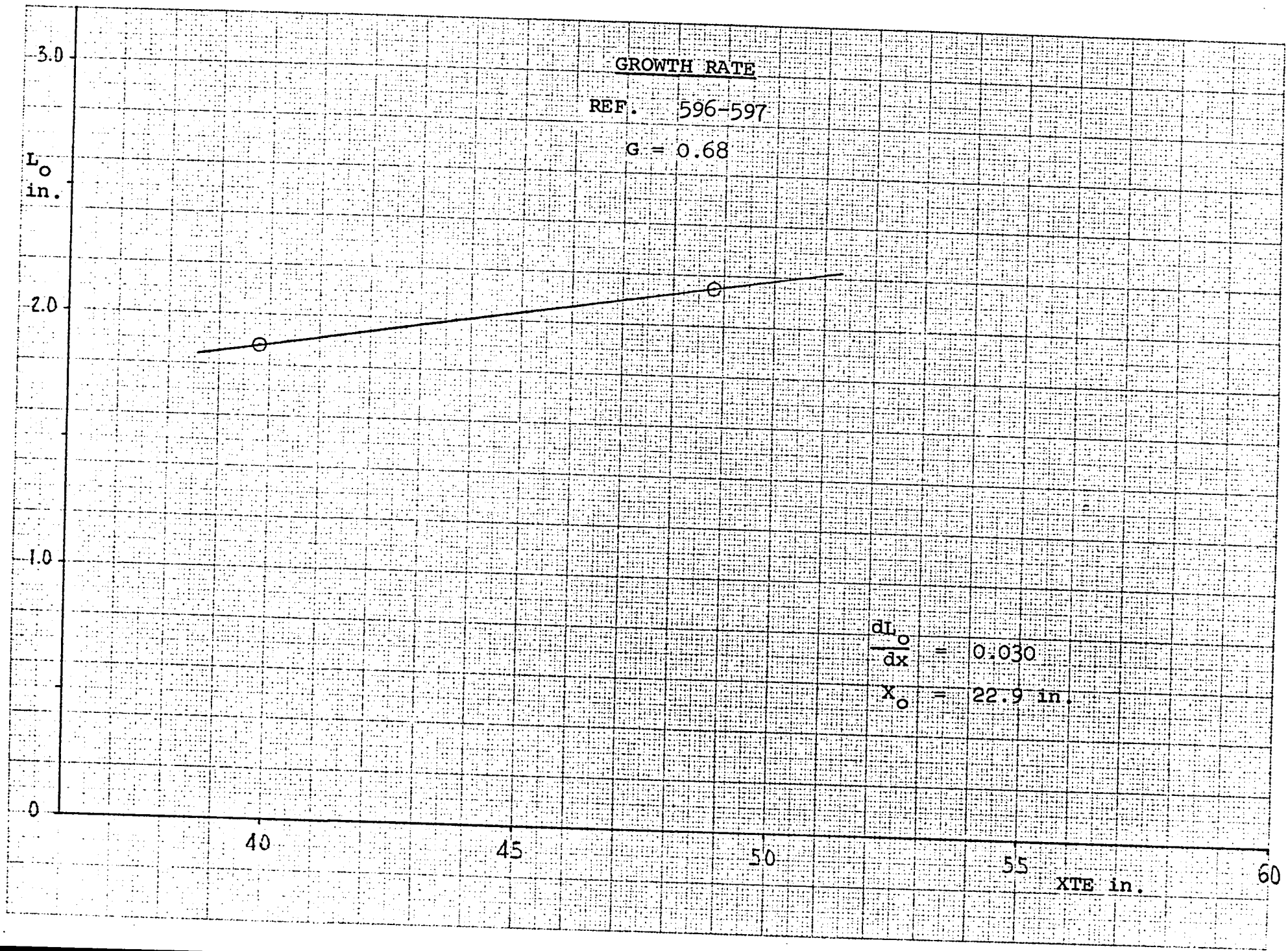
GROWTH RATE
REF. 596-597
G = 0.68
L_o in.
3.0
2.0
1.0
0
40
45
50
55
60
XTE in.
$\frac{dL_o}{dx}$ = 0.030
x_o = 22.9 in.

Fig. 19.b

VELOCITY DECAY

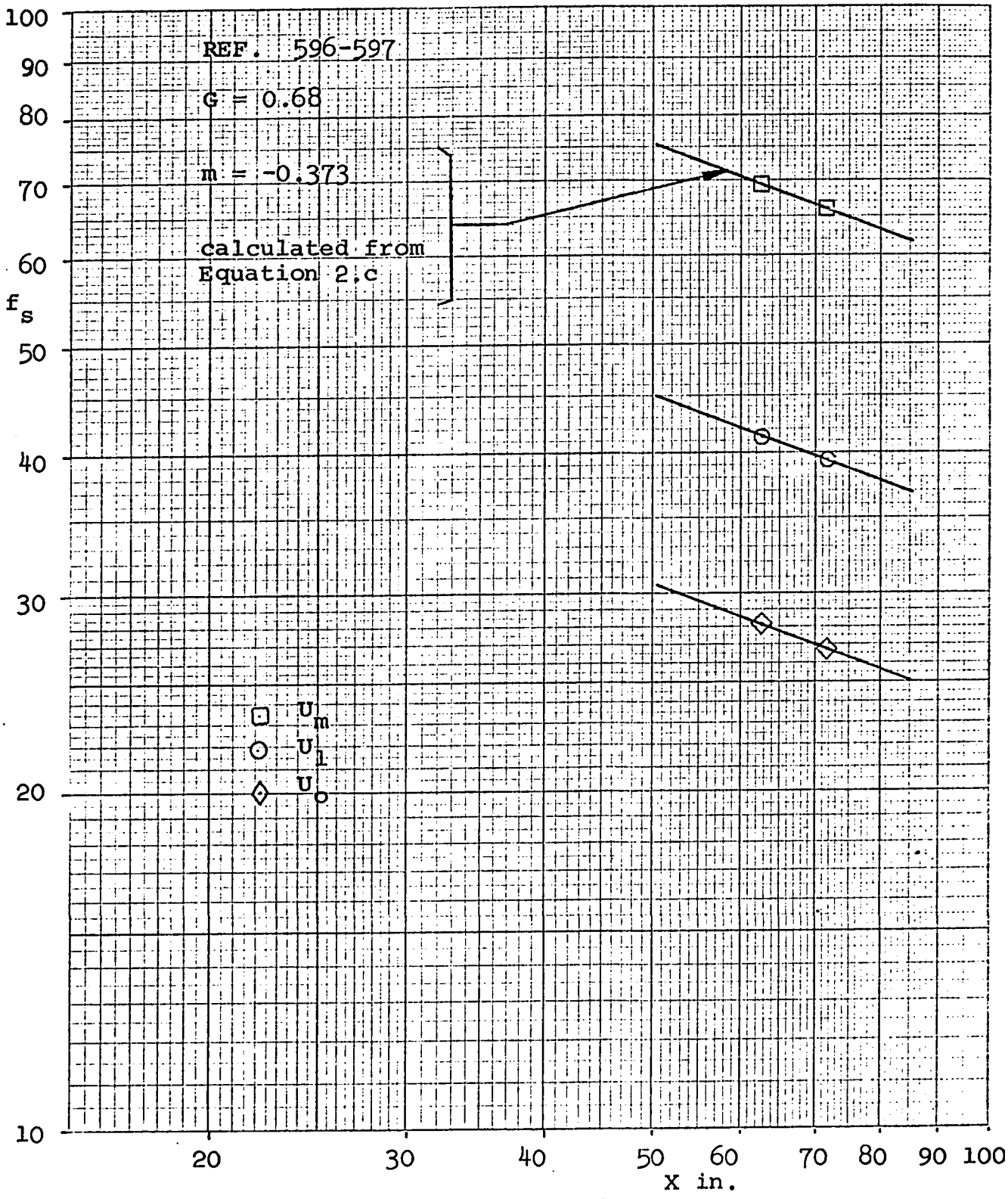

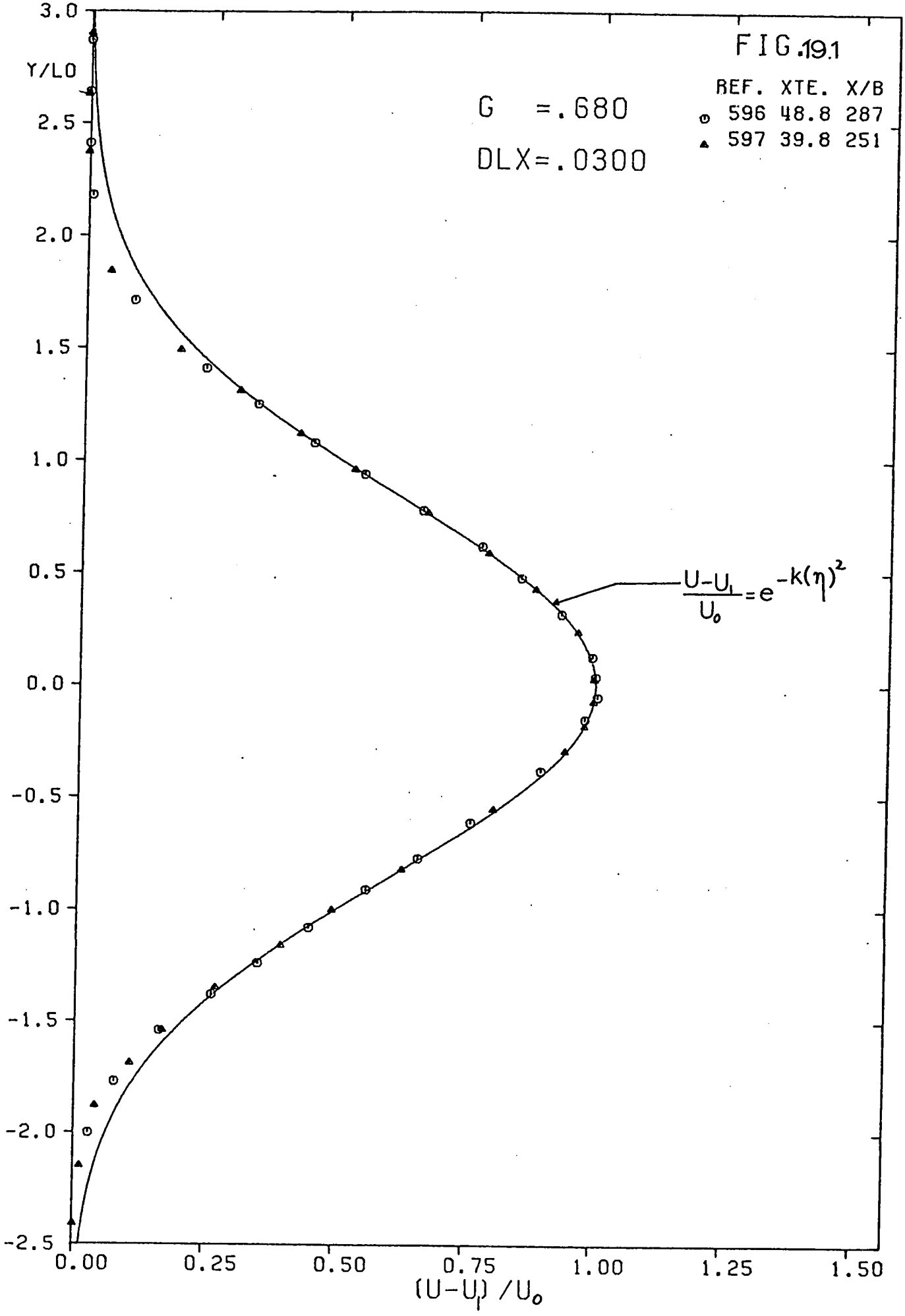
FIG.19.1
REF. XTE. X/B
596 48.8 287
597 39.8 251
G =.680
DLX=.0300
$\frac{U-U_1}{U_0} = e^{-k(\eta)^2}$
Y/LO
3.0
2.5
2.0
1.5
1.0
0.5
0.0
-0.5
-1.0
-1.5
-2.0
-2.5
0.00
0.25
0.50
0.75
1.00
1.25
1.50
$(U-U_1)/U_0$

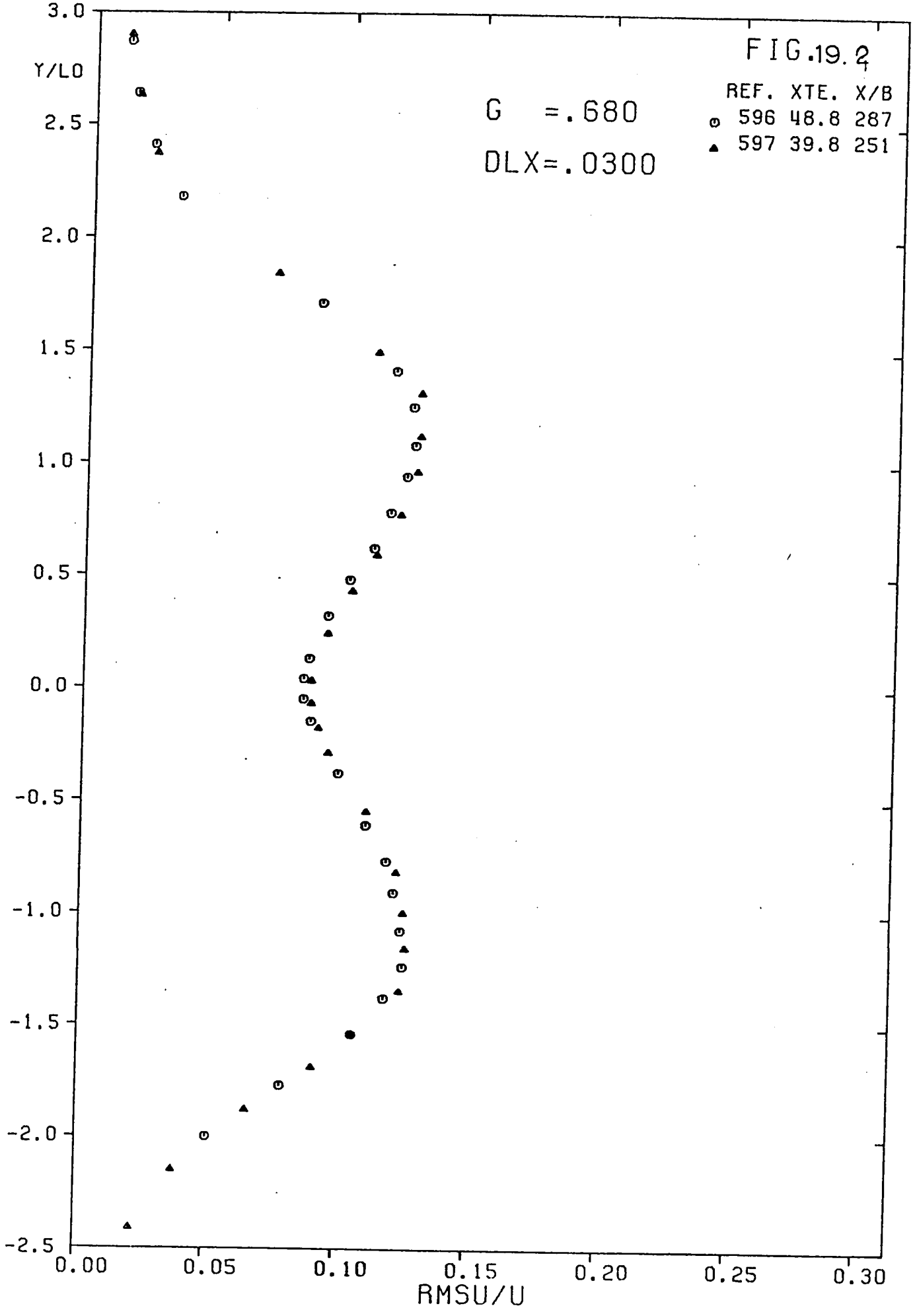
FIG.19.2
REF. XTE. X/B
596 48.8 287
597 39.8 251
G =.680
DLX=.0300
Y/LO
RMSU/U
3.0
2.5
2.0
1.5
1.0
0.5
0.0
-0.5
-1.0
-1.5
-2.0
-2.5
0.00
0.05
0.10
0.15
0.20
0.25
0.30

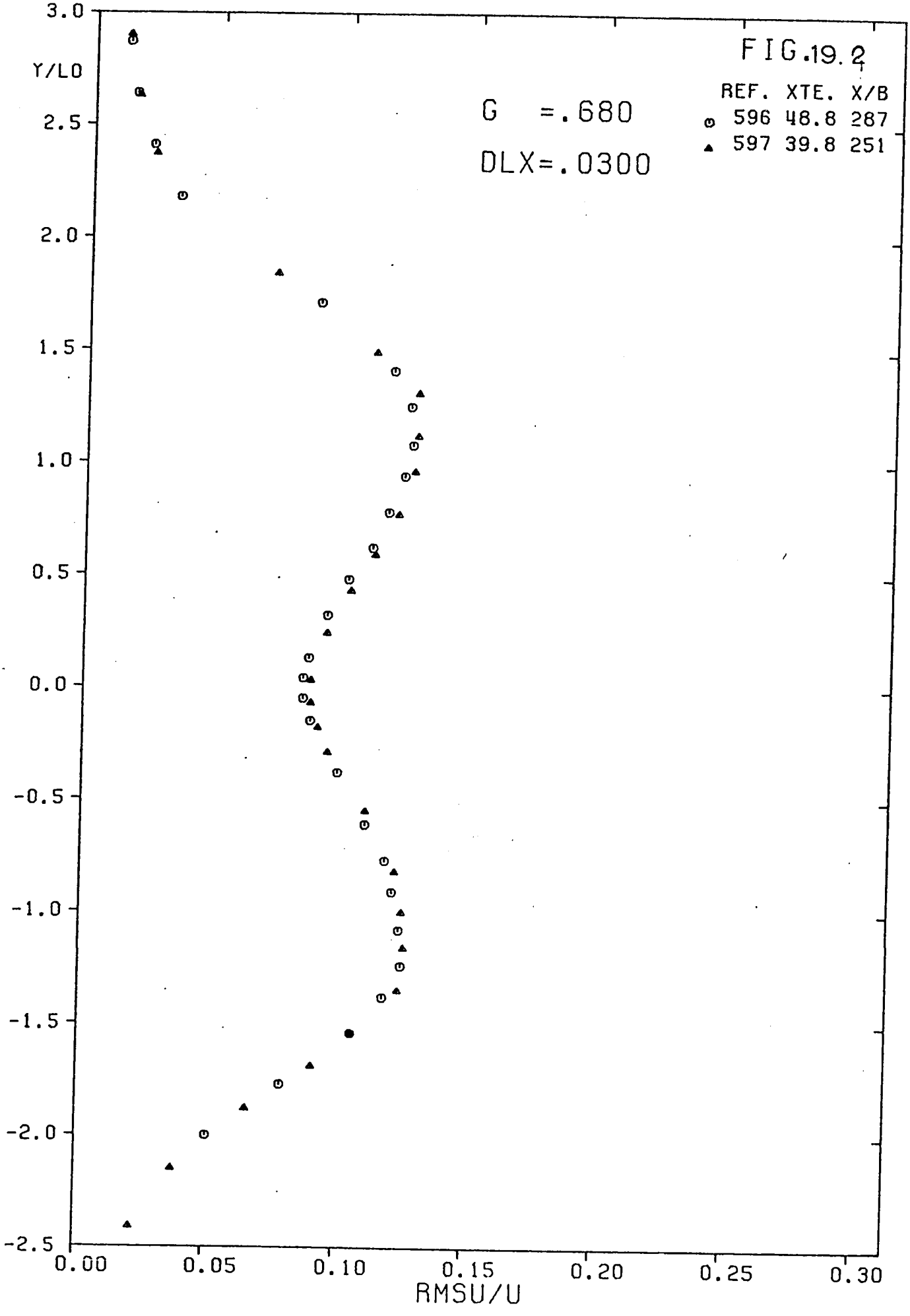
FIG.19.2
REF. XTE. X/B
596 48.8 287
597 39.8 251
G =.680
DLX=.0300
Y/LO
RMSU/U
3.0
2.5
2.0
1.5
1.0
0.5
0.0
-0.5
-1.0
-1.5
-2.0
-2.5
0.00
0.05
0.10
0.15
0.20
0.25
0.30

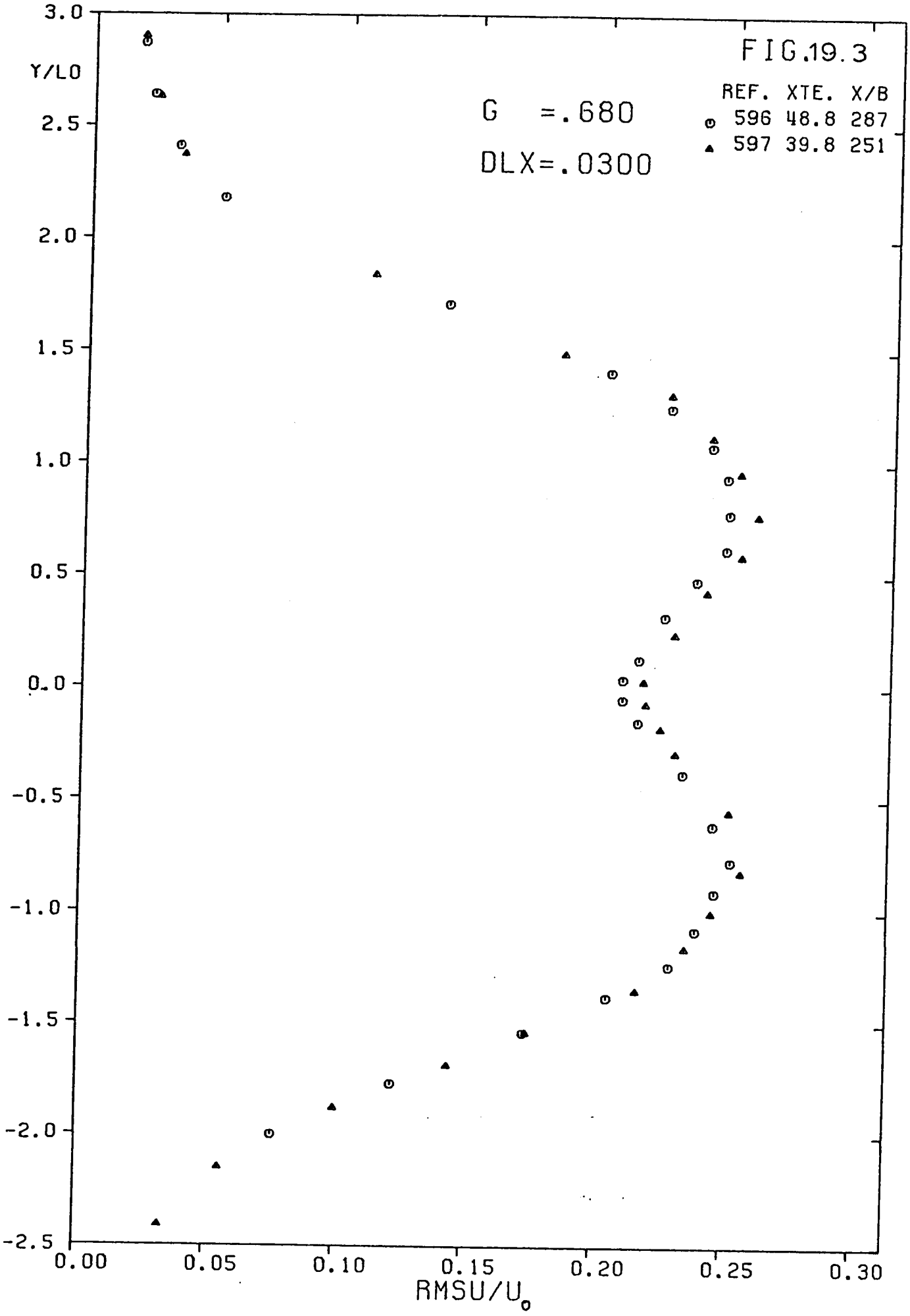
FIG.19.3
G =.680
DLX=.0300
REF. XTE. X/B
596 48.8 287
597 39.8 251
Y/LO
3.0
2.5
2.0
1.5
1.0
0.5
0.0
-0.5
-1.0
-1.5
-2.0
-2.5
0.00
0.05
0.10
0.15
0.20
0.25
0.30
RMSU/U0

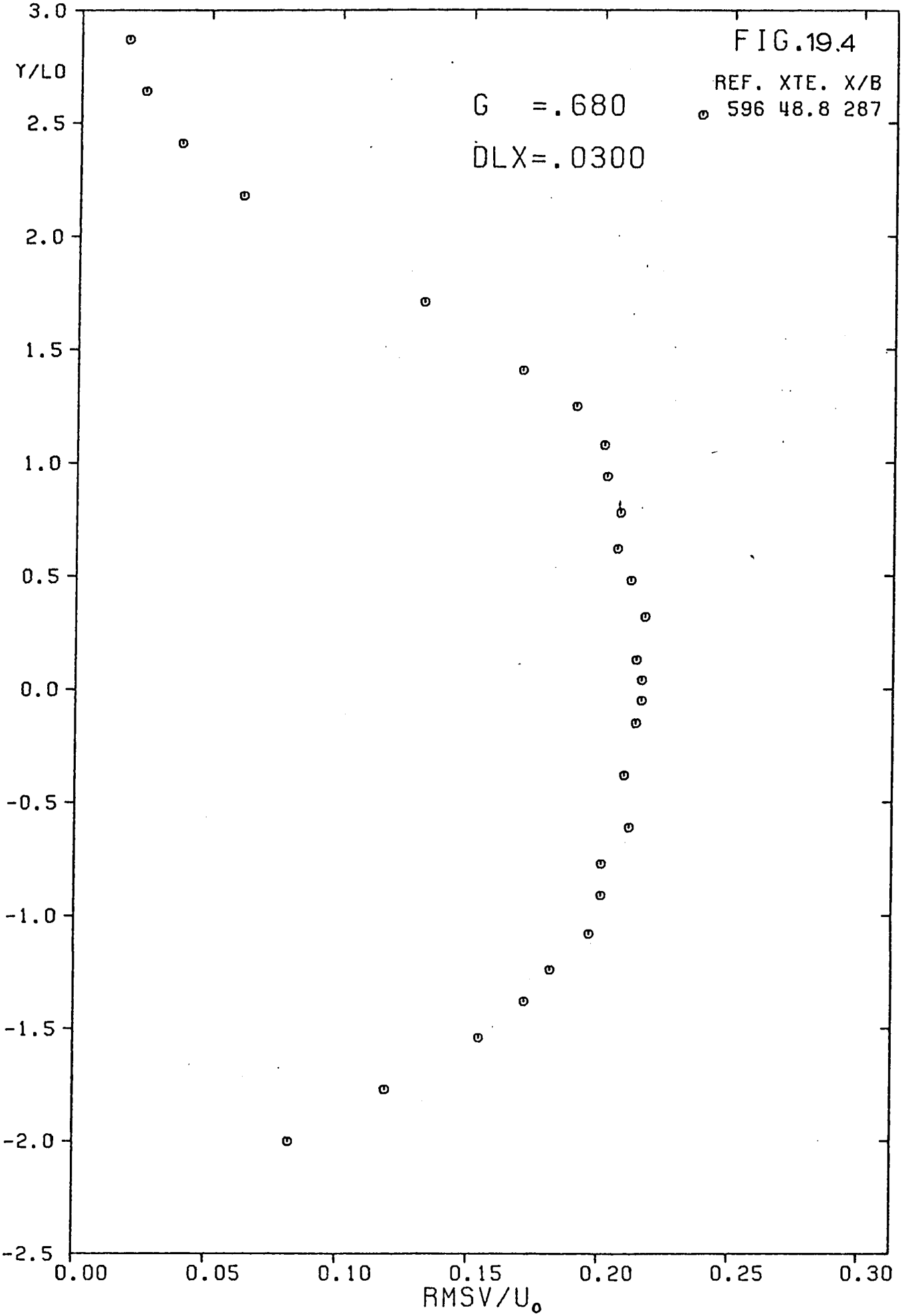
FIG.19.4
REF. XTE. X/B
596 48.8 287
G =.680
DLX=.0300
Y/LO
3.0
2.5
2.0
1.5
1.0
0.5
0.0
-0.5
-1.0
-1.5
-2.0
-2.5
0.00
0.05
0.10
0.15
0.20
0.25
0.30
RMSV/U0

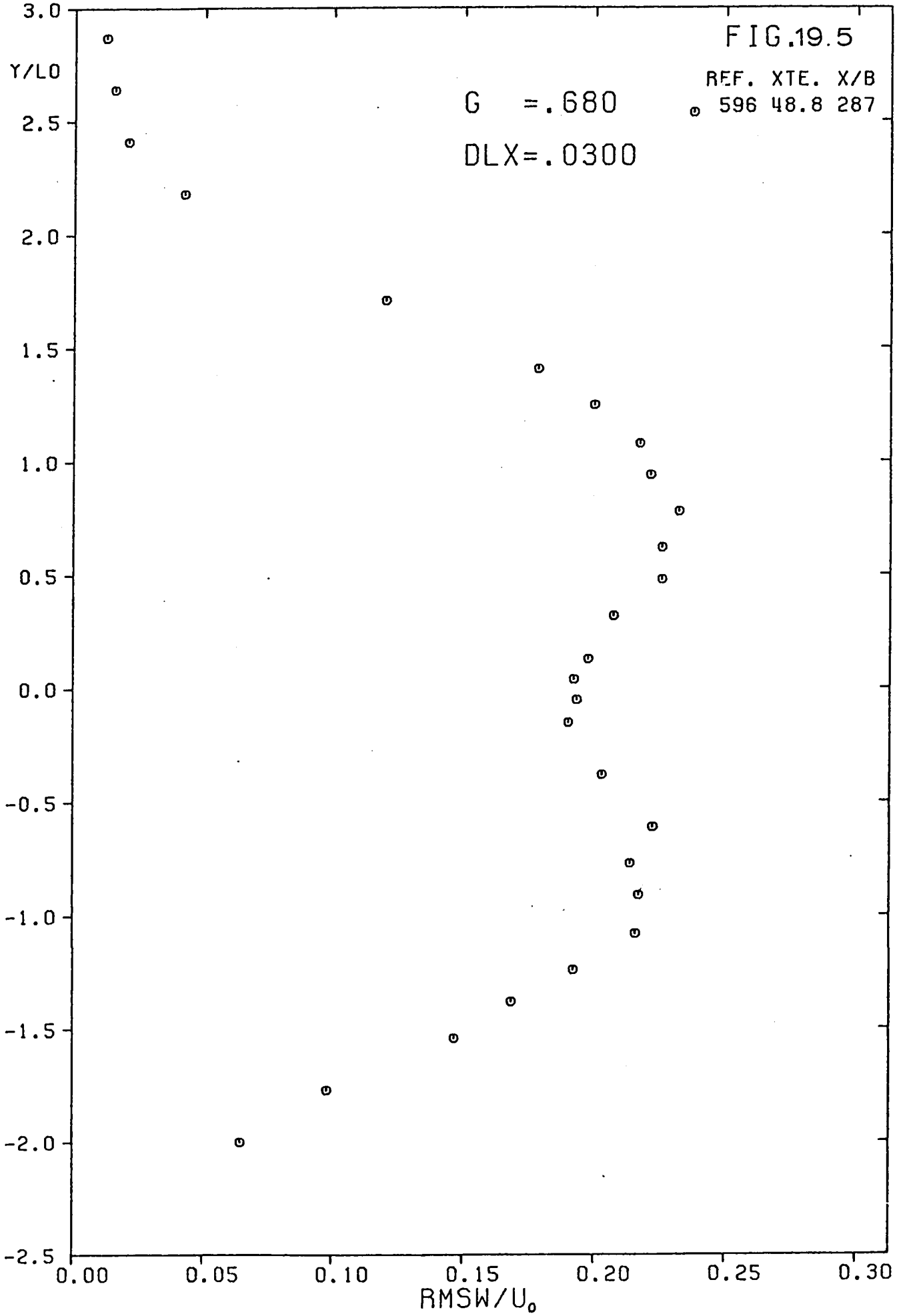
FIG.19.5
REF. XTE. X/B
596 48.8 287
G =.680
DLX=.0300
Y/LO
3.0
2.5
2.0
1.5
1.0
0.5
0.0
-0.5
-1.0
-1.5
-2.0
-2.5
0.00
0.05
0.10
0.15
0.20
0.25
0.30
RMSW/U0

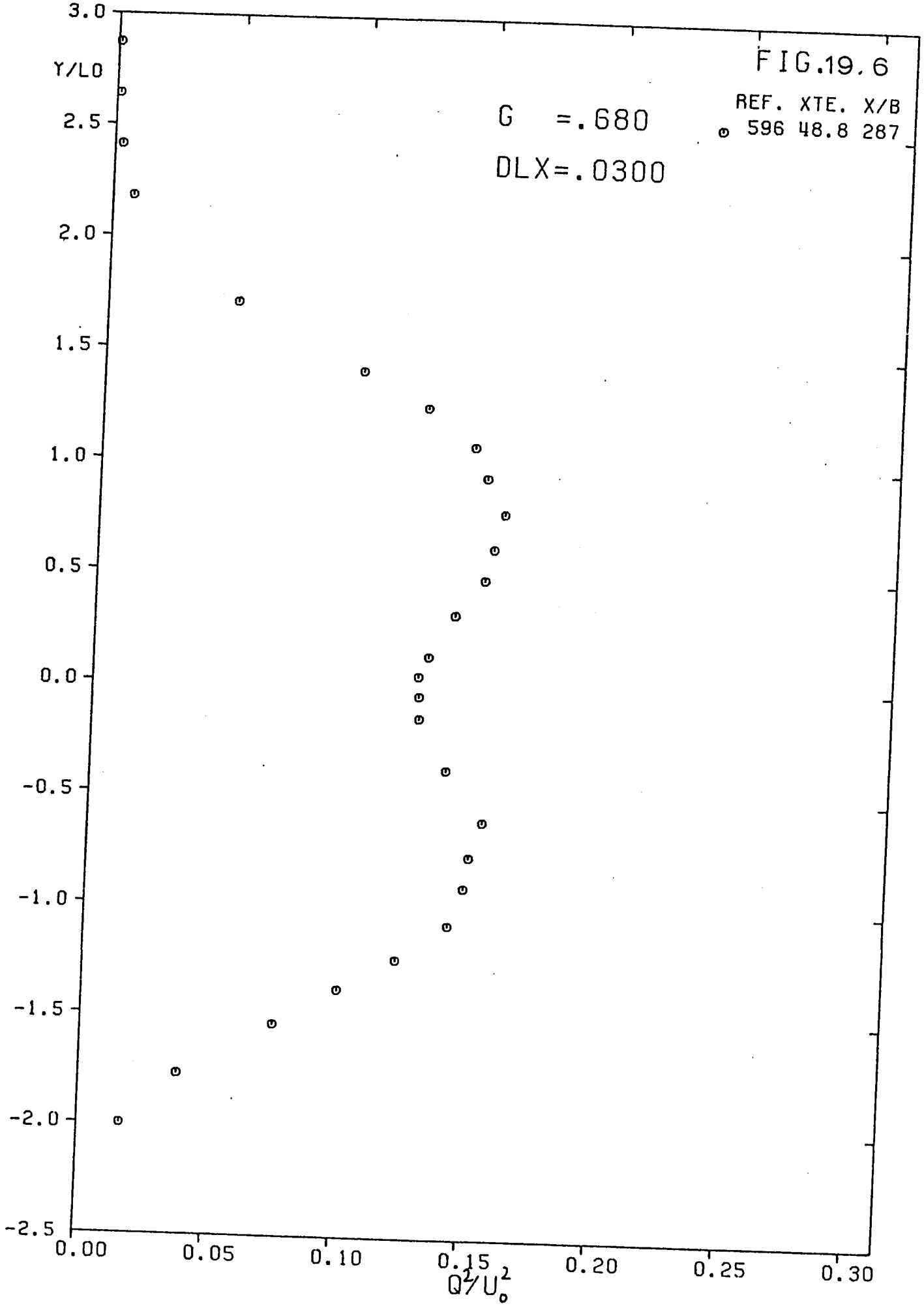
FIG.19.6
REF. XTE. X/B
596 48.8 287
G =.680
DLX=.0300
Y/LO
3.0
2.5
2.0
1.5
1.0
0.5
0.0
-0.5
-1.0
-1.5
-2.0
-2.5
0.00
0.05
0.10
0.15
0.20
0.25
0.30
Q^2/U_o^2

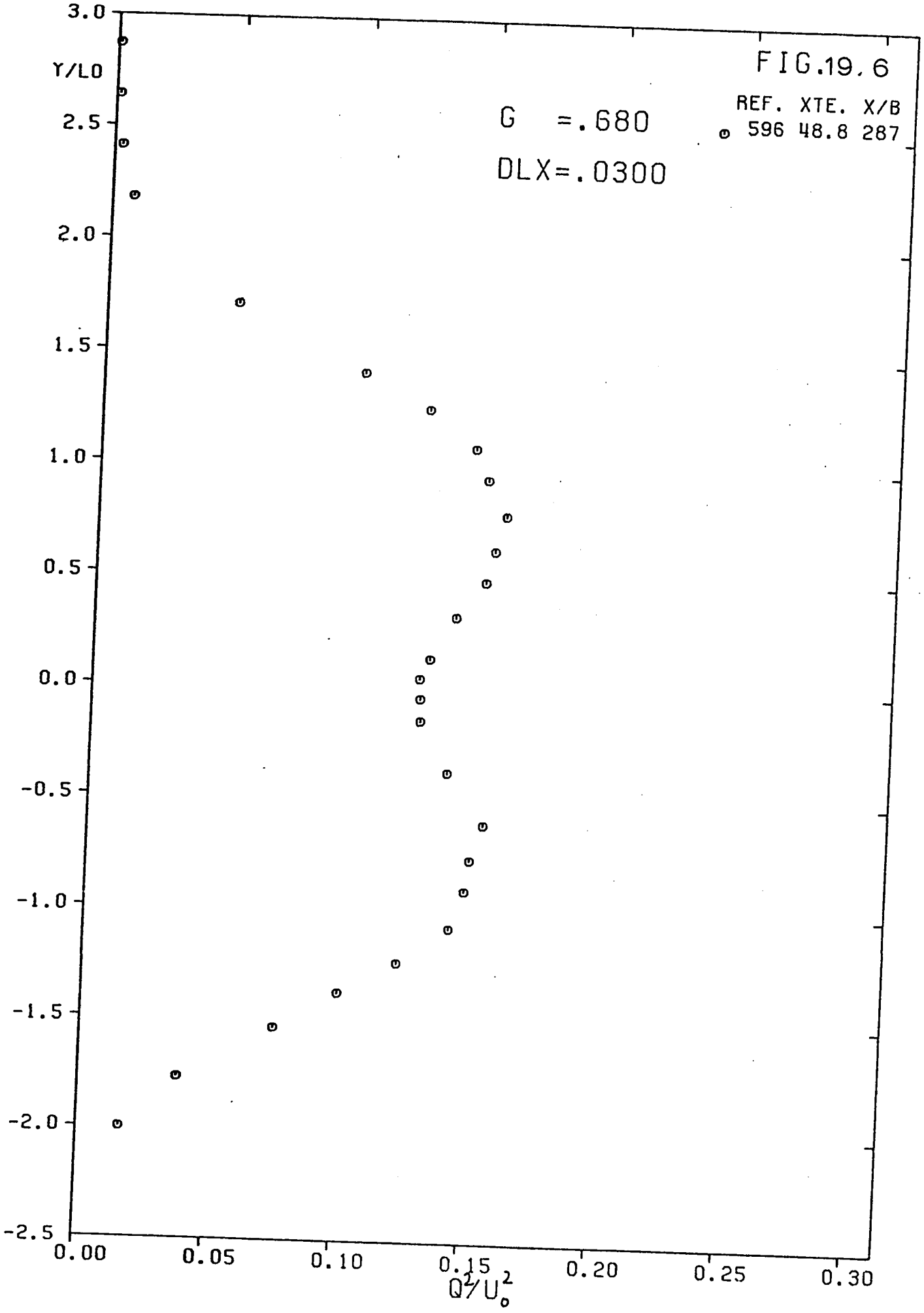
FIG.19.6
REF. XTE. X/B
596 48.8 287
G =.680
DLX=.0300
Y/LO
3.0
2.5
2.0
1.5
1.0
0.5
0.0
-0.5
-1.0
-1.5
-2.0
-2.5
0.00
0.05
0.10
0.15
0.20
0.25
0.30
Q^2/U_o^2

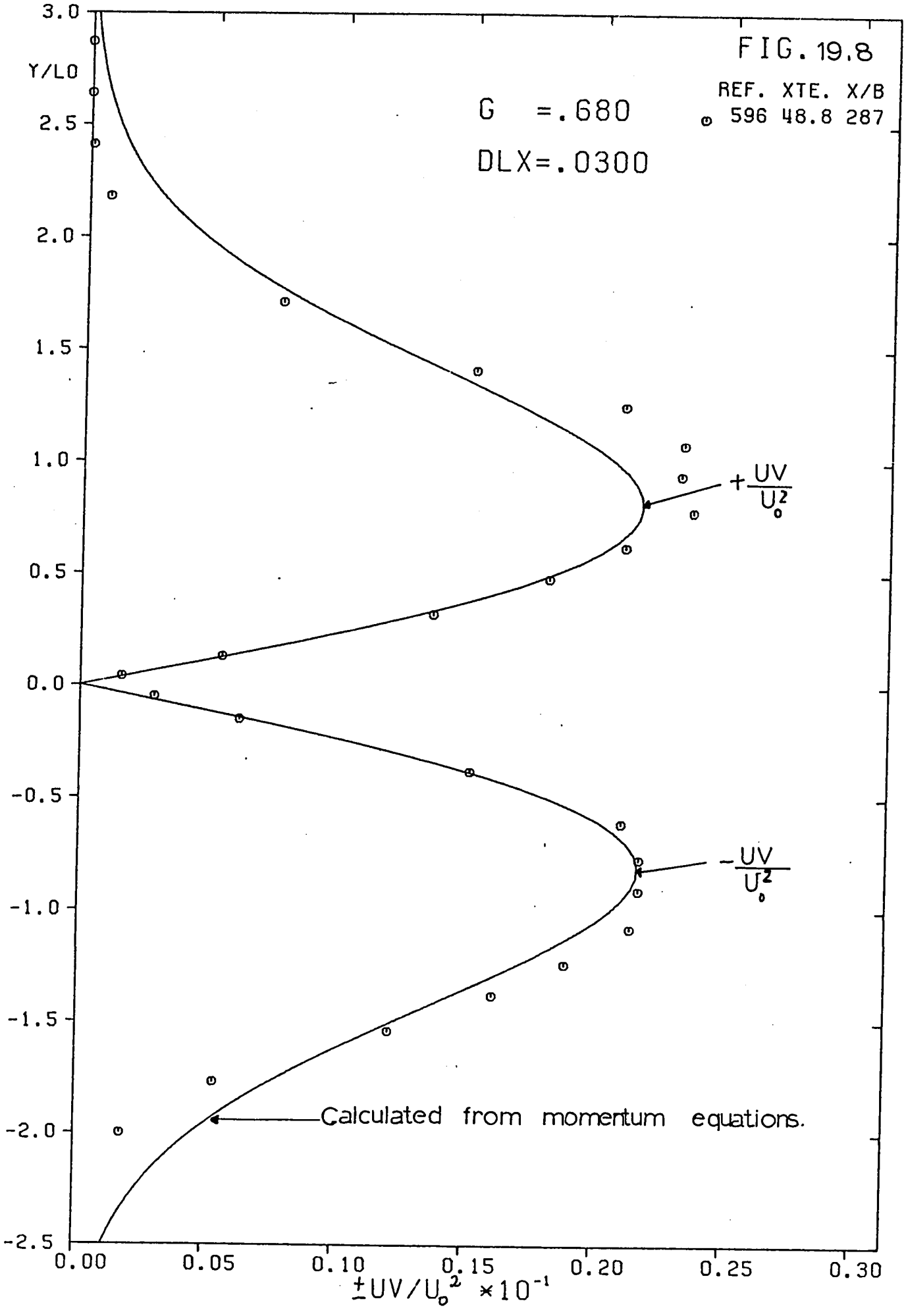
FIG. 19.8
REF. XTE. X/B
596 48.8 287
G =.680
DLX=.0300
Y/LO
3.0
2.5
2.0
1.5
1.0
0.5
0.0
-0.5
-1.0
-1.5
-2.0
-2.5
+UV/U₀²
-UV/U₀²
Calculated from momentum equations.
0.00
0.05
0.10
0.15
0.20
0.25
0.30
±UV/U₀² ×10⁻¹

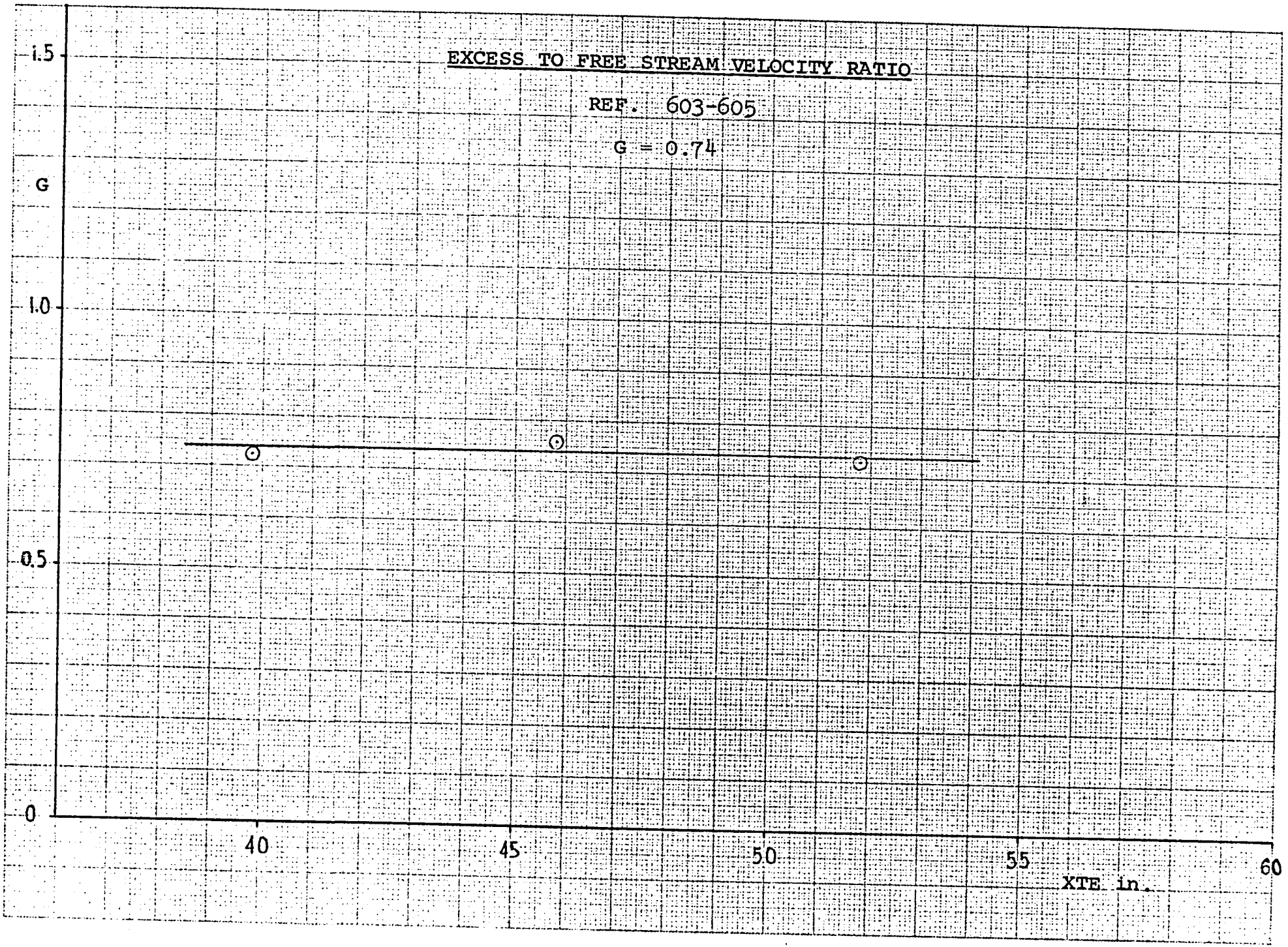
EXCESS TO FREE STREAM VELOCITY RATIO
REF. 603-605
G = 0.74
G
1.5
1.0
0.5
0
40
45
50
55
60
XTE in.

Fig. 20.a

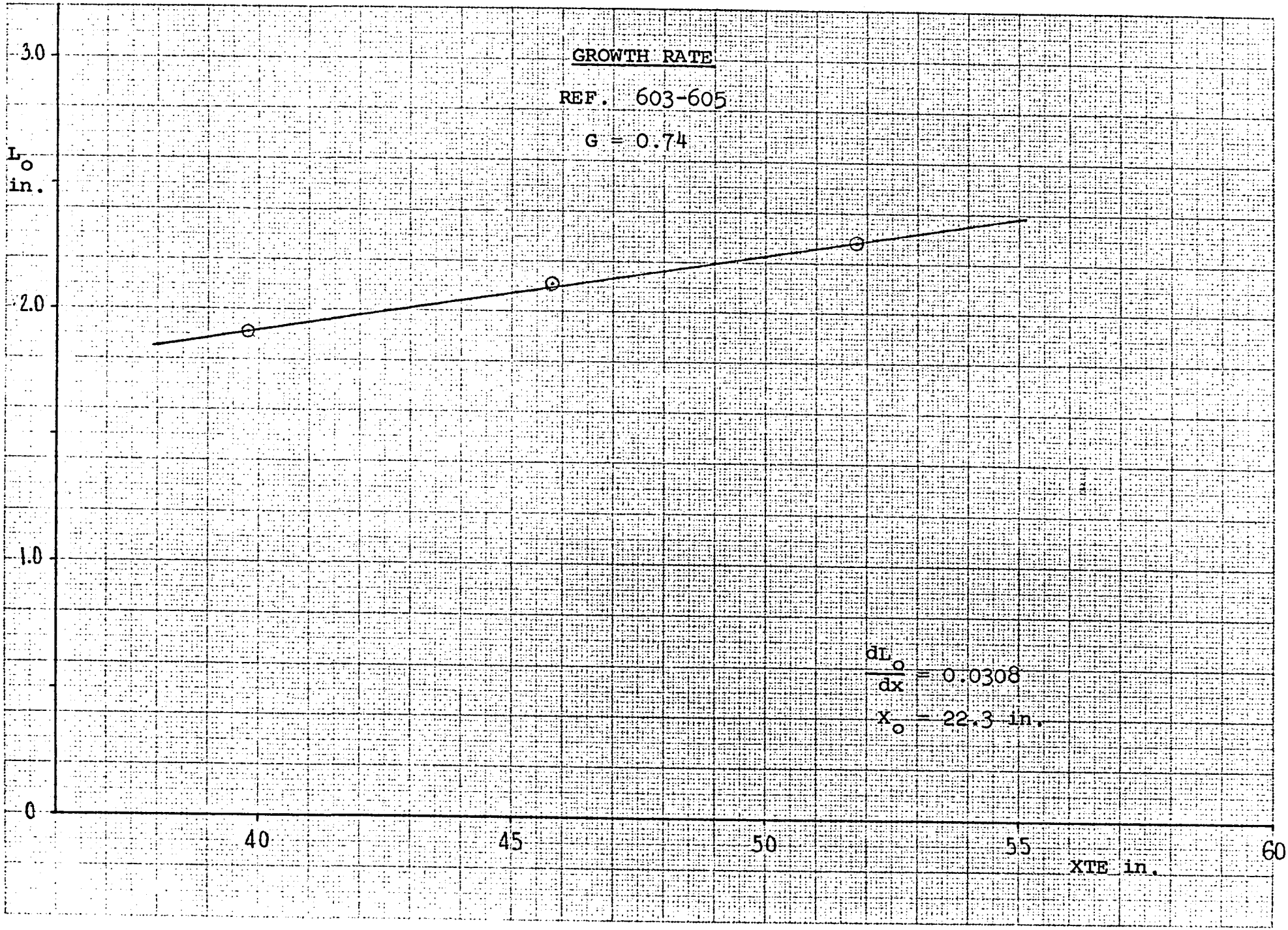
GROWTH RATE
REF. 603-605
G = 0.74
L_o in.
3.0
2.0
1.0
0
40
45
50
55
60
XTE in.
$\frac{dL_o}{dx} = 0.0308$
$x_o = 22.3$ in.

Fig. 20.b

VELOCITY DECAY

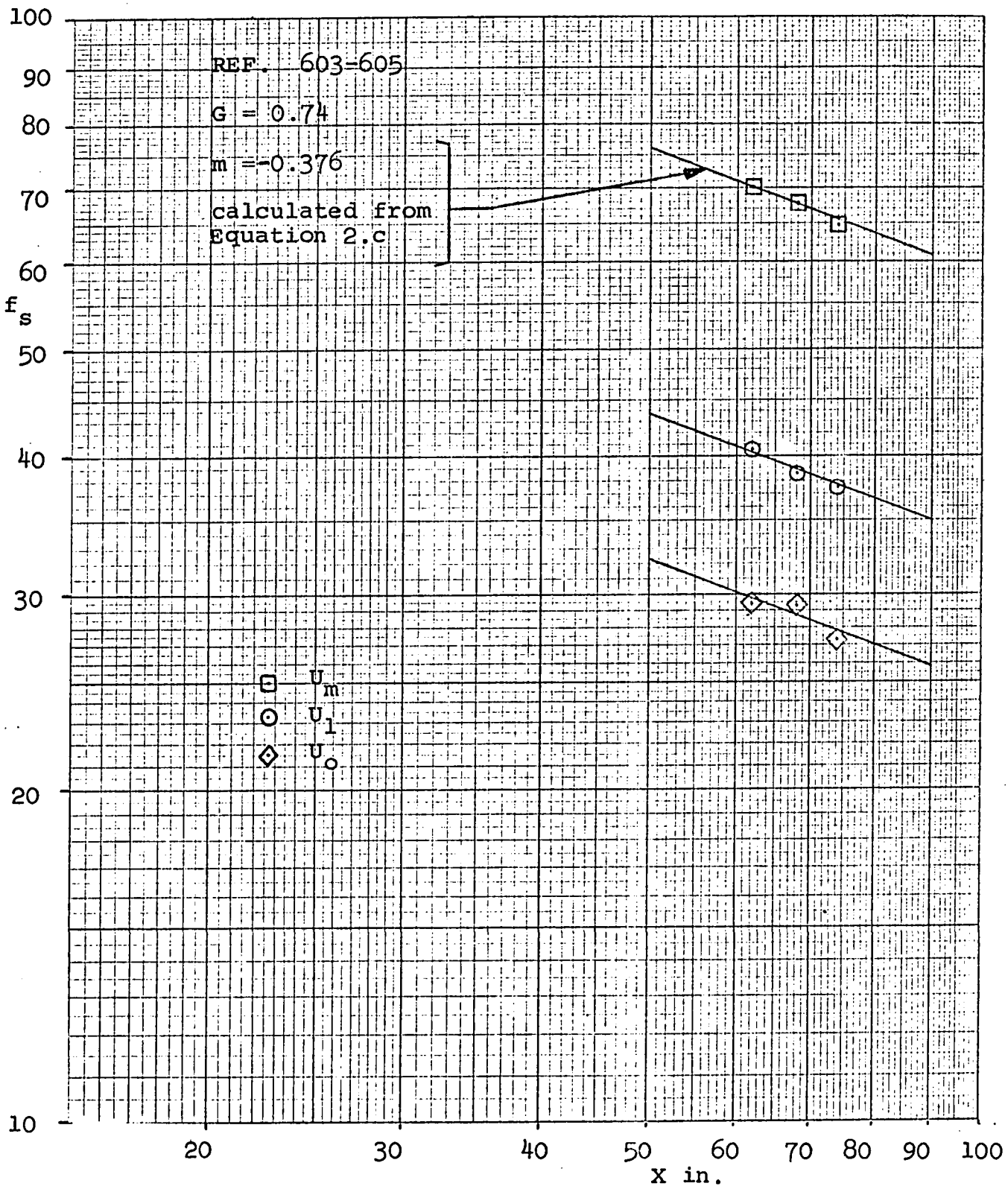

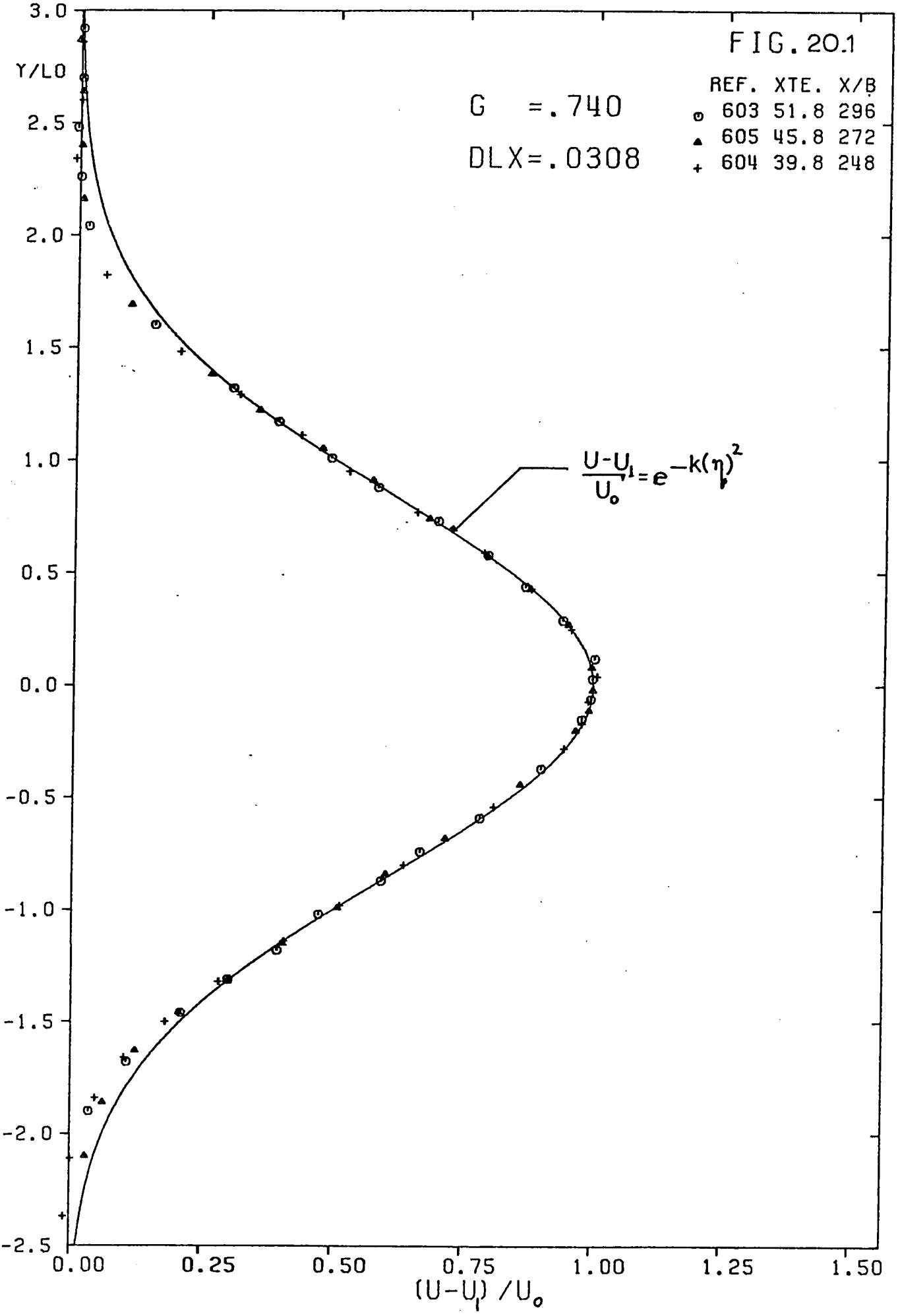
FIG. 20.1
G = .740
DLX = .0308
REF. XTE. X/B
603 51.8 296
605 45.8 272
604 39.8 248
$\frac{U-U_1}{U_o} = e^{-k(\eta)^2}$
Y/LO
3.0
2.5
2.0
1.5
1.0
0.5
0.0
-0.5
-1.0
-1.5
-2.0
-2.5
0.00
0.25
0.50
0.75
1.00
1.25
1.50
$(U-U_1)/U_o$

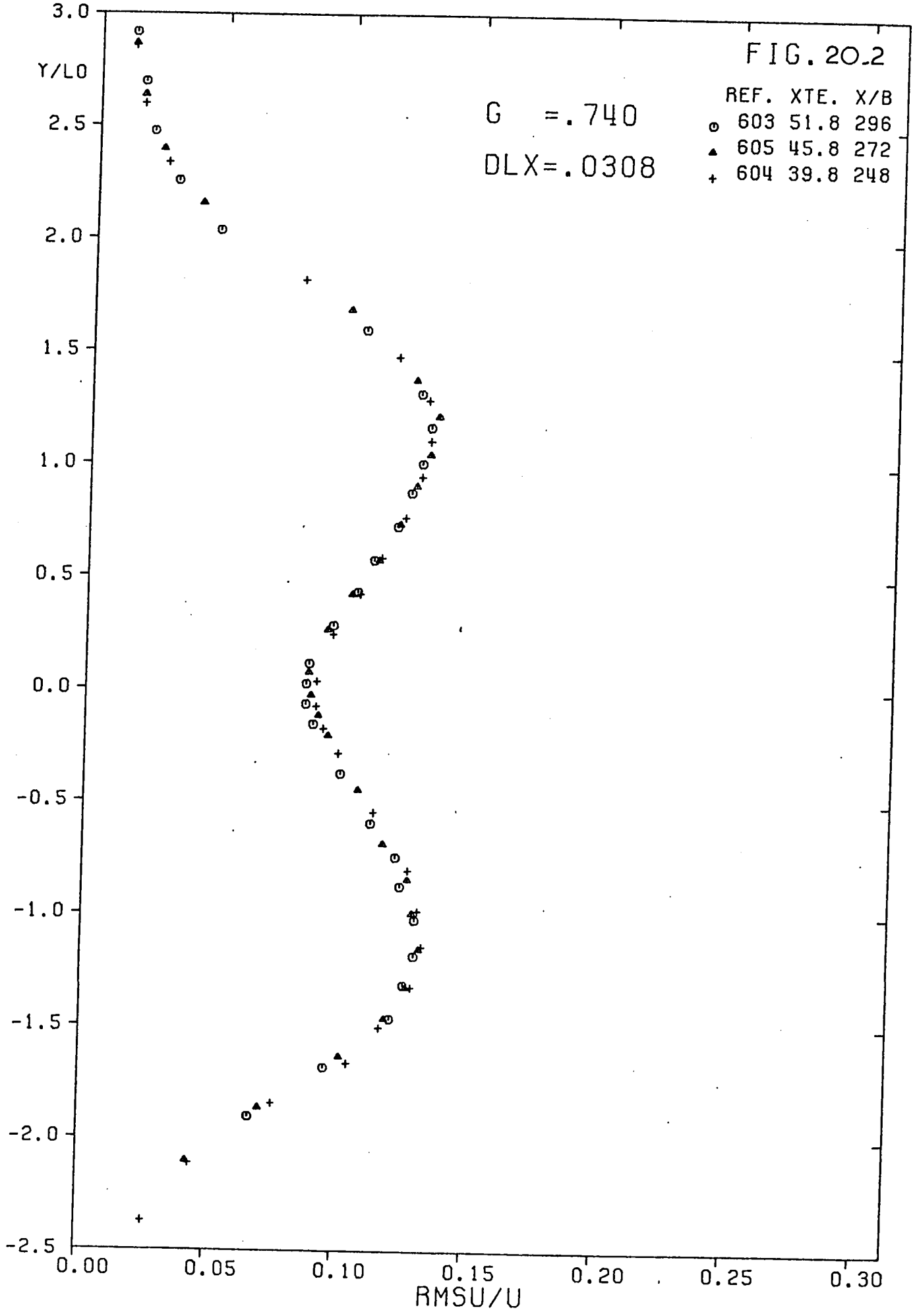
FIG. 20.2
G =.740
DLX=.0308
REF. XTE. X/B
603 51.8 296
605 45.8 272
604 39.8 248
Y/LO
RMSU/U
3.0
2.5
2.0
1.5
1.0
0.5
0.0
-0.5
-1.0
-1.5
-2.0
-2.5
0.00
0.05
0.10
0.15
0.20
0.25
0.30

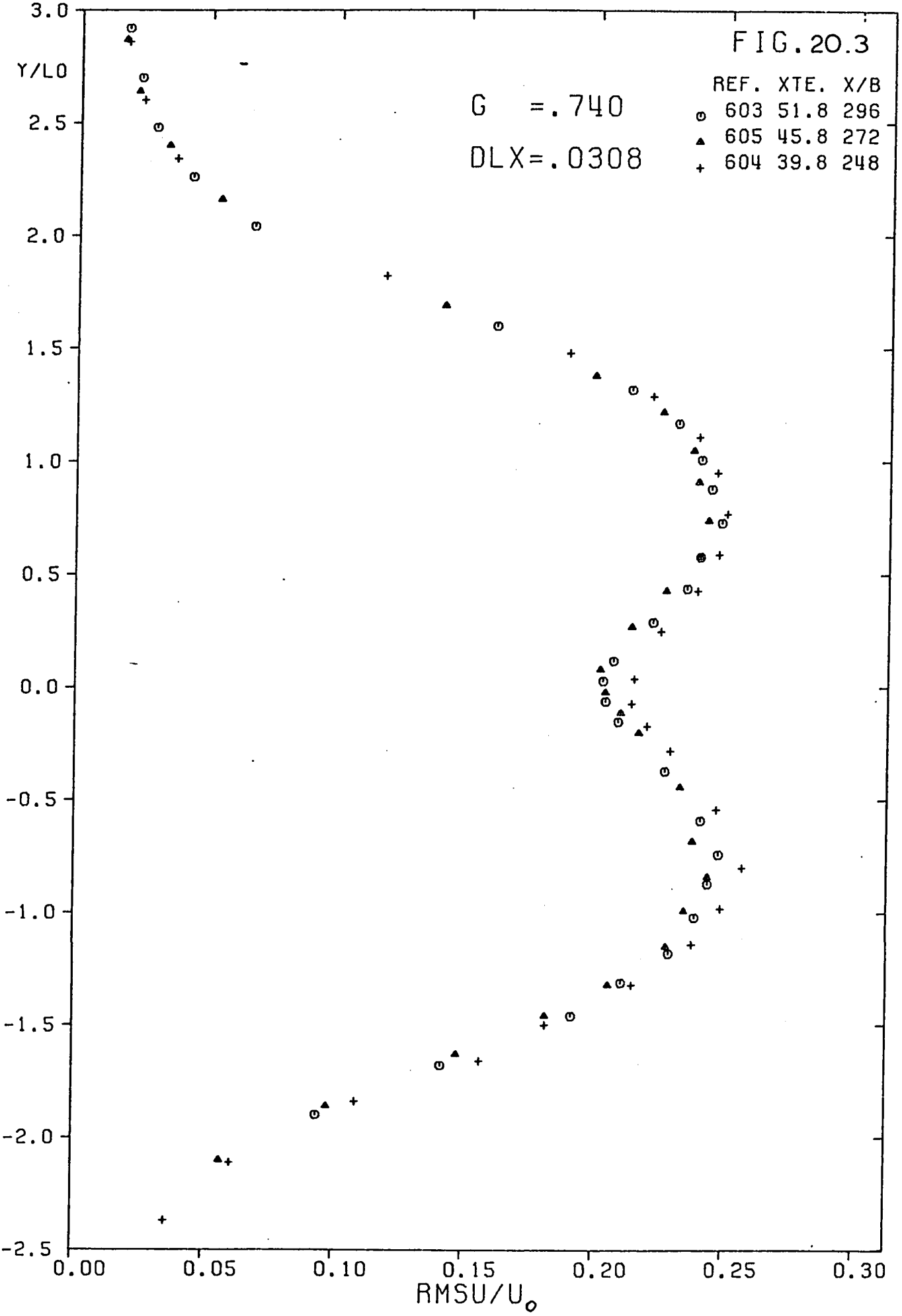
FIG. 20.3
G =.740
DLX=.0308
REF. XTE. X/B
603 51.8 296
605 45.8 272
604 39.8 248
Y/LO
3.0
2.5
2.0
1.5
1.0
0.5
0.0
-0.5
-1.0
-1.5
-2.0
-2.5
0.00
0.05
0.10
0.15
0.20
0.25
0.30
RMSU/U$_o$

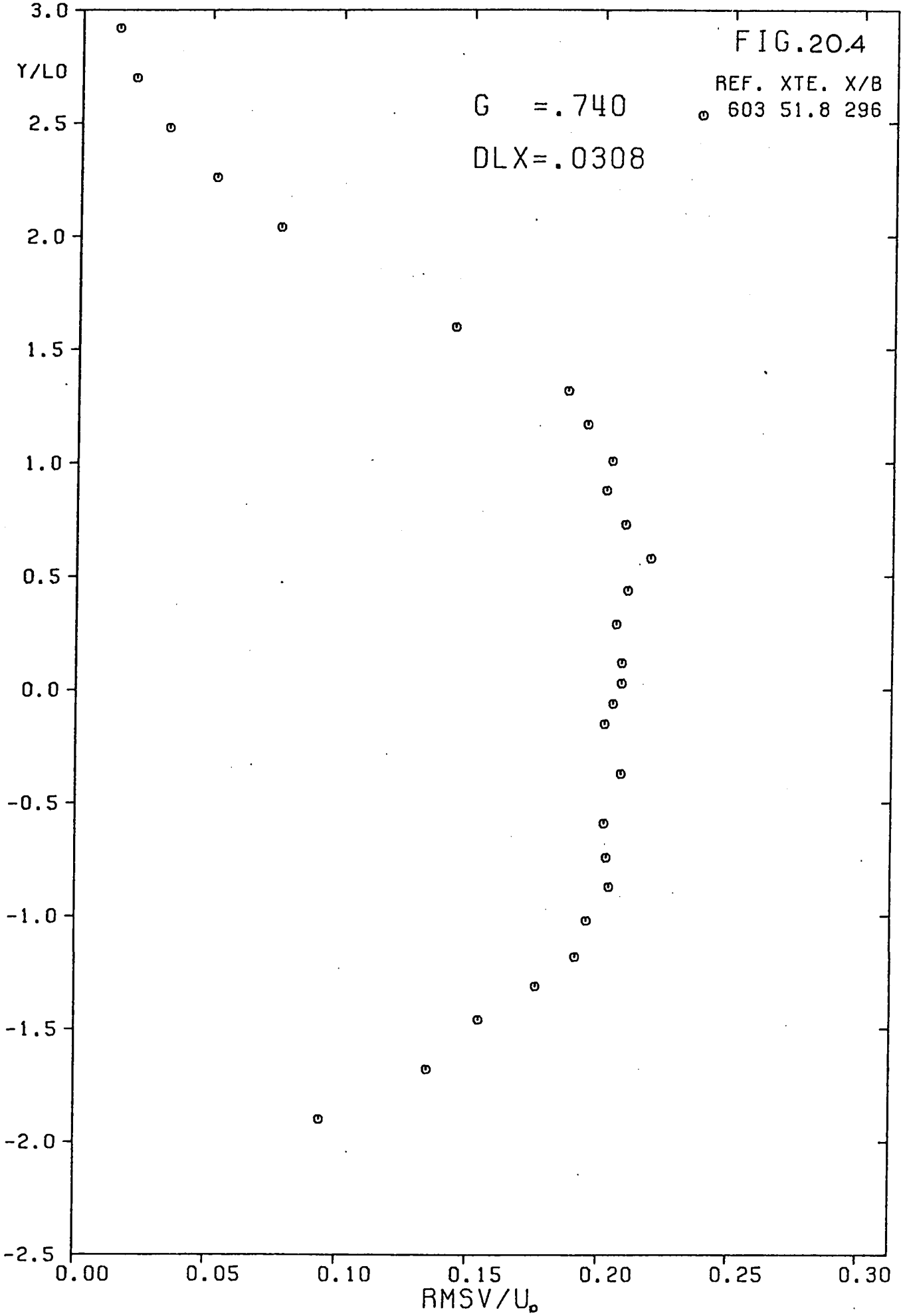
FIG.20.4
REF. XTE. X/B
603 51.8 296
G =.740
DLX=.0308
Y/LO
3.0
2.5
2.0
1.5
1.0
0.5
0.0
-0.5
-1.0
-1.5
-2.0
-2.5
0.00
0.05
0.10
0.15
0.20
0.25
0.30
RMSV/U∞

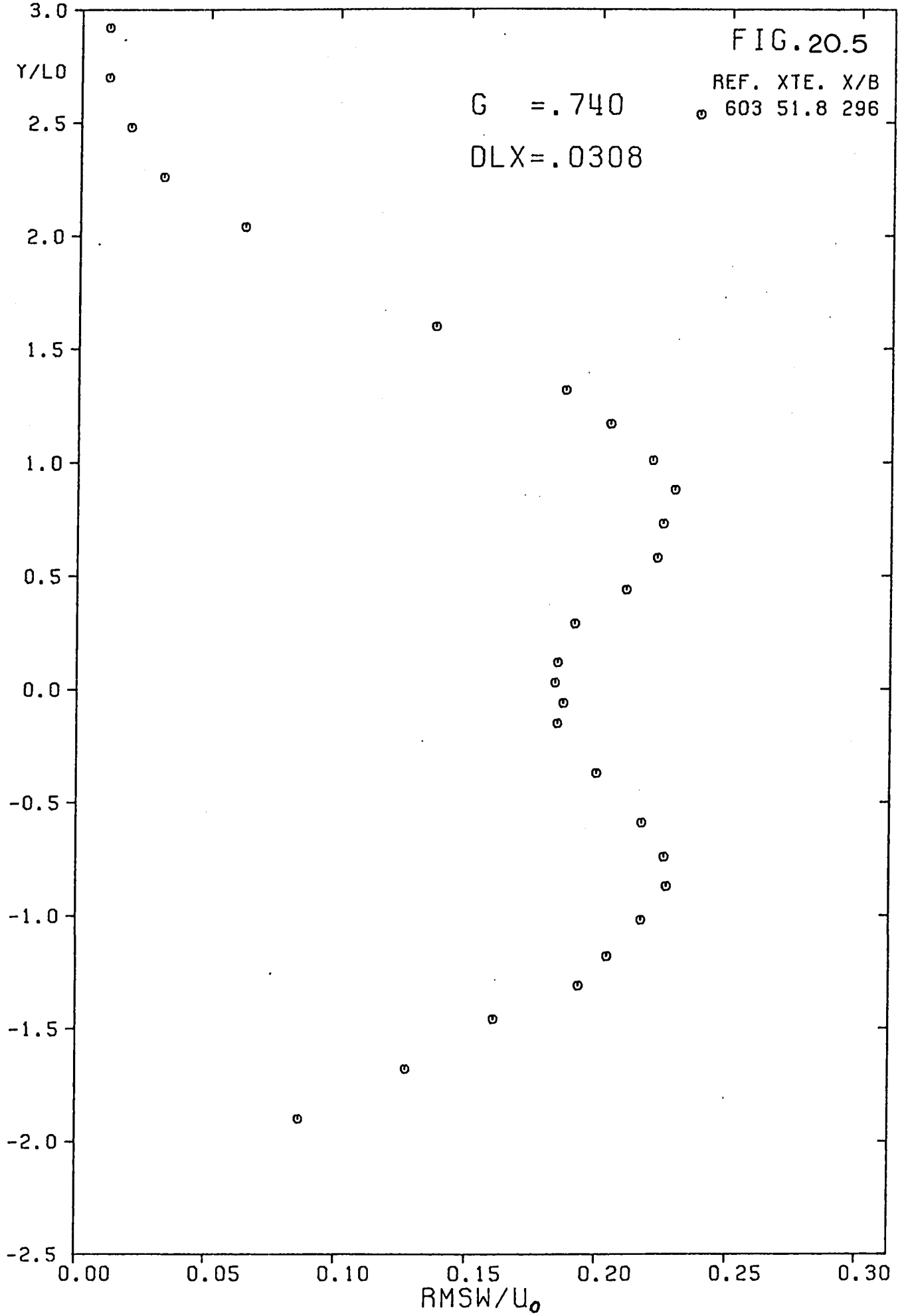
FIG. 20.5
REF. XTE. X/B
603 51.8 296
G =.740
DLX=.0308
Y/LO
3.0
2.5
2.0
1.5
1.0
0.5
0.0
-0.5
-1.0
-1.5
-2.0
-2.5
0.00
0.05
0.10
0.15
0.20
0.25
0.30
RMSW/U0

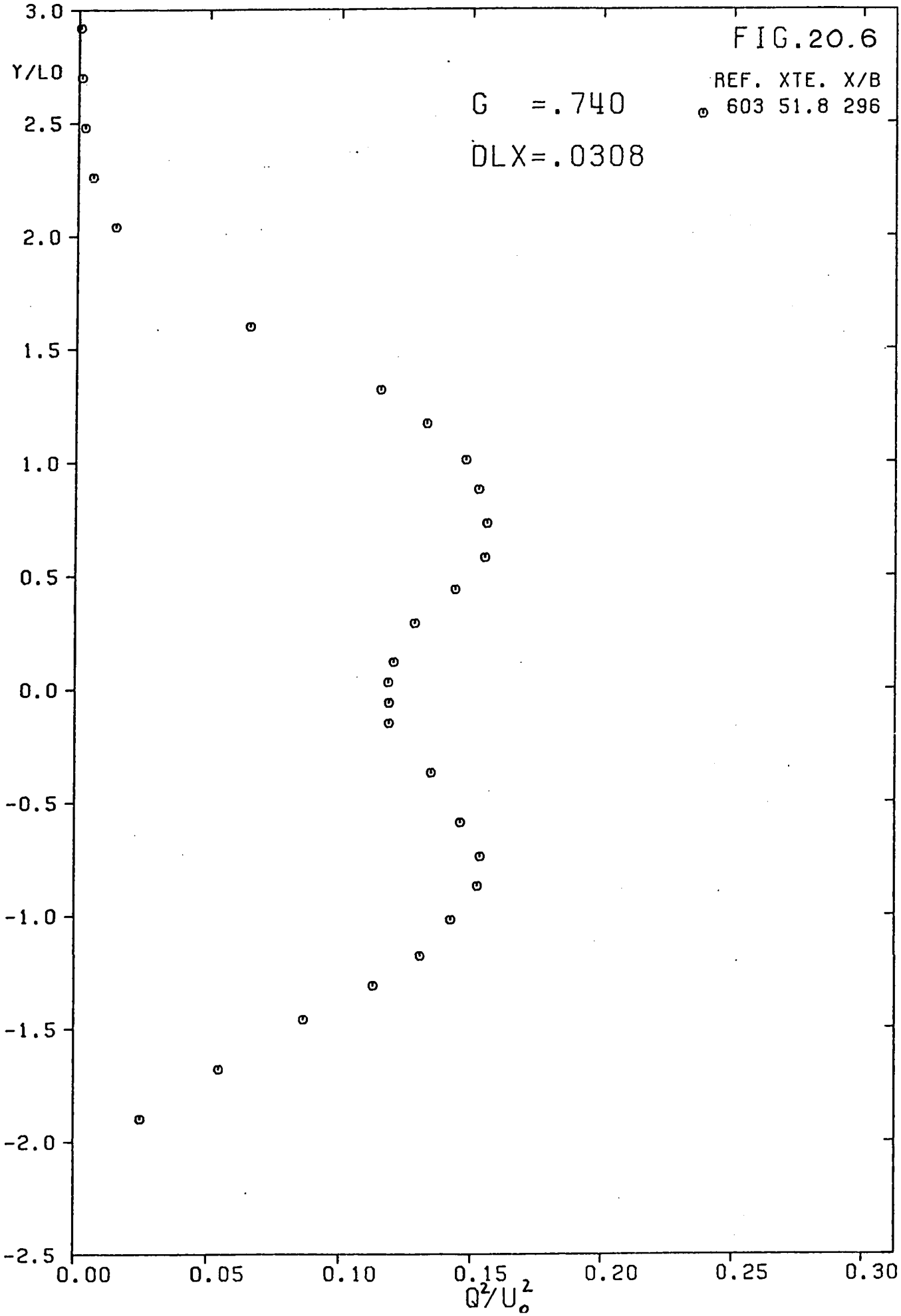
FIG.20.6
REF. XTE. X/B
603 51.8 296
G =.740
DLX=.0308
Y/LO
3.0
2.5
2.0
1.5
1.0
0.5
0.0
-0.5
-1.0
-1.5
-2.0
-2.5
0.00
0.05
0.10
0.15
0.20
0.25
0.30
Q²/U₀²

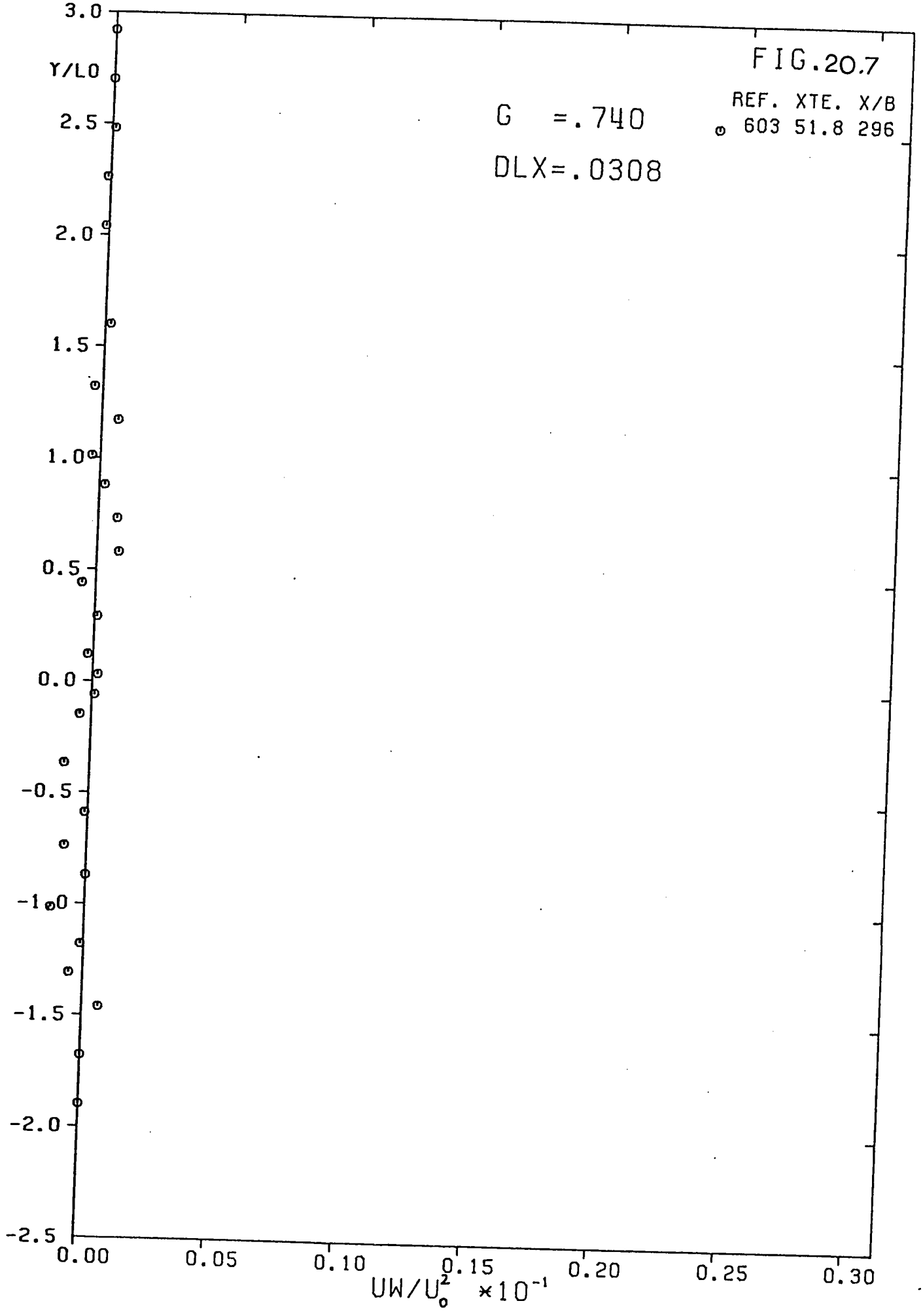
FIG.20.7
REF. XTE. X/B
603 51.8 296
G =.740
DLX=.0308
Y/LO
3.0
2.5
2.0
1.5
1.0
0.5
0.0
-0.5
-1.0
-1.5
-2.0
-2.5
0.00
0.05
0.10
0.15
0.20
0.25
0.30
UW/U$_0^2$ *10^{-1}

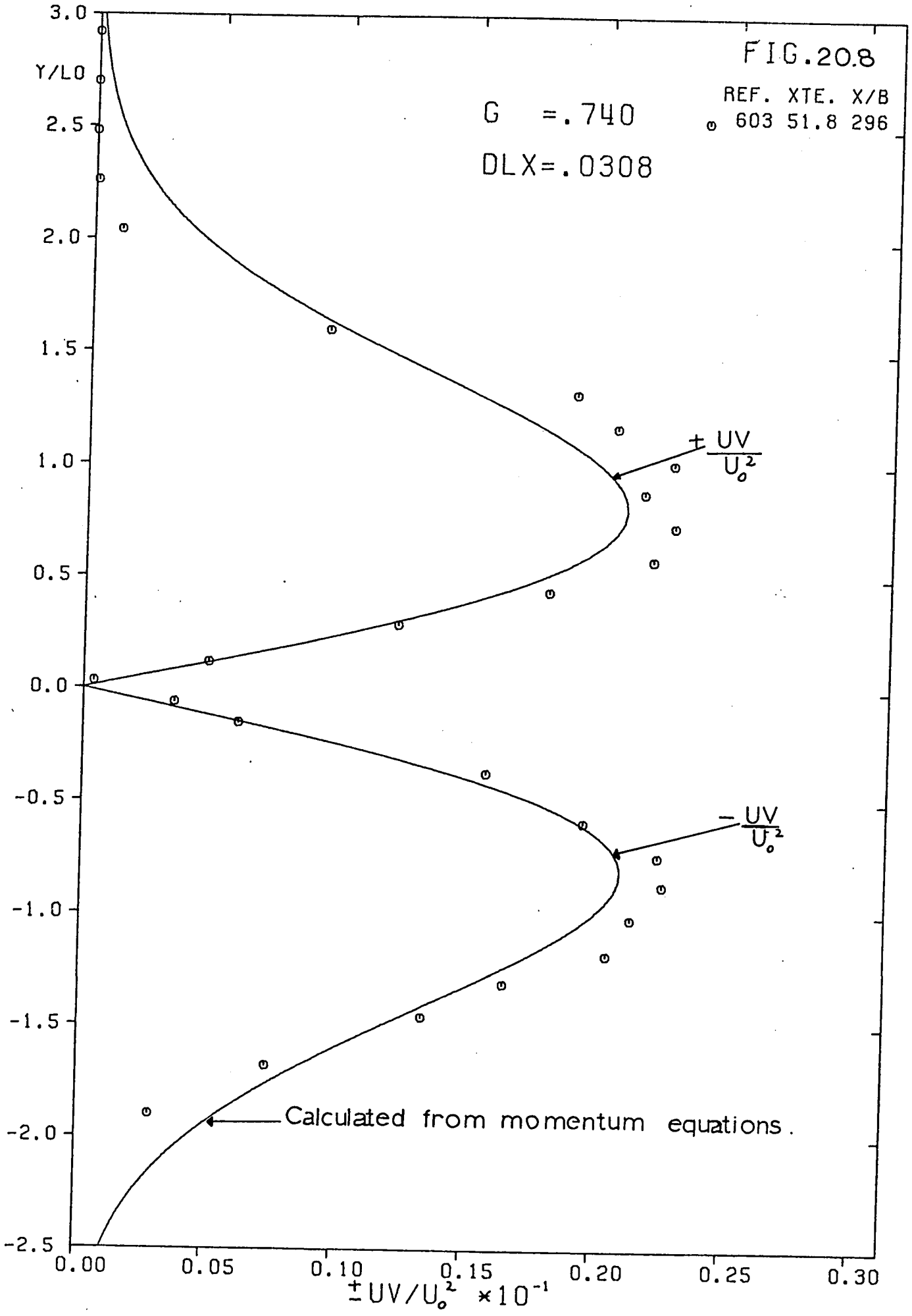
FIG.20.8
REF. XTE. X/B
603 51.8 296
G =.740
DLX=.0308
Y/LO
3.0
2.5
2.0
1.5
1.0
0.5
0.0
-0.5
-1.0
-1.5
-2.0
-2.5
± UV/U₀²
− UV/U₀²
Calculated from momentum equations.
0.00
0.05
0.10
0.15
0.20
0.25
0.30
±UV/U₀² *10⁻¹

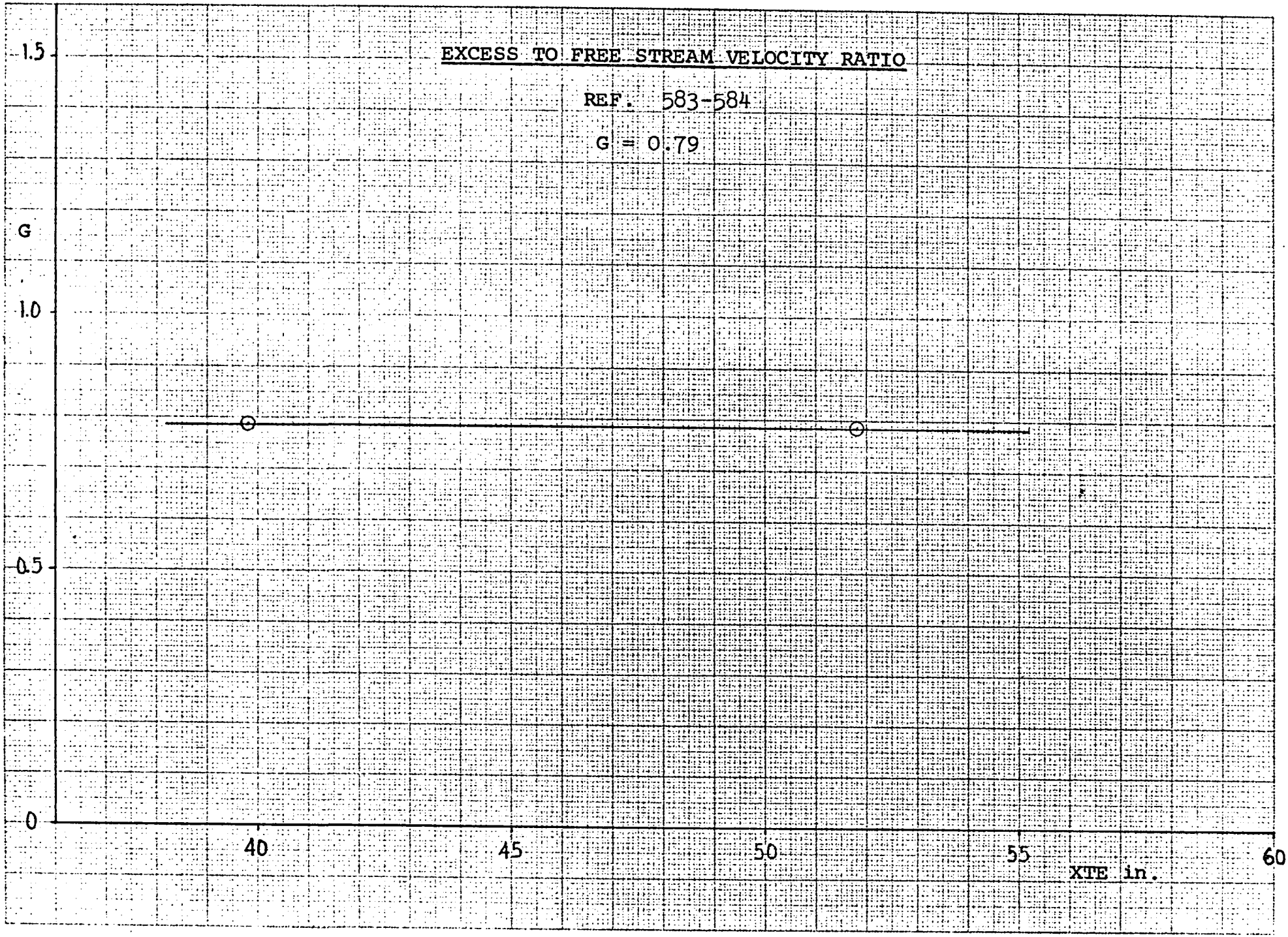
EXCESS TO FREE STREAM VELOCITY RATIO
REF. 583-584
G = 0.79
G
1.5
1.0
0.5
0
40
45
50
55
60
XTE in.

Fig. 21.a

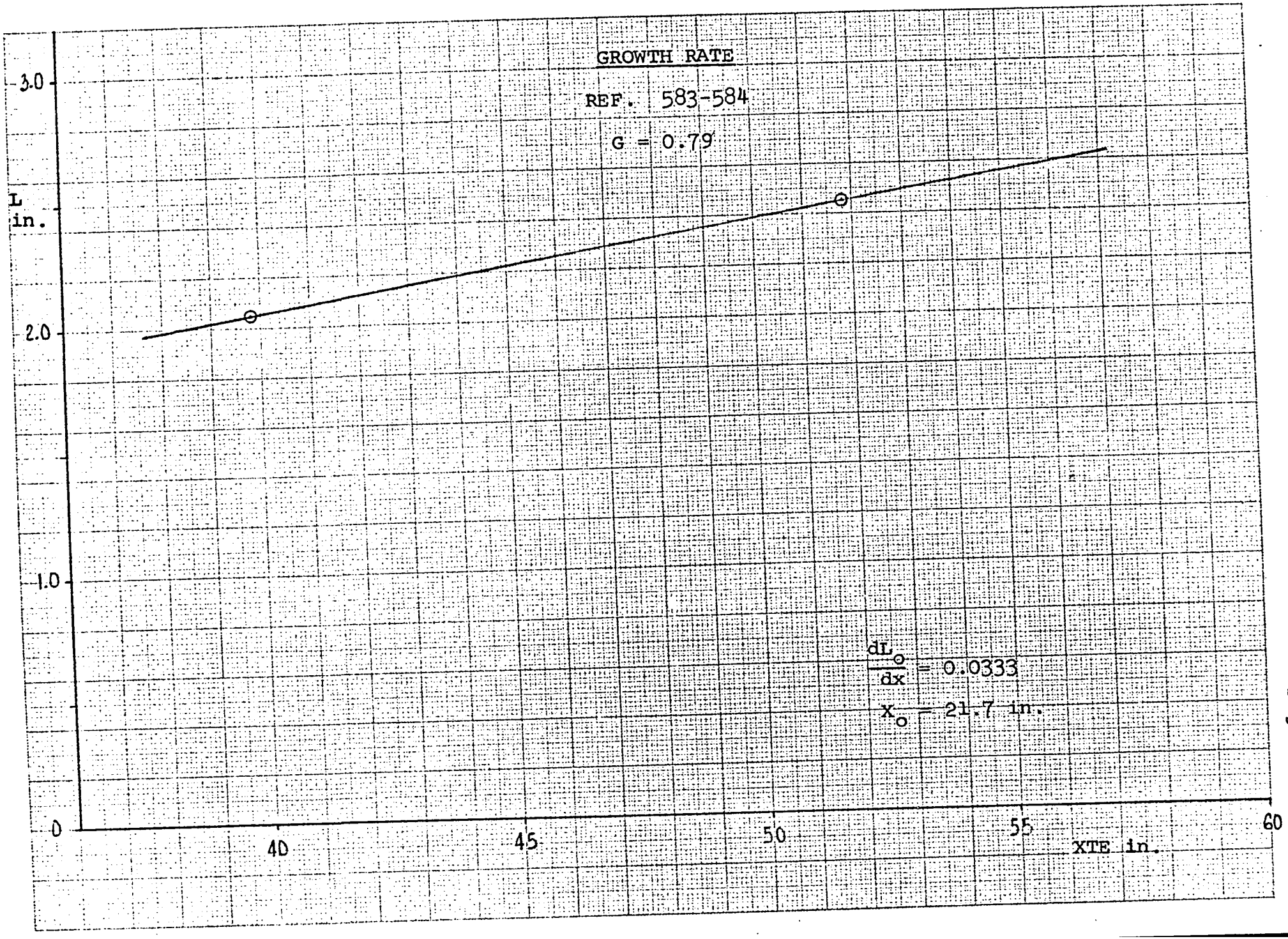
GROWTH RATE
REF. 583-584
G = 0.79
L in.
3.0
2.0
1.0
0
40
45
50
55
60
XTE in.
$\frac{dL_o}{dx} = 0.0333$
$X_o = 21.7$ in.

Fig. 21.b

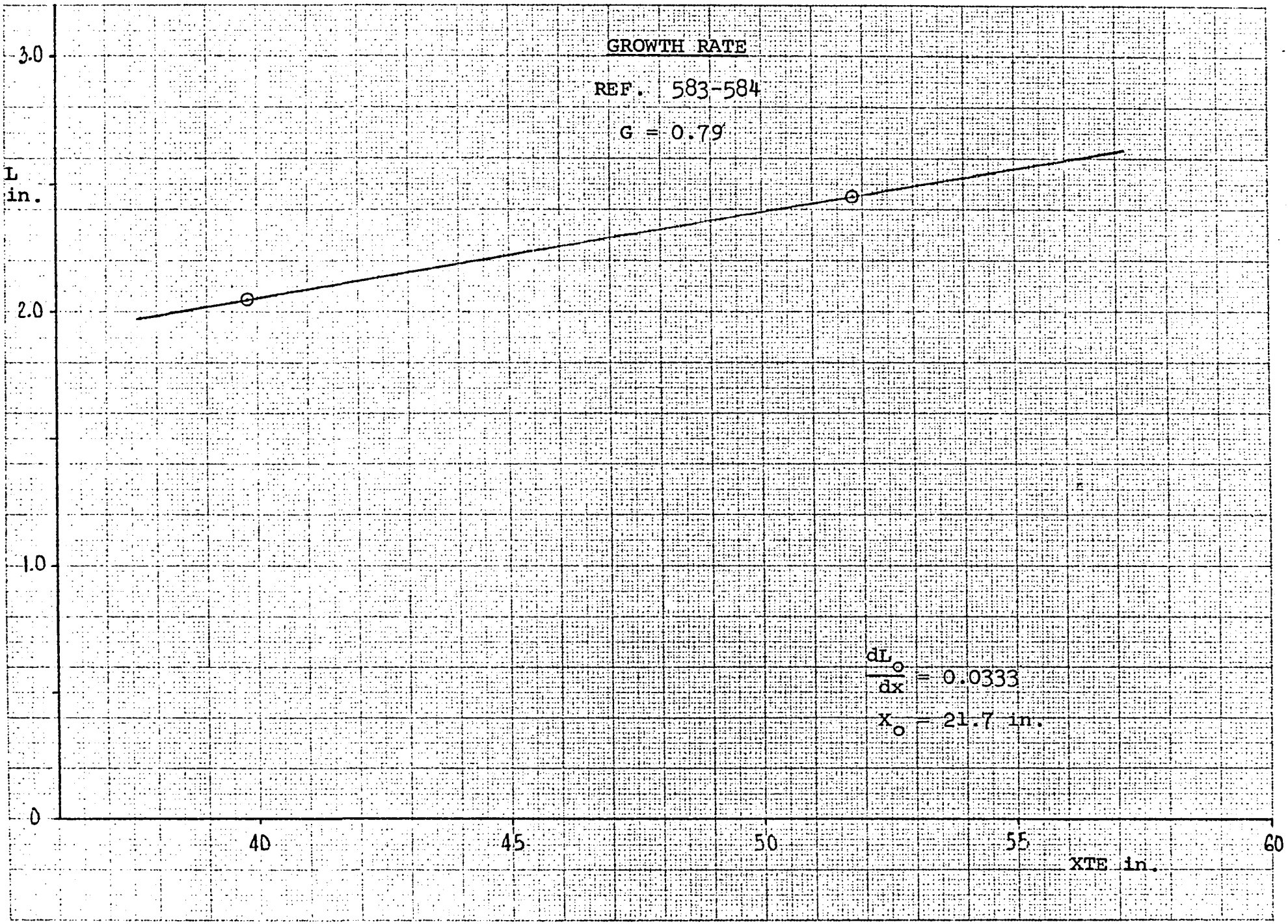
GROWTH RATE
REF. 583-584
G = 0.79
L
in.
3.0
2.0
1.0
0
40
45
50
55
60
XTE in.
dL_o/dx = 0.0333
X_o = 21.7 in.

Fig. 21.a

VELOCITY DECAY

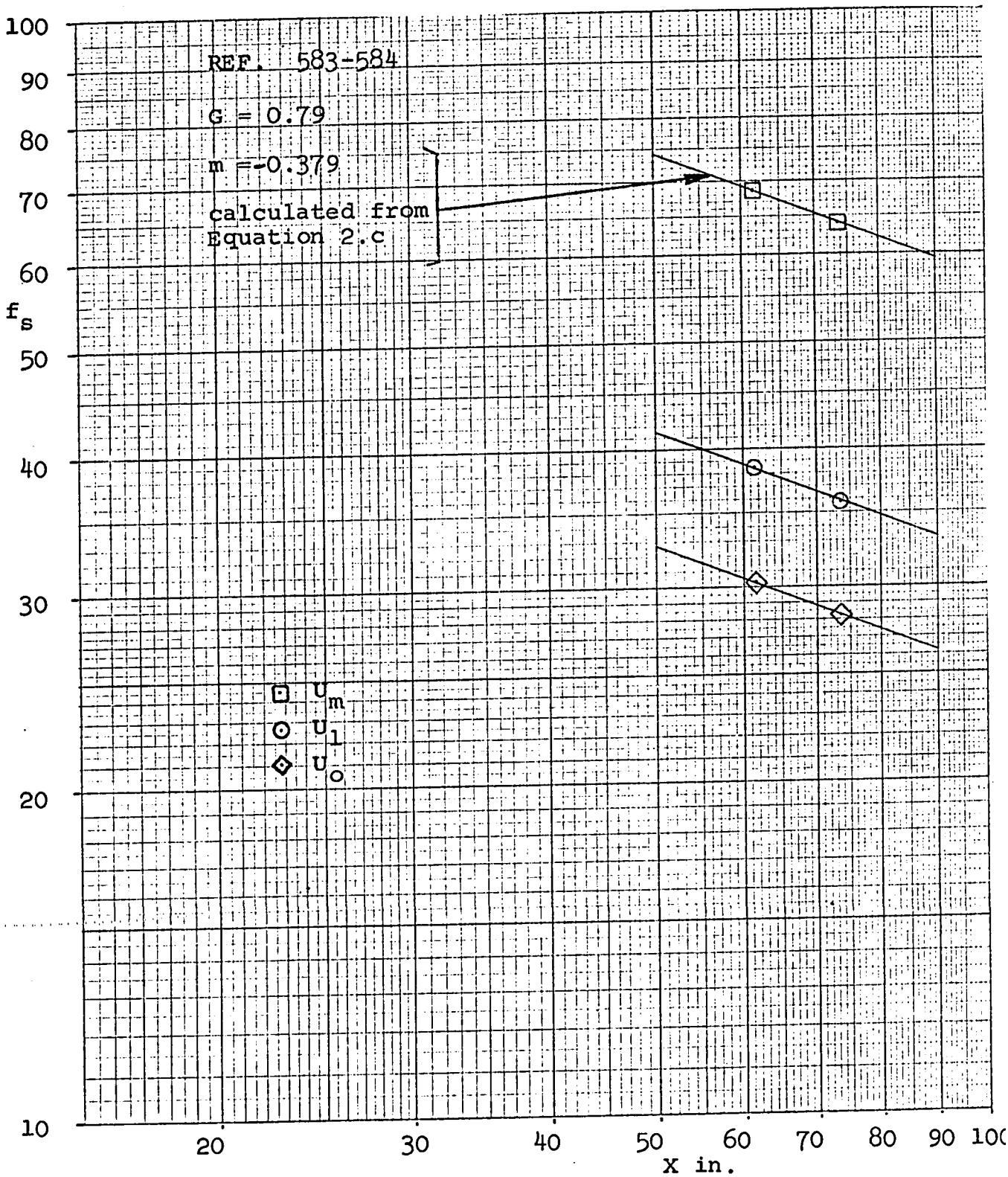

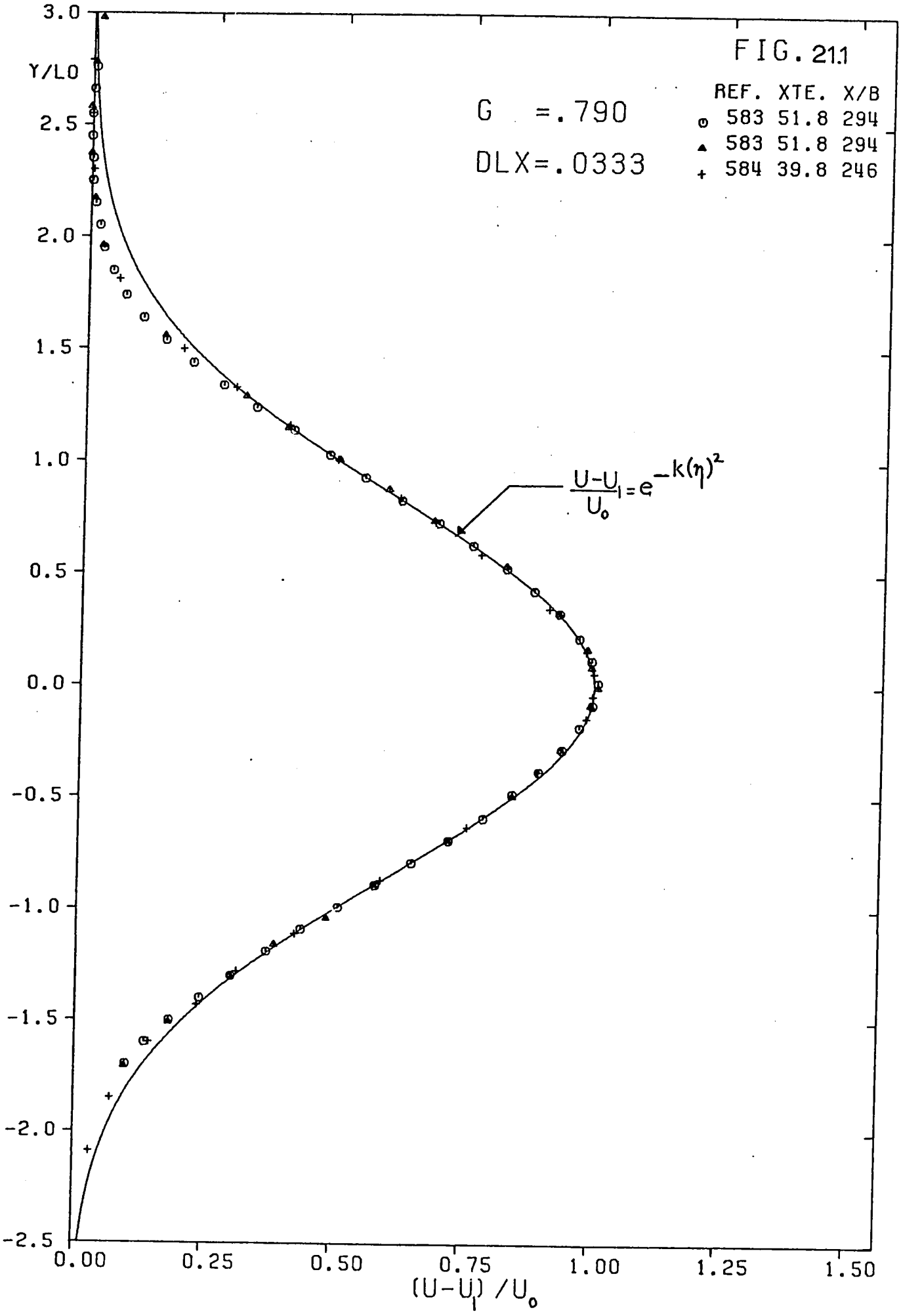
FIG. 21.1
G =.790
DLX=.0333
REF. XTE. X/B
583 51.8 294
583 51.8 294
584 39.8 246
$\frac{U-U_1}{U_0} = e^{-k(\eta)^2}$
Y/LO
3.0
2.5
2.0
1.5
1.0
0.5
0.0
-0.5
-1.0
-1.5
-2.0
-2.5
0.00
0.25
0.50
0.75
1.00
1.25
1.50
$(U-U_1)/U_0$

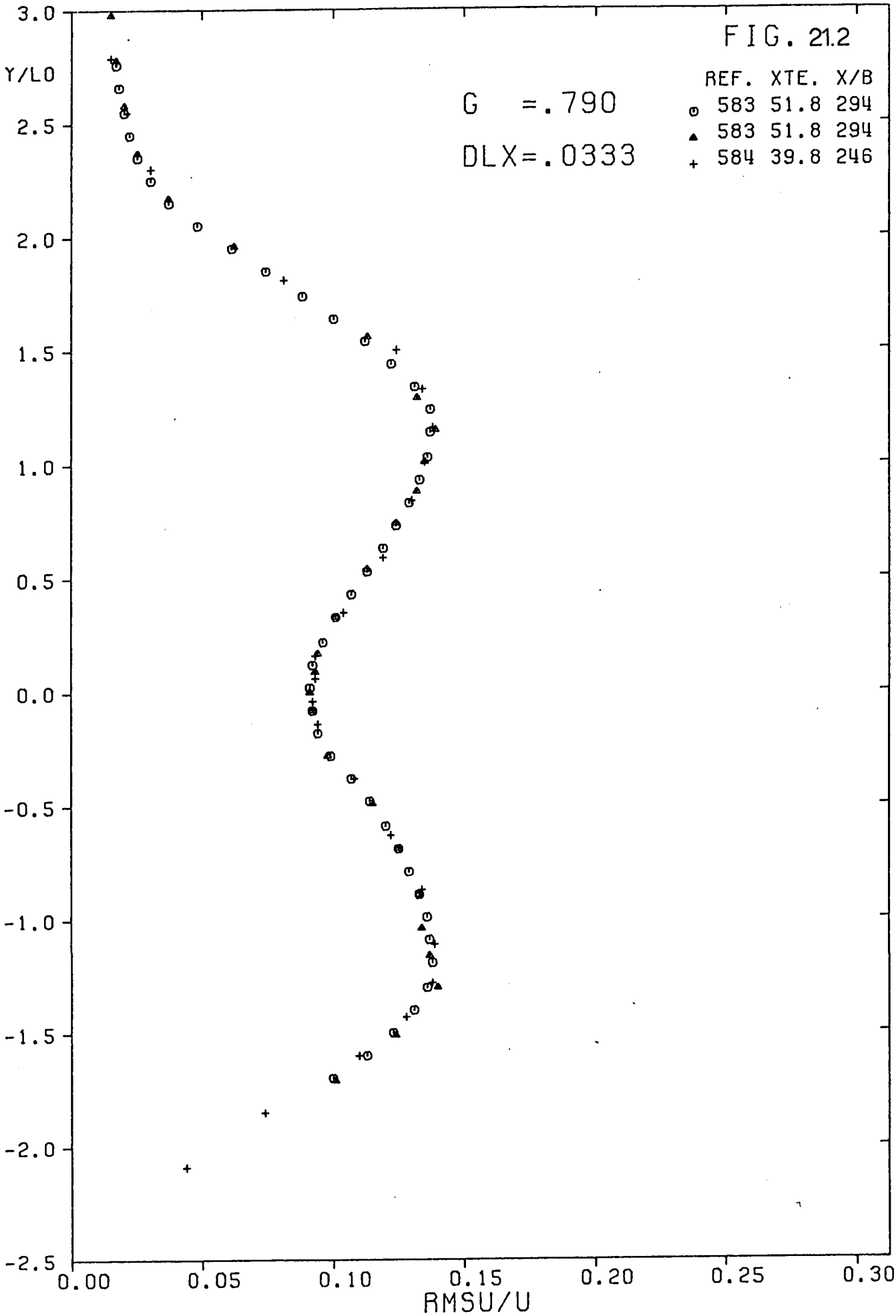
FIG. 21.2
G =.790
DLX=.0333
REF. XTE. X/B
583 51.8 294
583 51.8 294
584 39.8 246
Y/LO
3.0
2.5
2.0
1.5
1.0
0.5
0.0
-0.5
-1.0
-1.5
-2.0
-2.5
0.00
0.05
0.10
0.15
0.20
0.25
0.30
RMSU/U

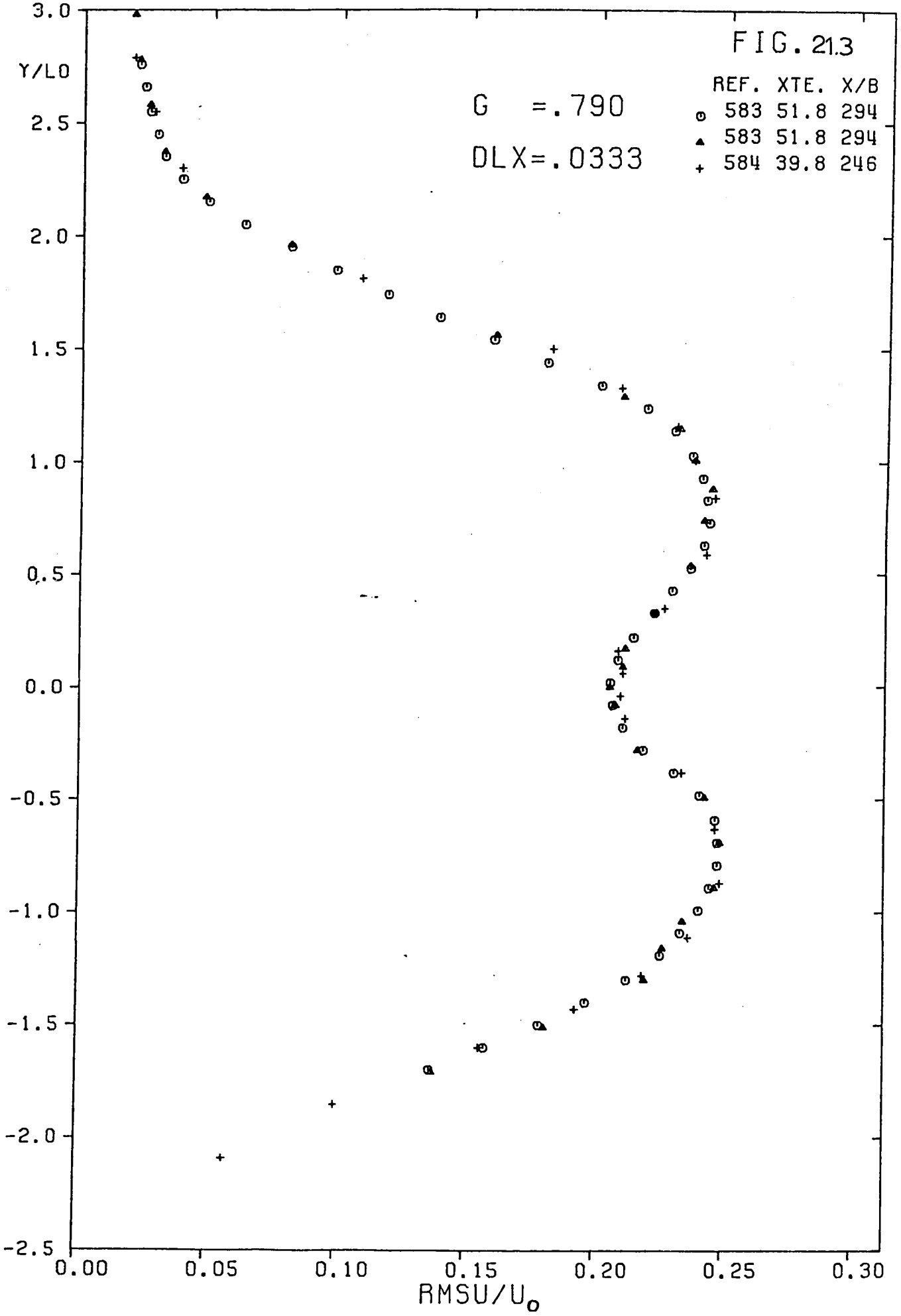
FIG. 21.3
G =.790
DLX=.0333
REF. XTE. X/B
583 51.8 294
583 51.8 294
584 39.8 246
Y/LO
3.0
2.5
2.0
1.5
1.0
0.5
0.0
-0.5
-1.0
-1.5
-2.0
-2.5
0.00
0.05
0.10
0.15
0.20
0.25
0.30
RMSU/U$_o$

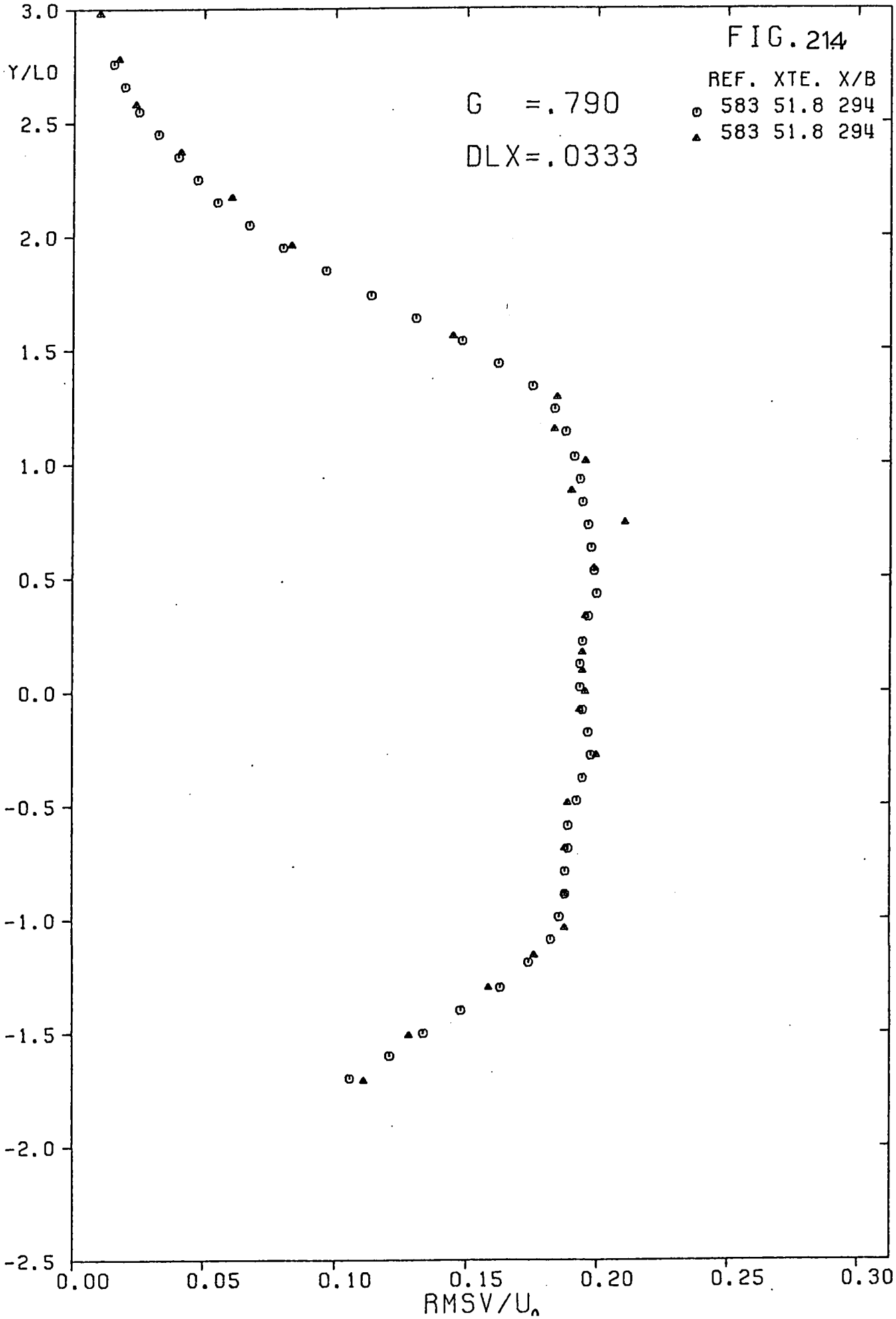
FIG. 214
REF. XTE. X/B
583 51.8 294
583 51.8 294
G =.790
DLX=.0333
Y/LO
3.0
2.5
2.0
1.5
1.0
0.5
0.0
-0.5
-1.0
-1.5
-2.0
-2.5
0.00
0.05
0.10
0.15
0.20
0.25
0.30
RMSV/U∞

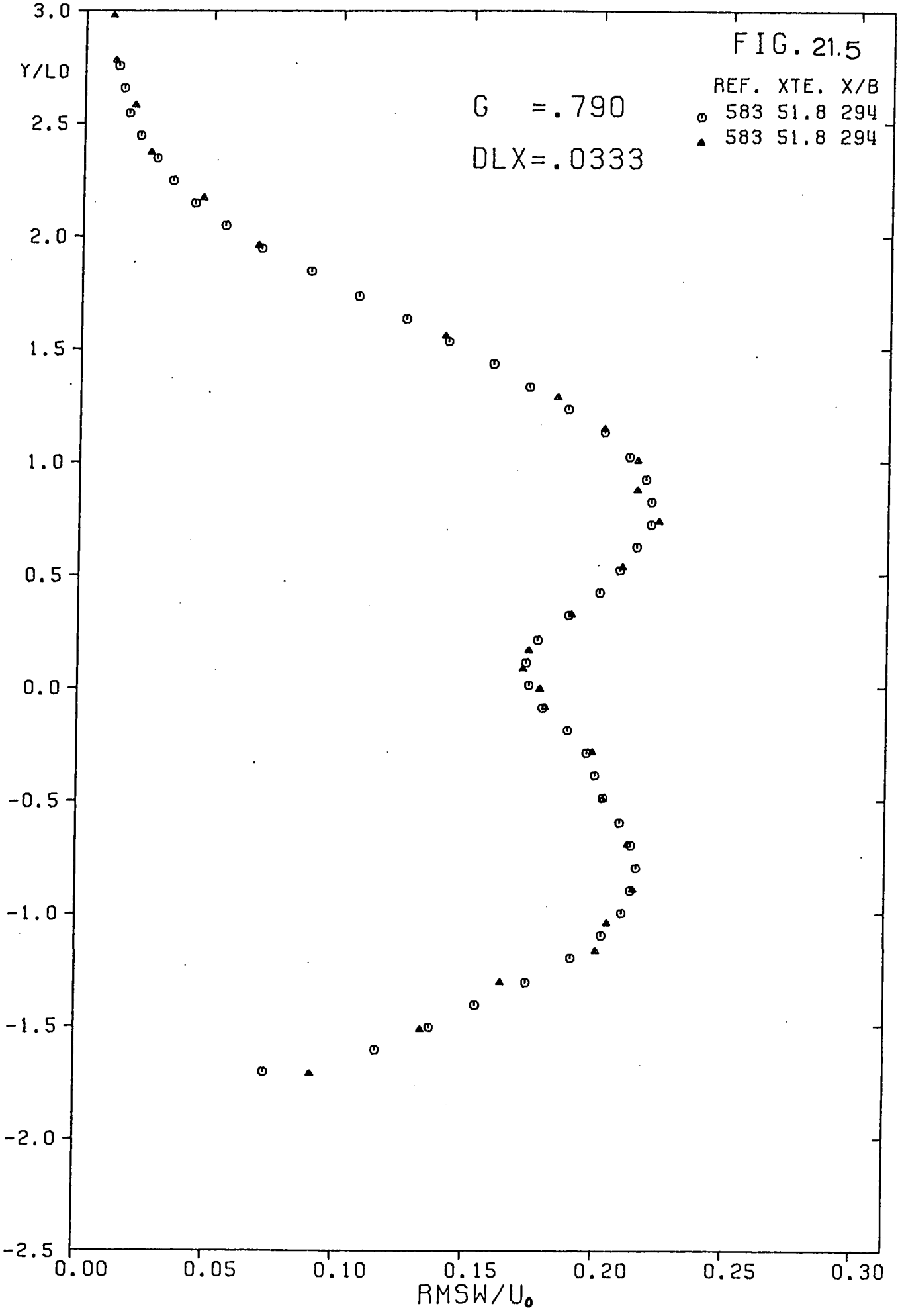
FIG. 21.5
REF. XTE. X/B
583 51.8 294
583 51.8 294
G =.790
DLX=.0333
Y/LO
3.0
2.5
2.0
1.5
1.0
0.5
0.0
-0.5
-1.0
-1.5
-2.0
-2.5
0.00
0.05
0.10
0.15
0.20
0.25
0.30
RMSW/U0

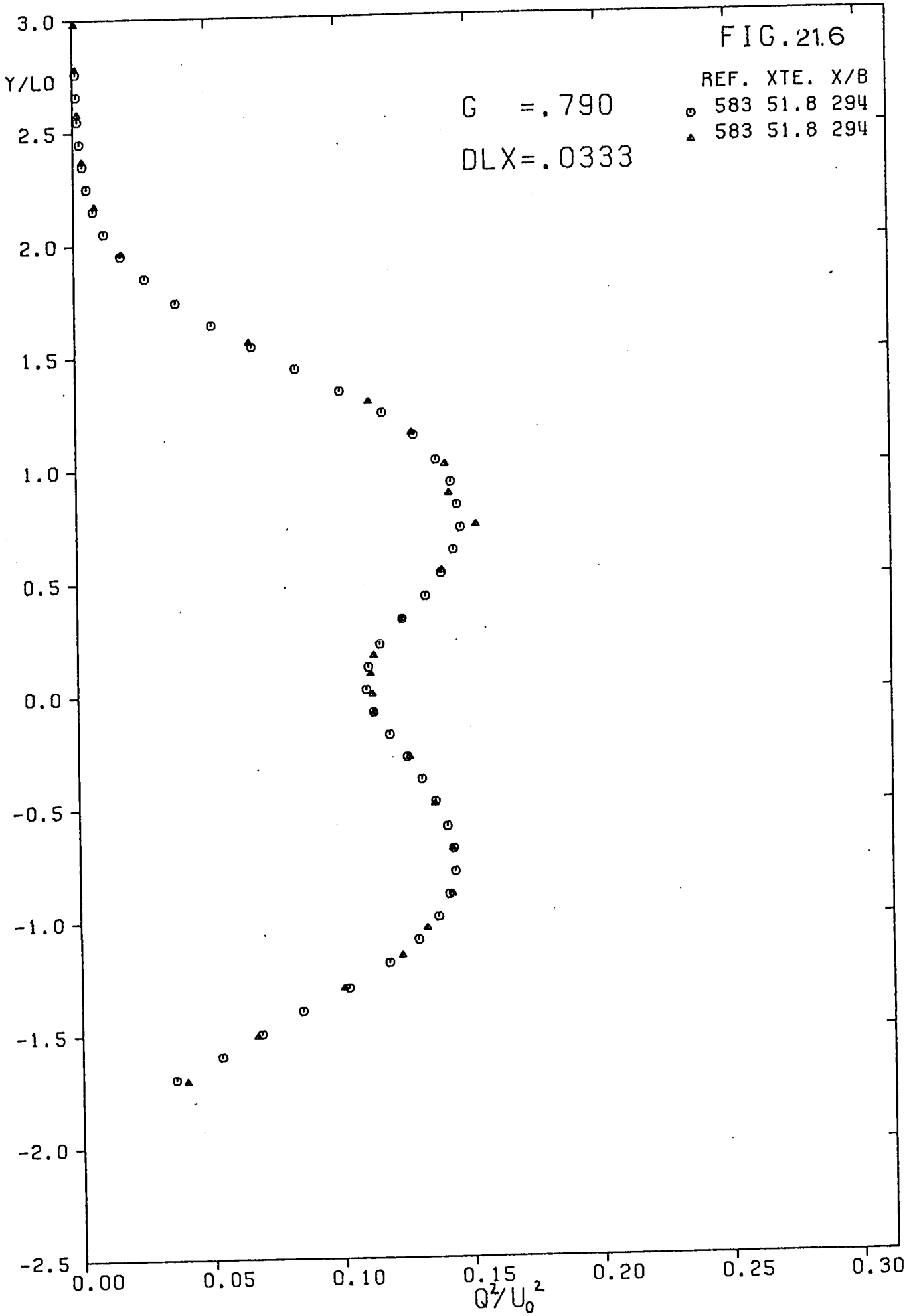
FIG. 21.6
REF. XTE. X/B
583 51.8 294
583 51.8 294
G =.790
DLX=.0333
Y/LO
3.0
2.5
2.0
1.5
1.0
0.5
0.0
-0.5
-1.0
-1.5
-2.0
-2.5
0.00
0.05
0.10
0.15
0.20
0.25
0.30
Q^2/U_0^2

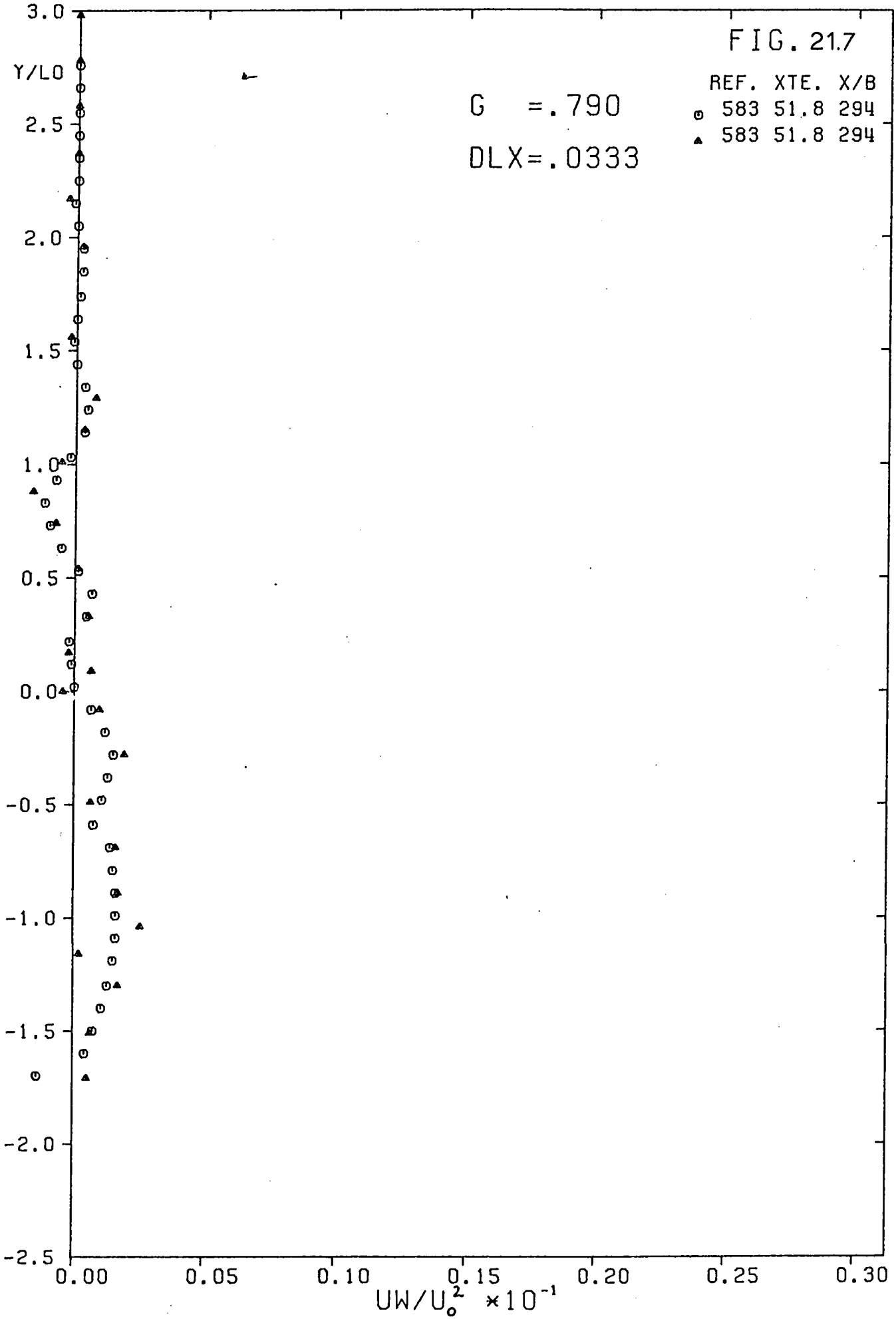
FIG. 21.7
G =.790
DLX=.0333
REF. XTE. X/B
583 51.8 294
583 51.8 294
Y/LO
3.0
2.5
2.0
1.5
1.0
0.5
0.0
-0.5
-1.0
-1.5
-2.0
-2.5
0.00
0.05
0.10
0.15
0.20
0.25
0.30
UW/U$_o^2$ ×10^{-1}

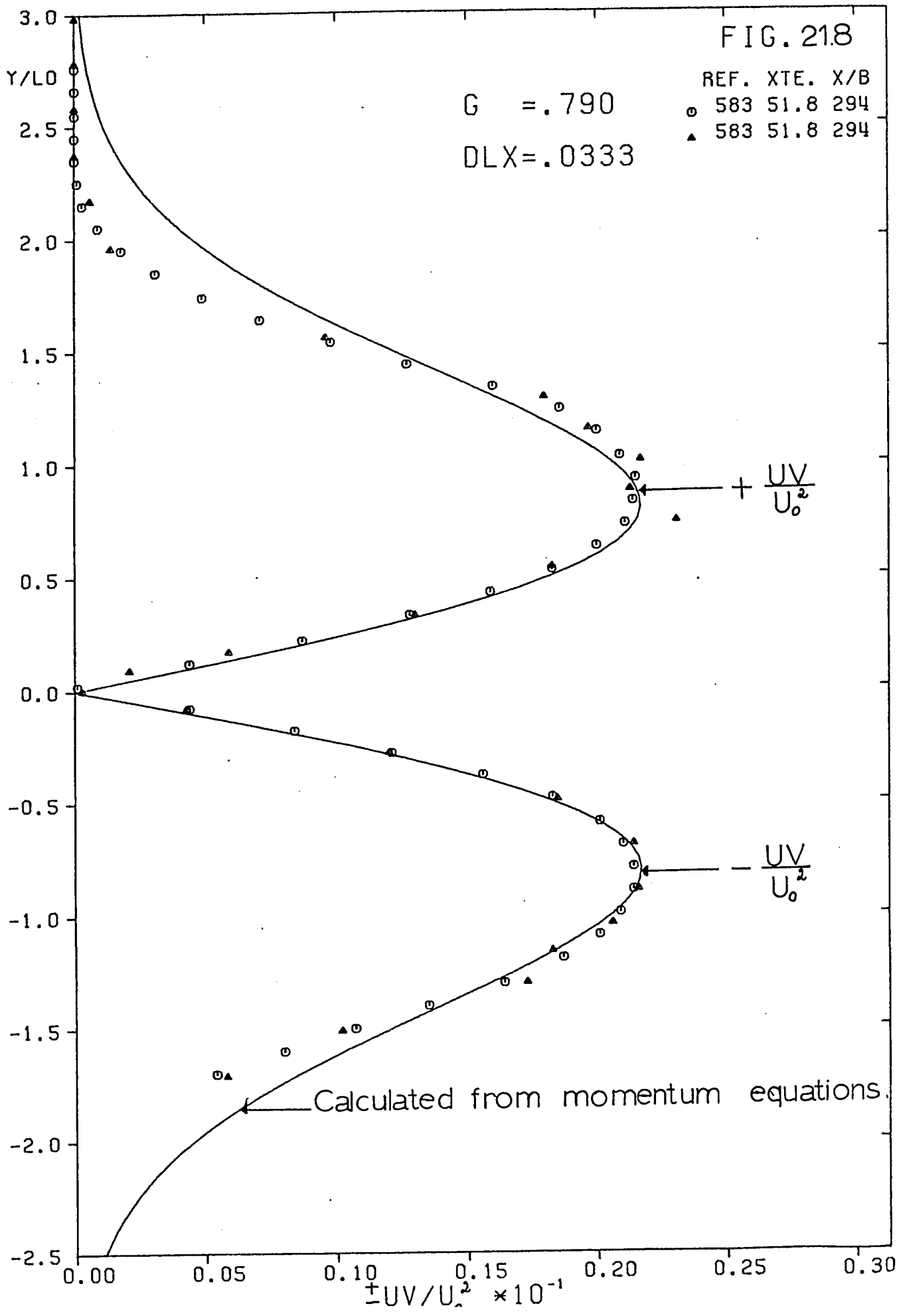
FIG. 21.8
REF. XTE. X/B
583 51.8 294
583 51.8 294
G =.790
DLX=.0333
Y/LO
3.0
2.5
2.0
1.5
1.0
0.5
0.0
-0.5
-1.0
-1.5
-2.0
-2.5
0.00
0.05
0.10
0.15
0.20
0.25
0.30
+ UV/U₀²
- UV/U₀²
Calculated from momentum equations.
±UV/U₀² ×10⁻¹

Fig. 21.9

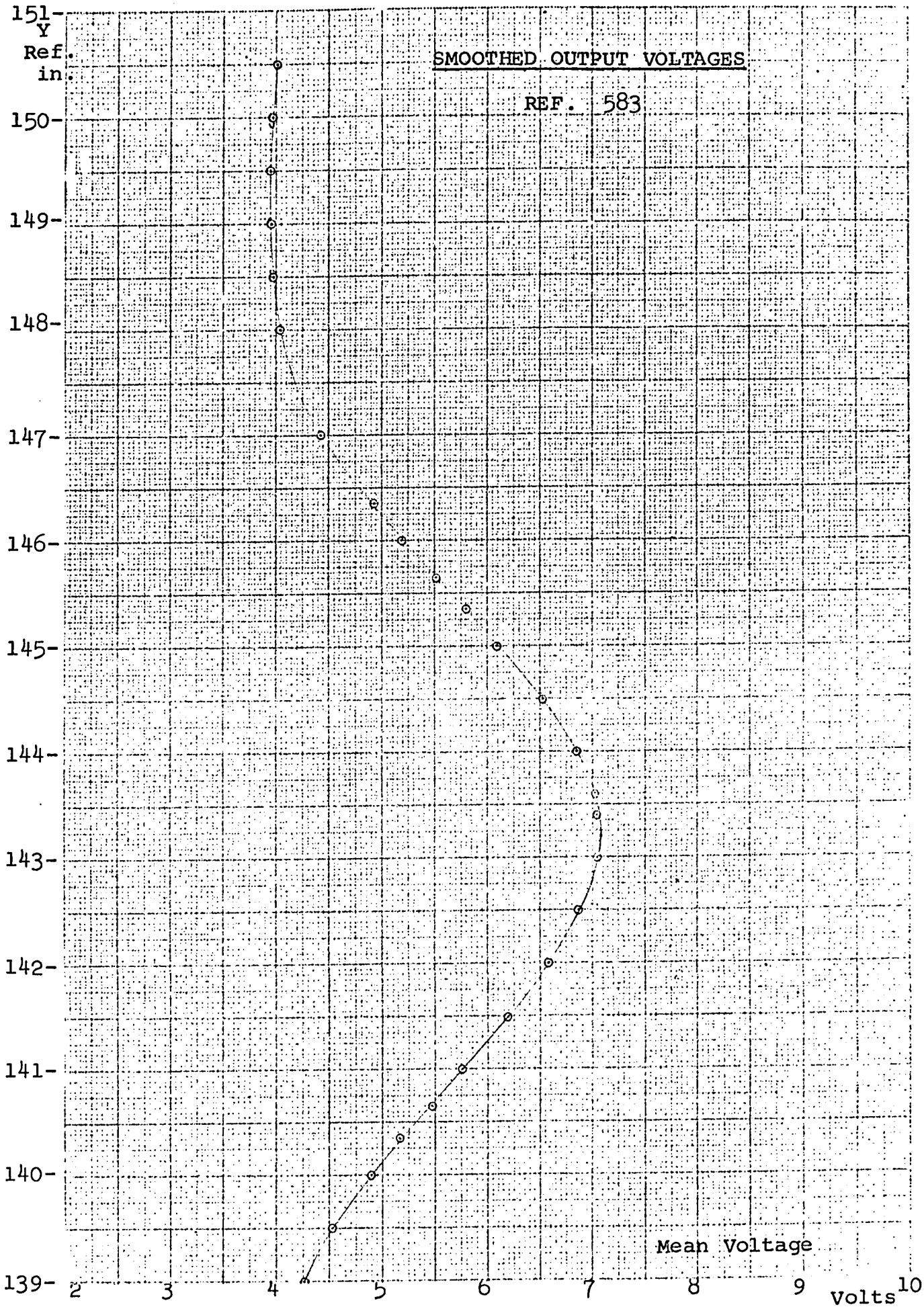
SMOOTHED OUTPUT VOLTAGES
REF. 583
Y Ref. in.
151
150
149
148
147
146
145
144
143
142
141
140
139
Mean Voltage
2
3
4
5
6
7
8
9
10
Volts

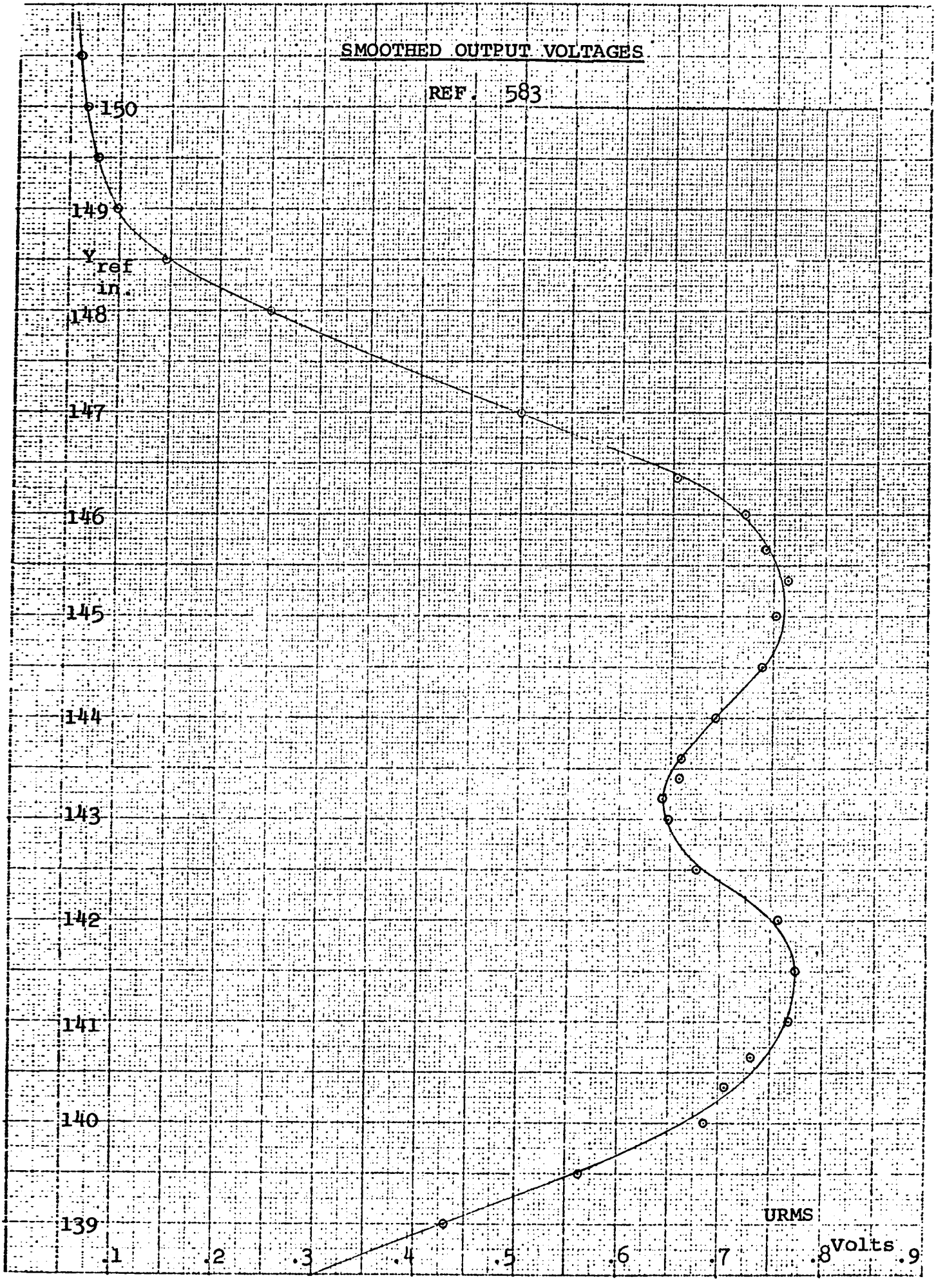
SMOOTHED OUTPUT VOLTAGES
REF. 583
150
149
Y_{ref} in.
148
147
146
145
144
143
142
141
140
139
.1
.2
.3
.4
.5
.6
.7
.8
.9
URMS
Volts

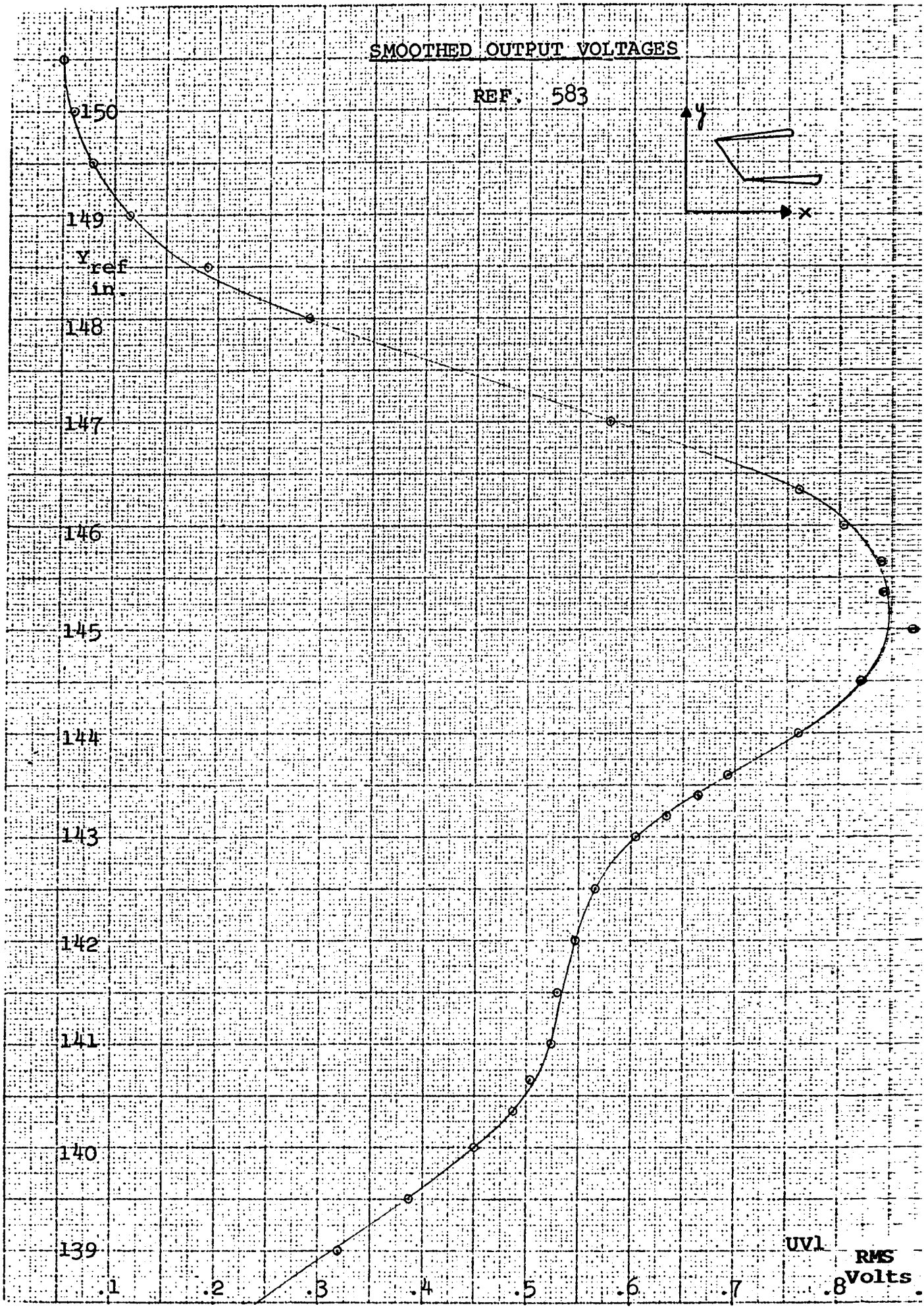
SMOOTHED OUTPUT VOLTAGES
REF. 583
y
x
150
149
Y ref in.
148
147
146
145
144
143
142
141
140
139
.1
.2
.3
.4
.5
.6
.7
.8
UV1
RMS Volts

Fig. 21.12

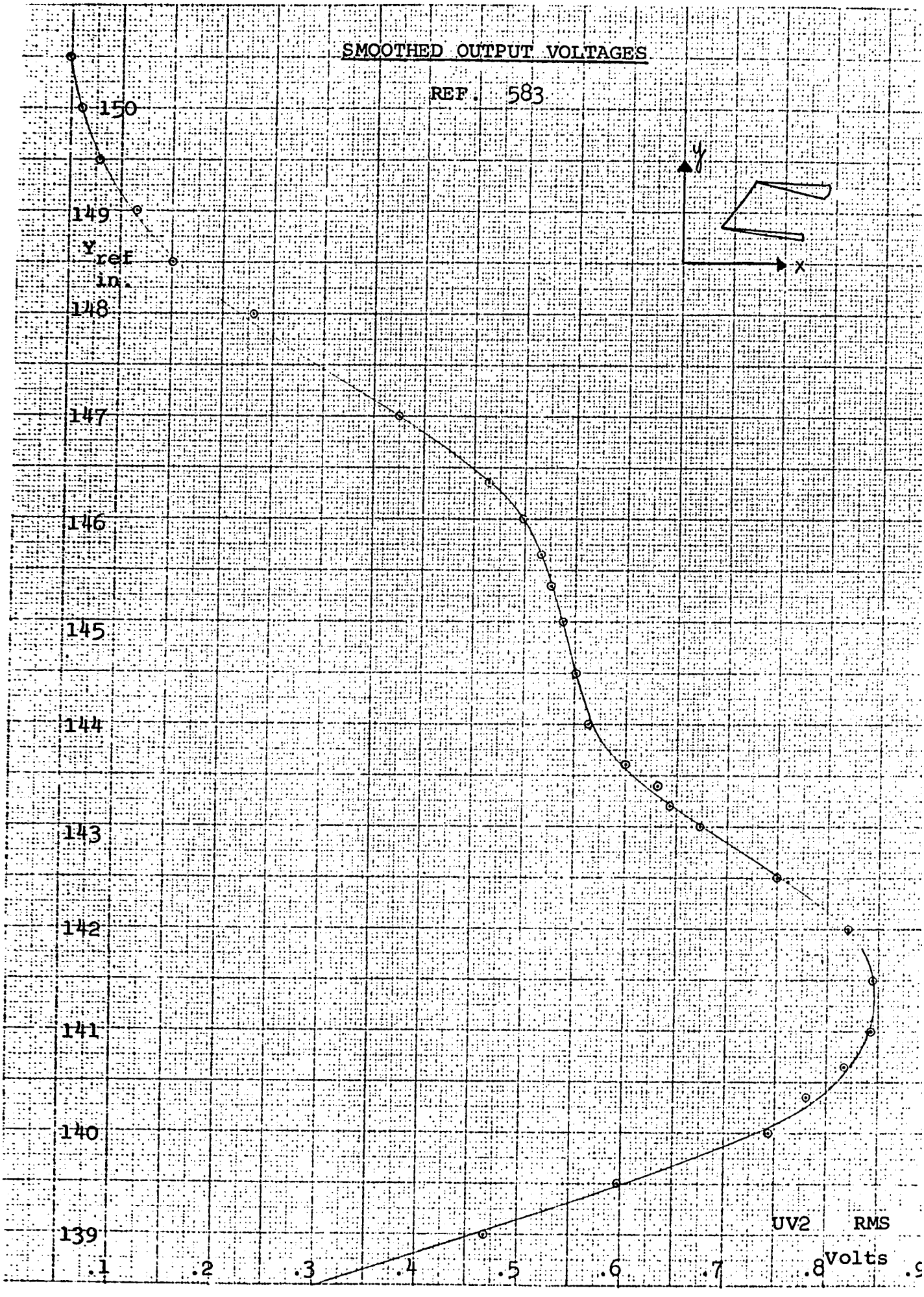
SMOOTHED OUTPUT VOLTAGES
REF. 583
y
x
150
149
Y ref in.
148
147
146
145
144
143
142
141
140
139
.1
.2
.3
.4
.5
.6
.7
.8
UV2 RMS
Volts

Fig. 21.13

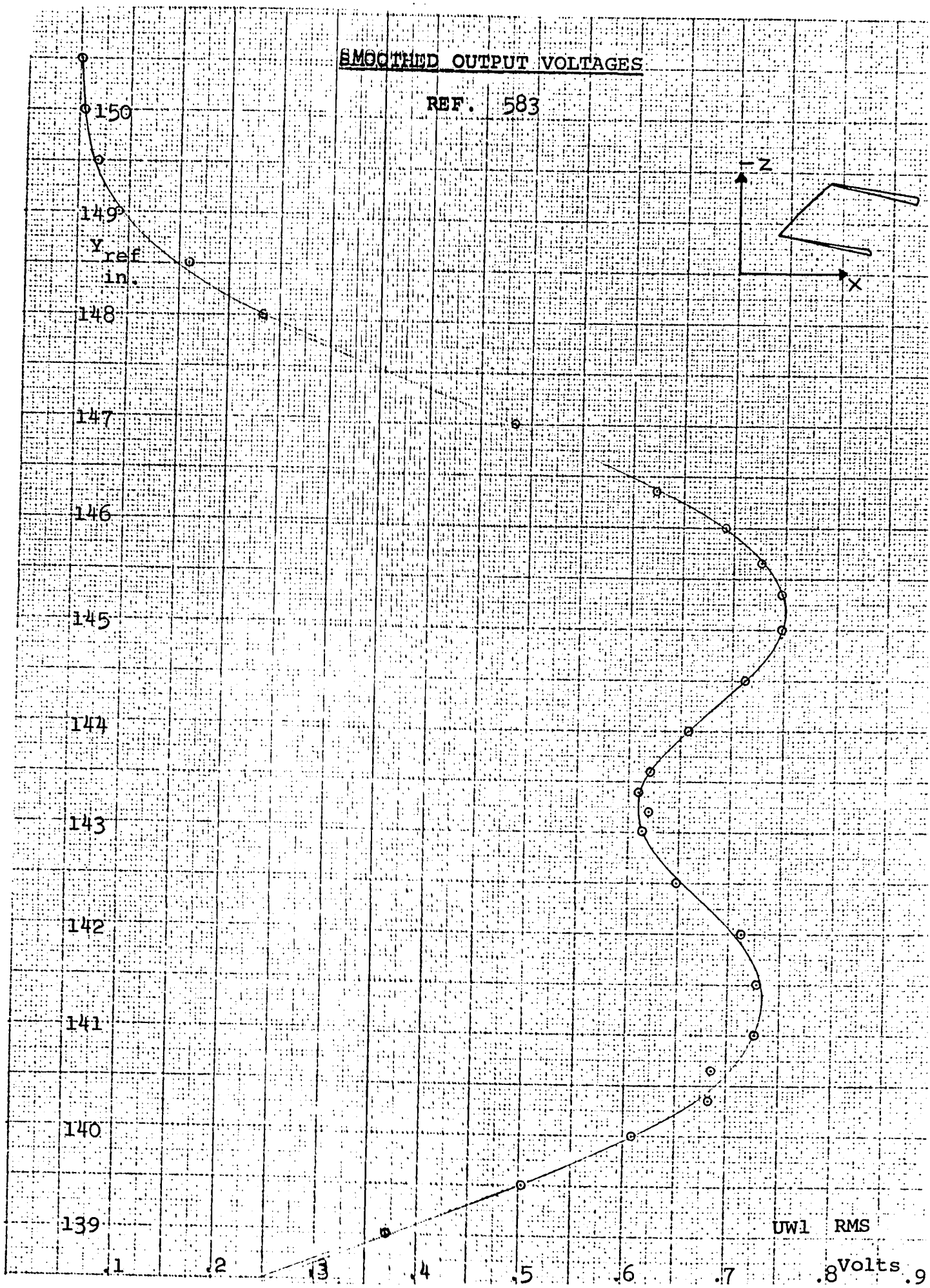
SMOOTHED OUTPUT VOLTAGES
REF. 583
-Z
X
150
149
Y ref in.
148
147
146
145
144
143
142
141
140
139
UW1 RMS
1
2
3
4
5
6
7
8
Volts
9

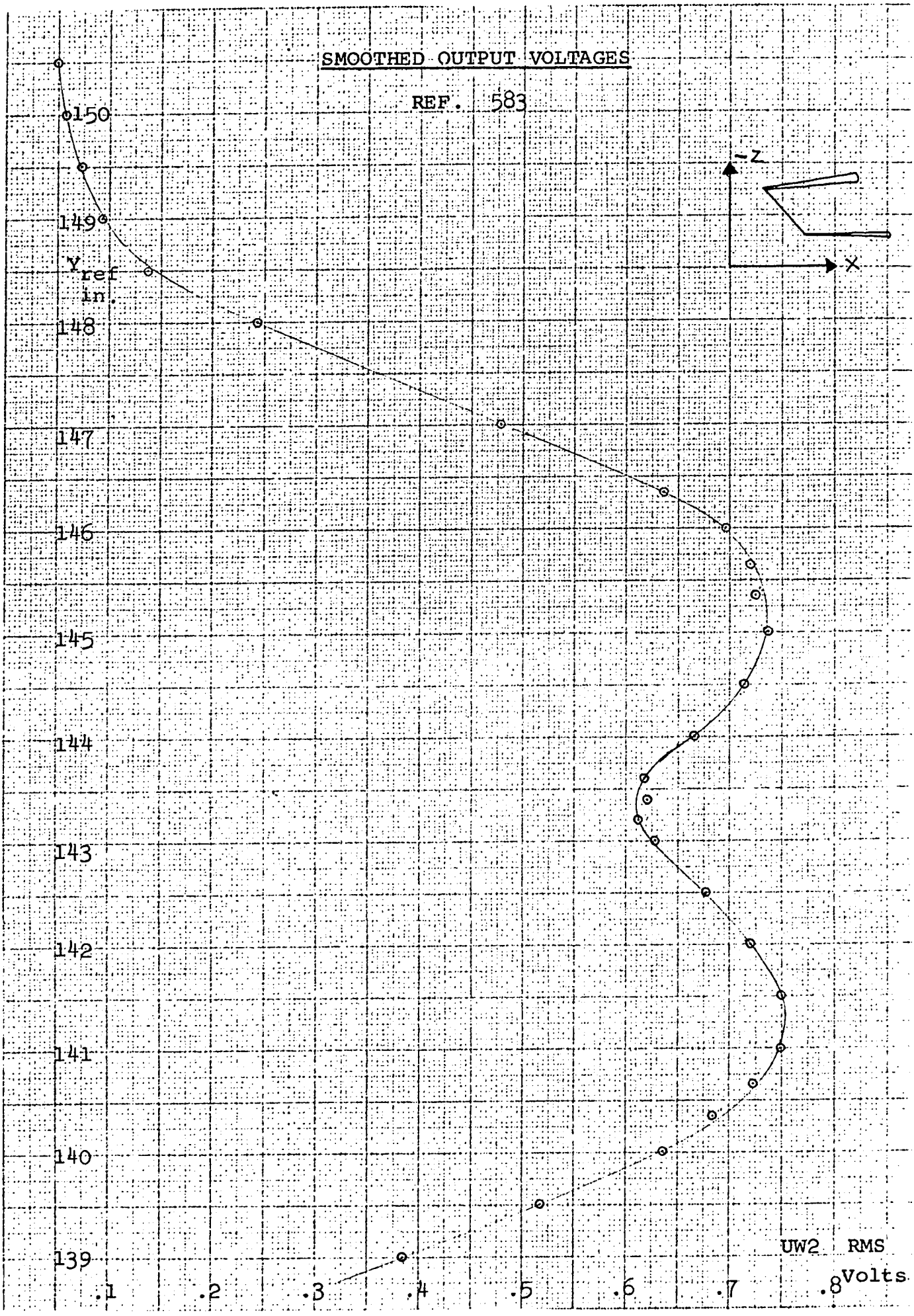
SMOOTHED OUTPUT VOLTAGES
REF. 583
-Z
X
150
149
Y_{ref} in.
148
147
146
145
144
143
142
141
140
139
.1
.2
.3
.4
.5
.6
.7
.8
UW2 RMS Volts

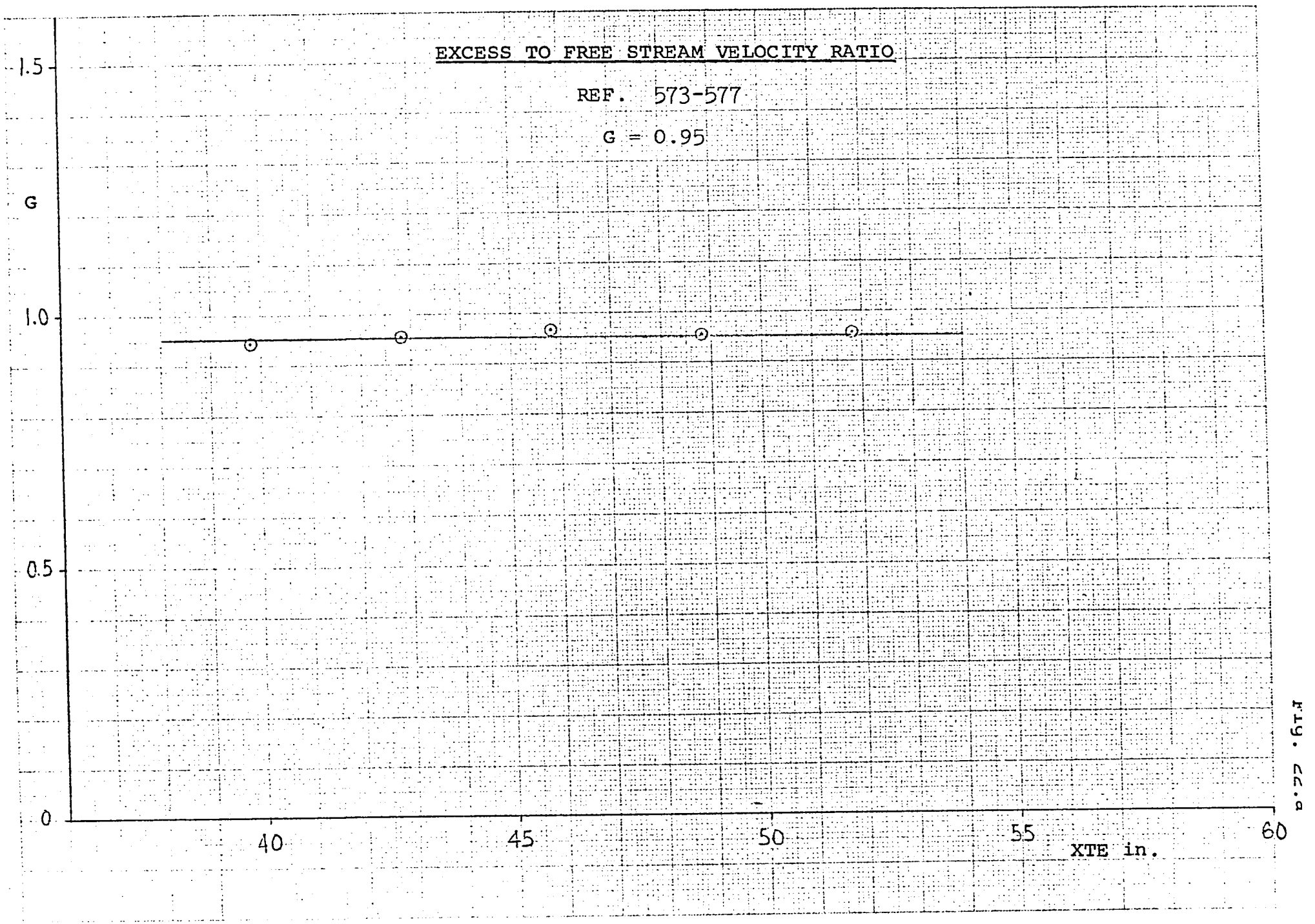
EXCESS TO FREE STREAM VELOCITY RATIO
REF. 573-577
G = 0.95
G
1.5
1.0
0.5
0
40
45
50
55
60
XTE in.

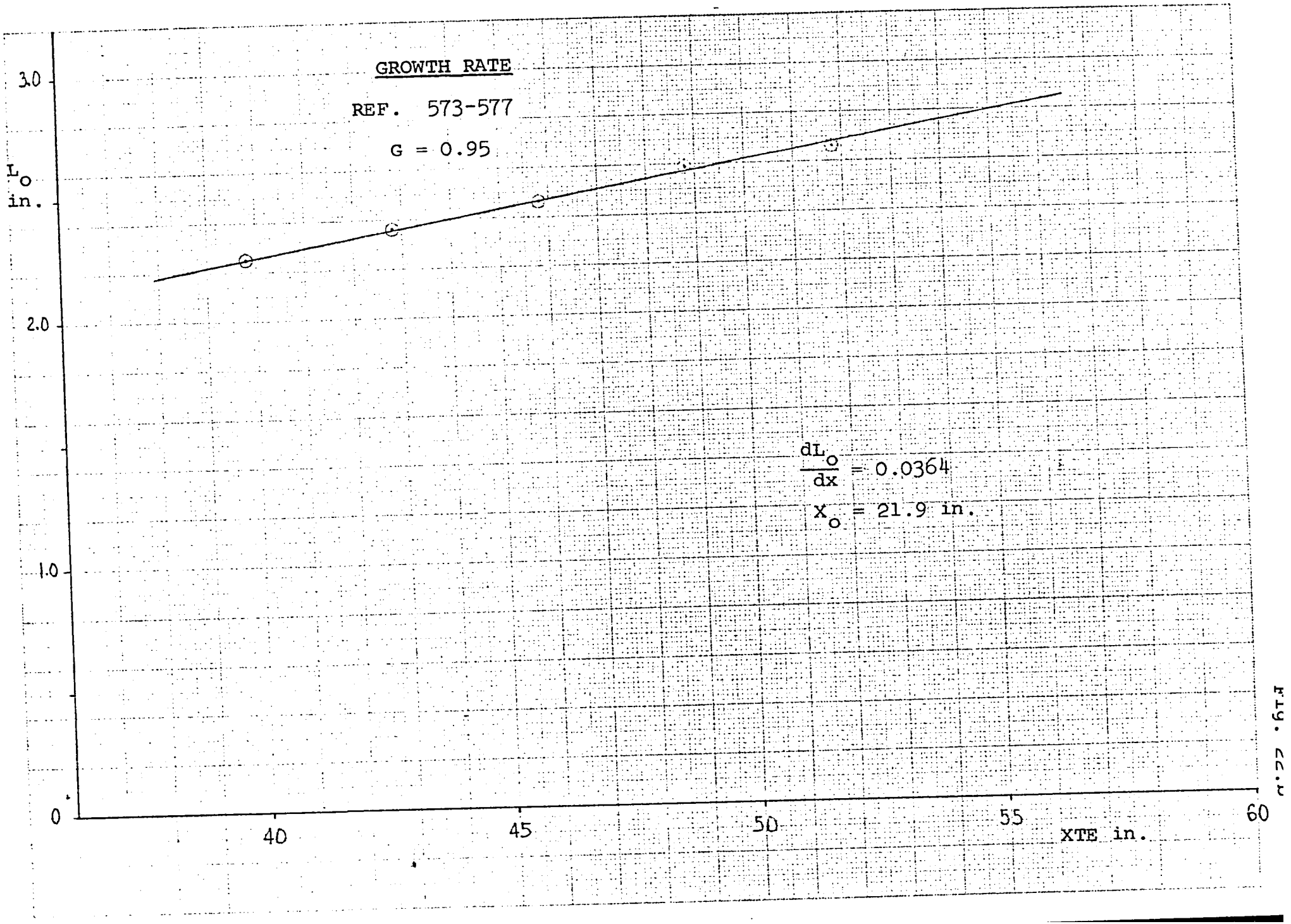
GROWTH RATE
REF. 573-577
G = 0.95
L_o in.
3.0
2.0
1.0
0
40
45
50
55
60
XTE in.
$\frac{dL_o}{dx} = 0.0364$
$X_o = 21.9$ in.

Fig. 22.2

VELOCITY DECAY

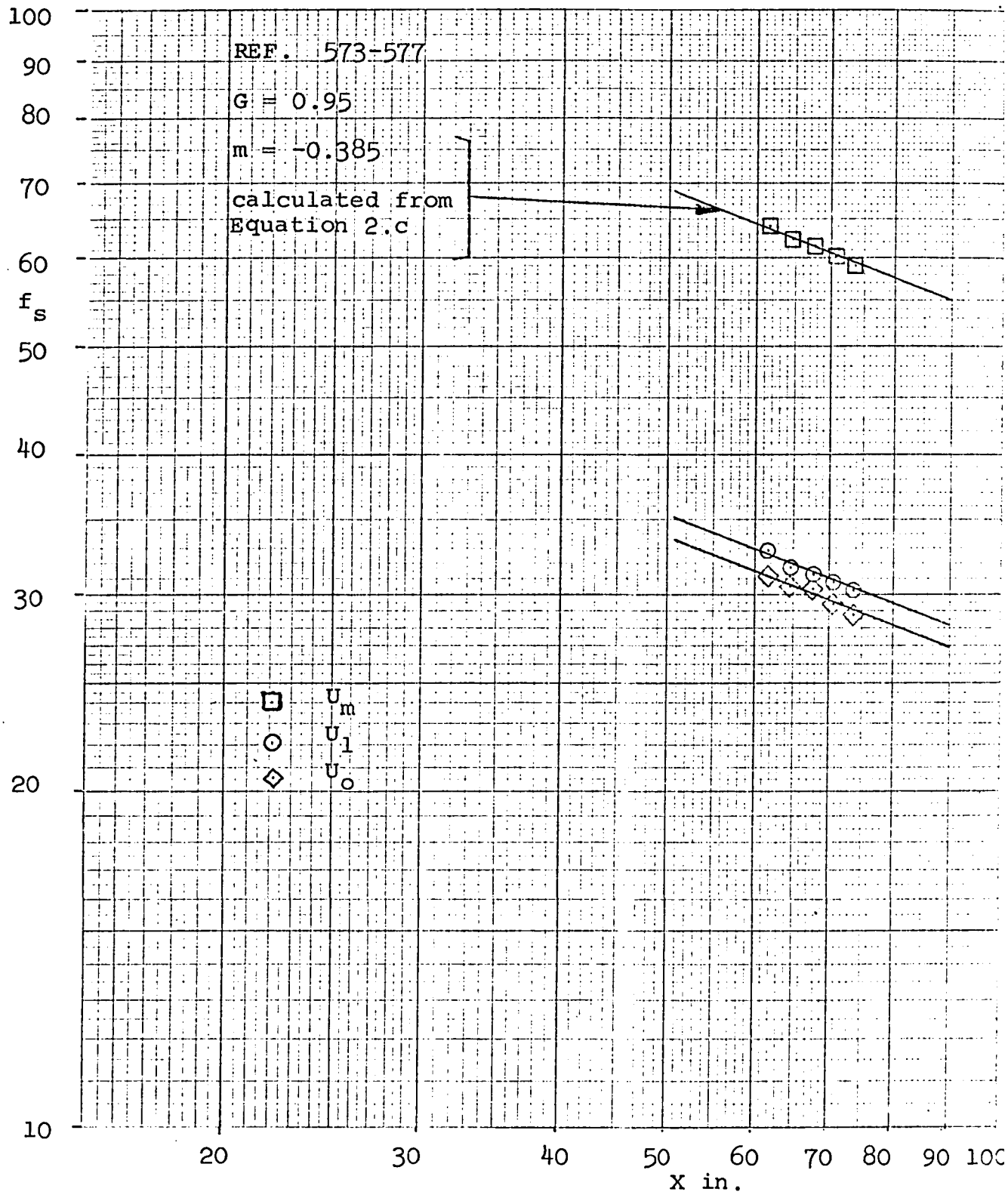

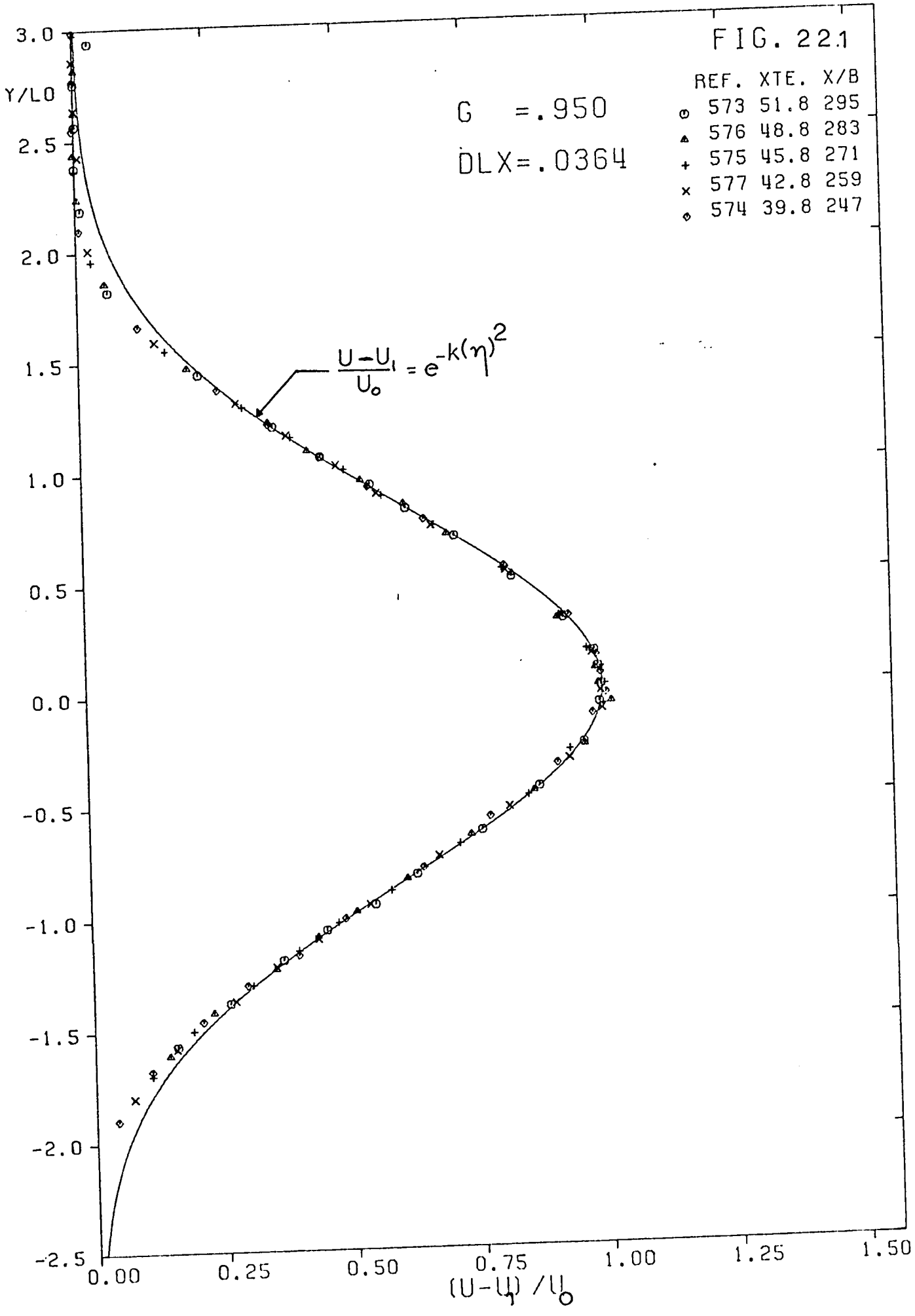
FIG. 22.1
G =.950
DLX=.0364
REF. XTE. X/B
573 51.8 295
576 48.8 283
575 45.8 271
577 42.8 259
574 39.8 247
$\frac{U-U_1}{U_o} = e^{-k(\eta)^2}$
Y/LO
3.0
2.5
2.0
1.5
1.0
0.5
0.0
-0.5
-1.0
-1.5
-2.0
-2.5
0.00
0.25
0.50
0.75
1.00
1.25
1.50
$(U-U_1)/U_o$

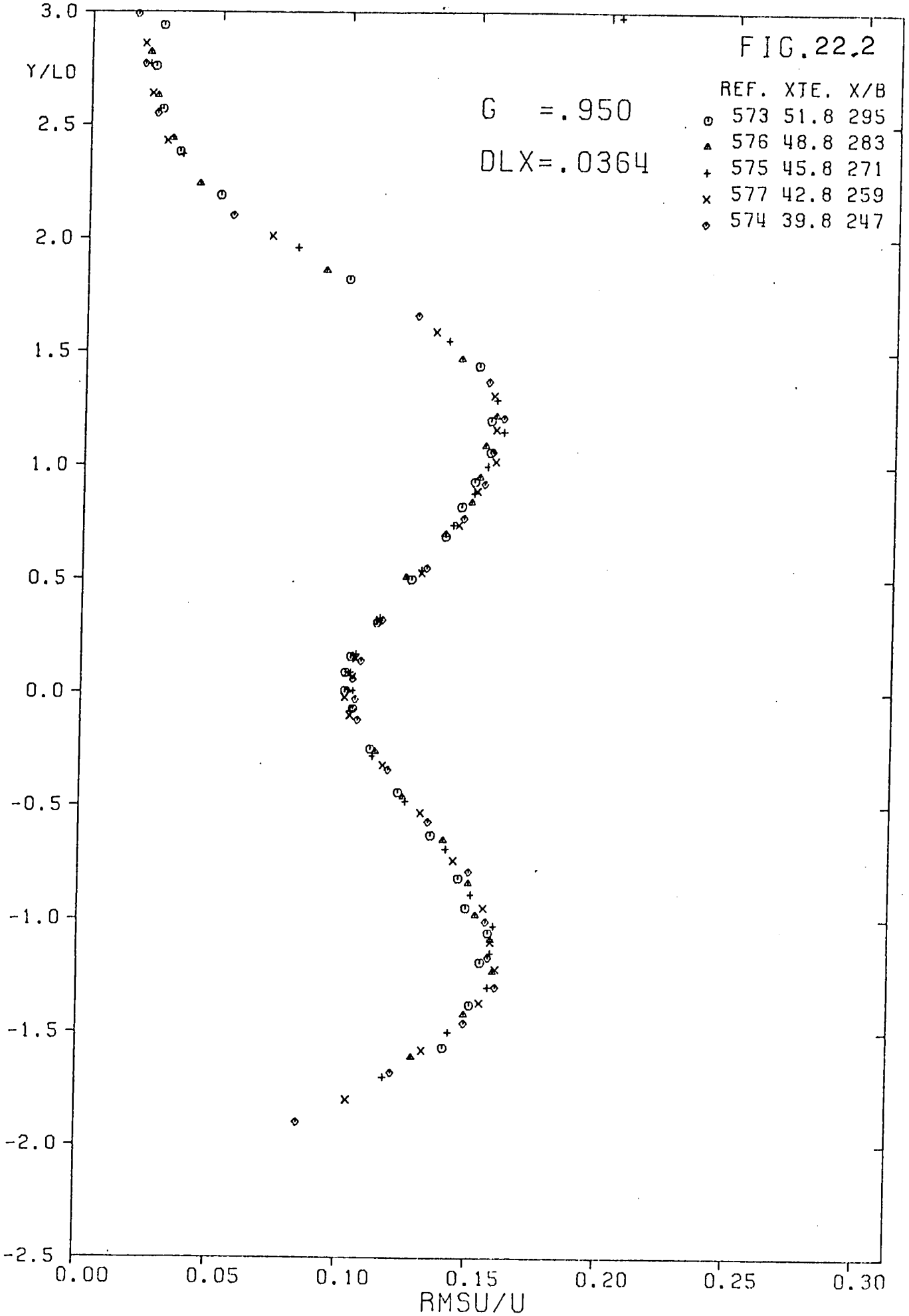
FIG.22.2
G =.950
DLX=.0364
REF. XTE. X/B
573 51.8 295
576 48.8 283
575 45.8 271
577 42.8 259
574 39.8 247
Y/LO
RMSU/U
3.0
2.5
2.0
1.5
1.0
0.5
0.0
-0.5
-1.0
-1.5
-2.0
-2.5
0.00
0.05
0.10
0.15
0.20
0.25
0.30

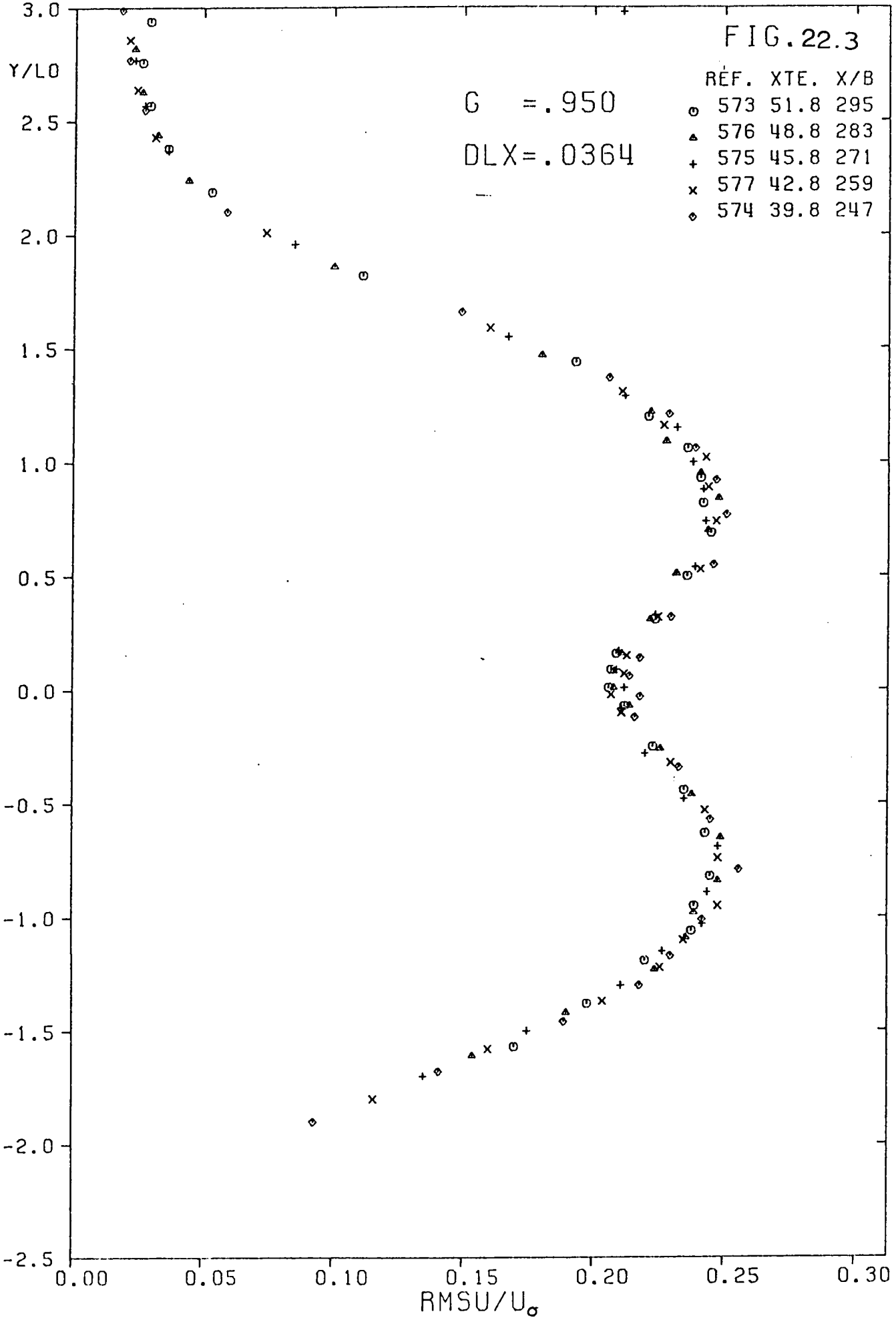
FIG.22.3
G =.950
DLX=.0364
REF. XTE. X/B
573 51.8 295
576 48.8 283
575 45.8 271
577 42.8 259
574 39.8 247
Y/LO
3.0
2.5
2.0
1.5
1.0
0.5
0.0
-0.5
-1.0
-1.5
-2.0
-2.5
0.00
0.05
0.10
0.15
0.20
0.25
0.30
RMSU/U$_\sigma$

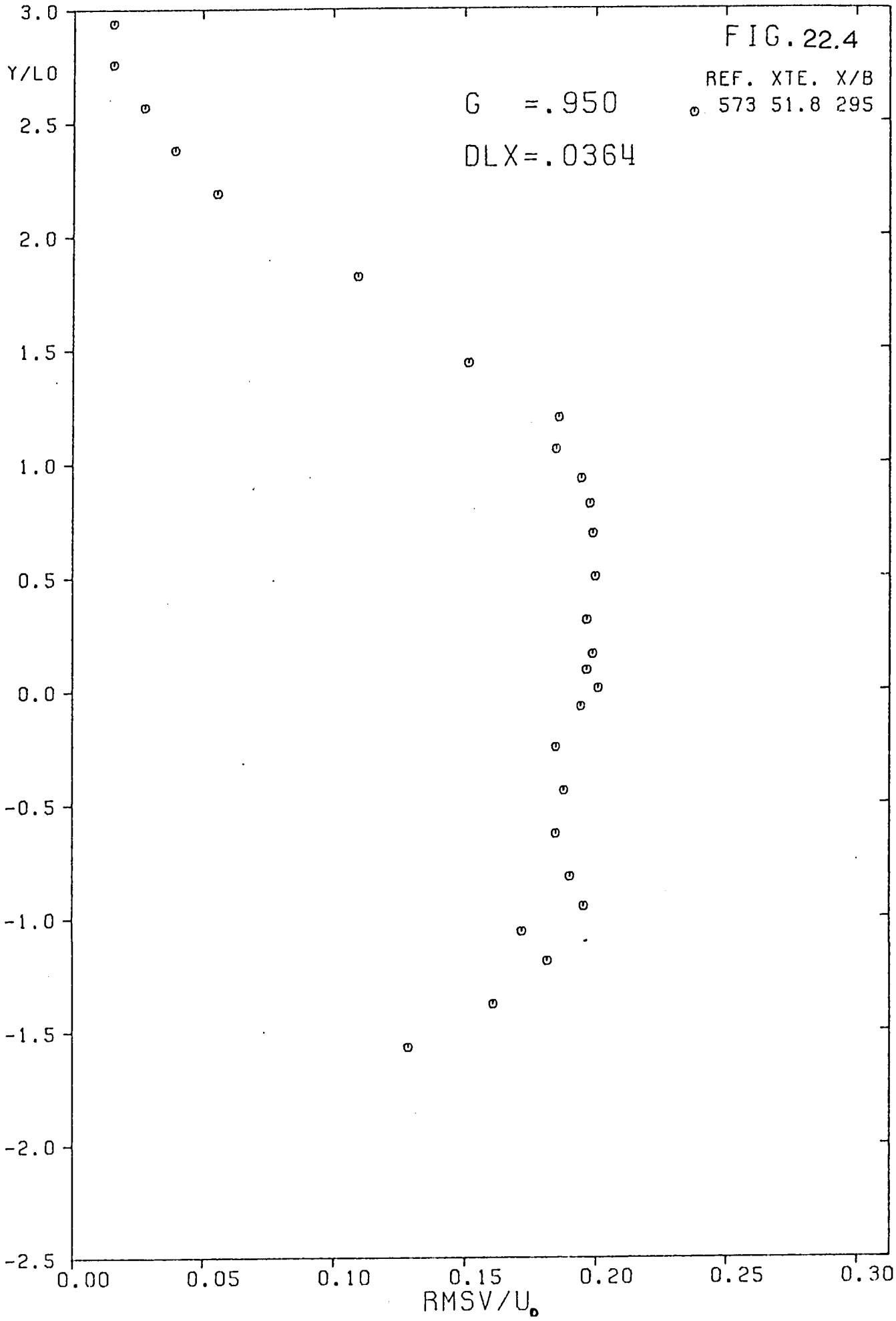
FIG. 22.4
REF. XTE. X/B
573 51.8 295
G =.950
DLX=.0364
Y/LO
3.0
2.5
2.0
1.5
1.0
0.5
0.0
-0.5
-1.0
-1.5
-2.0
-2.5
0.00
0.05
0.10
0.15
0.20
0.25
0.30
RMSV/U0

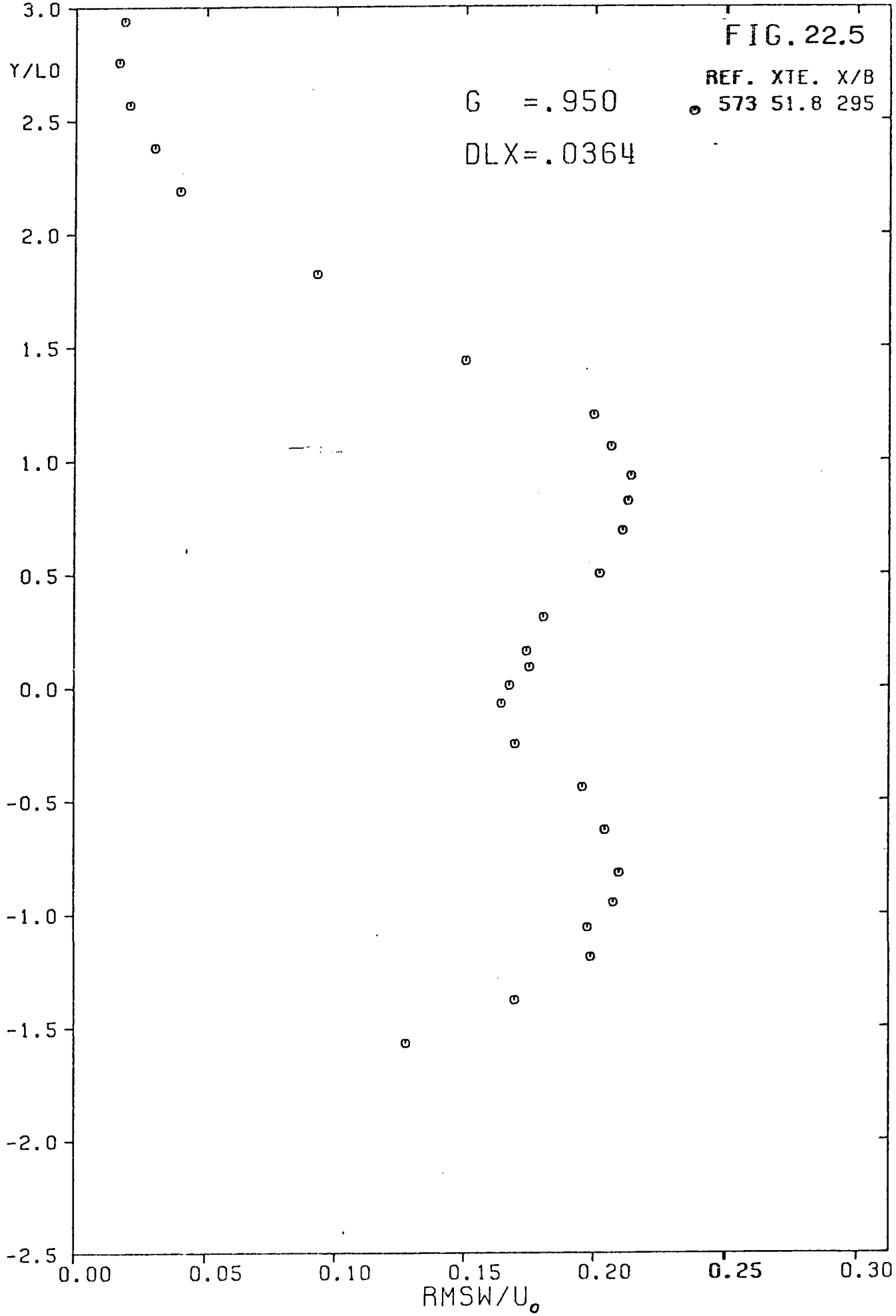
FIG. 22.5
REF. XTE. X/B
573 51.8 295
G =.950
DLX=.0364
Y/LO
3.0
2.5
2.0
1.5
1.0
0.5
0.0
-0.5
-1.0
-1.5
-2.0
-2.5
0.00
0.05
0.10
0.15
0.20
0.25
0.30
RMSW/U0

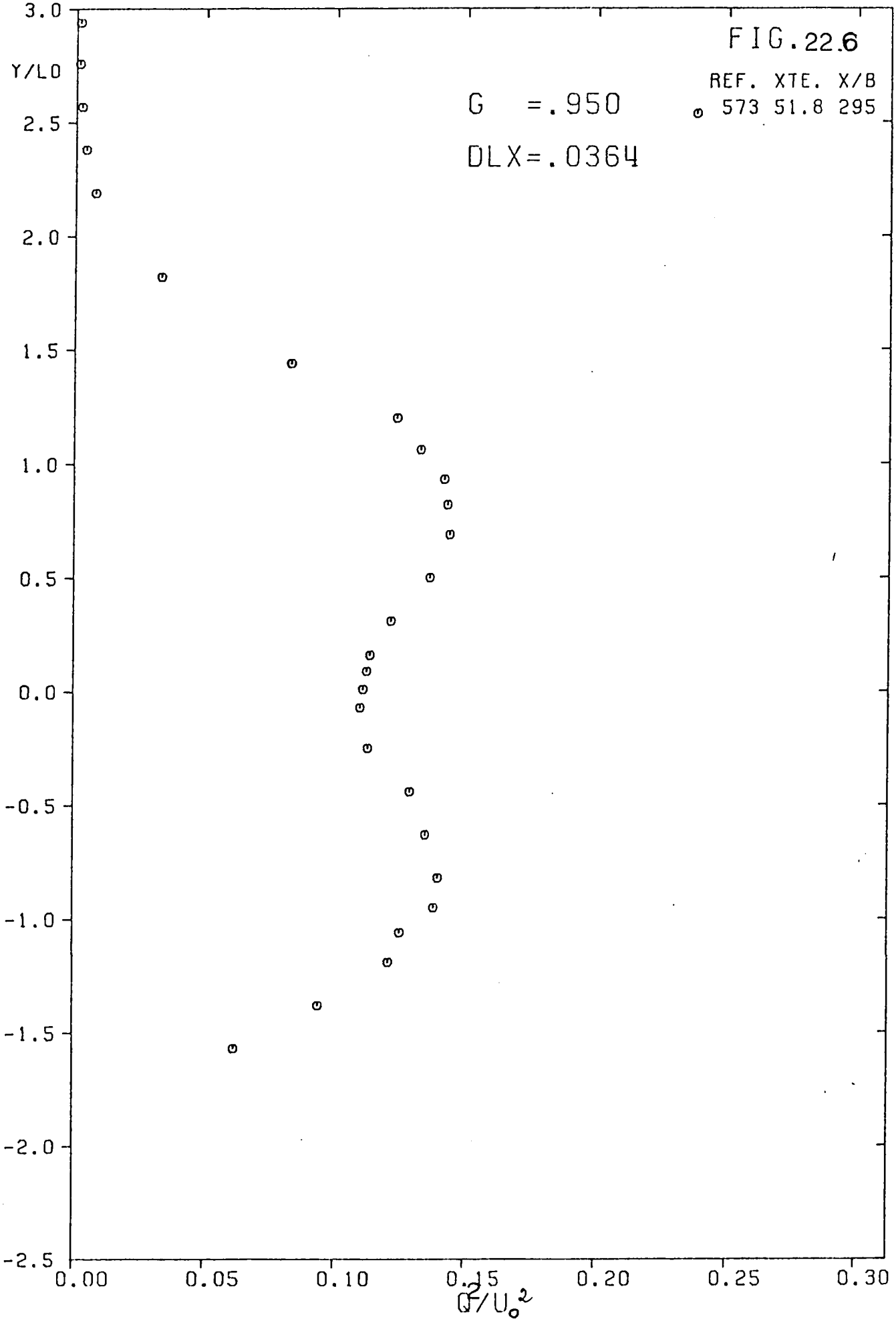
FIG. 22.6
REF. XTE. X/B
573 51.8 295
G =.950
DLX=.0364
Y/LO
3.0
2.5
2.0
1.5
1.0
0.5
0.0
-0.5
-1.0
-1.5
-2.0
-2.5
0.00
0.05
0.10
0.15
0.20
0.25
0.30
Q²/U₀²

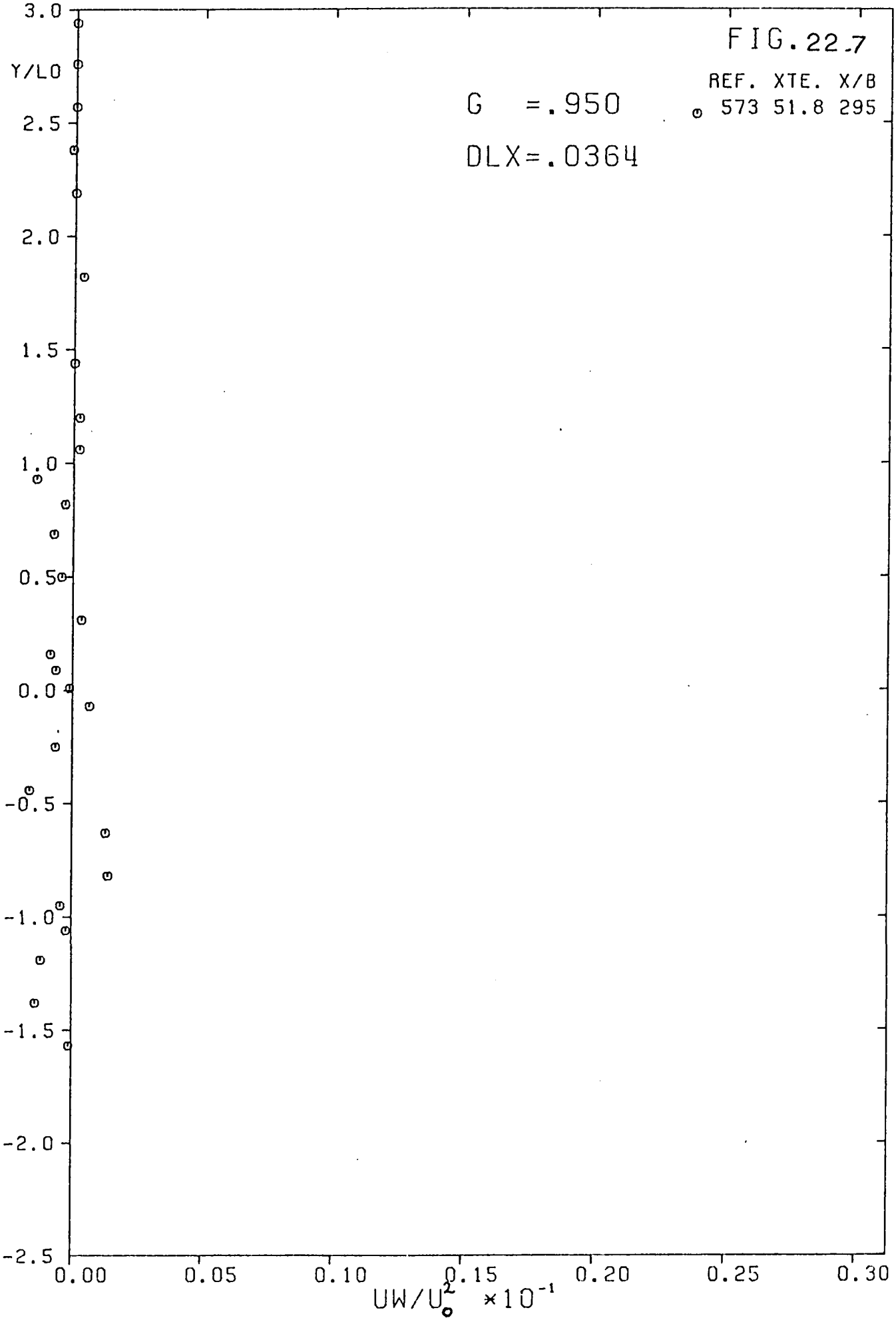
FIG. 22.7
REF. XTE. X/B
573 51.8 295
G =.950
DLX=.0364
Y/LO
3.0
2.5
2.0
1.5
1.0
0.5
0.0
-0.5
-1.0
-1.5
-2.0
-2.5
0.00
0.05
0.10
0.15
0.20
0.25
0.30
UW/U$_o^2$ ×10^{-1}

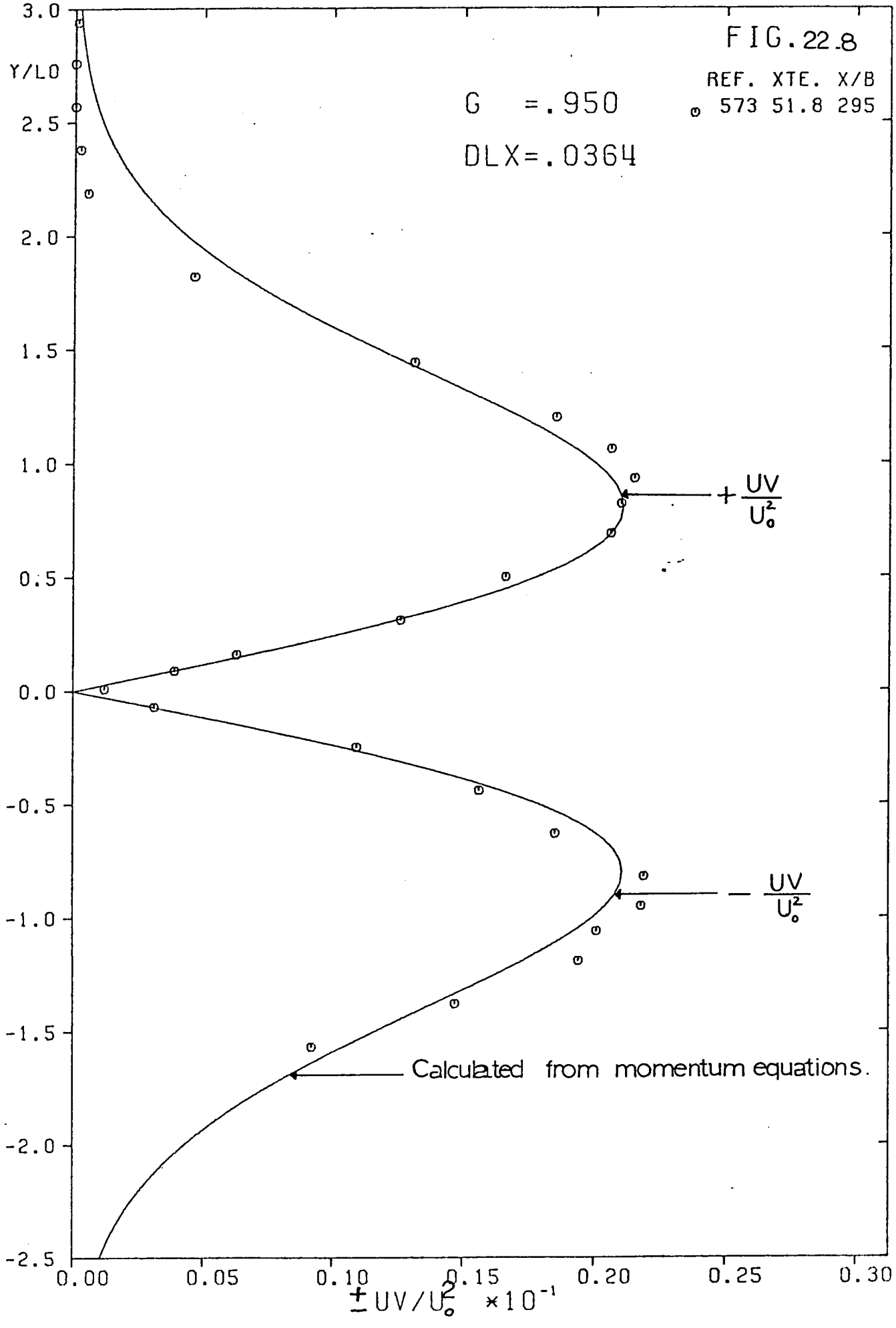
FIG. 22.8
REF. XTE. X/B
573 51.8 295
G = .950
DLX = .0364
Y/LO
3.0
2.5
2.0
1.5
1.0
0.5
0.0
-0.5
-1.0
-1.5
-2.0
-2.5
0.00
0.05
0.10
0.15
0.20
0.25
0.30
$+\frac{UV}{U_o^2}$
$-\frac{UV}{U_o^2}$
Calculated from momentum equations.
$\pm UV/U_o^2 \times 10^{-1}$

REF.NO.	XTE	DAY	MO	YR	WIRE NO.	WIRE MTL.	WIRE DIA.IN	WIRE ANGLE	WIRE CALIBRATION DV/DU	INTERCEPT	REF.VEL. RATIO
297	51.8	30	3	69	21	1	0.0002	90.00	0.1010	-0.4180	
323	51.9	31	3	69	8	1	0.0002	44.00	0.1170	-0.9610	1.01
321	51.8	31	3	69	8	1	0.0002	44.00	0.1170	-0.8610	1.01

REF. ORDINATE	MEAN VOLTAGE	H WIRE RMS VOLTS	SCALE FACTR	UV1 RMS VOLTS	SCALE FACTR	UV2 RMS VOLTS	SCALE FACTR	UW1 RMS VOLTS	SCALE FACTR	UW2 RMS VOLTS	SCALE FACTR
139.75	4.3020	0.31920	10.	0.16680	0.	0.17400	0.	0.13990	0.	0.13350	0.
139.00	4.3160	0.39430	10.	0.19370	0.	0.22650	0.	0.17820	0.	0.17970	0.
139.50	4.3770	0.20870	0.	0.29260	0.	0.39440	0.	0.32100	0.	0.29890	0.
140.00	4.5490	0.36610	0.	0.43530	0.	1.99600	1.	1.66700	1.	1.65700	1.
140.50	4.8450	0.51220	0.	0.55690	0.	2.71800	1.	2.36300	1.	2.29400	1.
141.00	5.2900	0.61370	0.	0.64320	0.	3.25500	1.	2.83200	1.	2.81100	1.
141.25	5.5000	0.65940	0.	0.67620	0.	3.47200	1.	3.02100	1.	2.96000	1.
141.50	5.7370	0.67300	0.	0.70790	0.	3.59800	1.	3.15000	1.	3.06000	1.
141.75	5.9920	0.68800	0.	0.72660	0.	3.59100	1.	3.18300	1.	3.11500	1.
142.00	6.1990	0.68700	0.	0.73290	0.	3.65400	1.	3.20600	1.	3.13500	1.
142.35	6.5240	0.67470	0.	0.75540	0.	3.55000	1.	3.12500	1.	3.07800	1.
142.65	6.7600	0.64580	0.	0.76770	0.	3.44200	1.	2.95900	1.	2.91500	1.
143.00	6.9580	0.61550	0.	0.78660	0.	3.17200	1.	2.82200	1.	2.78700	1.
143.20	7.0610	0.59940	0.	0.82510	0.	3.05600	1.	2.69500	1.	2.68400	1.
143.40	7.1110	0.59410	0.	2.72500	1.	2.98600	1.	2.67300	1.	2.67900	1.
143.60	7.0940	0.59780	0.	2.86800	1.	2.77600	1.	2.63300	1.	2.63500	1.
143.80	7.0670	0.60160	0.	2.97200	1.	2.64500	1.	2.72500	1.	2.71100	1.
144.00	6.9740	0.61750	0.	3.13100	1.	2.51000	1.	2.79600	1.	2.78000	1.
144.35	6.7620	0.65510	0.	3.41500	1.	2.43100	1.	2.97500	1.	2.96000	1.
144.65	6.5260	0.67580	0.	3.58700	1.	2.40400	1.	3.12100	1.	3.10900	1.
145.00	6.2190	0.69510	0.	3.62800	1.	2.37500	1.	3.11800	1.	3.18000	1.
145.25	5.9920	0.70510	0.	3.64000	1.	2.34200	1.	3.13600	1.	3.16500	1.
145.50	5.7410	0.68460	0.	3.59600	1.	2.24000	1.	3.06800	1.	3.11400	1.
145.75	5.4770	0.64500	0.	3.43600	1.	2.21300	1.	2.95600	1.	2.98700	1.
146.00	5.2750	0.62040	0.	3.25550	1.	2.08700	1.	2.75400	1.	2.83600	1.
146.50	4.8560	0.52350	0.	2.69900	1.	1.75900	1.	2.27700	1.	2.24900	1.
147.00	4.5380	0.37040	0.	2.01500	1.	1.37600	1.	1.56600	1.	1.59700	1.
147.50	4.3880	0.21700	0.	1.21800	1.	0.29450	0.	0.30640	0.	0.30830	0.
148.00	4.3320	0.40300	10.	0.21400	0.	0.19500	0.	0.16270	0.	0.17900	0.
148.50	4.3210	0.25670	10.	0.13220	0.	0.40300	1.	0.32510	1.	0.32740	1.
149.00	4.3230	0.17910	10.	0.27850	1.	0.29860	1.	0.22510	1.	0.23060	1.
149.50	4.3290	0.04544	0.	0.21200	1.	0.20650	1.	0.18690	1.	0.18600	1.
150.00	4.3410	0.03915	0.	0.17080	1.	0.16990	1.	0.15820	1.	0.15030	1.

Fig. 23.a

REF.NO.	XTE	DAY	MO	YR	WIRE NO.	WIRE MTL.	WIRE DIA.IN	WIRE ANGLE	WIRE CALIBRATION DV/DU	INTERCEPT	REF.VEL. RATIO
297	51.8	30	3	69	21	1	0.0002	90.00	0.1010	-0.4180	
323	51.8	31	3	69	8	1	0.0002	44.00	0.1170	-0.8610	1.01
321	51.8	31	3	69	8	1	0.0002	44.00	0.1170	-0.8610	1.01

X	X/B	LO	UO	UM	UJ	UO/U1	YCL	XO
79.9	320.	2.02	27.5	74.5	47.0	0.586	143.50	28.1

YREF	Y	U	U-U1	/U-U1/G	RMSU	MSU	MSV	MSW	UV	UW
138.75	-4.75	46.7	-0.2	0.6	0.999	0.999	1.087	0.368	-0.044	-0.031
139.00	-4.50	46.9	-0.1	0.9	1.203	1.448	1.735	0.863	-0.248	0.003
139.50	-4.00	47.5	0.5	1.8	2.066	4.270	4.395	2.699	-1.258	-0.247
140.00	-3.50	48.2	2.2	3.4	3.625	13.139	8.167	6.707	-3.756	-0.178
140.50	-3.00	52.1	5.2	6.0	5.071	25.718	12.450	13.689	-7.706	-0.578
141.00	-2.50	56.5	9.6	9.5	6.076	36.921	16.742	20.871	-11.612	-0.213
141.25	-2.25	58.6	11.6	11.6	6.529	42.624	18.007	22.382	-13.453	-0.656
141.50	-2.00	60.9	14.0	13.9	6.663	44.400	20.968	25.580	-14.266	-1.005
141.75	-1.75	63.5	16.5	16.4	6.821	46.523	19.747	25.507	-13.693	-0.770
142.00	-1.50	65.5	18.6	18.8	6.802	46.267	21.889	26.690	-14.349	-0.810
142.35	-1.15	68.7	21.8	22.0	6.680	44.625	21.981	25.210	-12.399	-0.524
142.65	-0.85	71.1	24.1	24.4	6.394	40.884	23.497	21.799	-10.704	-0.465
143.00	-0.50	73.0	26.1	26.4	6.094	37.138	21.808	20.006	-6.965	-0.353
143.20	-0.30	74.0	27.1	27.1	5.935	35.220	22.242	17.404	-4.550	-0.106
143.40	-0.10	74.5	27.6	27.5	5.783	33.445	23.130	17.817	-1.418	-0.325
143.60	0.10	74.4	27.4	27.5	5.820	33.870	22.416	16.610	1.624	0.019
143.80	0.30	74.1	27.2	27.1	5.956	35.479	21.891	18.233	3.303	-0.137
144.00	0.50	73.2	26.2	26.4	6.114	37.379	21.073	19.139	6.299	-0.160
144.35	0.85	71.1	24.1	24.3	6.486	42.070	21.901	21.941	10.344	-0.160
144.65	1.15	68.8	21.8	21.9	6.701	44.903	22.889	25.530	12.745	-0.134
145.00	1.50	65.7	18.7	18.7	6.882	47.364	21.141	24.721	13.526	0.702
145.25	1.75	63.5	16.5	16.3	6.981	48.737	19.624	23.503	13.963	0.329
145.50	2.00	61.0	14.0	13.9	6.781	45.985	19.411	23.491	14.205	0.511
145.75	2.25	58.4	11.4	11.6	6.386	40.783	19.985	23.307	12.423	0.331
146.00	2.50	56.4	9.4	9.5	6.143	37.731	16.743	19.093	11.220	0.824
146.50	3.00	52.2	5.3	5.9	5.187	26.906	10.958	10.471	7.536	-0.236
147.00	3.50	49.1	2.1	3.4	3.667	13.449	9.136	4.619	3.896	0.248
147.50	4.00	47.6	0.6	1.8	2.149	4.616	3.860	2.259	1.108	0.021
148.00	4.50	47.0	0.1	0.9	1.264	1.599	1.421	0.542	0.140	0.100
148.50	5.00	46.9	-0.0	0.4	0.804	0.646	0.569	0.137	0.022	0.003
149.00	5.50	46.9	-0.0	0.2	0.561	0.314	0.265	0.068	-0.010	0.005
149.50	6.00	47.0	0.0	0.1	0.450	0.202	0.115	0.053	0.004	-0.001
150.00	6.50	47.1	0.2	0.0	0.388	0.150	0.061	0.025	0.001	-0.004

Fig. 23.b

REF.NO.	XTF	DAY	MO	YR	WIRE NO.	WIRE MTL.	WIRE DIA.IN	WIRE ANGLE	WIRE CALIBRATION DV/DU	WIRE CALIBRATION INTERCEPT	REF.VEL. RATIO
297	51.8	30	3	69	21	1	0.0002	90.00	0.1010	-0.4190	
323	51.8	31	3	69	8	1	0.0002	44.00	0.1170	-0.8610	1.01
321	51.8	31	3	69	8	1	0.0002	44.00	0.1170	-0.8610	1.01

X	X/R	LO	UO	UM	UI	UO/UI	YCL	XO	DLX	G
79.9	320.	2.02	27.5	74.5	47.0	0.586	143.50	28.1	.02530	.99300

YREF	Y/LO	Y/X	U-UI / UO	/U-UI/G / UO	RMSU U	RMSU UO	RMSV UO	RMSW UO	MSU SU	MSU SUO	MSV SUO	MSW SUO	O2 SUO	UV SUO	MUV SUO	UW SUO	Y/LOX
138.75	-2.35	-.0594	-.009	0.021	0.021	0.036	0.041	0.024	0.0005	0.0013	0.0017	0.0006	0.004	-.0001	-.0017	-.0000	-2.35
139.00	-2.23	-.0563	-.008	0.032	0.026	0.044	0.052	0.034	0.0007	0.0019	0.0027	0.0013	0.006	-.0004	-.0024	0.0000	-2.22
139.50	-1.98	-.0500	0.010	0.046	0.044	0.075	0.082	0.064	0.0019	0.0056	0.0068	0.0042	0.017	-.0018	-.0045	-.0004	-1.98
140.00	-1.73	-.0438	0.081	0.124	0.074	0.132	0.112	0.102	0.0054	0.0173	0.0126	0.0103	0.040	-.0054	-.0076	-.0003	-1.73
140.50	-1.48	-.0375	0.187	0.216	0.097	0.184	0.138	0.145	0.0095	0.0340	0.0192	0.0211	0.074	-.0110	-.0117	-.0008	-1.48
141.00	-1.24	-.0312	0.347	0.346	0.108	0.221	0.161	0.179	0.0116	0.0488	0.0258	0.0321	0.107	-.0166	-.0160	-.0003	-1.23
141.25	-1.11	-.0281	0.423	0.423	0.111	0.237	0.167	0.196	0.0124	0.0563	0.0277	0.0345	0.119	-.0192	-.0179	-.0009	-1.11
141.50	-0.99	-.0250	0.502	0.502	0.109	0.242	0.180	0.198	0.0120	0.0586	0.0323	0.0394	0.130	-.0203	-.0193	-.0014	-0.99
141.75	-0.87	-.0219	0.600	0.595	0.107	0.248	0.174	0.198	0.0116	0.0614	0.0304	0.0393	0.131	-.0195	-.0200	-.0011	-0.86
142.00	-0.74	-.0187	0.674	0.693	0.104	0.247	0.184	0.203	0.0108	0.0611	0.0337	0.0411	0.136	-.0205	-.0200	-.0012	-0.74
142.25	-0.57	-.0143	0.791	0.790	0.097	0.243	0.184	0.197	0.0094	0.0594	0.0339	0.0388	0.132	-.0177	-.0182	-.0007	-0.57
142.65	-0.42	-.0106	0.876	0.895	0.090	0.232	0.190	0.193	0.0081	0.0540	0.0362	0.0336	0.124	-.0152	-.0150	-.0007	-0.42
143.00	-0.25	-.0062	0.969	0.959	0.083	0.221	0.193	0.176	0.0070	0.0490	0.0336	0.0308	0.113	-.0099	-.0096	-.0005	-0.25
143.20	-0.15	-.0037	0.985	0.985	0.080	0.216	0.189	0.164	0.0064	0.0465	0.0358	0.0269	0.109	-.0065	-.0059	-.0002	-0.15
143.40	-0.05	-.0012	1.003	0.998	0.078	0.210	0.189	0.166	0.0060	0.0442	0.0356	0.0274	0.107	-.0020	-.0020	-.0005	-0.05
143.60	0.05	0.0012	0.996	0.998	0.078	0.211	0.186	0.160	0.0061	0.0447	0.0345	0.0256	0.105	0.0023	0.0021	0.0000	0.05
143.80	0.15	0.0038	0.987	0.994	0.080	0.216	0.184	0.169	0.0065	0.0469	0.0337	0.0281	0.109	0.0047	0.0061	-.0002	0.15
144.00	0.25	0.0063	0.953	0.958	0.084	0.227	0.190	0.172	0.0070	0.0494	0.0325	0.0295	0.111	0.0090	0.0097	-.0002	0.25
144.35	0.42	0.0107	0.877	0.883	0.091	0.236	0.193	0.184	0.0083	0.0556	0.0336	0.0338	0.123	0.0148	0.0151	-.0002	0.42
144.65	0.57	0.0144	0.792	0.797	0.097	0.244	0.188	0.199	0.0095	0.0593	0.0353	0.0393	0.134	0.0182	0.0182	-.0002	0.57
145.00	0.75	0.0188	0.681	0.690	0.105	0.250	0.180	0.195	0.0110	0.0625	0.0326	0.0381	0.133	0.0193	0.0200	0.0010	0.74
145.25	0.87	0.0219	0.603	0.592	0.110	0.254	0.174	0.190	0.0121	0.0644	0.0302	0.0362	0.131	0.0199	0.0200	0.0005	0.87
145.50	0.99	0.0251	0.510	0.504	0.111	0.246	0.173	0.190	0.0124	0.0607	0.0299	0.0362	0.127	0.0203	0.0193	0.0007	0.99
145.75	1.12	0.0282	0.415	0.421	0.109	0.232	0.175	0.189	0.0120	0.0539	0.0308	0.0359	0.121	0.0177	0.0178	0.0005	1.11
146.00	1.24	0.0313	0.342	0.342	0.109	0.223	0.161	0.171	0.0119	0.0498	0.0258	0.0294	0.105	0.0160	0.0159	0.0012	1.24
146.50	1.49	0.0376	0.191	0.215	0.099	0.188	0.130	0.127	0.0099	0.0355	0.0169	0.0161	0.069	0.0107	0.0116	-.0003	1.49
147.00	1.74	0.0439	0.077	0.123	0.075	0.133	0.112	0.084	0.0056	0.0178	0.0125	0.0071	0.037	0.0056	0.0074	0.0004	1.73
147.50	1.99	0.0501	0.022	0.065	0.045	0.078	0.077	0.059	0.0020	0.0061	0.0059	0.0035	0.016	0.0016	0.0045	0.0000	1.98
148.00	2.23	0.0564	0.003	0.031	0.027	0.046	0.047	0.029	0.0007	0.0021	0.0022	0.0008	0.005	0.0002	0.0024	0.0001	2.23
148.50	2.49	0.0626	-.001	0.014	0.017	0.029	0.030	0.015	0.0003	0.0009	0.0009	0.0002	0.002	0.0000	0.0012	0.0000	2.48
149.00	2.73	0.0689	-.000	0.006	0.012	0.020	0.020	0.010	0.0001	0.0004	0.0004	0.0001	0.001	-.0000	0.0005	0.0000	2.72
149.50	2.98	0.0751	0.002	0.002	0.010	0.016	0.013	0.009	0.0001	0.0003	0.0002	0.0001	0.001	0.0000	0.0002	-.0000	2.97
150.00	3.23	0.0814	0.006	0.001	0.008	0.014	0.010	0.006	0.0001	0.0002	0.0001	0.0000	0.000	0.0000	0.0001	-.0000	3.22

Fig. 23.c

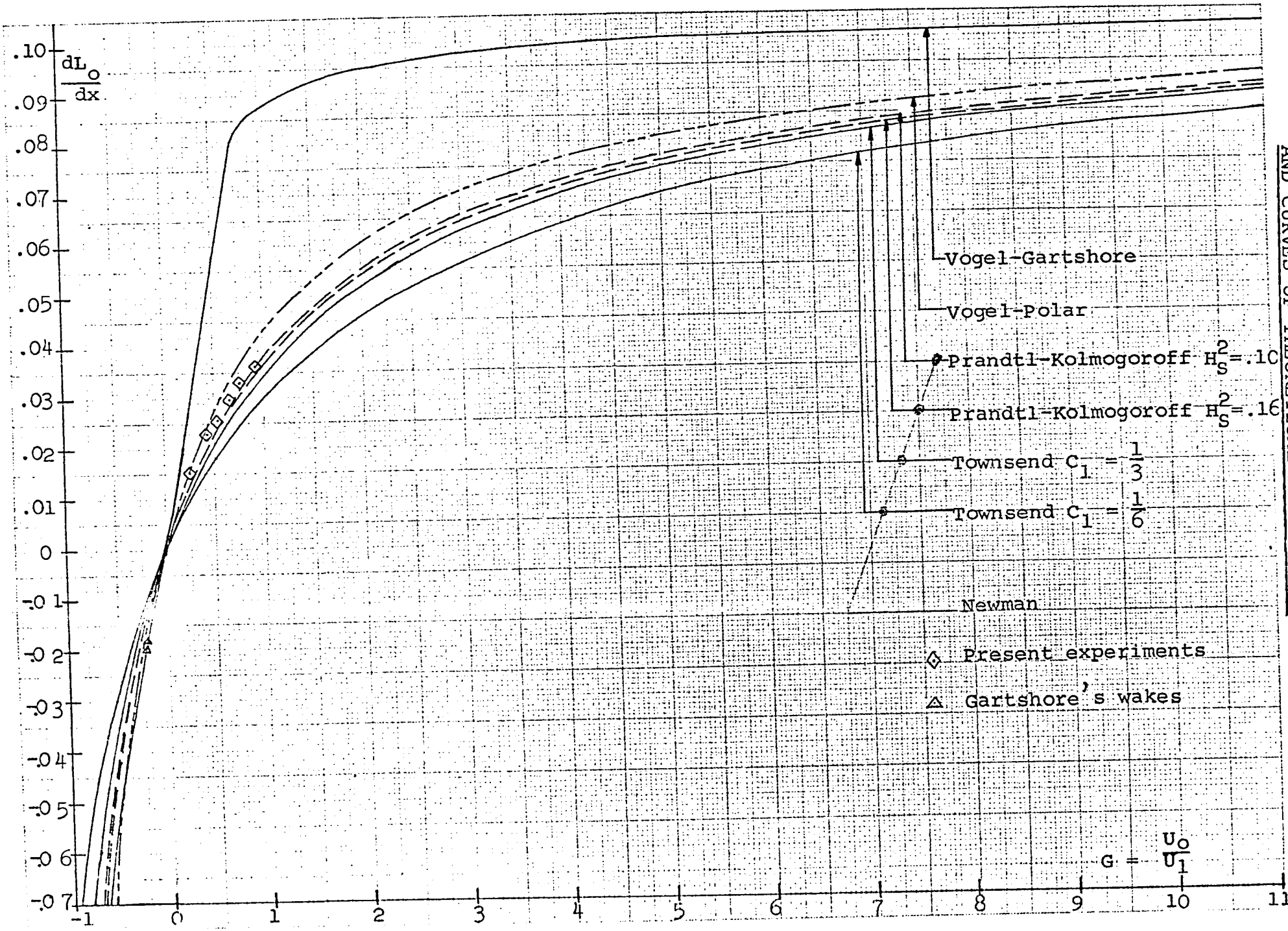

RATE OF SHEAR GROWTH ... AND CURVES OF THEORETICAL PREDICTIONS

Fig. 24

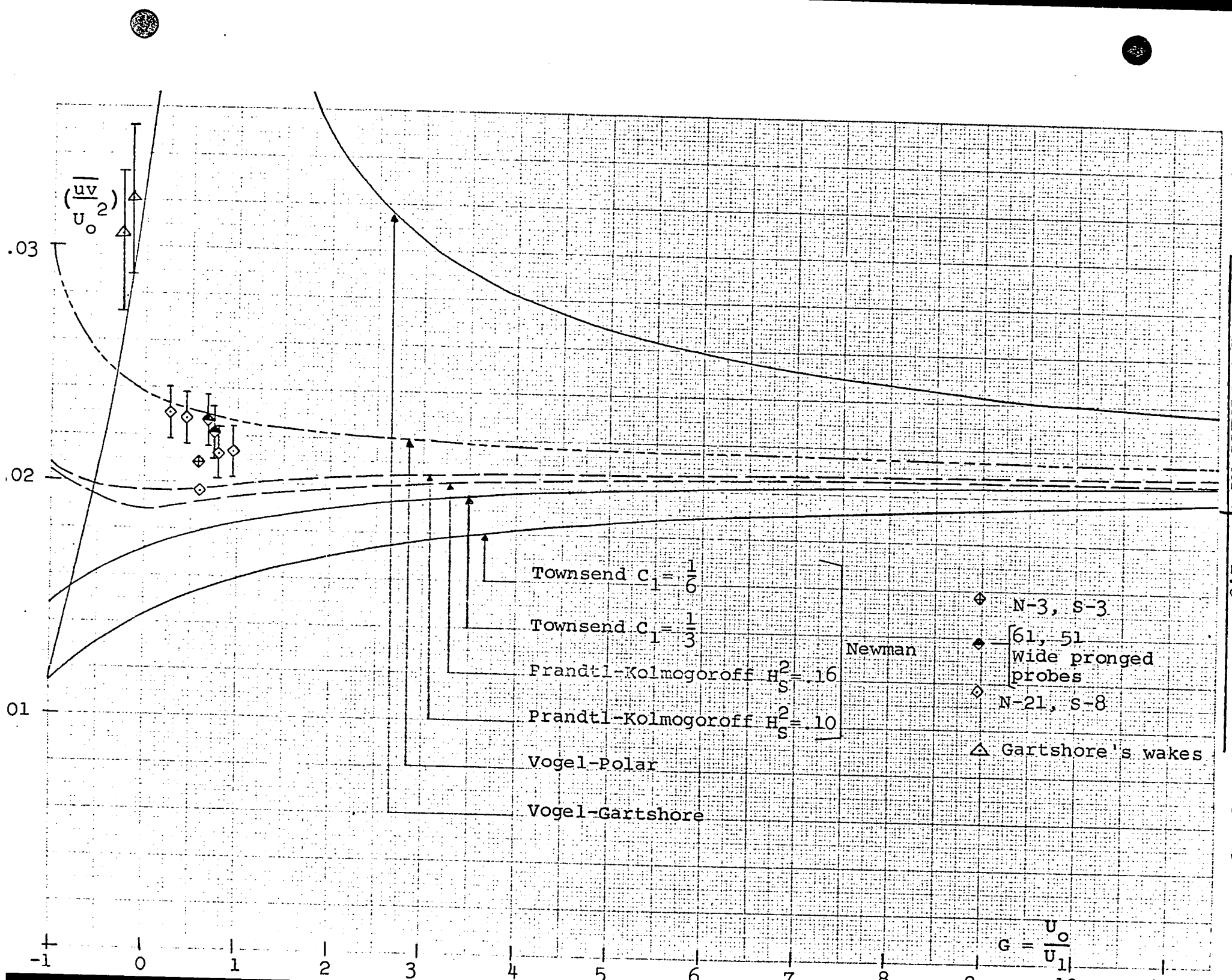

EXPERIMENTAL VALUES OF THE NON-DIMENSIONAL SHEAR STRESS AT $\eta = 1.0$

Fig. 25

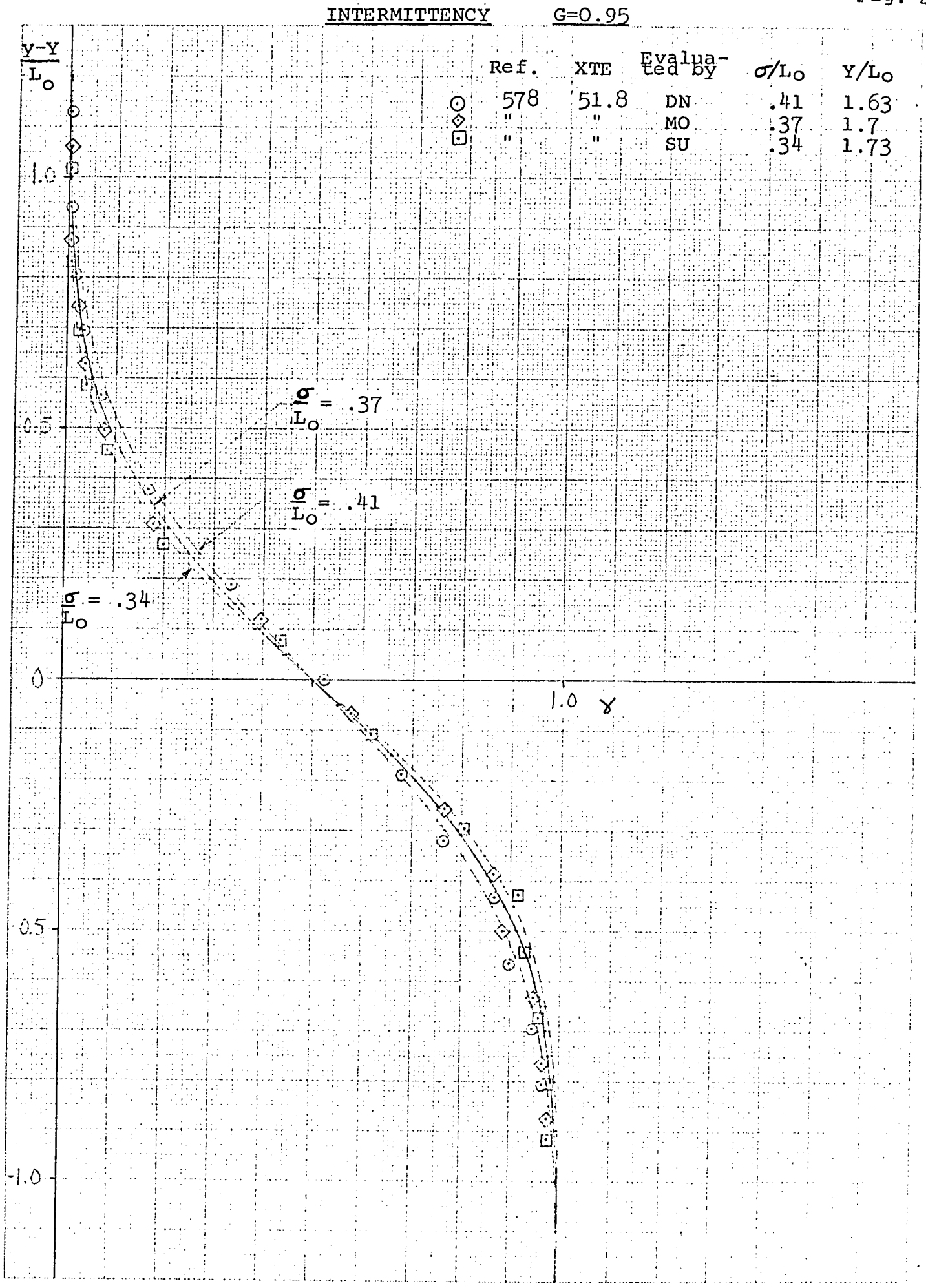
INTERMITTENCY G=0.95
y-Y / L_o
Ref. XTE Evaluated by σ/L_o Y/L_o
578 51.8 DN .41 1.63
" " MO .37 1.7
" " SU .34 1.73
σ/L_o = .37
σ/L_o = .41
σ/L_o = .34
1.0
0.5
0
0.5
-1.0
1.0 y

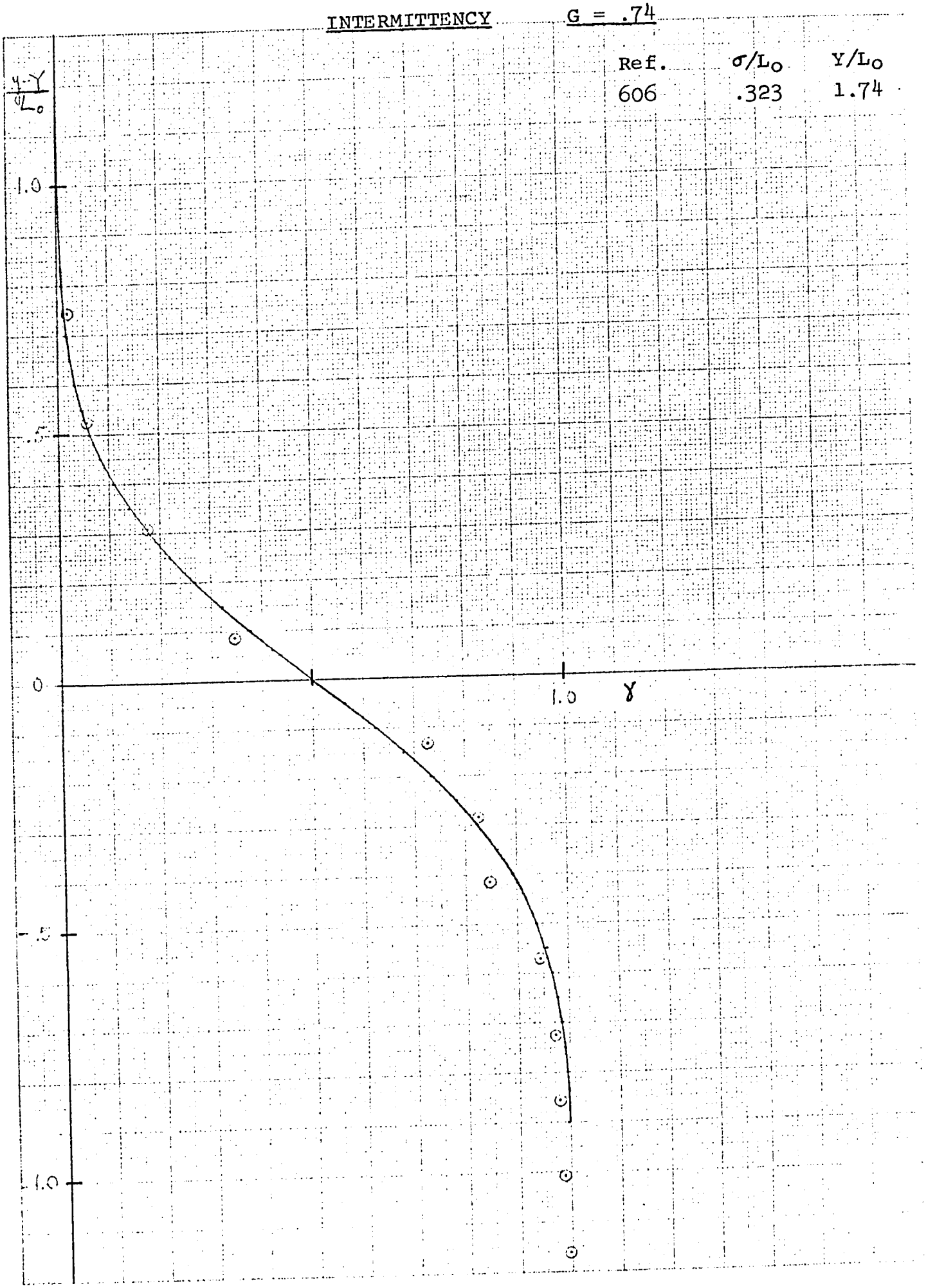
INTERMITTENCY
G = .74
Ref.
σ/L₀
Y/L₀
606
.323
1.74
1.0
.5
0
-.5
-1.0
1.0
Y

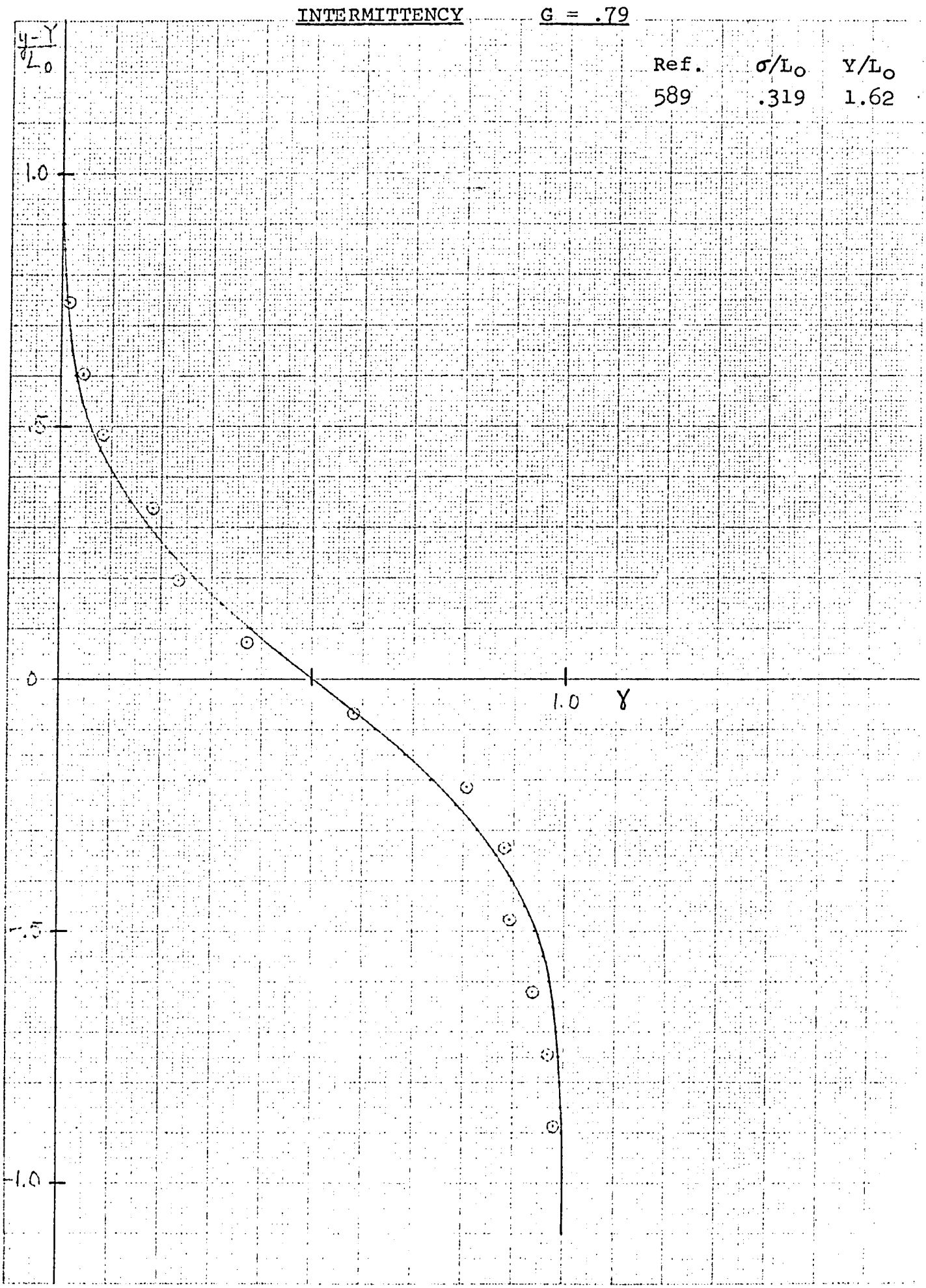
INTERMITTENCY
G = .79
Ref. σ/L_o Y/L_o
589 .319 1.62
(y-Y)/L_o
1.0
.5
0
-.5
-1.0
1.0
Y

INTERMITTENCY G = .57

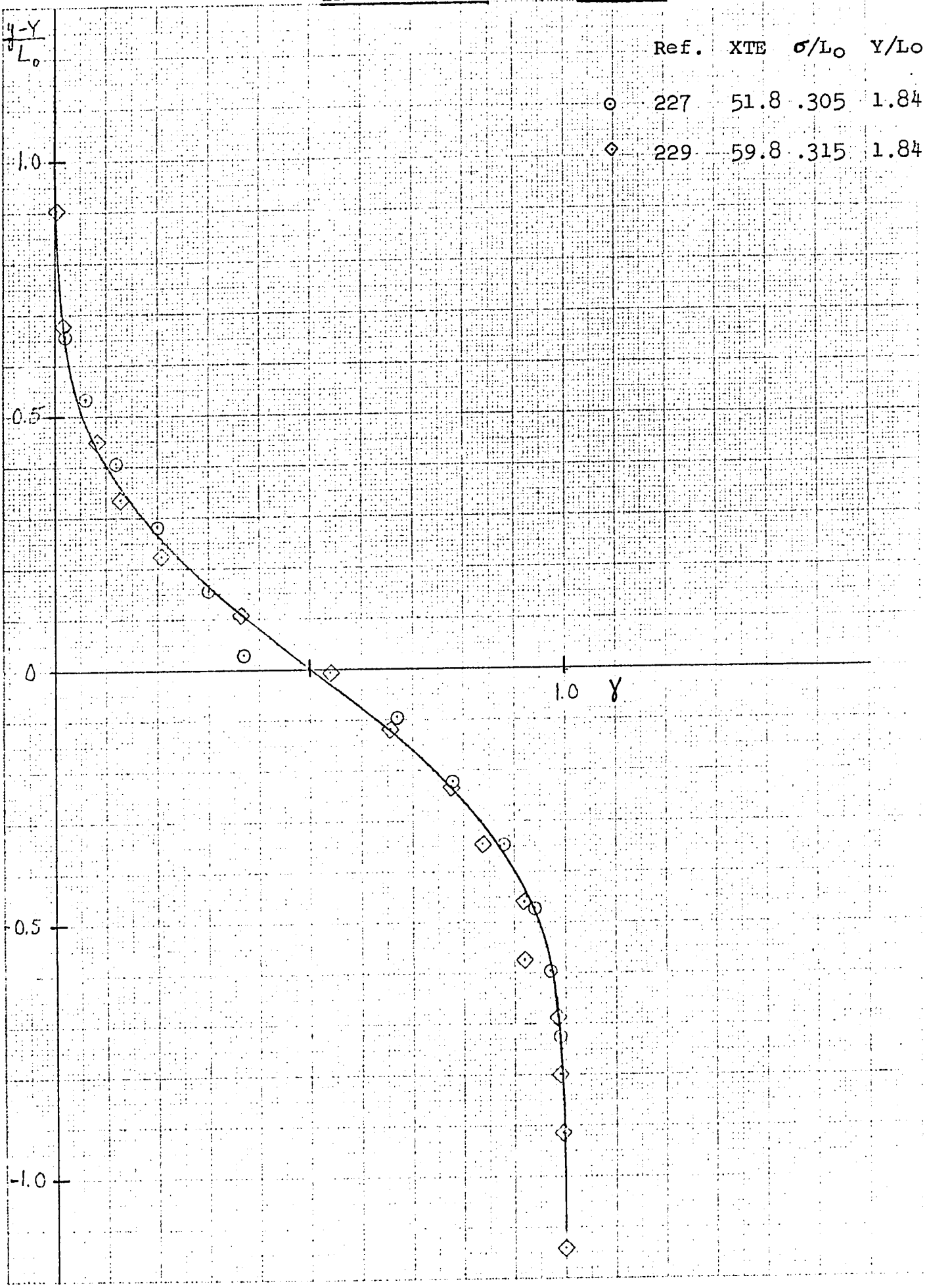

Ref.	XTE	σ/L_o	Y/Lo
⊙ 227	51.8	.305	1.84
◇ 229	59.8	.315	1.84

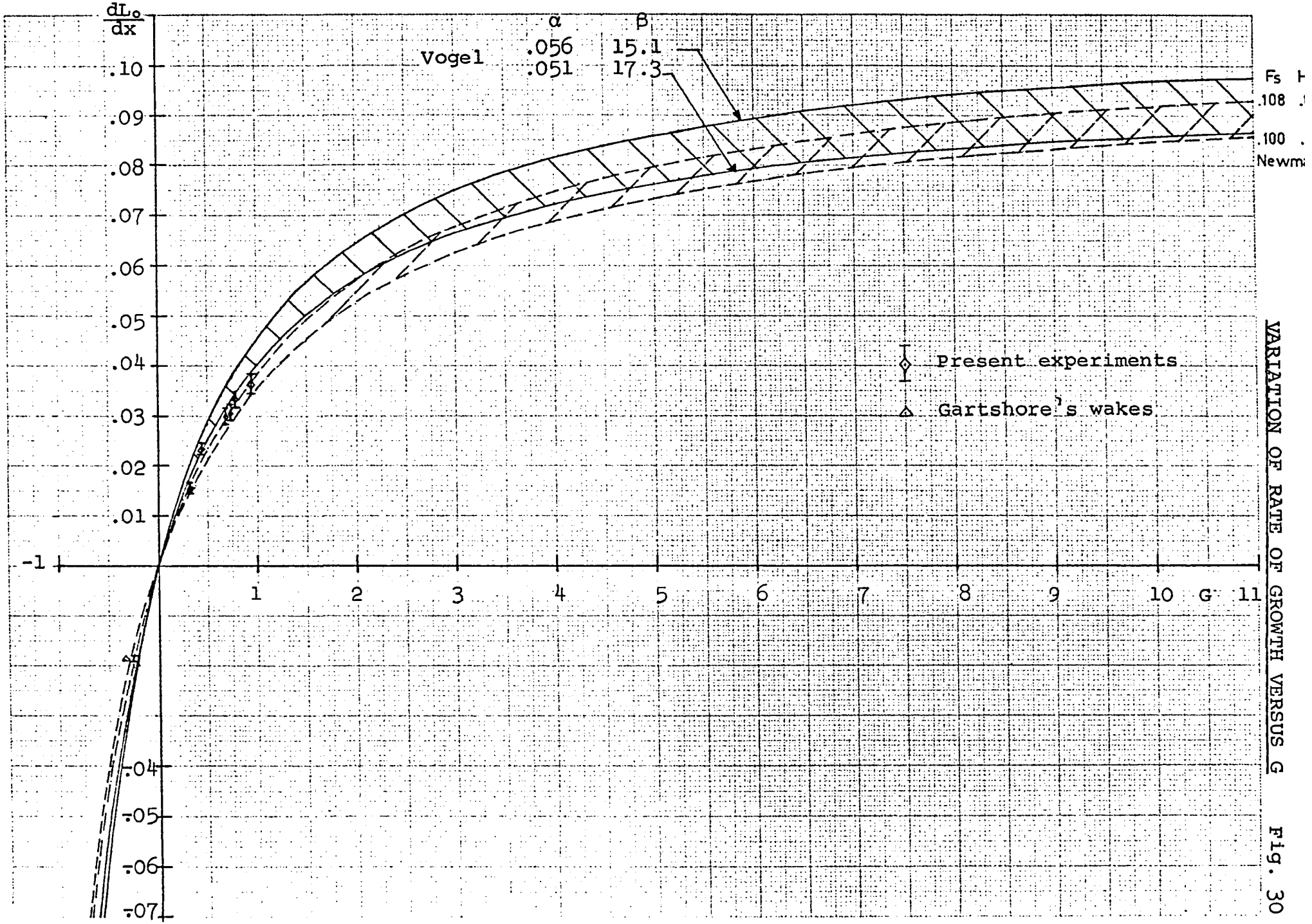

VARIATION OF RATE OF GROWTH VERSUS G

Fig. 30

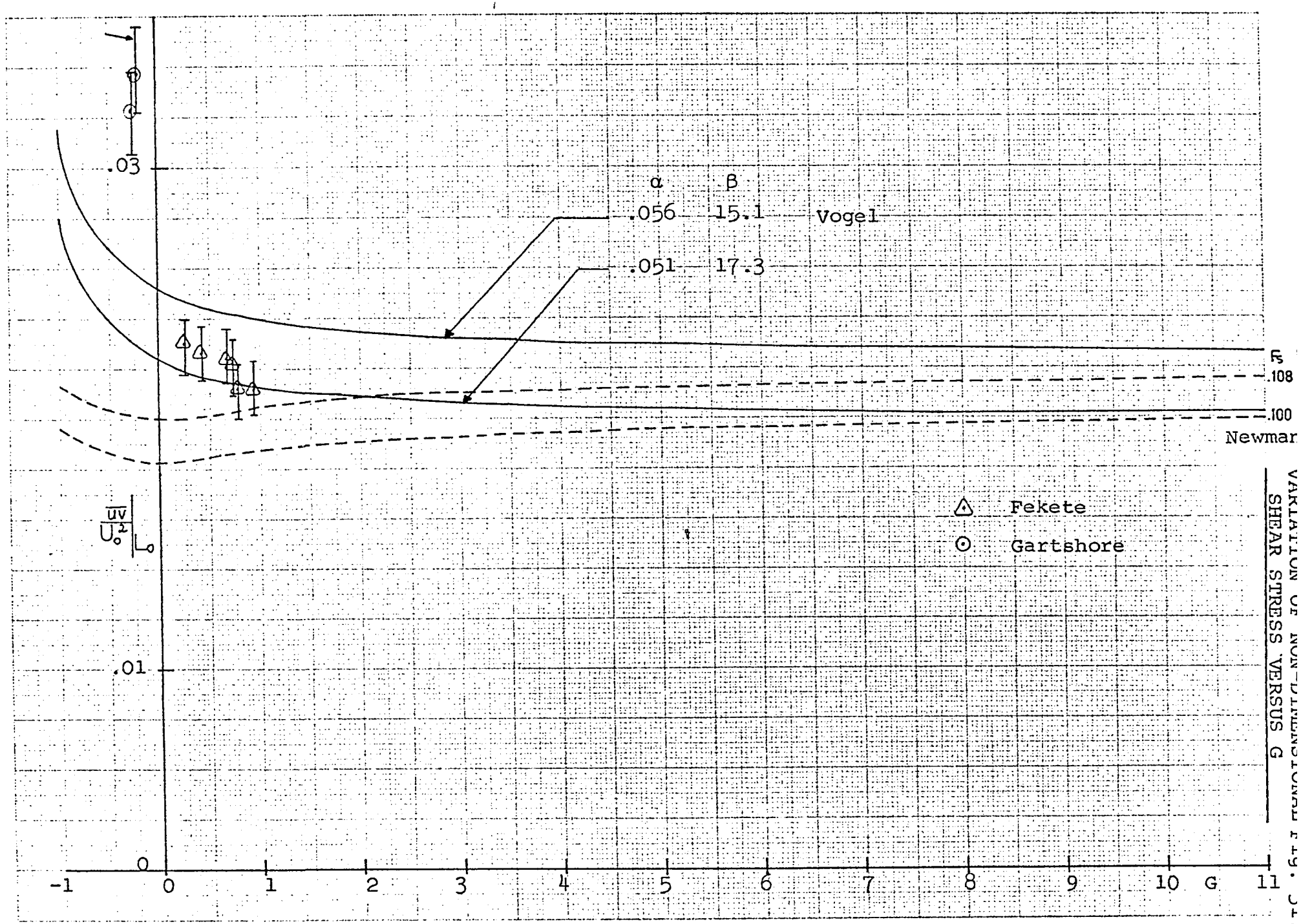
.03
.01
0
α
β
.056
15.1
Vogel
.051
17.3
.108
.100
Newmar
Fekete
Gartshore
-1
0
1
2
3
4
5
6
7
8
9
10
G
11
SHEAR STRESS VERSUS G

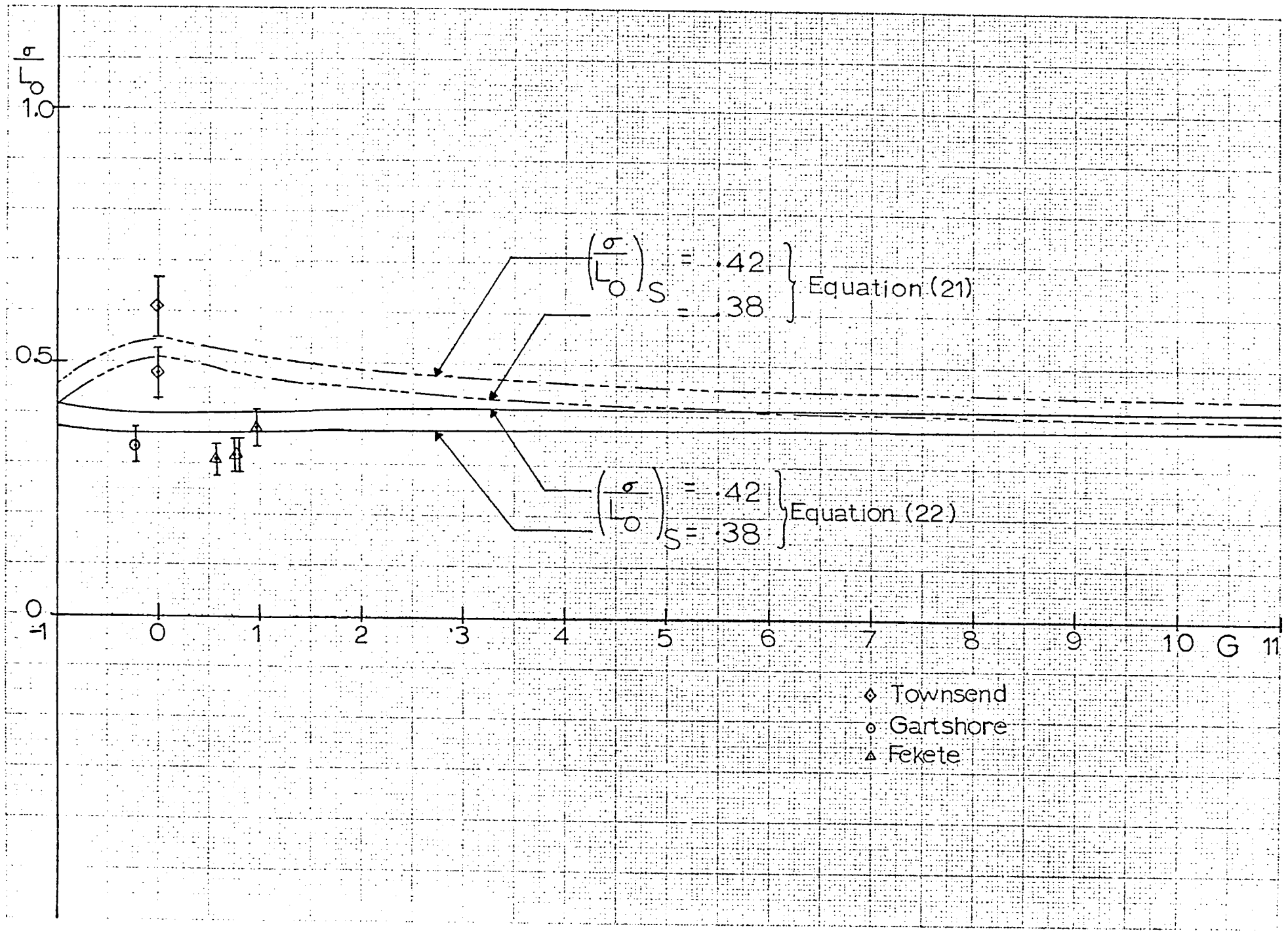

σ/L_o PLOTTED VERSUS G

Fig. 32.

AS A FUNCTION OF LARGE EDDY SCALE

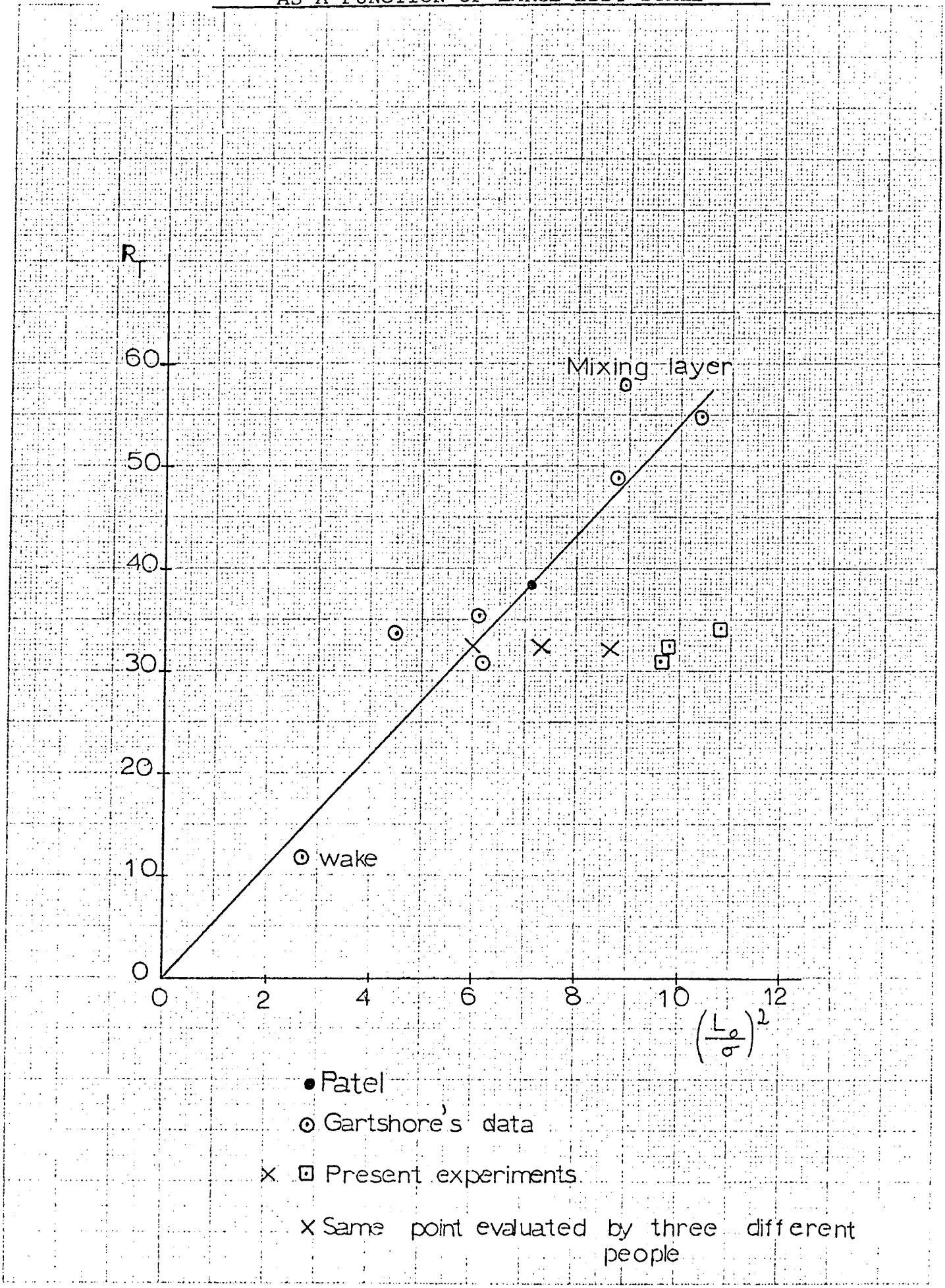

VALUES OF H^2 VERSUS G

Fig. 54.

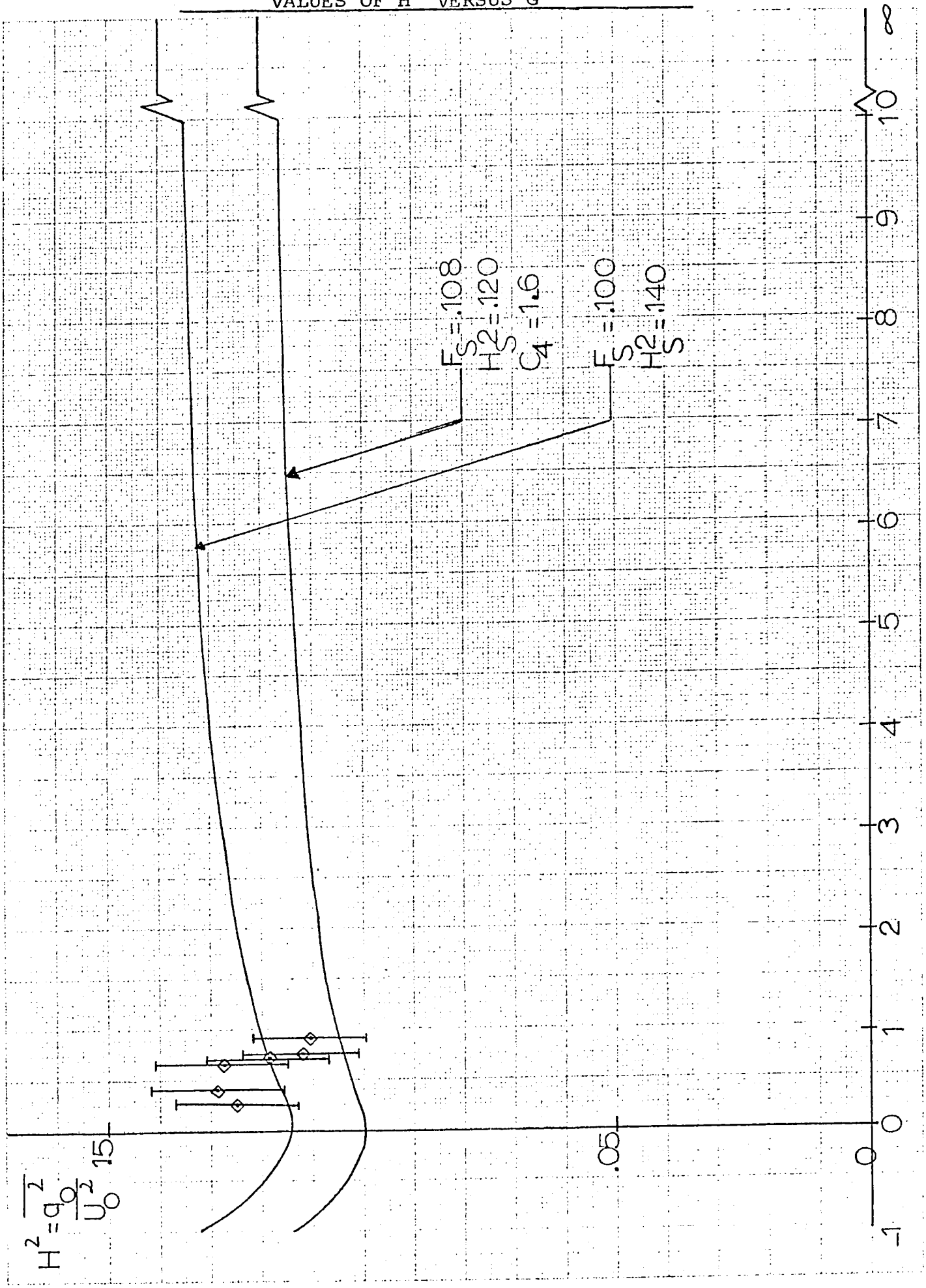

SKETCHES OF STREAMLINES

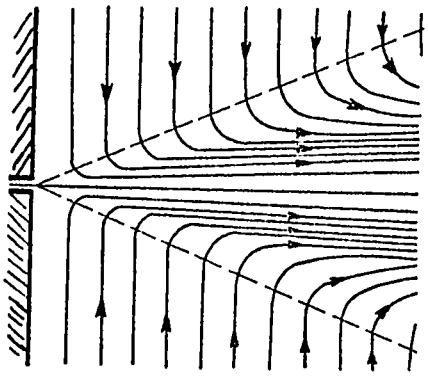

Fig. 35 (a). Sketch of Streamlines: Jet issuing from slot in wall.

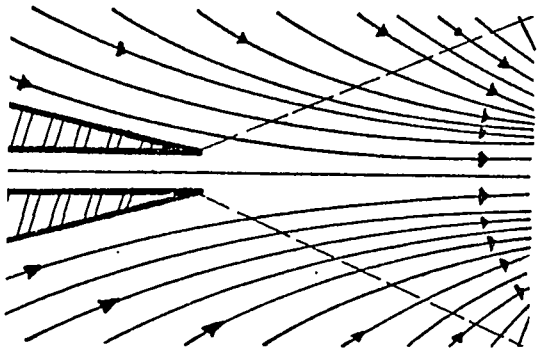

Fig. 35 (b). Sketch of Streamlines: Jet issuing from slot lip.